JSCSEN 79(6)627–757(2014)

ISSN 1820-7421(Online)

Journal of the Serbian Chemical Society

Electronic Version

VOLUME 79

No 6

BELGRADE 2014

Available on line at

www.shd.org.rs/JSCS/

Journal of the Serbian Chemical Society
JSCS-info@shd.org.rs • www.shd.org.rs/JSCS

J. Serb. Chem. Soc. Vol. 79, No. 6 (2014)

CONTENTS

Published by the Serbian Chemical Society
Karnegijeva 4/III, P. O. Box 36, 11120 Belgrade 35, Serbia
Printed by the Faculty of Technology and Metallurgy
Karnegijeva 4, P. O. Box 35-03, 11120 Belgrade, Serbia

Journal of the Serbian Chemical Society
JSCS-info@shd.org.rs • www.shd.org.rs/JSCS
J. Serb. Chem. Soc. 79 (6) 627–636 (2014) UDC 546.763–039.7+547.313–41:542.9:547.952
JSCS–4613 *Original scientific paper*

Diastereoselective addition of alkenylchromium(III) reagents to Garner's aldehyde. The Nozaki–Hiyama–Kishi coupling approach to sphingosines and ceramides

ZORANA FERJANČIĆ[1]*, RADOMIR MATOVIĆ[2] and FILIP BIHELOVIĆ[1]**

[1]*Faculty of Chemistry, University of Belgrade, Studentski trg 16, P. O. Box 158, 11000 Belgrade, Serbia and* [2]*ICTM – Center for Chemistry, Njegoševa 12, 11000 Belgrade, Serbia*

(Received 11 June, revised 18 June, accepted 19 June 2013)

Abstract: Intermolecular Nozaki–Hiyama–Kishi coupling between alkenylchromium(III) reagents, derived from either (*E*)-(2-bromoethenyl)benzene or (*E*)-1-iodo-1-pentadecene, and the conformationally rigid Garner's aldehyde resulted in the stereoselective formation of Felkin-type allylic alcohols in good yields, thus providing an easy access to sphingosines. In addition, when the protecting group in the Garner's aldehyde was changed (from Boc to *N*-octanoyl), a reversal of stereoselectivity was observed in the reaction with (*E*)--1-pentadecenylchromium(III), probably as the result of hydrophobic interactions between the long carbon chains of the reaction partners.

Keywords: Nozaki–Hiyama–Kishi reaction; sphingosine; Garner's aldehyde; organochromium reagent.

INTRODUCTION

Nozaki–Hiyama–Kishi (NHK) coupling is a versatile carbon–carbon bond forming reaction that involves nucleophilic addition of organochromium(III) species to carbonyl compounds under very mild conditions.[1,2] The NHK reaction showed good tolerance to a range of functional groups in both reaction partners. The great synthetic potential of the nickel-catalyzed addition of alkenylchromium reagents to aldehydes was demonstrated in the syntheses of various natural products,[3] including palytoxin,[4] halichondrin,[5] epothilone B and D,[6] pestalotiopsin A[7] and abyssomicin C.[8]

As alkenylchromium species are less basic than other organometallic reagents, their addition to chiral aldehydes proceed without epimerization at the α carbon atom.[2c] While the stereochemical outcome of intermolecular NHK reactions was thoroughly investigated with allylchromium species,[2,9] less attention has been paid to the stereoselectivity of the addition of alkenylchromium nuc-

Corresponding authors. E-mail: (*)zferjan@chem.bg.ac.rs; (**)filip@chem.bg.ac.rs
doi: 10.2298/JSC130611067F

leophiles. Intermolecular additions, as well as intramolecular reactions on conformationally more flexible substrates, often result in mixtures of diastereoisomers, sometimes even with a complete lack of diastereoselectivity.[8,10]

Garner's aldehyde (*tert*-butyl (4*S*)-4-formyl-2,2-dimethyloxazolidine-3-carboxylate) (**1**)[11] is a conformationally restricted *α*-nitrogen-substituted aldehyde, which represents a good substrate for probing the stereochemical outcome of alkenylchromium(III) addition. Nucleophilic additions of various organometallic species to Garner's aldehyde (**1**) are well studied.[12,13] Curiously, there is no report on alkenylchromium addition, although the addition of vinyl metals to Garner's aldehyde (**1**) represents a straightforward entry to sphingosines and ceramides (Fig. 1),[13c,d] sphingolipid key metabolites.[14] These compounds constitute a novel family of lipid second messengers[15] that play important roles in cell regulation and apoptosis,[16] as well as in higher-order physiological processes.[17]

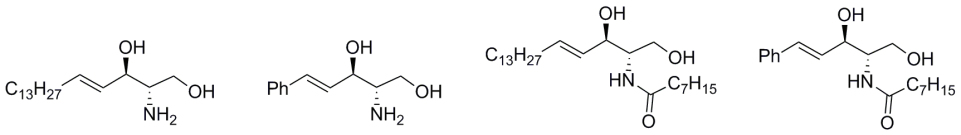

Fig. 1. Biologically important sphingosines and ceramides.

RESULTS AND DISCUSSION

Before exploring the diastereoselectivity of the addition of (*E*)-styrylchromium(III) to Garner's aldehyde (**1**),[18] the focus was initially directed to optimizing the reaction conditions. Attempts to use (*E*)-(2-iodoethenyl)benzene (**6a**) as a precursor of alkenylchromium(III) species had limited success, as the coupling products **7a** and **7b** were isolated in only 20 % yield (Scheme 1, Entry 1). However, the yield was improved by using (*E*)-(2-bromoethenyl)benzene (**6b**) as an (*E*)-styrylchromium(III) precursor (Scheme 1, Entry 2). Additionally, the reaction yield was shown to be highly dependent on chromium(II) concentration (Scheme 1, Entries 3 and 4) and tenfold excess of $CrCl_2$ was found to be the optimal loading. It is well known that, in practice, the NHK reaction requires the use of a large excess of $CrCl_2$.[2a]

Based on the available literature data,[19] it was anticipated that the stereochemistry of the addition would be in accordance with the non-chelated Felkin–Ahn Model (re-attack), thus favoring the formation of the *anti* product, due to the pronounced voluminosity of the *tert*-butoxycarbonyl group. Indeed, when performed at room temperature, the reaction stereoselectively provided allylic alcohol **7a** (*anti*:*syn* = 5:1).[20] This selectivity could be improved to 8.5:1 by performing the reaction at 0 °C, albeit with a drop in the reaction yield (Scheme 1,

Entry 5). The observed diastereoselectivity of the addition of (*E*)-styrylchromium(III) to Garner's aldehyde (**1**) was significantly higher than expected for an intermolecular NHK reaction (usually up to 3:1).[2c]

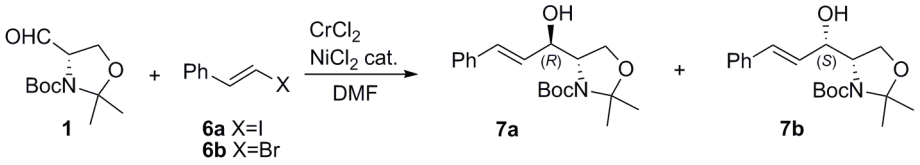

Entry	X	$CrCl_2$ eq.	Temp.	Yield **7a**,**b** %	dr(**7a** : **7b**)
1	I	4	r.t.	20	5 : 1
2	Br	4	r.t.	32	-
3	Br	6	r.t.	56	-
4	Br	10	r.t.	69	5 : 1
5	Br	10	0 °C	22	8.5 : 1

Scheme 1. Addition of (*E*)-styrylchromium(III) to Garner's aldehyde (**1**).

Next, attention was turned toward the most abundant sphingosine **2** in nature, which could be obtained through the addition of (*E*)-1-iodo-1-pentadecene (**8**)[21] to Garner's aldehyde (**1**, Scheme 2). With the previously optimized chromium(II) loading, N,O-protected sphingosines **9a** and **9b** were obtained with an even higher diastereoselectivity (*anti*:*syn* = 7:1).[20,22] Although the yield of this product was moderate (46 %), the straightforwardness of the NHK approach, coupled with its experimental simplicity, qualified it for synthetic application.

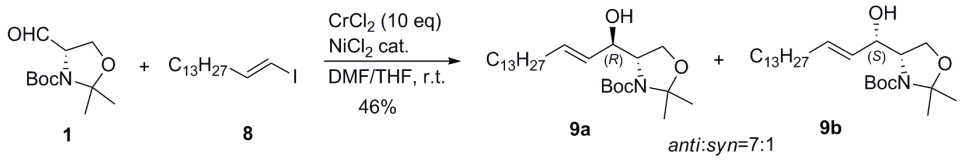

Scheme 2. Addition of (*E*)-1-pentadecenylchromium(III) to Garner's aldehyde (**1**).

Diastereoselectivity in the addition of (*E*)-1-pentadecenylchromium(III) to Garner's aldehyde (**1**) was somewhat higher, as compared to other approaches to sphingosines based on the addition of other vinylmetals (Li, Mg, Zn, Al; *anti*:*syn* ratio from 5:1 to 1:6).[19,23] Fürstner *et al*. showed that rhodium-catalyzed addition of 1-octenylboronic acid to Garner's aldehyde proceeded with a moderate diastereoselectivity (4:1).[13a] The diastereoselectivity in the addition of 1-(*E*)-alkenylzirconocene-zinc reagents, according to Murakami *et al*., is superior to other alkenylmetals (*anti*:*syn* ratio from 20:1 to 1:15). However in this method, different additives were required ($ZnBr_2$ for *syn*; Et_2Zn for *anti*).[13c]

Due to sensitivity of *N*-Boc-*N*,*O*-acetal moiety, aldehyde **10** (Scheme 3) was subjected to further research, by supstituing the octanoyl group for Boc. This

substrate is also expected to be conformationally restricted and, additionally, it would allow for a direct synthesis of protected ceramides. Aldehyde **10** was prepared from L-serine, according to Scheme 3. L-Serine was transformed into its methyl ester **11**,[24] which was then acylated with octanoyl chloride, and the resulting amide **12** was protected as *N*,*O*-acetal.[25] After subsequent reduction of ester moiety in **13**, aldehyde **10** was finally obtained by the oxidation of the intermediary alcohol **14** with Dess–Martin periodinane (DMP).

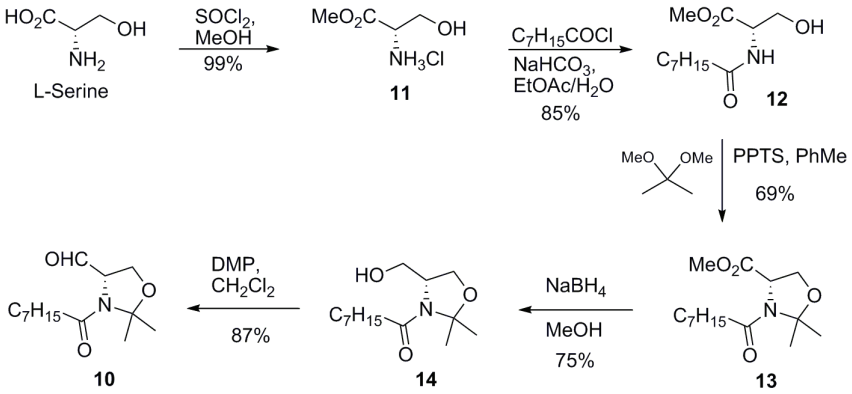

Scheme 3. Synthesis of aldehyde **10** from L-serine.

First, the reaction of the optically pure aldehyde **10** with (*E*)-1-pentadecenylchromium(III) (Scheme 4, Entry 1) was examined. This time, unfortunately, neither the yield (18 %) nor the diastereoselectivity (*anti*:*syn* = 1:2)[26] reached synthetically useful levels.

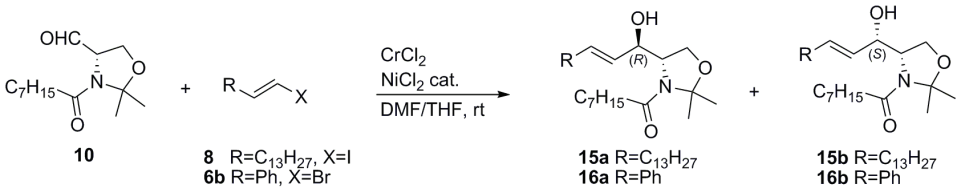

Entry	X	R	$CrCl_2$ eq.	Yield **15a,b** %	Yield **16a,b** %
1	I	$C_{13}H_{27}$	12	18	-
2	Br	Ph	7	-	55
3	Br	Ph	12	-	75

Scheme 4. Addition of alkenylchromium(III) to aldehyde **10**.

It is interesting to note that this reaction proceeded with a reversal of diastereoselectivity, with the predominant formation of the *syn*-product. The anti-Felkin stereochemical outcome could be the result of a stabilizing hydrophobic

interaction between the two long, aliphatic chains of the reaction partners. Due to this interaction, favored in polar media, alkenylchromium(III) species attack the carbonyl group from the opposite, *si*-face (Fig. 2).

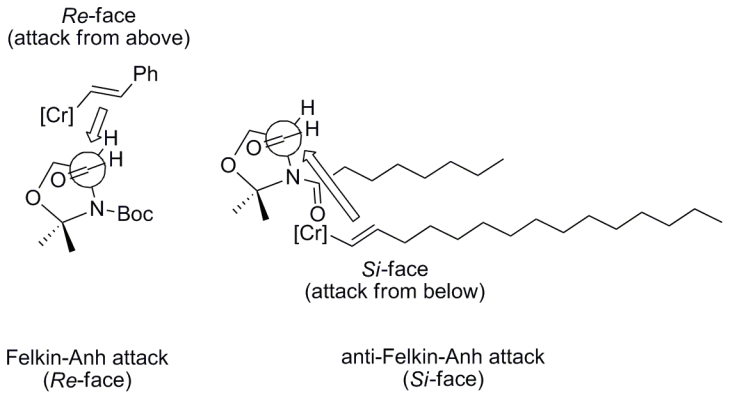

Fig. 2. *si*-Attack of (*E*)-1-pentadecenylchromium(III) on **10**, which is favored by hydrophobic interactions.

However, the treatment of aldehyde **10** with (*E*)-styrylchromium(III), prepared *in situ* from (*E*)-(2-bromoethenyl)benzene (**6b**), resulted in a smooth conversion, affording the desired products **16a** and **16b** in a good yield (Scheme 4, Entries 2 and 3). Contrary to the ^{1}H-NMR spectra of the diastereomeric mixtures **7a** and **b** or **9a** and **b**, it was difficult to determine directly the diastereomeric ratio (dr) of **16a** and **b** from the ^{1}H-NMR spectrum, as it consisted of broad and overlapping signals of rotamers, even at a higher temperature (60 °C). Therefore, it was decided to modify the work-up procedure by *in situ* hydrolysis, consequently leading to the formation of ceramides from aldehyde **10** in a single step (Scheme 5). Once the reaction was completed, the reaction mixture was treated with hydrochloric acid instead of sodium serinate,[25] and the thus-obtained free ceramides **5a** and 5**b** were analyzed by ^{1}H-NMR. Surprisingly, the ^{1}H-NMR analysis showed that the addition proceeded with almost complete lack of diastereoselectivity (*anti*:*syn* = 1.2:1), possibly as a result of the smaller steric hindrance of the *n*-octanoyl group, as compared to that of the *tert*-butoxycarbonyl group.

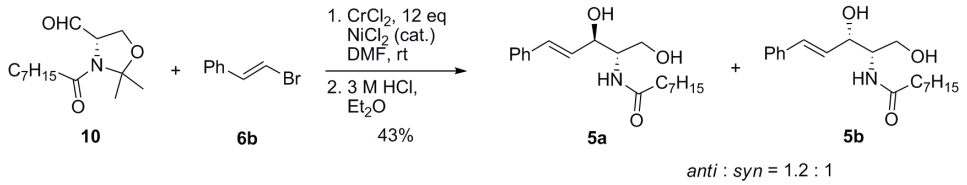

Scheme 5. Direct synthesis of ceramides **5a** and **5b** from aldehyde **10**.

EXPERIMENTAL

General experimental

All chromatographic separations[26] were performed on Silica 10–18, 60 Å, ICN Biomedicals, using petroleum ether (b. p. 65–70 °C). Standard techniques were used for the purification of the reagents and solvents.[27] The NMR spectra were recorded on a Bruker Avance III 500 (^{1}H-NMR at 500 MHz, ^{13}C-NMR at 125 MHz). The chemical shifts are expressed in ppm (δ) using tetramethylsilane as an internal standard, coupling constants (J) are in Hz. The IR spectra were recorded on a Nicolet 6700 FT instrument, and are expressed in cm^{-1}. The mass spectra were obtained on Agilent technologies 6210 TOF LC/MS instrument (LC: series 1200). The optical rotations were measured on Rudolph Research Analytical AUTOPOL IV automatic polarimeter.

Nozaki–Hiyama–Kishi couplings

*Addition of (*E*)-styrylchromium(III) to Garner's aldehyde **1***. Commercial chromium(II) chloride (113 mg; 0.924 mmol; 10 eq; 99.9 % purity) and anhydrous nickel(II) chloride (0.6 mg; 5 mol %) were suspended in freshly distilled and degassed dry DMF (0.4 mL), in a glovebox, under an argon atmosphere. A solution of **1** (21 mg; 0.0924 mmol) and **6b** (50 mg; 0.277 mmol; 3 eq) in DMF (0.4 mL) was added dropwise to the suspension, and the mixture was stirred at room temperature for 1 h. The reaction mixture was treated with 1 M sodium serinate (3 mL) and diethyl ether (10 mL) and vigorous stirring was continued for 1 h. The layers were separated, the aqueous layer was extracted with diethyl ether (2×10 mL), and the combined organic extract was washed with brine (2×5 mL), dried ($MgSO_4$), filtered, and concentrated under reduced pressure. Purification of the residue by column chromatography (eluent, petroleum ether:ethyl acetate:triethylamine = 80:20:1) afforded 21 mg (69 %) of mixture of allylic alcohols **7a** and **7b** (**7a**:**7b** = 5:1), as a colorless oil. The diastereoisomeric ratio was determined by integrating signals in ^{1}H-NMR spectrum (500 MHz, C_6D_6 at 60 °C, δ / ppm): δ (isomer **7a**) = 6.74 (1H, *d*, J = 16.0 Hz); δ (isomer **7b**) = 6.62 (1H, *d*, J = 15.5 Hz). The spectroscopic data were fully consistent with those previously reported.[13c]

*Addition of (*E*)-1-pentadecenylchromium(III) to Garner's aldehyde (**1**)*. Commercial chromium(II) chloride (80 mg; 0.654 mmol; 10 eq; 99.9 % purity) and anhydrous nickel(II) chloride (0.4 mg; 5 mol %) were suspended in freshly distilled and degassed dry DMF (0.4 mL), in a glovebox, under an argon atmosphere. A solution of **1** (15.0 mg; 0.0654 mmol) and **8** (66 mg; 0.196 mmol; 3 eq) in DMF/THF (V/V = 1/1; 0.4 mL) was added dropwise to the suspension, and the mixture was stirred at room temperature for 1 h. The reaction mixture was treated with 1 M sodium serinate (3 mL) and diethyl ether (10 mL) and vigorous stirring was continued for 1 h. The layers were separated, the aqueous layer was extracted with diethyl ether (2×10 mL), and the combined organic extract was washed with brine (2×5 mL), dried ($MgSO_4$), filtered and concentrated under reduced pressure. Purification of the residue by column chromatography (eluent, petroleum ether:ethyl acetate:triethylamine = 90:10:1) afforded 13.3 mg (46 %) of a mixture of allylic alcohols **9a** and 9**b** (**9a**:**9b** = 7:1), as a colorless oil. The diastereoisomeric ratio was determined by integrating signals in the ^{1}H-NMR spectrum (500 MHz, C_6D_6 at 60 °C, δ / ppm): δ (isomer **9a**) = 5.79 (1H, *dt*, J = 6.5 and 15.5 Hz); δ (isomer **9b**) = 5.71 (1H, *dt*, J = 6.5 and 15.5 Hz). The spectroscopic data were fully consistent with those previously reported.[13c,19a]

*Addition of (*E*)-1-pentadecenylchromium(III) to aldehyde **10***. Commercial chromium(II) chloride (122 mg; 0.993 mmol; 12 eq; 99.9 % purity) and anhydrous nickel(II) chloride (0.5 mg; 5 mol %) were suspended in freshly distilled and degassed dry DMF (0.5 mL), in a

glovebox, under an argon atmosphere. A solution of **10** (21.0 mg; 0.0827 mmol) and **8** (83 mg; 0.248 mmol) in DMF/THF (*V*/*V* = 1/1; 0.6 mL) was added dropwise to the suspension, and the mixture was stirred at room temperature for 1 h. The reaction mixture was treated with 1 M sodium serinate (2.1 mL) and diethyl ether (10 mL) and vigorous stirring was continued for 1 h. The layers were separated, the aqueous layer was extracted with diethyl ether (2×10 mL), and the combined organic extract was washed with brine (2×5 mL), dried ($MgSO_4$), filtered, and concentrated under reduced pressure. Purification of the residue by column chromatography (eluent, petroleum ether:ethyl acetate:triethylamine = 90:10:1) afforded 7.1 mg (18 %) of a mixture of allylic alcohols **15a** and **15b**, as a colorless oil.

The thus-obtained alcohols **15a** and **15b** (7.1 mg; 0.0152 mmol) were dissolved in 70 % acetic acid (0.5 mL) and the mixture was stirred overnight. The mixture was diluted with ethyl acetate, washed with water and brine, dried ($MgSO_4$), filtered and concentrated under reduced pressure. Purification of the residue by column chromatography (eluent, petroleum ether:ethyl acetate = 1:4) afforded 4.8 mg (73 %) of mixture of allylic alcohols **4a** and **4b** (**4a**:**4b** = 1:2), as a white wax. The diastereoisomeric ratio was determined by integrating signals in the ^{1}H--NMR spectrum (500 MHz, $CDCl_3$, δ / ppm): δ (isomer **4a**) = 6.26 (1H, *d*, *J* = 7.5 Hz); δ (isomer **4b**) = 6.13 (1H, *d*, *J* = 8.0 Hz). The spectroscopic data were fully consistent with those previously reported.[30]

*Addition of (*E*)-styrylchromium(III) to aldehyde **10***. Commercial chromium(II) chloride (173 mg; 1.41 mmol; 12 eq; 99.9 % purity) and anhydrous nickel(II) chloride (0.7 mg; 5 mol %) were suspended in freshly distilled and degassed dry DMF (0.8 mL), in a glovebox, under an argon atmosphere. A solution of **10** (30 mg; 0.117 mmol) and **6b** (64 mg; 0.352 mmol; 3 eq) in DMF (0.4 mL) was added dropwise to the suspension, and the mixture was stirred at room temperature for 1 h. Hydrochloric acid (3 M; 0.6 mL) was added to the reaction mixture and stirring was continued for 1 h, before the resulting mixture was diluted with ethyl acetate, and the layers were separated. The organic layer was washed with water and brine, dried ($MgSO_4$), filtered and concentrated under reduced pressure. Purification of the residue by column chromatography (eluent, petroleum ether:ethyl acetate = 1:2) afforded 16.3 mg (43 %) of a mixture of allylic alcohols **5a** and **5b** (**5a**:**5b** = 1.2:1), as a white wax. The diastereo-isomeric ratio was determined by integrating signals in the ^{1}H-NMR spectrum (500 MHz, $CDCl_3$, δ / ppm): δ (isomer **5a**) = 6.48 (1H, *d*, *J* = 8.0 Hz); δ (isomer **5b**) = 6.34 (1H, *d*, *J* = 8.0 Hz). The spectroscopic data were fully consistent with those previously reported.[31]

*Preparation of aldehyde **10***

*Synthesis of (*S*)-methyl 3-hydroxy-2-octanamidopropanoate (**12**)*. To a cold solution (–15 °C) of L-serine (1.0 g, 9.6 mmol) in anhydrous methanol (20 mL), thionyl chloride (1.37 g, 11.52 mmol) was added slowly using a syringe. The solution was stirred at –15 °C for 30 min and then at room temperature overnight. The reaction mixture was concentrated under reduced pressure to afford 1.47 g (99 %) of crude L-serine methyl ester hydrochloride (**11**), as a white powder, which was further used without purification.

L-Serine methyl ester hydrochloride (**11**, 1.47 g, 8.75 mmol) was added to a solution of sodium bicarbonate (1.08 g, 17.49 mmol) in water (27 mL), followed by the addition of ethyl acetate (27 mL). Octanoyl chloride (1.78 g, 10.94 mmol) was added to the vigorously stirred reaction mixture and stirring was continued for 1 h. The reaction mixture was extracted with ethyl acetate (3×20 mL) and the combined organic extract was washed with brine and dried over $MgSO_4$. After removal of the solvent under reduced pressure, the residue was purified by dry-flash chromatography (eluent, petroleum ether:ethyl acetate = 1:1), to afford 1.81 g (85 %) of **12** as a colorless, viscous oil.

*Synthesis of (*S*)-methyl 2,2-dimethyl-3-octanoyloxazolidine-4-carboxylate (**13**)*. A solution of 2,2-dimethoxypropane (8.9 g; 85.7 mmol), pyridinium *p*-toluenesulfonate (122 mg; 0.48 mmol) and the amide alcohol **12** (660 mg; 2.69 mmol) in toluene (11 mL) was heated at 90 °C for 20 h. The reaction mixture was diluted with dichloromethane, washed with saturated $NaHCO_3$ and water. The organic extract was dried over anh. $MgSO_4$ and concentrated under reduced pressure. Purification of the crude product by dry-flash chromatography (eluent, petroleum ether:ethyl acetate = 85:15) afforded 530 mg (69 %) of compound **13**, as a colorless oil.

*Synthesis of (*R*)-1-(4-(hydroxymethyl)-2,2-dimethyloxazolidin-3-yl)-1-octanone (**14**)*. A solution of **13** (720 mg; 2.52 mmol) in methanol (5 mL) was treated with sodium borohydride (429 mg; 11.34 mmol) for 1 h at room temperature. The reaction was quenched with saturated NH_4Cl and the resulting mixture was stirred for 5 min. After dilution with water, the reaction mixture was extracted twice with dichloromethane and the extract was dried over anh. $MgSO_4$. Concentration under reduced pressure, followed by purification of the residue by dry-flash chromatography (eluent, petroleum ether:ethyl acetate = 1:1) gave alcohol **14** (490 mg; 75%), as a colorless, viscous oil.

*Synthesis of (*S*)-2,2-dimethyl-3-octanoyloxazolidine-4-carboxaldehyde (**10**)*. Dess–Martin periodinane (1,1,1-triacetoxy-1,1-dihydro-1,2-benziodoxol-3(1*H*)-one, 372 mg; 0.87 mmol) was added to a solution of alcohol **14** (30 mg; 0.19 mmol) in dichloromethane (3 mL) and the reaction mixture was stirred for 30 min at room temperature. The reaction mixture was diluted with dichloromethane and washed with 10% $Na_2S_2O_3$ and saturated $NaHCO_3$. The organic extract was dried over anh. $MgSO_4$ and concentrated under reduced pressure. Purification of the crude product by dry-flash chromatography (eluent, petroleum ether:ethyl acetate = 1:1) afforded 26 mg (87 %) of the title compound, as a colorless oil.

The physical and spectral data for aldehyde **10** and the isolated intermediates in its preparation **12**–**14** are given in the Supplementary material to this paper.

CONCLUSIONS

In conclusion, it was shown that alkenylchromium(III) species add to conformationally rigid Garner's aldehyde (**1**) in a stereoselective manner. The predominant formation of Felkin-type products is in accordance with non-chelation control in the transition state. In addition, it was shown that a nonpolar interaction between two long, aliphatic chains of the reaction partners may play an important role in diastereofacial selectivity, thus favoring the formation of the anti-Felkin product. Therefore, Nozaki–Hiyama–Kishi reaction with Garner's aldehyde (**1**) offers an alternative synthetic route toward sphingosines. This coupling approach also allows for a direct, but non-stereoselective preparation of aromatic ceramide analogue **5**, in a good yield.

SUPPLEMENTARY MATERIAL

The physical and spectral data for aldehyde **10** and the isolated intermediates **12**–**14** are available electronically from http://www.shd.org.rs/JSCS/, or from the corresponding author on request.

Acknowledgments. Financial support of the Ministry of Education, Science and Technological Development of the Republic of Serbia is acknowledged (Project No. 172027). We are grateful to Prof. Radomir N. Saicic (Faculty of Chemistry, University of Belgrade, Serbia) for helpful discussions.

ИЗВОД

ДИЈАСТЕРЕОСЕЛЕКТИВНЕ АДИЦИЈЕ АЛКЕНИЛХРОМ(III) РЕАГЕНАСА НА ГАРНЕРОВ АЛДЕХИД. СИНТЕЗА СФИНГОЗИНА И ЦЕРАМИДА НОЗАКИ–ХИЈАМА–КИШИЈЕВИМ КУПЛОВАЊЕМ

ЗОРАНА ФЕРЈАНЧИЋ[1], РАДОМИР МАТОВИЋ[2] и ФИЛИП БИХЕЛОВИЋ[1]

[1]*Хемијски факултет Универзитета у Београду, Студентски трг 12–16, п. пр. 158, 11 000 Београд и* [2]*ИХТМ-Центар за хемију, Универзитет у Београду, Његошева 12, 11 000 Београд*

У интермолекулском Нозаки–Хијама–Кишијевом куповању алкенилхром(III) реагенаса, изведених из (*E*)-2-бромстирена или (*E*)-1-јод-1-пентадецена, и конформационо ригидног Гарнеровог (*Garner*) алдехида стереоселективно се добијају алилни алкохоли Фелкиновог (*Felkin*) типа у добрим приносима, што омогућује лак приступ сфингозинима. Такође, промена заштитне групе у Гарнеровом алдехиду (из *терц*-бутоксикарбонил- у октаноил-), резултује обрнутом дијастереоселективношћу у случају (*E*)-1-пентадеценилхрома(III), вероватно као последица хидрофобних интеракција између дугих угљоводоничних ланаца реакционих партнера.

(Примљено 11. јуна, ревидирано 18. јуна, прихваћено 19. јуна 2013)

REFERENCES

1. a) Y. Okude, S. Hirano, T. Hiyama, H. Nozaki, *J. Am. Chem. Soc.* **99** (1977) 3179; b) T. Hiyama, K. Kimura, H. Nozaki, *Tetrahedron Lett.* **22** (1981) 1037; c) T. Hiyama, Y. Okude, K. Kimura, H. Nozaki, *Bull. Chem. Soc. Jpn.* **55** (1982) 561; d) K. Takai, K. Kimura, T. Kuroda, T. Hiyama, H. Nozaki, *Tetrahedron Lett.* **24** (1983) 5281
2. For recent reviews on Cr-mediated reactions, see: a) A. Fürstner, *Chem. Rev*. **99** (1999) 991; b) L. A. Wessjohann, G. Scheid, *Synthesis* (1999) 1; c) K. Takai, *Org. React.* **64** (2004) 253 and references cited therein
3. For review on the application of the Nozaki–Hiyama–Kishi reaction in the syntheses of complex natural products see: E. M. Daly, R. E. Taylor, *Chemtracts* **20** (2007) 1
4. R. W. Armstrong, J.-M. Beau, S. H. Cheon, W. J. Christ, H. Fujioka, W.-H. Ham, L. D. Hawkins, H. Jin, S. H. Kang, Y. Kishi, M. J. Martinelli, W. W. McWhorter, M. Mizuno, M. Nakata, A. E. Stutz, F. X. Talamas, M. Taniguchi, J. A. Tino, K. Ueda, J.-I. Uenishi, J. B. White, M. Yonaga, *J. Am. Chem. Soc.* **111** (1989) 7525
5. T. D. Aicher, K. R. Buszek, F. G. Fang, C. J. Forsyth, S. H. Jung, Y. Kishi, M. C. Matelich, P. M. Scola, D. M. Spero, S. K. Yoon, *J. Am. Chem. Soc*. **114** (1992) 3162
6. R. E. Taylor, Y. Chen, *Org. Lett.* **3** (2001) 2221
7. a) K.-I. Takao, N. Hayakawa, R. Yamada, T. Yamaguchi, U. Morita, S. Kawasaki, K.-I. Tadano, *Angew. Chem. Int. Ed.* **47** (2008) 3426; b) T. M. Baker, D. J. Edmonds, D. Hamilton, C. J. O'Brien, D. J. Procter, *Angew. Chem. Int. Ed.* **47** (2008) 5631
8. F. Bihelovic, R.N. Saicic, *Angew. Chem. Int. Ed.* **51** (2012) 5687
9. a) M. D. Lewis, Y. Kishi, *Tetrahedron Lett.* **23** (1982) 2343; b) J. Mulzer, T. Schulze, A. Strecker, W. Denzer, *J. Org. Chem.* **53** (1988) 4098; c) Y. Aoyagi, H. Inaba, Y. Hiraiwa, A. Kuroda, A. Ohta, *J. Chem. Soc., Perkin Trans. 1* (1998) 3975; d) T. Nagamitsu, T. Sunazuka, H. Tanaka, S. Omura, P. A. Sprengeler, A. B. Smith, *J. Am. Chem. Soc.* **118** (1996) 3584; e) P. Ciapetti, M. Falorni, M. Taddei, *Tetrahedron* **52** (1996) 7379; f) W. R. Roush, D. S. Coffey, D. Madar, A. D. Palkowitz, *J. Braz. Chem. Soc*. **7** (1996) 327
10. a) E. Piers, A. M. Kaller, *Tetrahedron Lett.* **37** (1996) 5857; b) A. Lubineau, I. Billault, *J. Org. Chem.* **63** (1998) 5668; c) K. M. Foote, M. John, G. Pattenden, *Synlett* (2002) 365

11. a) P. Garner, *Tetrahedron Lett.* **25** (1984) 5855; b) P. Garner, J. M. Park, *J. Org. Chem.* **52** (1987) 2361; c) P. Garner, J. M. Park, *Org. Synth.* **70** (1991) 18
12. For review article on the Garner's aldehyde, see: X. Liang, J. Andersch, M. Bols, *J. Chem. Soc., Perkin Trans. 1* (2001) 2136
13. a) A. Fürstner, H. Krause, *Adv. Synth. Catal.* **343** (2001) 343; b) K. Sa-Ei, J. Montgomery, *Tetrahedron* **65** (2009) 6707; c) T. Murakami, K. Furusawa, *Tetrahedron* **58** (2002) 9257; d) T. Murakami, R. Hirono, K. Furusawa, *Tetrahedron* **61** (2005) 9233
14. For recent review on the syntheses of sphingosines, see: J. A. Morales-Serna, J. Llaveria, Y. Diaz, M. I. Matheu, S. Castillón, *Curr. Org. Chem.* **14** (2010) 2483
15. a) Y. A. Hannun, *Science* **274** (1996) 1855; b) Y. A. Hannun, *Sphingolipid-Mediated Signal Transduction*, Chapman and Hall, New York, 1997
16. a) Y. A. Hannun, L. M. Obeid, *Trends Biochem. Sci.* **20** (1995) 73; b) S. Mathias, L. A. Pena, R. N. Kolesnick, *Biochem. J.* **335** (1998) 465; c) H. Birbes, S. E. Bawab, L. M. Obeid, Y. A. Hannun, *Adv. Enzyme Regul.* **42** (2002) 113
17. a) M. El Alwani, B. X. Wu, L. M. Obeid, Y. A. Hannun, *Pharmacol. Ther.* **112** (2006) 171; b) K. M. Argraves, B. A. Wilkerson, W. S. Argraves, P. A. Fleming, L. M. Obeid, C. J. Drake, *J. Biol. Chem.* **279** (2004) 50580
18. Garner's aldehyde (**1**) was prepared according to a previously published procedure: M. Trajkovic, Z. Ferjancic, R. N. Saicic, *Tetrahedron Asymmetr.* **23** (2012) 602
19. a) P. Garner, J. M. Park, E. Malecki, *J. Org. Chem.* **53** (1988) 4395; b) X. Liang, J. Andersch, M. Bols, *J. Chem. Soc., Perkin Trans. 1* (2001) 2136
20. This pair of diastereomeric products exists as mixture of rotamers, and its ^{1}H-NMR spectrum shows broad and overlapping signals at room temperature. The *anti*/*syn* ratio was determined by ^{1}H-NMR at 60 °C
21. J. Llaveria, A. Beltran, M. M. Diaz-Requejo, M. I. Matheu, S. Castillon, P. J. Perez, *Angew. Chem. Int. Ed.* **49** (2010) 7092
22. THF was used as a cosolvent, in order to overcome the problem of a poor solubility of (*E*)-1-iodo-1-pentadecene in DMF
23. a) R. S. Coleman, A. J. Carpenter, *Tetrahedron Lett.* **33** (1992) 1697; b) K. Soai, K. Takahashi, *J. Chem. Soc., Perkin Trans. 1* (1994) 1257; c) K. Suzuki, T. Hasegawa, T. Imai, H. Maeta, S. Ohba, *Tetrahedron* **51** (1995) 4483
24. K. Gu, L. Bi, M. Zhao, C. Wang, J. Ju, S. Peng, *Bioorg. Med. Chem.* **15** (2007) 6273
25. W. Wu, R. Li, S. S. Malladi, H. J. Warshakoon, M. R. Kimbrell, M. W. Amolins, R. Ukani, A. Datta, S. A. David, *J. Med. Chem.* **53** (2010) 3198
26. The *anti*/*syn* ratio was determined by ^{1}H-NMR of the unprotected (3*R*)- and (3*S*)-epimers of ceramide **4**, obtained after acidic hydrolysis (70 % acetic acid) of the acetal moiety in **15a** and 15**b**
27. D. P. Stamos, X. C. Sheng, S. S. Chen, Y. Kishi, *Tetrahedron Lett.* **38** (1997) 6355
28. For a description of the technique of dry-flash chromatography, see: a) L. M. Harwood, *Aldrichim. Acta* **18** (1985) 25; b) A. I. Vogel, A. R. Tatchell, B. S. Furnis, A. J. Hannaford, P. W. G. Smith, *Vogel's Textbook of Practical Organic Chemistry*, Longman Scientific & Technical, 5th ed., London, 1989, p. 220; c) An account which includes some improvements of the separation technique: D. S. Pedersen, C. Rosenbohm, *Synthesis* (2001) 2431
29. D. D. Perrin, W. L. F. Armarego, *Purification of Laboratory Chemicals*, 3rd ed., Pergamon Press, Oxford, 1988
30. N. Karasavvas, R. K. Erukulla, R. Bittman R. Lockshin, Z. Zakeri, *Eur. J. Biochem.* **236** (1996) 729
31. M. Moreno, C. Murruzzu, A. Riera, *Org. Lett.* **13** (2011) 5184.

Journal of the Serbian Chemical Society
JSCS@tmf.bg.ac.rs • www.shd.org.rs/JSCS
J. Serb. Chem. Soc. 79 (6) S58–S59 (2014) *Supplementary material*

SUPPLEMENTARY MATERIAL TO

Diastereoselective addition of alkenylchromium(III) reagents to Garner's aldehyde. The Nozaki–Hiyama–Kishi coupling approach to sphingosines and ceramides

ZORANA FERJANČIĆ[1]*, RADOMIR MATOVIĆ[2] and FILIP BIHELOVIĆ[1]**

[1]*Faculty of Chemistry, University of Belgrade, Studentski trg 16, P. O. Box 158, 11000 Belgrade, Serbia and* [2]*ICTM – Center for Chemistry, Njegoševa 12, 11000 Belgrade, Serbia*

J. Serb. Chem. Soc. 79 (6) (2014) 627–636

PHYSICAL AND SPECTRAL DATA FOR COMPOUNDS **10** AND **12**–**14**

*(S)-2,2-Dimethyl-3-octanoyloxazolidine-4-carboxaldehyde (**10**)*. Yield: 87 %; Colorless oil; IR (film, cm^{-1}): 3399, 2955, 2930, 1826, 1738, 1657, 1409, 1372, 1252, 1216, 1157, 1069; ^{1}H-NMR (500 MHz, DMSO-d_6, δ / ppm): 9.61 (1H, *s*), 4.81 (1H, *d*, *J* = 6.5 Hz), 4.32 (1H, *dd*, *J* = 1.0 and 10.0 Hz), 4.07 (1H, *dd*, *J* = 6.5 and 9.5 Hz), 2.21 (1H, *dt*, *J* = 7.5 and 16.0 Hz), 1.95 (1H, *dt*, *J* = 7.5 and 16.0 Hz), 1.48 (3H, *s*), 1.45 (3H, *s*), 1.45–1.41 (2H, *m*), 1.29–1.21 (8H, *m*), 0.86 (3H, *t*, *J* = 7.0 Hz); ^{13}C-NMR (125 MHz, DMSO-d_6, δ / ppm): 200. 04 (C), 169.94 (C), 95.41 (C), 65.54 (CH), 63.47 (CH_2), 35.02 (CH_2), 31.64 (CH_2), 28.99 (2×CH_2), 25.80 (CH_3), 24.68 (CH_2), 23.50 (CH_3), 22.51 (CH_2), 14.37 (CH_3); HRMS (ESI-TOF high acc) Calcd. for $C_{14}H_{26}NO_3$ (MH^+): 256.1907. Found: 256.1906. $[\alpha]_D^{20}$ (*c*=0.64, $CHCl_3$): –38.9.

*(S)-Methyl 3-hydroxy-2-octanamidopropanoate (**12**)*. Yield: 85 %; Colorless, viscous oil; IR (film, cm^{-1}): 3370, 2956, 2930, 2858, 1751, 1655, 1543, 1463, 1440, 1223, 1084; ^{1}H-NMR (500 MHz, $CDCl_3$, δ / ppm): 6.55 (1H, *d*, *J* = = 7.5 Hz), 4.67 (1H, *dt*, *J* = 4.0 and 7.5 Hz), 3.98–3.96 (1H, *m*), 3.91–3.88 (1H, *m*), 3.79 (3H, *s*), 3.13 (1H, *bs*), 2.26 (2H, *t*, *J* = 7.5 Hz), 1.67–1.61 (2H, *m*), 1.32––1.26 (8H, *m*), 0.88 (3H, *t*, *J* = 7.0 Hz); ^{13}C-NMR (125 MHz, $CDCl_3$, δ / ppm): 173.84 (C), 171.07 (C), 63.35 (CH_2), 54.58 (CH), 52.66 (CH_3), 36.44 (CH_2), 31.61 (CH_2), 29.13 (CH_2), 28.93 (CH_2), 25.51 (CH_2), 22.54 (CH_2), 13.99 (CH_3); HRMS (ESI-TOF high acc): Calcd. for $C_{12}H_{23}NO_4Na$ (MNa^+): 268.1519. Found: 268.1509; $[\alpha]_D^{20}$ (*c*=0.48, $CHCl_3$): +23.9.

*(S)-Methyl 2,2-dimethyl-3-octanoyloxazolidine-4-carboxylate (**13**)*. Yield: 69 %; Colorless oil; IR (film, cm^{-1}): 2956, 2931, 2857, 1755, 1650, 1461, 1411, 1368, 1256, 1210, 1079, 1056; ^{1}H-NMR (500 MHz, DMSO-d_6; 60 °C, δ / ppm):

*,** Corresponding authors. E-mail: (*)zferjan@chem.bg.ac.rs; (**)filip@chem.bg.ac.rs

4.77 (1H, *bt*, *J* = 4.0 Hz), 4.13 (2H, *m*), 3.73 (3H, *s*), 2.25 (1H, *dt*, *J* = 7.5 and 16.0 Hz), 2.00 (1H, *dt*, *J* = 7.0 and 15.5 Hz), 1.55 (3H, *s*), 1.49 (1H, *bt*, *J* = 6.5 Hz), 1.46 (3H, *s*), 1.30-1.25 (8H, *m*), 0.87 (3H, *t*, *J* = 7.0 Hz); ^{13}C-NMR (125 MHz, DMSO-d_6, δ / ppm): 171.01 (C), 169.15 (C), 94.89 (C), 66.20 (CH_2), 58.60 (CH), 55.12 (CH_3), 34.27 (CH_2), 30.80 (CH_2), 28.20 (CH_2), 28.12 (CH_2), 24.85 (CH_3), 23.79 (CH_2), 23.10 (CH_3), 21.66 (CH_2), 13.46 (CH_3); HRMS (ESI-TOF high acc) Calcd. for $C_{15}H_{28}NO_4$ (MH^+): 286.2013. Found: 286.2004; $[\alpha]_D^{20}$ (*c*=1.4, $CHCl_3$): –47.0.

*(*R*)-1-(4-(Hydroxymethyl)-2,2-dimethyloxazolidin-3-yl)-1-octanone* (***14***). Yield: 75 %; Colorless, viscous oil; IR (film, cm^{-1}): 3420, 2956, 2931, 2873, 1627, 1464, 1423, 1372, 1251, 1209, 1079, 1059; ^{1}H-NMR (500 MHz, DMSO-d_6, δ / ppm): 5.05 (1H, *dd*, *J* = 5.0 and 6.5 Hz), 3.92–3.84 (3H, *m*), 3.42–3.39 (1H, *m*), 3.32–3.27 (1H, *m*), 2.38–2.23 (1H, *m*), 2.29–2.23 (1H, *m*), 1.53–1.47 (2H, *m*), 1.47 (3H, *s*), 1.41 (3H, *s*), 1.30–1.21 (8H, *m*), 0.86 (3H, *t*, *J* = 7.0 Hz); ^{13}C-NMR (125 MHz, DMSO-d_6, δ / ppm): 169.31 (C), 93.81 (C), 64.87 (CH_2), 61.44 (CH_2), 58.50 (CH), 34.35 (CH_2), 31.22 (CH_2), 28.65 (CH_2), 28.60 (CH_2), 26.75 (CH_3), 24.71 (CH_2), 22.74 (CH_3), 22.07 (CH_2), 13.94 (CH_3); HRMS (ESI-TOF high acc) Calcd. for $C_{14}H_{28}NO_3$ (MH^+): 258.2064. Found: 258.2053; $[\alpha]_D^{20}$ (*c*=0.6, $CHCl_3$): –9.3.

Journal of the Serbian Chemical Society
JSCS-info@shd.org.rs • www.shd.org.rs/JSCS
J. Serb. Chem. Soc. 79 (6) 637–648 (2014)
JSCS–4614
UDC 547.585+547.855.1+547.233:548.7:543.42–74:547.415
Original scientific paper

Structural, spectral and thermal properties of 2-(2-pyridylamino)pyridinium trihydrogen pyromellitate

DEJAN POLETI[1*#], JELENA ROGAN[1#], LIDIJA RADOVANOVIĆ[2#] and MARKO RODIĆ[3#]

[1]*Department of General and Inorganic Chemistry, Faculty of Technology and Metallurgy, University of Belgrade, Karnegijeva 4, 11000 Belgrade, Serbia,* [2]*Innovation Center, Faculty of Technology and Metallurgy, University of Belgrade, Karnegijeva 4, 11000 Belgrade, Serbia and* [3]*Faculty of Sciences, University of Novi Sad, Trg Dositeja Obradovića 3, 21000 Novi Sad, Serbia*

(Received 7 June, revised 24 October, accepted 25 October 2013)

Abstract: The title compound, (Hdipya)(H_3pyr), where Hdipya is protonated 2,2′-dipyridilamine and H_3pyr is the monoanion of pyromellitic acid (H_4pyr), was obtained from a reaction mixture containing Zn(II) ions, dipya, Na_4pyr (in the mole ratio 2:2:1) and HNO_3. The products (micro- and single-crystalline) were characterized by X-ray structure determination, FT-IR spectroscopy and TG/DSC analysis. The most striking structural feature of (Hdipya)(H_3pyr) are short inter- and extremely short intramolecular hydrogen bonds. These bonds mutually connect cations and anions making thin layers parallel to the crystallographic (223) plane. In addition, quite unusual, linear proton-bound polymeric $\{H(H_2pyr)^-\}_n$ were identified in the structure. The results of crystal structure determination are compared with FT-IR and TG/DSC data. The low position of the ν_{as}(COO) vibration at 1660 cm^{-1} is in accordance with strong hydrogen bonding. This value could be used as a measure of the C=O bond order, which was calculated to be 1.81.

Keywords: pyromellitic acid; 2,2′-dipyridylamine; crystal structure; FT-IR spectra; TG/DSC analysis.

INTRODUCTION

Pyromellitic or 1,2,4,5-benzenetetracarboxylic acid (H_4pyr), one of 12 benzenepolycarboxylic acids, is used in the production of polyesters and polyamides. Anions of H_4pyr, in particular pyr^{4-}, are well-known as very prospective ligands in coordination chemistry due to the presence of eight O atoms as potential ligating sites that can coordinate up to ten metal centers.[1] The crystal structure of

* Corresponding author. E-mail: dejan@tmf.bg.ac.rs
# Serbian Chemical Society member.
doi: 10.2298/JSC130706115P

H_4pyr was published in 1971,[2] and earliest transition metal (TM) complexes with the tetra-anion of H_4pyr were published just after that.[3] The first structurally characterized complexes were described at the beginning of the 1990s.[4] Later, during structural studies of TM complexes, it was shown that the tetra-anion pyr^{4-} usually acts as a centrosymmetric bridging ligand and can build discrete,[5] chain,[6] layered,[7] or framework[8] structures. A survey of the Cambridge Structural Database, CSD,[9] showed that the partially deprotonated forms: $Hpyr^{3-}$, H_2pyr^{2-} and H_3pyr^- are, as a rule, not coordinated.

Binary and ternary TM complexes with anions of aromatic polycarboxylic acids have been studied for a long time.[10] In line with this subject, attempts were made to prepare mixed ligand Mn(II) and Zn(II) complexes with pyr^{4-} and 2,2′--dipyridylamine (dipya) as an *N*,*N*′ ligand. Surprisingly, the title compound containing only potential ligands was obtained instead. Such compounds can be classified into two major groups, as co-crystals (adducts) or organic salts (proton-transfer complexes),[11] but between them there are so-called "disordered solid forms",[12,13] where hydrogen atoms are not undoubtedly located or they are disordered. Although such compounds are much less frequent in comparison with single-component organics or the corresponding complexes, the number of studied examples permanently increases since their possible importance for pharmaceutical chemistry was recognized.[14,15] Even ferroelectric properties were found in some compounds.[16] Therefore, it seemed worthwhile to study the obtained compound in detail.

In the CSD[9] there is a very limited number of structurally characterized compounds concerning molecule of H_4pyr or its partially deprotonated ions. There are, however, several similar organic salts: (Hpy)(H_3pyr), where py is pyridine,[13] (NMe_4)(H_3pyr),[17] a series of H_2pyr^{2-} salts with different pyridinium derivatives,[18] (cytosinium)$_2$(H_2pyr)·H_2O,[19] and (Hbipy)$_2$(H_2pyr)(H_4pyr), where bipy is 2,2′-bipyridine, which was characterized structurally[20] and by FT-IR and NMR spectroscopy.[21]

On the other hand, dipya is well known as a chelating ligand. A search of the CSD revealed some 170 compounds containing dipya.[9] Most of them were TM complexes, and there were no examples of uncoordinated dipya in its neutral form. At the same time, there were only eight compounds containing protonated dipya, which can be present as monoprotonated 2-(2-pyridylamino)pyridinium, Hdipya, or diprotonated 2,2′-iminodipyridinium(2+), H_2dipya. Such protonated forms are not coordinated, and in five out of eight cases tetrahalidometalates, $[MX_4]^{2-}$ (M = Co, Cu or Hg; X = Cl or Br), were present as counter ions.[9]

Herein, crystal structure of the title compound, (Hdipya)(H_3pyr), together with its FT-IR spectral and thermal properties are described and correlated with each other.

EXPERIMENTAL

The starting reagents pyromellitic acid (> 95 %), 2,2′-dipyridylamine (98 %), Mn(II) nitrate solution, 45–50 % in dilute nitric acid (all Sigma–Aldrich) and $Zn(NO)_3 \cdot 6H_2O$ (*p.a.* Kemika, Zagreb) were used without any purifications.

Preparation of the microcrystalline product. Into 100 cm^3 of an aqueous solution containing 0.74 g (2.5 mmol) of $Zn(NO_3)_2 \cdot 6H_2O$, first 5 cm^3 of HNO_3 solution (c = 1 mol dm^{-3}), then 0.43 g of dipya (2.5 mmol) dissolved in 10 cm^3 of an EtOH/H_2O mixture (3:1 volume ratio) was added. The pH value of this mixture was 2. Then, 50 cm^3 of an aqueous solution of Na_4pyr (0.32 g; 1.25 mmol) was slowly added under stirring. The final pH value was 4. After standing for 24 h, the obtained precipitate was filtered and rinsed with H_2O, EtOH and Et_2O. Yield: 84.6 %; Anal. Calcd. for $C_{20}H_{15}N_3O_8$: C, 56.48; H, 3.55; N, 9.88 %. Found: C, 56.27, H, 3.62, N, 9.91 %; FT-IR (KBr, cm^{-1}): 3470 (*bw*), 3117 (*m*), 3097 (*m*), 3061 (*m*), 3024 (*m*), 2993 (*m*), 2920 (*w*), 1715 (*m*), 1660 (*s*), 1604 (*s*), 1562 (*s*), 1451 (*s*), 1311 (*w*), 1292 (*w*), 1270 (*w*), 1250 (*w*), 1170 (*m*), 1151 (*m*), 1005 (*m*), 955 (*m*), 901 (*m*), 771 (*s*), 748 (*s*), 594 (*m*), 559 (*w*), 532 (*m*). The compound was soluble in DMSO but insoluble in H_2O and EtOH.

A similar procedure using Mn(II) instead of Zn(II) ions resulted in a white microcrystalline powder in a comparable yield (78.9 %). As revealed by elemental analysis and FT-IR spectroscopy, this product was identical to the product obtained in the presence of Zn(II) ions.

Preparation of single-crystals. Into 50 cm^3 of an aqueous suspension containing 0.25 g (1 mmol) of H_4pyr was added 0.17 g of dipya (1 mmol) dissolved in 5 cm^3 of EtOH. Then, 50 cm^3 of an aqueous solution containing 0.30 g (1 mmol) of $Zn(NO_3)_2 \cdot 6H_2O$ was added dropwise under continuous stirring. The mixture was gently heated at 50 °C for 3 h, filtered to remove a small quantity of unreacted H_4pyr, and left standing under ambient conditions. The first crystals appeared after 24 h, but single-crystals of appropriate size were collected after 10 days.

Characterization. The FT-IR spectra were recorded on a Bomem MB-100 (Hartmann Braun) spectrophotometer (4000–600 cm^{-1} region) using KBr pellets. The thermal properties of the compound were examined from room temperature up to 380 °C using an SDT Q600 TGA/DSC instrument (TA Instruments) in a dry nitrogen atmosphere (flow rate: 100 cm^3 min^{-1}) at a heating rate of 20 °C min^{-1}. The sample mass was 8.14 mg.

Room temperature (22 °C) single-crystal X-ray diffraction data were collected on an Oxford Gemini S diffractometer equipped with CCD detector, using monochromatized Cu $K\alpha$ radiation (λ = 1.5418 Å). A multi-scan correction for absorption was applied. The structure was solved by direct methods (SIR97)[22] and refined on F^2 by full-matrix least-squares using the programs SHELXL97[23] and WinGX.[24] All non-hydrogen atoms were refined anisotropically. The positions of the C- and N2-bonded H atoms were calculated geometrically and refined by the riding model with U_{iso} = 1.2U(C,N). H atoms from OH groups were found in ΔF maps and refined with the U_{iso} = 1.5U(O) constraint. The Hdipya cation was disordered over a centre of symmetry with congener atoms having 0.5 site occupancies; the individual pyridyl groups were refined using the FLAT constraint with equal displacement parameters for the corresponding A and B atoms. Attempts to determine the H atom that protonates dipya were unsuccessful, very likely because this atom was spread over four positions (N1A, N1B and their centrosymmetric counterparts, see Fig. 1. Selected crystal data and refinement results are listed in Table I. CCDC 948070 contains supplementary crystallographic data for this paper. This data can be obtained free of charge at http://www.ccdc.cam.ac.uk/cgi-bin/catreq.cgi.

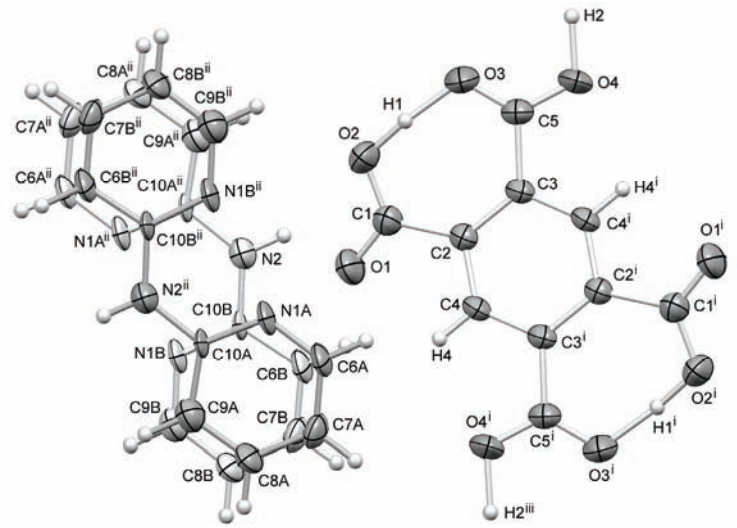

Fig. 1. Molecular structure of (Hdipya)(H_3pyr) with atomic numbering scheme. Displacement ellipsoids are drawn at the 50 % probability level. Disordered Hdipya ions are marked by different shades of gray. Symmetry codes: (*i*) 1 – *x*, 1 – *y*, 1 – *z*; (*ii*) 1 – *x*, 1 – *y*, –*z*; (*iii*) 1 + *x*, 1 + *y*, –*z*.

TABLE I. Crystal data and structure refinement for (Hdipya)(H_3pyr)

Empirical formula	$C_{20}H_{15}N_3O_8$
M / g mol^{-1}	425.35
Crystal system	Triclinic
Space group	$P\bar{1}$
a, b, c / Å	3.8268(2), 9.2726(6), 13.3494(8)
α, β, γ / °	74.761(6), 81.845(5), 82.935(6)
V / Å^3	450.59(5)
Z	1
ρ_c / g cm^{-3}	1.568
μ / mm^{-1}	1.056
F(000)	220
Crystal dimensions, mm	0.09×0.10×0.31
θ_{max} / °	72.12
Range of h, k, l	$-4 \le h \le 3$, $-11 \le k \le 11$, $-16 \le l \le 16$
Reflections collected	7605
Independent reflections	1770 (R_{int} = 0.0361)
Completeness, %	99.6
Data/restraints/parameters	1770/6/169
$(\Delta/\sigma)_{max}$	0.001
S	1.116
R indices ($I > 2\sigma(I)$)	R_1 = 0.0533, wR_2 = 0.1282
R indices (all data)	R_1 = 0.0631, wR_2 = 0.1341
$\Delta\rho_{max}$, $\Delta\rho_{min}$ (both in e Å^{-3})	0.150, –0.205

RESULTS AND DISCUSSION

Synthesis

As described in the Experimental, the title compound was obtained during attempts to synthesize ternary Zn(II)–dipya-pyr complexes or their Mn(II) analogues. This demonstrates the difficulties in the preparation of such complexes, in spite of being known.[9] A similar experience was already published by Ha,[25] when $(Hdipya)_2[MnCl_4]$ was obtained instead of the expected Mn(II)–dipya complex, and it was not reported previously for Zn(II) complexes. Such behavior can be partly explained by an increase on the thermodynamic stability of the protonated dipya in respect to the neutral molecule,[26] but since dipya complexes of many TMs are known, the specific role of Zn(II)/Mn(II) ions and the pH of the reaction mixture should not be neglected.

Crystal structure

In the structure of $(Hdipya)(H_3pyr)$, both the Hdipya and H_3pyr ions are positioned around the symmetry centre, and only half of each species belongs to the asymmetric unit (Fig. 1). Besides, Hdipya is disordered over a centre of symmetry with equal allocation of both entities. A comparable disorder was found in some organostannates,[26] and in the analogous (Hdipya)(Hpht), where Hpht is the hydrogen phthalate ion.[27] One of pyridyl N atoms has to be protonated, but it was not possible to locate the corresponding H atom. Both N atoms from the pyridyl rings could be protonated because N1A···O1 and N1B···O1 distances are 3.018(7) and 3.121(5) Å, respectively, *i.e.*, they could form hydrogen bonds. Therefore, the H atom is very likely spread over four possible positions.

The whole Hdipya is practically perfectly planar with a negligible dihedral angle between the mean-planes of the two pyridyl rings. In three known dipya polymorphs and five crystallographically different dipya molecules, this angle varied between about 4 and 40°.[28] A very similar variety of angles was also found in some TMs–dipya complexes.[10] The planarity of Hdipya might be explained by symmetry constraints or by extended delocalization of the π electrons. However, the influence of intramolecular (intra-H) and intermolecular (inter-H) hydrogen bonds could also be important. According to Haddad *et al.*,[29] weak intra-H bonding is also possible between the protonated and unprotonated N atom from adjacent pyridyl rings (Fig. 1, atoms N1A and N1B). As usual, pyridyl rings are less regular than benzene rings.

At first sight, the H_3pyr ion (Fig. 1) is fully protonated, *i.e.*, it should be described as a neutral H_4pyr molecule, not as a monoanion. However, the H2 atom is in special position (site symmetry: $\bar{1}$) and with a 0.5 site occupancy factor. The geometry data for the H_3pyr anion are listed in Table II. While the C–C bond distances are as expected, the angles, in particular C1–C2–C3 and C2–C3–C5, strongly deviate from the values found in $H_4pyr{\cdot}2H_2O$ (max. 121.7°).[30] This is the consequence of the stress caused by the presence of the

intra-H bond O2–H1···O3 and the formation of seven-membered, S(7), pseudo--rings. In respect to the aromatic ring, the C–COO groups are inclined in the opposite sides, with the corresponding angles of 13.3° for the C2C1O1O2 group and 73.6° for the C3C5O3O4 group. This intra-H bond is extremely short and clearly asymmetrical (Table III, Fig. 1). Very similar geometries were already found in H_2pyr and H_3pyr anions.[13,18–20] and in some Hpht complexes.[31,32]

TABLE II. Bond distances and angles in H_3pyr ion (For O–H bond distances, see Table III)

Bond distance, Å			
O1–C1	1.202(4)	O2–C1	1.297(3)
O3–C5	1.225(3)	O4–C5	1.251(3)
C1–C2	1.527(3)	C2–C3	1.406(3)
C2–C4	1.391(3)	C3–C4	1.391(3)
C3–C5	1.513(3)		
Bond angle, °			
O1–C1–O2	121.2(3)	O1–C1–C2	118.9(2)
O2–C1–C2	119.9(2)	C1–C2–C3	129.2(2)
C1–C2–C4	113.0(2)	C3–C2–C4	117.8(2)
C2–C3–C4	118.0(2)	C2–C3–C5	126.8(2)
C4–C3–C5	115.2(2)	C2–C4–C3	124.2(2)
C2–C4–H4	117.9(2)	C3–C4–H4	117.9(2)
O3–C5–O4	122.2(3)	O3–C5–C3	121.9(2)
O4–C5–C3	115.8(2)		

TABLE III. Geometry of hydrogen bonds in (Hdipya)(H_3pyr); Symmetry codes: (iv) $-x, -y + 2, -z + 1$; (v) $x - 1, y, z$

D–H···A	*d*(D–H) / Å	*d*(H···A) / Å	Angle (DHA) / °	*d*(D···A) / Å
O2–H1···O3	1.11(4)	1.34(4)	167(3)	2.435(3)
O4–H2···O4^{iv}	1.24[a]	1.24[a]	180[a]	2.477(2)
N2–H2A···O1^{v}	0.86	1.87	165	2.706(4)

[a]Atom H2 is in a special position and its coordinates were fixed during refinement

Another, inter-H bond O4–H2···O4^{iv} ((iv) $-x, -y + 2, -z + 1$) is symmetrical and also very short, but a little longer than the intra-H bond (Table III). In comparison to typical O···O distances found in related Hpht compounds,[27] the intra-H bond is slightly longer, whereas inter-H bond is shorter than expected. This shows how strong the inter-H bond is in this case. Being that the inter-H bond is symmetrical, H_3pyr could also be viewed as a polymeric proton-bound trihydrogen pyromellitate anion, $\{H(H_2pyr)^-\}_n$ (Fig. 2). Again, there is great similarity with Hpht compounds, in which proton-bound anions are also found.[33–35] The main difference is that $\{H(H_2pyr)^-\}_n$ is polymeric, while $[H(Hpht)_2]^-$ ions are only dimeric. This is because H_4pyr could be considered as developed from H_2pht by mirroring two COOH groups in the *ortho*-position to another pair of COOH groups. Thus, only H_3pyr^- and H_2pyr^{2-} can make polymeric proton-bound anions,

while $Hpht^-$ is restricted to dimeric forms.[36] To the best of our knowledge, a similar polyanion was found only in $(NMe_4)(H_3pyr)$, described by Rodriguez-Cuamatzi *et al.*[17] However, those chains were of a zig–zag type, while here the presented chains are linear (Fig. 2) and so could be regarded as unprecedented.

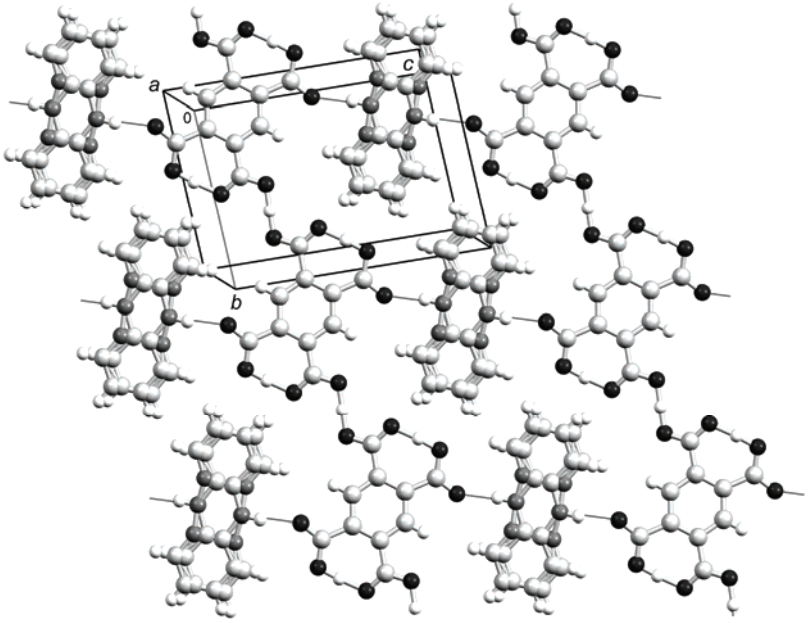

Fig. 2. Motif of hydrogen bonds (thin dark lines) in the (223) crystallographic plane. Color codes for atoms: H – white, C – light gray, N – dark gray and O – black.

In the structure, there is another hydrogen bond between the amine N2 atom and O1 (Fig. 1, Table III). Since all hydrogen bonds are concentrated in one plane, thin layers approximately parallel to the crystallographic (223) plane are formed (Fig. 2). The $\{H(H_2pyr)^-\}_n$ and Hdipya ions are assembled in alternating rows making a non-rectangular grid. The layers are stacked together by short parallel--displaced π–π interactions. For example, all distances between the plane of one benzene ring and benzene C atoms from the nearest layer are 3.490(5) Å. Analogous layers also exist in $(cytosinium)_2(H_2pyr)\cdot H_2O$,[19] and in $(NMe_4)(H_3pyr)$.[17]

Spectral and thermal properties

A sequence of weak and sometimes broad IR bands between 3500 and 3200 cm^{-1} is indicative for numerous hydrogen bonds. According to the literature,[21] even weak and very broad bands centered at 2900, 2430 and 1900 cm^{-1} could also be ascribed to strong hydrogen bonding. In some cases, they could be extremely strong and broad.[37] Bands between about 3120 and 2990 cm^{-1} are characteristic for stretching N–H and C–H vibrations in secondary amines and aromatic rings.

It seems that the stretching N–H band was shifted from 3244 cm^{-1} in dipya to 3117 or 3097 cm^{-1} in (Hdipya)(H_3pyr), suggesting stronger hydrogen bonding.

In the "fingerprint" region, there are bands of different origin typical for substituted benzene rings and secondary amines; they agree with the bands in the individual components. Especially characteristic for dipya is a prominent doublet due to N–H out of plane bending at 771 and 748 cm^{-1}. Both vibrations were slightly shifted with respect to pure dipya (768 and 735 cm^{-1}) and very likely overlap with the corresponding C–H vibrations.[38]

The most interesting part of the FT-IR spectrum is the 1720–1250 cm^{-1} region (Fig. 3), where many strong bands are expected: asymmetrical and symmetrical stretching vibrations of COOH and the corresponding COO groups, C–C and C–N stretching vibrations of aromatic rings and N–H bending in a secondary aromatic amine.[39] (Asymmetrical ν_{as}(COOH) vibrations, characteristic for organic acids, are often labelled ν(C=O) and called carbonyl, due to the presence of double C=O bond). Consistent to the literature,[37] ν_{as}(COOH) and ν_s(COOH) frequencies for H_4pyr are at 1710 and 1266 (as doublet at 1278 and 1255) cm^{-1}, respectively, and the present experimental data agree within ±5 cm^{-1} with these values. These bands are broad and usually the most intense in the spectrum.[38] Surprisingly, the corresponding bands in the FT-IR spectrum of (Hdipya)(H_3pyr) are medium to weak, but one additional very prominent band at 1660 cm^{-1} appeared. At first sight, this band could be attributed to the secondary amine N–H bending group frequency, which is located at 1604 cm^{-1} in dipya. However, such high wavenumbers are observed only in the case of coordinated dipya and the band is typically very sharp.[10] Therefore, the band at 1660 cm^{-1} should be ascribed to the ν_{as}(COOH) or carbonyl C=O vibrations. Such a low position of ν_{as}(COOH) is not expected,[38] and, together with no unambiguous identification of ν_s(COOH) vibrations, has to be correlated to the extremely short and strong hydrogen bonds involving all O atoms from H_3pyr. In (Hbipy)$_2$(H_2pyr)(H_4pyr),[20,21] just the opposite behavior was observed, ν_{as}(COOH) is shifted to the higher wavenumbers (1726 cm^{-1}), which was explained by the absence of hydrogen bonds.

In the tetrathiafulvalene–*p*-chloranil (TTF–CA) complex, which is a widely studied charge-transfer organic compound,[40] the position of C=O vibrations was used to determine the degree of charge transfer from TTF to CA. In other words, ν_{as}(COOH)/ν(C=O) could be related to the C=O bond order. For H_4pyr ν_{as}(COOH) was at 1710 cm^{-1},[39] and this corresponds to a bond order of 2. In alkali metal salts, the COOH groups are ionized and, due to delocalization of the electrons in COO groups, the bond order should be 1.5. The available data for the two alkali metal salts K_4pyr[39] and Na_4pyr (this study) give an identical value, 1580 cm^{-1} for ν_{as}(COO). From these values, it is easy to calculate the C=O bond order in (Hdipya)(H_3pyr), which was 1.81. By analogy to the "degree of charge transfer" this quantity could be used to measure the "degree of proton transfer",[41] and should be correlated to the geometry of hydrogen bonding in (Hdipya)(H_3pyr).

However, the observed geometry of H_3pyr ions (Table II) does not enable a simple explanation of the calculated value. For O1–C1 and O2–C1 pair, bond distances can be judged as normal when compared to the H_4pyr and common COOH values.[2] Nevertheless, O3–C5 bond is longer than expected and O4–C5 bond distance corresponds to the typical values found in ionized COO groups.[9] This could be a possible cause for the low value of ν_{as}(COOH), although an extensive coupling of vibrational modes should also be kept in mind.

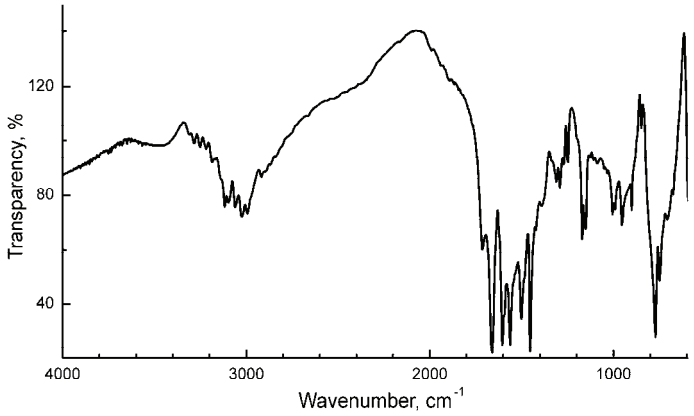

Fig. 3. FT-IR spectrum (KBr pellets) of (Hdipya)(H_3pyr).

As shown in Fig. 4, the decomposition of (Hdipya)(H_3pyr) began at 237 °C (onset temperature) and ended at about 325 °C with a total mass loss. No melting

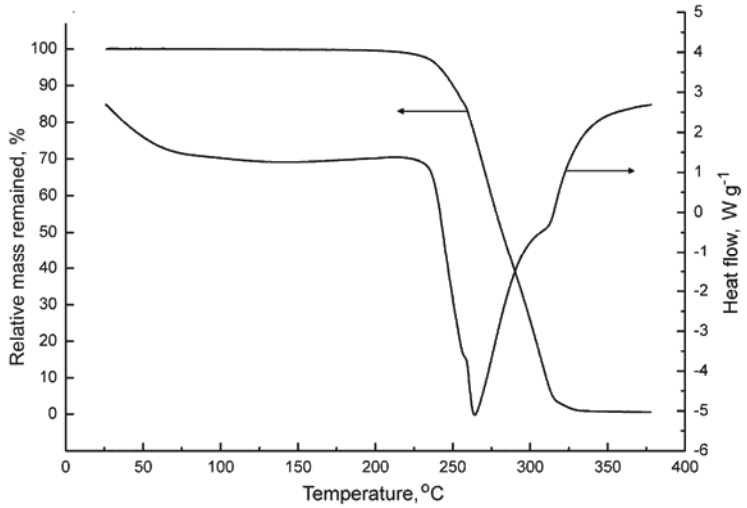

Fig. 4. TG/DSC curves of (Hdipya)(H_3pyr) under a dynamic N_2 atmosphere at a heating rate of 20 °C min^{-1} (exotherm up).

was observed and the decomposition started around the boiling point of dipya (222 °C), suggesting that this molecule escaped first. Although the TG curve decreased rapidly, the shape of the DSC curve indicated that the disintegration occurred in at least three, probably four, highly overlapped steps, which could not be resolved. The total molar decomposition enthalpy was relatively high, $\Delta_{dec}H_m^o = 461.2$ kJ mol^{-1}. In comparison to TM complexes with dipya and some polycarboxylate ligands,[10] the initial decomposition temperature of (Hdipya)(H_3pyr) was lower, very likely owing to the absence of coordinative bonds. In analogous systems (py)$_2$(H_2tpht), where H_2tpht is terephthalic acid, and (py)$_3$(H_3tms), where H_3tms is trimesic acid, the total degradation was found to be at 339 and 366 °C, respectively.[13] There, however, loss of py molecules started just above room temperature, although the boiling point of py is 115 °C.

CONCLUSIONS

A new organic salt (Hdipya)(H_3pyr) was prepared unpredictably during efforts to obtain ternary Zn(II) or Mn(II) complexes with dipya and pyr ligands. Besides the higher stability of Hdipya with respect to dipya,[26] the presence of Zn^{2+} or Mn^{2+} ions, as well as a starting mixture pH value of 4 most likely affected the reaction mechanism and the formation of (Hdipya)(H_3pyr). The compound consisted of disordered Hdipya cations and H_3pyr anions connected by hydrogen bonds. There were short inter- and extremely short intra-H bonds. In this way, thin layers parallel to the (223) plane were formed. Due to the very strong and symmetrical inter-H bond, the H_3pyr anions could furthermore be regarded as polymeric $\{H(H_2pyr)^-\}_n$ anions. The position and shape of the characteristic bands revealed by FT-IR spectroscopy undoubtedly confirmed the structural findings in (Hdipya)(H_3pyr), and the value of ν_{as}(COO) vibration was used for measuring the “degree of proton transfer”, which was calculated to be 1.81. The TG/DSC analysis proved that (Hdipya)(H_3pyr) decomposed in several overlapping steps and a total molar decomposition enthalpy of 461.2 kJ mol^{-1} was calculated.

SUPPORTING INFORMATION

Crystallographic data can be obtained free of charge at http://www.ccdc.cam.ac.uk/cgi--bin/catreq.cgi.

Acknowledgement. This study was financially supported by the Ministry of Education, Science and Technological Development of the Republic of Serbia (Grant No. 45007).

И З В О Д

СТРУКТУРНА, СПЕКТРАЛНА И ТЕРМИЧКА СВОЈСТВА 2-(2-ПИРИДИЛАМИНО)ПИРИДИНИЈУМ-ТРИХИДРОГЕНПИРОМЕЛИТАТА

ДЕЈАН ПОЛЕТИ[1], ЈЕЛЕНА РОГАН[1], ЛИДИЈА РАДОВАНОВИЋ[2] и МАРКО РОДИЋ[3]

[1]Катедра за општу и неорганску хемију, Технолошко–металуршки факултет,Универзитет у Београду, Карнегијева 4, 11000 Београд, [2]Иновациони центар Технолошко–металуршког факултета, Универзитет у Београду, Карнегијева 4, 11000 Београд и [3]Природно–математички факултет, Универзитет у Новом Саду, Трг Доситеја Обрадовића 3, 21000 Нови Сад

Описано једињење, (Hdipya)(H_3пуг), где је Hdipya протоновани 2,2′-дипиридиламин, а H_3пуг моноанјон пиромелитне киселине (H_4пуг), добијено је из реакционе смеше која је садржала Zn(II) јоне, dipya, Na_4пуг (молски однос 2:2:1) и HNO_3. Производи (микро- и монокристални) окарактерисани су рендгенском структурном анализом, FT-IR спектроскопијом и TG/DSC анализом. Врло необично структурно својство (Hdipya)(H_3пуг) јесте присуство кратких интер- и екстремно кратких интрамолекулских водоничних веза, које међусобно повезују катјоне и анјоне градећи танке слојеве паралелне кристалографској равни (223). Такође, у структури су нађени до сада веома ретки, линеарни полимерни анјони $\{H(H_2пуг)^-\}_n$ настали повезивањем преко протона. Резултати рендгенске структурне анализе упоређени су са подацима добијеним FT-IR спектроскопијом и TG/DSC анализом. Ниска фреквенција ν_{as}(COO) вибрације на 1660 cm^{-1} у сагласности је са постојањем јаких водоничних веза. Ова вредност искоришћена је за одређивање реда C=O везе (“степена преноса протона”) и израчунато је да он износи 1,81.

(Примљено 7. јуна, ревидирано 24. октобра, прихваћено 25. октобра 2013)

REFERENCES

1. Y.-G. Li, N. Hao, E.-B. Wang, Y. Lu, Ch.-W. Hu, L. Xu, *Eur. J. Inorg. Chem.* (2003) 2567
2. F. Takusagawa, K. Hirotsu, A. Shimada, *Bull. Chem. Soc. Jpn.* **44** (1971) 1274
3. a) T. Ota, H. Imai, *Technol. Rep. Kansai Univ.* **13** (1972) 25; b) T. Ota, H. Imai, *Technol. Rep. Kansai Univ.* **15** (1974) 61
4. a) B. T. Usubaliev, A. N. Shnulin, H. S. Mamedov, *Koord. Khim.* **8** (1982) 1532; b) D. L. Ward, D. C. Luehrs, *Acta Crystallogr., Sect. C: Cryst. Struct. Commun.* **39** (1983) 1370
5. a) D. Poleti, B. Prelesnik, R. Herak, Đ. Stojaković, *Acta Crystallogr., C* **44** (1988) 242; b) A. M. Atria, G. Corsini, L. Gonzalez, M. T. Garland, R. Baggio, *Acta Crystallogr., C* **65** (2009) m250
6. a) D. Poleti, Lj. Karanović, *Acta Crystallogr., C* **45** (1989) 1716; b) A. Majumder, V. Gramlich, G. M. Rosair, S. R. Batten, J. D. Masuda, M. S. El Fallah, J. Ribas, J.-P. Sutter, C. Desplanches, S. Mitra, *Cryst. Growth Des.* **6** (2006) 2355
7. a) J. C. Geng, L. W. Liu, S. L. Xiao, G. H. Cui, *Transition Met. Chem.* **38** (2013) 143; b) X.-Y. Yu, J. Lu, J.-H. Yu, X. Zhang, J.-Q. Xu, T.-G. Wang, *Z. Anorg. Allg. Chem.* **633** (2007) 490
8. a) Sh.-Y. Yang, L.-Sh. Long, R.-B. Huang, L. S. Zheng, S. W. Ng, *Acta Crystallogr., E* **59** (2003); m731; b) Sh.-Y. Yang, L.-Sh. Long, R.-B. Huang, L. S. Zheng, S. W. Ng, *Acta Crystallogr., E* **59** (2003) m921; c) D. Poleti, Lj. Karanović, *J. Serb. Chem. Soc.* **70** (2005) 1441
9. F. R. Allen, *Acta Crystallogr., Sect. B: Struct. Sci.* **58** (2002) 380

10. a) J. Rogan, D. Poleti, *Thermochim. Acta* **413** (2004) 227; b) J. Rogan, D. Poleti, Lj. Karanović, *Z. Anorg. Allg. Chem.* **632** (2006) 133; c) J. Rogan, D. Poleti, Lj. Karanović, Z. Jagličić, *J. Mol. Struct.* **985** (2011) 371
11. A. D. Bond, *CrystEngComm* **9** (2007) 833
12. S. Mohamed, D. A. Tocher, M. Vickers, P. G. Karamertzanis, S. L. Price, *Cryst. Growth Des.* **9** (2009) 2881
13. S. H. Dale, M. Elsegood, M. Hemmings, A. L. Wilkinson, *CrystEngComm* **6** (2004) 207
14. P. Vishweshwar, J. A. McMahon, J. A. Bis, M. J. Zaworotko, *J. Pharm. Sci.* **95** (2006) 499
15. A. Lemmerer, J. Bernstein, V. Kahlenberg, *J. Chem. Crystallogr.* **41** (2011) 991
16. S. Horiuchi, Y. Tokura, *Nat. Mater.* **7** (2008) 357
17. P. Rodriguez-Cuamatzi, O. I. Arillo-Flores, M. I. Bernal-Uruchurtu, H. Hopfl, *Supramol. Chem.* **19** (2007) 559
18. K. Biradha, M. J. Zaworotko, *Cryst. Eng.* **1** (1998) 67
19. R. Thomas, G. U. Kulkarni, *J. Mol. Struct.* **873** (2008) 160
20. D. Mrvoš-Sermek, Z. Popović, D. Matković-Čalogović, *Acta Crystallogr., C* **52** (1996) 2538
21. P. Novak, S. Sekušak, D. Vikić-Topić, Z. Popović, *J. Chem. Soc., Faraday Trans.* **94** (1998) 1051
22. A. Altomare, M. C. Burla, M. Camalli, G. L. Cascarano, C. Giacovazzo, A. Guagliardi, A. G. G. Moliterni, G. Polidori, R. Spagna, *J. Appl. Crystallogr.* **32** (1999) 115
23. G. M. Sheldrick, *Acta Crystallogr., Sect. A: Found. Crystallogr.* **64** (2008) 112
24. L. J. Farrugia, *J. Appl. Crystallogr.* **32** (1999) 837
25. K. Ha, *Z. Kristallogr. New Cryst. Struct.* **225** (2010) 653
26. S. W. Ng, *Acta Crystallogr., Sect. C: Cryst. Struct. Commun.* (1999) IUC9900098
27. A. Langkilde, D. Madsen, S. Larsen, *Acta Crystallogr., B* **60** (2004) 502
28. a) J. E. Johnson, R. A. Jacobson, *Acta Crystallogr., B* (1973) 1669; b) G. J. Pyrka, A. A. Pinkerton, *Acta Crystallogr., C* **48** (1992) 91; c) H. Schodel, C. Nather, H. Bock, F. Butenschon, *Acta Crystallogr., B* **52** (1996) 842
29. S. F. Haddad, B. F. Ali, R. H. Al-Far, *Polyhedron* **30** (2011) 1061
30. S. H. Dale, M. R. J. Elsegood, *Acta Crystallogr., E* **59** (2003) o1087
31. H. Küppers, *Z. Kristallogr.* **192** (1990) 97
32. X. Wang, Ch. Qin, E. Wang, L. Xu, *J. Mol. Struct.* **737** (2005) 49
33. J. B. Benedict, T. Bullard, W. Kaminsky, B. Kahr, *Acta Crystallogr., C* **60** (2004) m551
34. H. Küppers, *Z. Kristallogr.* **146** (1977) 269
35. a) S. G. Baca, Y. Simonov, M. Gdaniec, N. Gerbeleu, I. G. Filippova, G. A. Timco, *Inorg. Chem. Commun.* **6** (2003) 685; b) S. G. Baca, I. G. Filippova, C. Ambrus, M. Gdaniec, Y. A. Simonov, N. Gerbeleu, O. A. Gherco, S. Decurtins, *Eur. J. Inorg. Chem.* (2005) 3118
36. D. Poleti, J. Rogan, *Acta Crystallogr., C* **69** (2013) 841
37. D. C. Luehrs, B. C. Cornilsen, C. B. Lover, T. L. Niels, *Inorg. Chim. Acta* **145** (1988) 81
38. E. Castellucci, L. Angeloni, N. Neto, G. Sbrana, *Chem. Phys.* **43** (1979) 365
39. J. Coates, in: *Encyclopedia of Analytical Chemistry*, R. A. Meyers, Ed., Wiley, Chichester, 2000, p. 10815
40. a) A. Girlando, R. Bozio, C. Pecile, J. B. Torrance, *Phys. Rev. B* **26** (1982) 2306; b) P. García, S. Dahaoui, C. Katan, M. Souhassoua, C. Lecomte, *Faraday Discuss.* **135** (2007) 217; c) A. Nagahori, N. Kubota, C. Itoha, *Eur. Phys. J., B* **86** (2013) 109
41. S. L. Johnson, K. A. Rumon, *J. Phys. Chem.* **69** (1965) 74.

Journal of the Serbian Chemical Society
JSCS-info@shd.org.rs • www.shd.org.rs/JSCS
J. Serb. Chem. Soc. *79* (6) 649–658 (2014)
JSCS–4615
UDC 547.415.1+547.313.2+547.26'11+542.913:615.277
Original scientific paper

Synthesis and high *in vitro* cytotoxicity of some (*S*,*S*)-ethylenediamine-*N*,*N*'-di-2-propanoate dihydrochloride esters

NEBOJŠA PANTELIĆ[1], BOJANA B. ZMEJKOVSKI[2], TATJANA P. STANOJKOVIĆ[3], VERICA V. JEVTIĆ[4], GORDANA P. RADIĆ[4], SREĆKO R. TRIFUNOVIĆ[4#], GORAN N. KALUĐEROVIĆ[5*] and TIBOR J. SABO[6**#]

[1]*Faculty of Agriculture, University of Belgrade, Nemanjina 6, 11080 Belgrade-Zemun, Serbia,* [2]*Department of Chemistry, Institute of Chemistry, Technology and Metallurgy, University of Belgrade, Njegoševa 12, 11000 Belgrade, Serbia,* [3]*Institute of Oncology and Radiology, 11000 Belgrade, Serbia;* [4]*Institute of Chemistry, Faculty of Science, University of Kragujevac, R. Domanovića 12, 34000 Kragujevac, Serbia,* [5]*Department of Bioorganic Chemistry, Leibniz Institute of Plant Biochemistry, Weinberg 3, D-06120 Halle (Saale), Germany and* [6]*Faculty of Chemistry, University of Belgrade, P. O. Box 158, 11001 Belgrade, Serbia*

(Received 5 December 2013, revised 13 March, accepted 17 March 2014)

Abstract. A novel (*S*,*S*)-R_2eddip ester, *O*,*O*′-diisopentyl-(*S*,*S*)-ethylenediamine--*N*,*N*′-di-2-propanoate dihydrochloride (**1**) was synthesized and characterized by IR, ^{1}H- and ^{13}C-NMR spectroscopy, mass spectroscopy and elemental analysis. *In vitro* antitumor action of **1**, and two more R_2eddip esters, dialkyl (*S*,*S*)-ethylenediamine-*N*,*N*′-di-2-propanoate dihydrochlorides, obtained before (alkyl = *n*-Bu or *n*-Pe, **2** and **3**, respectively), was determined against cervix adenocarcinoma (HeLa), human melanoma (Fem-x), human chronic myelogenous leukemia (K562) cells, and a non-cancerous cell line human embryonic lung fibroblast (MRC-5), using the microculture tetrazolium test MTT assay. Esters **1**–**3** showed higher cytotoxicity and better selectivity in comparison to cisplatin, used as reference compound. The highest activity was expressed by **1**, with IC_{50}(Fem-x) value of 1.51±0.09 μM.

Keywords: R_2edda-type esters; characterization; cytotoxicity; selectivity.

INTRODUCTION

Cancer is one of the most widespread and feared diseases in the world because it is very difficult to cure as cancer cells are not foreign to the body but are simply subtly mutated forms of normal human cells that multiply without control.[1–3]

Corresponding authors. E-mail: (*)goran.kaluderovic@ipb-halle.de; (**)tsabo@chem.bg.ac.rs
[#] Serbian Chemical Society member.
doi: 10.2298/JSC130512022P

The majority of drugs used for the treatment of cancer today are cytotoxic (cell-killing) drugs that work by interfering in some way with the operation of the cell's DNA.

Over the last fifty years, about 500,000 natural and synthetic chemical compounds have been tested for their anticancer activity, but only about 25 of these are in wide use today.[4] A major challenge is to design new drugs that will be more selective for cancer cells, and thus have fewer side effects.

Cisplatin showed potent antitumor activity in the 70's and nowadays it is routinely used in the treatment of many types of cancers.[5–9] Unfortunately, it also causes severe side-effects, such as nephro-, oto- and neuro-toxicity.[10,11] Many platinum complexes were synthesized with hope for better pharmacological properties.[12–14] Besides cisplatin, only carboplatin and oxaliplatin are in worldwide clinical use.[15]

During the last decade, our research group has been engaged in the synthesis, characterization and investigation of the antitumor activity of platinum(II) and platinum(IV) complexes with *N*,*N*′ bidentate ligands, R_2edda-type esters.[16–26] These ligands, obtained by structural variations of the aminocarboxylato arms and alkyl groups of the ester moiety (normal, branched chains, rings), yielded a large library of such molecules (Fig. 1). In most cases, high cytotoxic action was accomplished when coordinating to platinum ions, but some of the esters, in fact, showed serious activity themselves.[27,28]

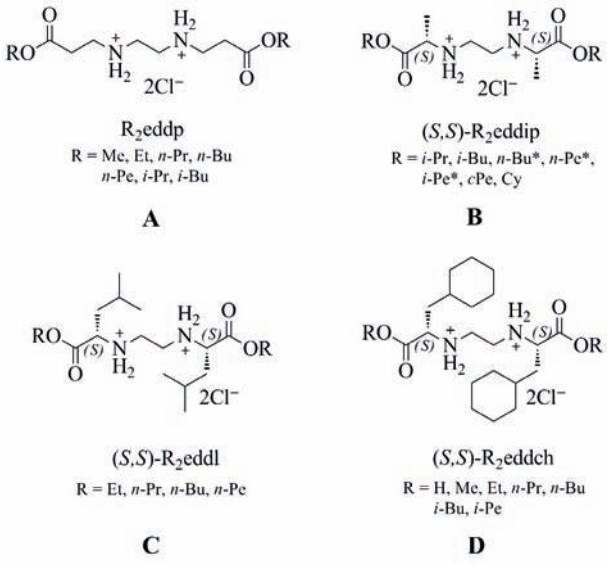

Fig. 1. R_2edda-type esters (* – esters investigated in this work).

These compounds (R_2edda-type esters, R = alkyl; eddp = ethylenediamne-*N*,*N*′-di-3-propanoate, Fig. 1, A; (*S*,*S*)-eddip = (*S*,*S*)-ethylenediamne-*N*,*N*′-di-2--propanoate, Fig. 1, B; (*S*,*S*)-eddl = (*S*,*S*)-*N*,*N*′-1,2-ethanediylbisleucinate, Fig. 1, C; (*S*,*S*)-eddch = (*S*,*S*)-α,α'-(1,2-ethanediyldiimino)biscyclohexanepropanoate, Fig. 1, D) were tested against various cancer lines and normal cells and moderate or low activity was found,[20,21,23,24,29,30] except for (*S*,*S*)-Et_2eddch that had the lowest IC_{50} values *ca*. 11 μM against HL-60, U251, C6, L929 and B16 cell lines.[27,28]

Herein, the synthesis, characterization and antiproliferative activity of one novel R_2edda-type ester: diisopentyl (*S*,*S*)-ethylenediamine-*N*,*N*′-di-2-propanoate dihydrochloride (**1**) is reported. This newly synthesized compound, along with already reported[22] di(*n*-butyl) (*S*,*S*)-ethylenediamine-*N*,*N*′-di-2-propanoate dihydrochloride (**2**) and di(*n*-pentyl) (*S*,*S*)-ethylenediamine-*N*,*N*′-di-2-propanoate dihydrochloride (**3**), were tested against cervix adenocarcinoma cell line (HeLa), human melanoma (Fem-x), human chronic myelogenous leukemia (K562) cells, and a non-cancerous cells MRC-5 (human embryonic lung fibroblast), with the aim of assessing their cytotoxic actions.

EXPERIMENTAL

Material and methods

All reagents were of analytical grade. (*S*,*S*)-Ethylenediamine-*N*,*N*′-di-2-propanoic acid hydrochloride, (*S*,*S*)-H_2eddip·HCl, was prepared by a standard procedure.[31]

Elemental analyses were realized on an Elemental Vario EL III microanalyzer. The infrared spectra were recorded using a Nicolet 6700 FT-IR spectrophotometer (Thermo Scientific), ATR technique (smart accessory orbit with diamond crystal) in the range of 4000–400 cm^{-1}. The NMR spectra were recorded on Varian Gemini 200 and Bruker Avance III 500 spectrometers. The chemical shifts for the ^{1}H- and ^{13}C-NMR spectra were referenced to residual ^{1}H and ^{13}C present in DMSO-d_6. The mass spectra were recorded with a 6210 Time-of-Flight LC–MS instrument (G1969A, Agilent Technologies). An Agilent Technologies 1200 series HPLC instrument (Agilent Technologies, Waldbronn, Germany) equipped with auto sampler, binary pump, DAD detector and ZDV cell, was used for the introduction of the sample dissolved in methanol into the mass spectrometer. As the mobile phase 0.2 % formic acid in water/acetonitrile (*V*/*V* = 50/50) at a flow of 0.15 mL min^{-1} was used. The mass spectra were recorded in the positive mode under the following conditions: capillary voltage 2500 V, gas temperature 250 °C, drying gas flow 7 L min^{-1}, nebulizer pressure 30 psig, fragmentor voltage 50 V, mass range 100–1500 *m*/*z*. For data collection and interpretation, MassHunter Workstation software was used.

An automatic polarimeter AUTOPOL® IV, Rudolph Research Analytical, a sodium lamp (589 nm) with a 1-dm cell was used to determine the specific rotation.

Synthesis of (S,S)-(i-*Pe*)$_2$*eddip 2HCl* (***1***)

The R_2edda-type ester, **1**, was prepared using the esterification reaction previously described for similar compounds.[18,32] Thionyl chloride (4 ml, 55 mmol) was introduced into a flask containing 40 ml of ice-cooled isopentyl alcohol (3-methyl-1-butanol), (*t* = 0 °C, anhydrous conditions) during 1 h through a dropping funnel. Subsequently, 1.50 g (5.41 mmol) of

(*S*,*S*)-ethylenediamine-*N*,*N*′-di-2-propanoic acid hydrochloride, (*S*,*S*)-H_2eddp·HCl, was added to the flask and the suspension was refluxed for 16 h at ≈130 °C. The mixture was filtered hot, immediately after reflux and the filtrate was left for a few days at 4 °C yielding the white product.

Yield: 1.22 g, 54 %. Anal. Calcd. for $C_{18}H_{38}N_2O_4Cl_2 \cdot 0.75H_2O$: C, 50.17; H, 9.23; N, 6.50 %. Found: C, 50.07; H, 8.77; N, 6.44 %; IR (cm^{-1}): 2961, 2862, 2636, 2598, 2416, 1733, 1236, 1160, 803; ^{1}H-NMR (500 MHz, DMSO-d_6, δ / ppm): 0.90 (12H, *d*, $^3J_{H,H}$ = 6.5 Hz, CH_3−*i*-Pe), 1.48–1.55 (10H, *m*, CH_2−*i*-Pe, CH_3), 1.68 (2H, *sep*, $^3J_{H,H}$ = 6.5 Hz, CH−*i*-Pe), 3.31–3.47 (4H, *m*, CH_2-(en)), 4.03 (2H, *q*, $^3J_{H,H}$ = 4.0 Hz, CH), 4.16–4.28 (4H, *m*, CH_2O−*i*-Pe), 10.09 (4H, *brs*, NH_2^+); ^{13}C-NMR (50 MHz, DMSO-d_6, δ / pm): 14.4 (CH_3), 22.4 (CH_3−*i*-Pe), 24.5 (CH−*i*-Pe), 36.7 (CH_2−*i*-Pe), 54.5 (CH_2-(en)) 64.6 (CH), 70.2 (CH_2O−*i*-Pe), 169.4 (COO−*i*-Pe); ESI−MS (CH_3OH), positive mode: Calcd. 345.27478. Found *m*/*z*: 345.27449 $[M–2Cl–H]^+$; $[\alpha]_D^{20}$ = –15° (CH_3OH, 1.1 mg/mL).

Biological experiments

Cell lines. Cervix adenocarcinoma cell line (HeLa), human melanoma (Fem-x), human chronic myelogenous leukemia (K562) cells, and a non-cancerous cell line, MRC-5 (human embryonic lung fibroblast) were grown in RPMI-1640 medium (Sigma Aldrich, St. Louis, MO, USA). The media were supplemented with 10 % fetal bovine serum, L-glutamine, and penicillin–streptomycin (Sigma Aldrich, St. Louis, MO, USA).

Treatment of cell lines. The target cells HeLa (2000 cells per well), Fem-x (5000 cells per well), K562 (5000 cells per well), and non-cancerous MRC-5 (5000 cells per well) were seeded into wells of a 96-well flat-bottomed microtitre plate. Twenty-four hours later, after cell adherence, different concentrations of the investigated compounds were added to the wells, except for the control cells to which the nutrient medium only was added. The final chosen concentrations range was 1–100 μM (1.0, 8.25, 16.5, 33.0 and 100.0 μM). The final concentration of DMSO solvent never exceeded 0.5 %, which was non-toxic to the cells. Especially, compounds were applied to the suspension of K562 cells 2 h after cell seeding. All concentrations were set up in triplicate. Nutrient medium with corresponding concentrations of investigated compounds, but without cells, was used as a blank, also in triplicate. The cultures were incubated for 72 h.

Determination of cell survival. The effect of the prepared compounds on cancer cell survival was determined by the microculture tetrazolium test (MTT) according to Mosmann[33] with modification by Ohno and Abe[34] 72 h after addition of the compounds, as described earlier. Briefly, 20 μl of methylthiazoletetrazolium bromide, 2-(4,5-dimethyl-2-thiazolyl)-3,5-diphenyl-2*H*-tetrazolium bromide (MTT) solution (5 mg ml^{-1} phosphate-buffered saline) was added to each well. Samples were incubated for a further 4 h at 37 °C in a humidified atmosphere of 95 vol. % air/5 vol. % CO_2. Then 100 μL of 100 g L^{-1} sodium dodecyl sulfate solution was added to extract the insoluble product formazan resulting from the conversion of the MTT dye by viable cells. The number of viable cells in each well was proportional to the intensity of the absorbance of light, which was read in an enzyme-linked immunosorbent assay (ELISA) plate reader at 570 nm. The absorbance (*A*) at 570 nm was measured 24 h later. To determine cell survival (%), the *A* of a sample with cells grown in the presence of various concentrations of the investigated compounds was divided by the control optical density (the *A* of control cells grown only in nutrient medium) and multiplied by 100. Absorbance of the blank was always subtracted from the A of the corresponding sample with target cells. The IC_{50} is defined as the concentration of an agent inhibiting cell survival by 50 % compared

with an untreated control. Cisplatin was used as the positive control. All experiments were performed in triplicate.

The selectivity index. The selectivity index (*SI*) is defined as the ratio of the IC_{50} obtained from the experiments on normal cells to that obtained on cancer cells. As the selectivity index (*SI*) demonstrates the differential activity of a pure compound, the greater the SI value is, the more selective is the compound.[35,36]

Statistical analysis

Results are presented as the mean ± standard deviation (*SD*) of triplicate observations from the representative of three experiments. The significance of the difference between treatments and control was analyzed by ANOVA followed by the Student-Newman-Keuls test $P < 0.05$ was considered significant.

RESULTS AND DISCUSSION

Spectroscopic studies

In the reaction of (*S*,*S*)-ethylenediamine-*N*,*N*′-di-2-propanoic acid hydrochloride, (*S*,*S*)-H$_2$eddip·HCl (crystal structure was described recently),[37] with absolute isopentyl alcohol (3-methyl-1-butanol) in the presence of thionyl chloride, diisopentyl (*S*,*S*)-ethylenediamine-*N*,*N*′-di-2-propanoate dihydrochloride (**1**) was obtained (Scheme 1).

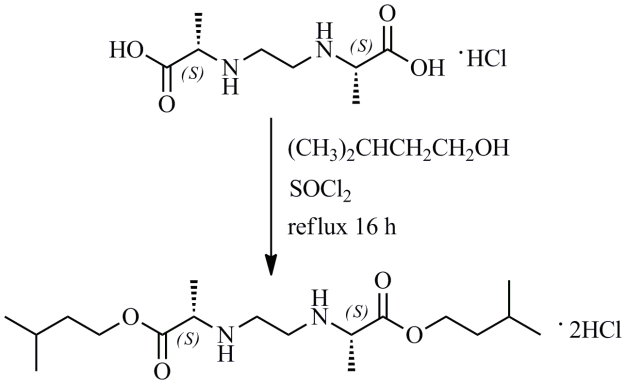

Scheme 1. Synthesis of (*S*,*S*)-(*i*-Pe)$_2$eddip·2HCl (**1**).

The IR spectrum of **1** showed characteristic absorption bands for this class of compounds.[22,23,28] A strong absorption stretching band ν(C=O) was found at 1733 cm^{-1}, while a band arising from ν(C−O) appeared at 1236 cm^{-1}. Asymmetric CH_3 stretching vibrations of medium intensity were found at ν(CH_3) 2961 cm^{-1} and 2862 cm^{-1}. Furthermore, an asymmetric ν(C−N) stretching vibration was found at 803 cm^{-1}.

In the ^{1}H-NMR spectrum resonances of methyl hydrogen atoms from the isopentyl moieties were found at 0.90 ppm as a doublet. Chemical shifts of the hydrogen atoms from isopentyl-CH_2 groups, overlapped with CH_3 protons

(L-alanine moiety), were found as a multiplet at 1.48–1.55 ppm, while CH_2 protons belonging to carbon atoms attached to ester oxygen could be seen at 4.21 ppm. Hydrogen atoms belonging to tertiary carbon atoms (isopentyl groups) were found as a septet at 1.69 ppm. The CH protons from the L-alanine moiety were detected at 4.03 ppm. The chemical shifts assignable to −N−C**H**$_2$−C**H**$_2$−N− protons were found at 3.31–3.47 ppm. Resonances of hydrogen atoms belonging to secondary ammonium groups were found at 10.09 ppm as broad singlets.

In the ^{13}C-NMR spectrum, the carbonyl carbon atoms peak was found at 169.4 ppm as expected for this class of compounds.[23,29] The ethylenediamine carbon atoms resonated at 54.5 ppm. The carbon atoms bonded to the ester oxygens were detected at 70.2, but resonances of all other carbon atoms (from isopentyl and L-alanine moieties) were found below 40 ppm, as expected.[22] The high resolution mass spectrum (positive mode) of **1** showed the presence of $[M–2Cl–H]^+$.

In vitro *studies*

Cytotoxicity. The *in vitro* cytotoxicity of esters **1–3** toward HeLa cervix adenocarcinoma, Fem-x human melanoma, K562 human chronic myelogenous leukemia cell lines and non-cancerous MRC-5 human embryonic lung fibroblast cells were determined by MTT assay. Cisplatin was used as a reference. The results are summarized in Table I, while Fig. 2 depicts the cytotoxic curves from the MTT assay showing the survival of target cells grown for 72 h in the presence of increasing concentrations of **1–3**.

TABLE I. IC_{50} values (μM) for **1**–**3** and cisplatin on the malignant HeLa, Fem-x and K562 cell lines and non-cancerous MRC-5 normal cells; the IC_{50} values are expressed as the mean±*SD* determined from the results of the MTT assay in three independent experiments

Compound	Cell line			
	HeLa	Fem-x	K562	MRC-5
1	2.01±0.19	1.51±0.09	5.22±0.55	51.09±1.06
2	2.22±0.81	2.25±0.91	3.27±0.58	>100
3	1.75±0.44	2.31±0.79	2.13±1.45	53.79±0.84
Cisplatin	2.10±0.20	5.51±0.31	5.54±1.03	14.21±1.54

The investigated compounds demonstrated a remarkable cytotoxic activity, as the IC_{50} values are in range from 1.51 to 5.22 μM against all the tested malignant cell lines. The IC_{50} values of these compounds against all cancer cell lines were in the micromolar range, similar to or better than those of the antitumor drug cisplatin. Namely, **1**–**3** and cisplatin showed no significant difference in *in vitro* activity against HeLa cells. Furthermore, all compounds exhibited significantly higher activity than cisplatin against K562 and Fem-x cell lines, except complex **1** against K562 cells.

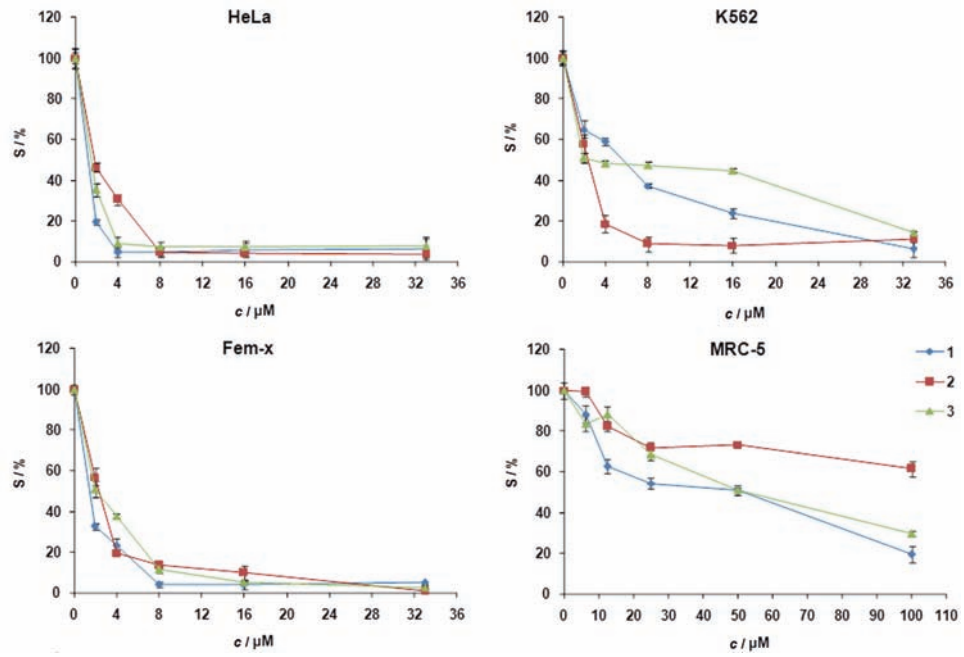

Fig. 2. Representative graphs show the survival of HeLa, K562, Fem-x, and MRC-5 cells grown for 72 h in the presence of increasing concentrations of **1**–**3**.

These findings indicate that the described compounds are extremely important for the future screening of their biological activity. In addition, from the obtained results, it could be concluded that compounds **1–3** show very slight differences in their cytotoxic effects against the tested cancer cells. Obviously, the presence of the isopentyl, *n*-butyl or *n*-pentyl groups in the structure of these compounds does not lead to significant differences in their activities.

Selectivity. Against the non-cancerous lung fibroblasts (MRC-5), all of the compounds exhibited a significantly weaker activity compared to cisplatin. The toxicity of compounds **1** and **3** in the lung fibroblasts was almost four times lower than that of cisplatin (Table I), and ten to fifty times weaker in the healthy cells compared to all the tested cancerous cells (Table II). Remarkably, compound **2** showed no cytotoxicity to normal non-cancerogenic MRC-5 cells (IC_{50} > 100 μM). The present *in vitro* experiments showed that compounds **1**–**3** express very high cytotoxic activity to cancerous cells with great selectivity (Table II), whereby compound **2** had no cytotoxic activity against mammalian normal cells (in the investigated concentration range). The effects of these compounds towards cancer and normal cells indicate to the necessity for further studies with *in vitro* and/or *in vivo* tests.

TABLE II. Selectivity index ($SI = IC_{50}$(MRC-5)/IC_{50}(cell line))

Compound	Cell		
	HeLa	Fem-x	K562
1	25.42±0.19	33.83±2.14	9.79±1.05
2	> 45.05	> 44.44	> 30.58
3	30.74±7.74	23.29±7.97	25.25±17.20
Cisplatin	6.77±0.98	2.58±0.31	2.56±0.55

CONCLUSIONS

The R_2eddip ester, diisopentyl (*S*,*S*)-ethylenediamine-*N*,*N*′-di-2-propanoate dihydrochloride (**1**) was synthesized. The compound was characterized by IR, ^{1}H- and ^{13}C-NMR spectroscopy, mass spectrometry and by elemental analysis. This novel R_2eddip·2HCl, **1**, ester along with earlier reported di(*n*-butyl) (*S*,*S*)-ethylenediamine-*N*,*N*′-di-2-propanoate dihydrochloride (**2**) and di(*n*-pentyl) (*S*,*S*)-ethylenediamine-*N*,*N*′-di-2-propanoate dihydrochloride (**3**) were tested against cervix adenocarcinoma cell line (HeLa), human melanoma (Fem-x), human chronic myelogenous leukemia (K562) cells and the non-cancerous cell line human embryonic lung fibroblast (MRC-5), using the MTT assay. Esters **1**–**3** showed similar or higher cytotoxicity, but much better selectivity, in comparison to cisplatin. (*S*,*S*)-(*i*-Pe)$_2$eddip (**1**) expressed the highest activity against Fem-x cells (IC_{50} = 1.51±0.09 μM).

Acknowledgments. This research was supported by the Ministry of Education, Science and Technological Development of the Republic of Serbia, Grants No. 172035 and 175011.

И З В О Д

СИНТЕЗА И ВИСОКА *IN VITRO* ЦИТОТОКСИЧНОСТ НЕКИХ (*S*,*S*)-ЕТИЛЕНДИАМИН-*N*,*N*′-ДИ-2-ПРОПАНОАТ-ДИХИДРОХЛОРИД ЕСТАРА

НЕБОЈША ПАНТЕЛИЋ[1], БОЈАНА Б. ЗМЕЈКОВСКИ[2], ТАТЈАНА П. СТАНОЈКОВИЋ[3], ВЕРИЦА В. ЈЕВТИЋ[4], ГОРДАНА П. РАДИЋ[4], СРЕЋКО Р. ТРИФУНОВИЋ[4], ГОРАН Н. КАЛУЂЕРОВИЋ[5] и ТИБОР Ј. САБО[6]

[1]Пољопривредни факултет, Универзитет у Београду, Немањина 6, 11080 Београд-Земун, [2]Центар за хемију – Институт за хемију, технологију и металургију, Универзитет у Београду, Његошева 12, 11000 Београд, [3]Институт за онкологију и радиологију, 11000 Београд, [4]Институт за хемију, Природно–математички факултет, Универзитет у Крагујевцу, Р. Домановића 12, 34000 Крагујевац, [5]Department of Bioorganic Chemistry, Leibniz Institute of Plant Biochemistry, Weinberg 3, D-06120 Halle (Saale), Germany и [6]Хемијски факултет, Универзитет у Београду, п.пр. 158, 11001 Београд

Нов (*S*,*S*)-R_2eddip естар, *O*,*O*′-диизопентил-(*S*,*S*)-етилендиамин-*N*,*N*′-ди-2-пропаноат-дихидрохлорид (**1**), синтетисан је и окарактерисан уз помоћ IR, NMR и масене спектрометрије и елементалне анализе. *In vitro* антитуморска активност једињења **1**, и још два R_2eddip естра, *O*,*O*′-диалкил-(*S*,*S*)-етилендиамин-*N*,*N*′-ди-2-пропаноат-дихидрохлорида, који су раније објављени (алкил = *n*-Bu или *n*-Pe, **2** и **3**, редом) испитивани су на хуманим ћелијским линијама аденокарцинома материце (HeLa), малигног меланома (Fem-x), и мијелоидне леукемије (K562), као и на нормалној ћелијској линији MRC-5 (фетални плућни фибробласти), уз помоћ MTT теста. Естри **1**–**3** су показали високу цитотоксичност и бољу селективност у поређењу са цисплатином која је коришћена као

референтна супстанца. Највећу активност је показао естар **1** са IC_{50}(Fem-x) вредношћу 1,51±0,09 μM.

(Примљено 5. децембра 2013, ревидирано 13. марта, прихваћено 17. марта 2014)

REFERENCES

1. F. Jadidi-Niaragh, G. Ghalamfarsa, M. Yousefi, M. N. Tabrizi, F. Shokri, *Tumor Biol*. **34** (2013) 2031
2. B. Vogelstein, K. W. Kinzler, *Nature Med.* **10** (2004) 789
3. G. Ghalamfarsa, A. Hadina, M. Yousefi, F. Jadidi-Niaragh, *Tumor Biol*. **34** (2013) 1349
4. M. Mubeen, S. G. Kini, *Int. J. Ther. Appl*. **5** (2012) 29
5. E. Lindauer, E. Holley, *Biochem. Pharm*. **52** (1996) 7
6. M. Viale, S. Minetti, M. Ottone, R. Lerza, B. Parodi, I. Pannacciulli, *Anti-Cancer Drugs* **14** (2003) 163
7. C. Molenaar, J. M. Teuben, R. J. Heetebrij, H. J. Tanke, J. Reedijk, *J. Biol. Inorg. Chem*. **5** (2000) 655
8. E. G. Talman, W. Bruning, J. Reedijk, A. L. Speek, N. Veldman, *Inorg. Chem*. **36** (1997) 854
9. P. M. Takahara, A. C. Rosenzweig, C. A. Frederick, S. J. Lippard, *Nature* **377** (1995) 649
10. M. A. Jakupec, M. Galanski, B. K. Keppler, *Rev. Physiol. Biochem. Pharmacol*. **146** (2003) 1
11. D. Wang, S. J. Lippard, *Nature Rev. Drug Discov*. **4** (2005) 307
12. F. Bouyer, J. Moretto, D. Pertuit, A. Szollosi, M. A. Locaille-Dubois, Y. Blache, B. Chauffert, N. Desbois, *J. Inorg. Biochem.* **110** (2012) 51
13. A. Merlino, L. Otero, D. Gambino, E. L. Coitino, *Eur. J. Med. Chem*. **46** (2011) 2639
14. A. Bakalova, H. Varbanov, R. Buyukliev, S. Stanchev, G. Momekov, D. Ivanov, *Inorg. Chim. Acta* **363** (2010) 1568
15. L. Kelland, *Nat. Rev. Cancer* **7** (2007) 573
16. G. N. Kaluđerović, V. M. Đinović, Z. D. Juranić, T. P. Stanojković, T. J. Sabo, *J. Inorg. Biochem.* **99** (2005) 488
17. G. N. Kaluđerović, Đ. Miljković, M. Momčilović, V. M. Đinović, M. M. Stojković, T. J. Sabo, V. Trajković, *Int. J. Cancer* **116** (2005) 479
18. G. N. Kaluđerović, T. J. Sabo, *Polyhedron* **21** (2002) 2277
19. G. N. Kaluđerović, H. Schmidt, S. Schwieger, C. Wagner, R. Paschke, A. Dietrich, T. Mueller, D. Steinborn, *Inorg. Chim. Acta* **361** (2008) 1395
20. G. N. Kaluđerović, H. Schmidt, D. Steinborn, T. J. Sabo, in: *Inorganic Biochemistry. Research Progress*, J. G. Hughes, A. J. Robinson, Eds., Nova Science Publishers, Hauppauge, NY, 2008, p. 305
21. G. N. Kaluđerović, H. Kommera, S. Schwieger, A. Paethanon, M. Kunze, H. Schmidt, R. Paschke, D. Steinborn, *Dalton Trans.* **48** (2009) 10720
22. G. P. Vasić, V. V. Glodjovic, I. D. Radojević, O. D. Stefanović, L. R. Comić, V. M. Djinović, S. R. Trifunović, *Inorg. Chim. Acta* **363** (2010) 3606
23. B. B. Krajčinović, G. N. Kaluđerović, D. Steinborn, H. Schmidt, C. Wagner, Ž. Žizak, Z. D. Juranić, S. R. Trifunović, T. J. Sabo, *J. Inorg. Biochem.* **102** (2008) 892
24. G. N. Kaluđerović, S. A. Mijatović, B. B. Zmejkovski, M. Z. Bulatović, S. Gomez-Ruiz, M. K. Mojić, D. Steinborn, D. M. Miljković, H. Schmidt, S. Stošić-Grujičić, *Metallomics* **4** (2012) 979
25. S. Mijatović, D. Maksimović-Ivanić, J. Radović, D. Miljković, G. N. Kaluđerović, T. J. Sabo, V. Trajković, *Cell. Mol. Life Sci.* **62** (2005) 1275

26. S. Gómez, D. Maksimović-Ivanić, S. Mijatović, G. N. Kaluđerović, *Bioinorg. Chem. Appl*. **2012** (2012), article ID 140284
27. S. Misirić Dencić, J. Poljarević, U. Vilimanovich, A. Bogdanović, A. J. Isaković, S. Kravić, M. Dulović, N. Zogović, A. M. Isaković, S. Grgurić-Sipka, *Chem. Res. Toxicol*. **25** (2012) 931
28. J. M. Lazić, L. Vučićević, S. Grgurić-Sipka, K. Janjetović, G. N. Kaluđerović, M. Misirkić, M. Gruden-Pavlović, D. Popadić, R. Paschke, V. Trajković, T. J. Sabo, *ChemMedChem* **5** (2010) 881
29. B. B. Zmejkovski, G. N. Kaluđerović, S. Gomez-Ruiz, Ž. Žizak, D. Steinborn, H. Schmidt, R. Paschke, Z. D. Juranić, T. J. Sabo, *Eur. J. Med. Chem.* **44** (2009) 3452
30. J. M. Vujić, M. Cvijović, G. N. Kaluđerović, M. Milovanović, B. B. Zmejkovski, V. Volarević, N. Arsenijević, T. J. Sabo, S. R. Trifunović, *Eur. J. Med. Chem.* **45** (2010) 3601
31. L. N. Schoenberg, D. W. Cooke, C. F. Liu, *Inorg. Chem.* **7** (1968) 2386
32. D. B. Haydock, T. P. C. Mulholland, *J. Chem. Soc. C* (1971) 2389
33. T. Mosmann, *J. Immunol. Methods* **65** (1983) 55
34. M. Ohno, T. Abe, *J. Immunol. Methods* **145** (1991) 199
35. P. Prayong, S. Barusrux, N. Weerapreeyakul, *Fitoterapia* **79** (2008) 598
36. A. Koch, P. Tamez, J. Pezzuto, D. Soejarto, *J. Ethnopharmacol*. **101** (2005) 95
37. V. V. Glodjović, G. P. Radić, S. M. Stanić, F. W. Heinemann, S. R. Trifunović *J. Serb. Chem. Soc.* **76** (2011) 995.

Journal of the Serbian Chemical Society
JSCS-info@shd.org.rs • www.shd.org.rs/JSCS
J. Serb. Chem. Soc. 79 (6) 659–668 (2014)
JSCS–4616
UDC 631.8+633.15:338.431.002.2
Original scientific paper

Microencapsulated fertilizers for improvement of plant nutrition

CIPRIAN TOLESCU[1], IRINA FIERASCU[2]*, CONSTANTIN NEAMTU[2], IULIA ANTON[3] and RADU CLAUDIU FIERASCU[2]

[1]Siemens S.R.L., 24 Preciziei Bvd., H3, 062204, Bucharest, Romania, [2]National R & D Institute for Chemistry and Petrochemistry – ICECHIM Bucharest, 202 Spl. Independentei, 060021, Romania and [3]National R & D Institute For Soil Science Agro-Chemistry and Environment – ICPA, 61 Marasti Bvd, 011464, Bucharest, Romania

(Received 4 October, revised 2 December, accepted 6 December 2013)

Abstract: Given the need to reduce the impact of the use of chemical fertilizers on the quality of food crop production, it is necessary to develop fertilizer formulations enabling the gradual and controlled release of the active substance, which could be achieved by encapsulation, thereby allowing its almost complete metabolization by plants. The study reported herein was intended to test such fertilizer compositions with controlled release, achieved by encapsulation in polymeric structures, by monitoring the biological activity of the new products, using maize and sunflower crops as the target plants, *i.e.*, crops having a major impact in the agricultural sector. To achieve this objective, solid microstructures were obtained, which allowed, on one hand, the incorporation of the fertilizing composition and, on the other, the controlled release of the active components over a period of time chosen so that advanced absorption in the plants could occur. Based on the presented findings, the tested fertilizers could ensure high quality fertilization in terms of a greater degree of nutrient recovery, lower doses without reducing plant productivity and reduced chemical pollution of soil.

Keywords: fertilizer; maize; sunflower; production increase; controlled release.

INTRODUCTION

The use of excessive amounts of mineral fertilizers leads inevitably to the emergence of crops containing large amounts of chemicals from the fertilizers, ultimately reaching the food chain and affecting the health of the consumers, thus having an extremely negative impact on the environment.[1] Given the need to reduce the impact of the use of chemical fertilizers on the quality of food crop production, it is therefore necessary to develop fertilizing formulation with gra-

* Corresponding author. E-mail: dumitriu.irina@yahoo.com
doi: 10.2298/JSC131004147T

dual and controlled release of the active substance, *e.g.*, by encapsulation, so that the fertilizer could be almost completely metabolized by the plants.

Due to the many advantages of the encapsulation process, the field has grown exponentially in recent years. The classes of compounds considered in this technique are extremely varied, ranging from medications,[2] food ingredients[3] and enzyme systems[4] to the encapsulation of highly toxic chemical residues, for their detoxification.[5] Thus, a number of studies have been performed worldwide regarding the microencapsulation of mineral fertilizers, in which various techniques were employed in order to obtain a controlled release fertilizer, thereby avoiding overdosing with the accompanying negative effects.[6,7]

The present paper intends to characterize such fertilizer compositions with controlled release, achieved by encapsulation in polymeric structures, by testing the biological activity of the new products, using maize and sunflower crops as target plants, crops with a major impact in the agricultural sector. To achieve this objective, solid microstructures were obtained to allow, on one hand, the incurporation of the fertilizing composition and, on the other, the controlled release of the active components in a period of time chosen so that advanced absorption in the plants could occur.[8]

EXPERIMENTAL

Materials

The fertilizers intended for use in the biological efficiency tests were microencapsulated urea; 1–1–0 NPK (nitrogen–phosphorous–potassium) complex; 1–1–1 NPK complex; 2–1–1 NPK complex. The methods for the synthesis of the proposed structures were presented in previous papers.[9–11]

The raw materials used for the fertilizers formulation were: urea (granules, SC Donau Chem SRL Turnu Magurele, Romania); formaldehyde aqueous solution (37 %, SC Chimreactiv SRL Bucharest, Romania); paraformaldehyde (solid, containing minimum 98 % formaldehyde, BDH Chemicals Ltd., UK); monoammonium phosphate (SC UTCHIM SRL Rm. Valcea, Romania); potassium chloride (SC Chimreactiv SRL Bucharest, Romania); phosphoric acid aqueous solution (85 % SC Chimreactiv SRL Bucharest, Romania); potassium hydroxide (aqueous standard solution, concentration 40±1 %); *n*-hexane (Vega Ploiesti, Romania); sodium tetraphenylborate (Fluka). All the materials are commercially available and were used as received, with no further purification.

Methods

The process of determining the degree of leaching of fertilizer on a column with sandy soil consisted of the following:

– The use of an installation consisting of columns of the following dimensions: I = 60 cm. d = 20 cm and 314 cm^2 column inner area, having a vessel at the bottom for collection of the solution.

– Incorporation at the top of the column filled with sand to a depth of 20 cm at a dose of 20 g fertilizer.

– Filling the columns with sandy soil with the following characteristics: 0.2 % humus content; total nitrogen 0.3 %; phosphorus <15 mg kg^{-1}; mobile potassium: 20 mg kg^{-1}; pH 6.5.

Given the humus content, the N/P/K content and the soil reaction as factors influencing plant nutrition, it was established that the testing of the microencapsulated and coated fertilizers must be realized on psamosoil (sandy soil) with a very low content of humus, nutrients and with a neutral reaction. With high permeability, very low content of humus and nutrients, sandy soil meets the optimum qualities to determine the leaching of fertilizers.

Regarding leaching producing irrigation, from the maximum standards set out in the literature for a main culture, *i.e.*, 4000–5000 m^3 water ha^{-1} (400–500 L m^{-2}) over 6–10 waterings of 600–700 m^3 water ha^{-1} (60–70 L m^{-2}) each, was considered effective and justified the application in columns of 8 waterings of 60 litres volume, every 8 days.[12] For irrigation, potable water from Bucharest was used. Product quantity – 20 g, nutrient content (**NPK**): **100** – 6.76 g N_t (33.82 %); **110** – 4.094 g N_t (20.47 %), 4.306 g P_2O_5 (21.53 %); **111** – 2.942 g N_t (14.71 %), 2.833 g P_2O_5 (14.16 %), 2.705 g K_2O (13.52 %); **211** – 4.336 g N_t (21.68 %), 2.417 g P_2O_5 (12.08 %), 2.387 g K_2O (11.93 %).

At the end of each eight-day cycle, the percolated water from the sand column was measured and analysed and the following standardized analyses were performed: determination of nitrogen by mineralization and distillation (Kjeldahl method); determination of phosphorus by the quinoline phosphomolybdate method; determination of potassium by the tetraphenylborate method [13]

Water leaching tests were performed and the results, from the point of view of the influence on plant nutrition, were compared with those obtained using classic fertilizers, commercial and non-encapsulated in a polymeric matrix.

The experimentation was conducted in a greenhouse in Mitscherlich vegetation vessels with 20 kg of soil, vermic chernozem, which is widely spread on the Romanian plain and various important areas on the Barlad Plateau, Transylvania and the Banat plain.

Chemical analysis (Table I) showed that the soil on which the tests were organized was fertile.

TABLE I. Chemical analysis of vermic chernozem; N_t – total nitrogen; P_t – total phosphorus; P_{AL} – phosphorus assimilable from the soil; K_{AL} –potassium assimilable from the soil

Soil type	Component						
	Humus	N_t	P_t	P_{AL}	K_{AL}	Ca	Mg
	%			mg kg^{-1}			
Vermic chernozem	3.5	0.18	0.015	35	56	180	65

The soil was introduced into the vegetation vessels (20 kg per vessel) and well levelled. Each variant was realized in three replications. Fertilization was performed pre-sowing by application of the product in the upper third of the soil in the vessel.

For the maize crop, the Talman simple hybrid was used, while for the sunflower, the Favourite variety was introduced. Maintenance of the crops was specific for the two species. Crop watering was ensured permanently at 70 % of field capacity of the soil. Harvesting was performed at crop maturity. The experimental results were expressed as the main product increase (maize grains, sunflower seeds) in g per vessel, % and in product grams per gram of active substance fertilizer (AS). The dose of fertilizer used was 20 g fertilizer per vessel.

RESULTS AND DISCUSSIONS

The main quality of microencapsulated fertilizers is the release of nutrients by slow solubilisation, over a period of time significantly longer than non-encap-

sulated mineral fertilizers, which are water soluble. Thus, the plants benefited from the improved nutrition through these fertilizers for a longer period and which ensured higher yields due to the higher ratio of nutrients used.[9]

Mineral fertilizers selected to be microencapsulated, either with one element (ureic nitrogen, for urea), two elements (nitrogen and phosphorus), or all three essential nutrients (nitrogen. phosphorus and potassium), once incorporated into the soil fill the nutrients reserve at optimal levels for the crop. The amounts of nutrients incorporated in microcapsules are leached (those with nitrogen), downgraded by reaction with the in soil existing calcium (those with phosphorus), respectively degraded in smaller amounts. Thus, fertilization doses can be reduced to a certain degree without reducing plant productivity and the fertility of the soil, thereby substantially reducing chemical pollution.[14]

Since this type of fertilizer has as its main feature the slow and controlled release of nutrients over time, thus preventing their leaching from the soil layer down to a depth of 60 cm, where the roots of most plant are widespread, the preliminary tests involved the characterization of each type of fertilizer obtained, in dependence on the leaching degree in an intensively pluviometric percolation regime.

Preliminary tests consisted of determining the leaching degree of the nutrient constituents (N_2, P_2O_5 and K_2O). Experimental results are given in Table II.

TABLE II. Leaching degree of the nutrient constituents

Percolation	Fertilizer (N:P:K)								
	1:0:0	1:1:0		1:1:1			2:1:1		
	N	N	P	N	P	K	N	P	K
P1	0.630	0.360	0.145	0.420	0.0192	0.0584	0.3944	0.0752	0.06
P2	0.595	0.345	0.122	0.2744	0.0968	0.0816	0.4248	0.1328	0.1152
P3	0.313	0.220	0.109	0.1144	0.1408	0.1168	0.2136	0.176	0.0848
P4	0.165	0.168	0.098	0.0792	0.1256	0.1112	0.170	0.176	0.068
P5	0.036	0.085	0.09	0.0352	0.104	0.064	0.1448	0.1136	0.0325
P6	0.015	0.070	0.086	0.0184	0.0768	0.0448	0.090	0.0696	0.028
P7	0.015	0.065	0.085	0.0184	0.0744	0.0408	0.080	0.0656	0.028
P8	0.014	0.040	0.083	0.0168	0.0664	0.0336	0.0752	0.06	0.0248
Total	1.783	1.353	0.8185	0.9768	0.704	0.5512	1.5928	0.8688	0.4413
	(26.4 %)	(33.0 %)	(19.0 %)	(33.2 %)	(24.8 %)	(19.4 %)	(36.7 %)	(35.9 %)	(18.5%)

From Table II, it could be seen that the forms of NPK fertilizer NPK 110 and 111 provide a uniform release over time of the macronutrient content (compared to the original content), while presenting a very good leaching resistance ("slow--release" activity), which recommended these formulations to be considered for future work.

The results of the leaching degree tests proved that the nitrogen incorporated into microencapsulated fertilizers was released slowly, over a long period, providing improved nutrition and reduction of pollution. Phosphorus and nitrogen

applied simultaneously had positive influences on the root surface and on the absorption process due to changes in the ratios between the ions present in the layer adjacent to the root surface. Nitrogen also promoted the release of phosphorus from combinations of energy transfer, increasing its effect in the cells of the plant root. Phosphorus affects nitrogen uptake by increasing root respiration.[15–17]

The test results showed the effectiveness of microencapsulation in prolonged maintenance of the solubility of phosphorus ($P–H_2PO_4^-$), which leached for up to 64 days compared to the downgraded ($H_2PO_4^-$), which occurred within a few days after incorporation into the soil.

Romanian soils are well supplied with assimilable potassium. Fertilizers containing this element can be used on sandy and luvic soils, or eroded as well as on other well-supplied soils under intensive cultivation of agricultural plants, fertilized with high doses of fertilizers. Microencapsulated potassium fertilizers are of interest for high-dose intensive fertilization.

Conventional, commercial fertilizers ensure the production increases given in Table III.

TABLE III. Production increases (%) of maize and sunflower ensured by fertilizers

Culture	Urea	NPK 110	NPK 111	NPK 211
Maize	10–12[a]	70–75[a]	Max. 40[b]	180–190[a]
Sun flower	15–17[a]	85–90[a]		150–160[a]

[a]source – field tests conducted using classic, commercial products, of the same compositions as those used in this study under the same conditions as those used for testing the developed fertilizers; [b]NPK 111 (15 % nitrogen, 15 % phosphorus, 15 % potassium), Azomures commercial product, the manufacturers guaranteed maximum increase

It could be seen that the smallest increases are provided by urea, which is only a source of nitrogen, and does not provide phosphorus and potassium, required by plants. On the other hand, the higher increases were obtained with conventional fertilizers, NPK 211. The disadvantage of this formulation in comparison to the NPK 111 is the higher cost of manufacturing. In addition, these increases are obtained with greater amounts of fertilizers, as several side fertilizations are necessary in order to compensate the losses caused by physical or chemical processes in the soil.

The efficiency of microencapsulated fertilizer on maize is presented in Table IV. The production increase relative to the total amount of active substance (AS) was differentiated according to the presence of the fertilizer components: N, NP and NPK, as well as the relationship between the elements N, P and K contained in the ternary fertilizers. The lowest growth increase (42.38 %) compared to the control unfertilized samples, was recorded for microencapsulated urea, but the increase was substantially higher (91.62 %) with the binary NP fertilizer (110).

This increase is due to the essential effects of nitrogen and phosphorus applied in combination on plant nutrition. The production increase obtained with the ternary complex fertilizer NPK 111 was superior to that of the binary one, 136.6 % higher compared to the control.

TABLE IV. Efficiency of microencapsulated fertilizer on maize

No.	Fertilizer	Quantity g per vessel	Grain production g per vessel	Increase		Production increase g per g of fertilizer
				g per vessel	%	
1	Unfertilized	–	51.2	–	100.00	–
2	100	6.76	72.9	21.7	142.38	2.89
3	110	8.40	98.11	46.91	191.62	5.58
4	211	9.14	104.86	53.66	204.80	5.87
5	111	8.48	121.14	69.94	236.60	8.24

Production increases presented with N, NP and NPK minimum dose of 6.76 to 9.14 g AS per vessel, certified that, to ensure optimum plant nutrition for intensive agriculture, all three elements are required, even for fertile soils.

Significantly greater production increases were obtained with NP and NPK complex fertilizers containing these elements in different ratios.

Thus, the microencapsulated NPK 110 complex fertilizer achieved an increase of 91.62 %, *i.e.*, 5.58 g grains per g of fertilizer, compared with the unfertilized control sample.

The use of microencapsulated NPK 111 complex fertilizer was favourable for maize, resulting in an increase of 136.60 %, *i.e.*, 8.24 g grains per g fertilizer, compared to the unfertilized control.

For urea the lowest production increase was recorded, as the plant assimilates nitrogen to a lesser extent in the absence of phosphorus.

In conclusion, all microencapsulated fertilizers tested led to considerable improvements in maize plant nutrition embodied in their proper vegetative development, which resulted in significant yield increases.

The effectiveness of the microencapsulated fertilizers applied to sunflower is presented in Table V.

TABLE V. Effectiveness of the microencapsulated fertilizers applied to sunflower

No.	Fertilizer	Quantity g per vessel	Grain production g per vessel	Increase		Production increase g increase per g of fertilizer
				g per vessel	%	
1	Unfertilized	–	27.3	–	100.00	–
2	100	7.12	46.13	18.83	168.97	2.64
3	110	8.40	66.98	39.68	245.34	4.72
4	211	9.14	69.4	42.1	254.21	4.60
5	111	8.48	78.8	51.5	288.64	6.07

Microencapsulated urea increased the production of seeds by 68.97 % (2.64 g seeds increase per g fertilizer). The binary complex NPK 110 fertilizer enhanced the yield by 145.34 % (4.72 g seeds per g fertilizer), while with the complex NPK 211 fertilizer the increase was 154.21 % (4.60 g seeds per g fertilizer). The ratio of the NPK complex fertilizers was also important for seed production. The complex NPK 111 fertilizer led to a yield increase of 188.64 % (6.07 g seeds per g fertilizer). The achieved production increases, lower than in the case of maize, could be explained by the fact that sunflower responded best to the NPK 111 fertilizer, while maize is a higher consumer of nutrients.

In conclusion, it could be stated that the microencapsulated fertilizers provided for significant production increases for sunflower.

Table VI presents a summary of Tables IV and V, and contains specific production increases (production increase in grams, compared to the amount of fertilizer used), obtained for both maize and sunflower crops.

TABLE VI. Specific production obtained for both maize and sunflower crops

No.	Fertilizer	Specific production increase g increase per g of fertilizer		Average production increase g increase per g of fertilizer
		Maize	Sunflower	
1	Unfertilized	–	–	
2	Microencapsulated urea	2.89	2.64	2.76
3	NPK 110	5.58	4.72	5.15
4	NPK 211	5.87	4.60	5.24
5	NPK 111	8.24	6.07	7.16

It should be noted that for maize with microencapsulated NPK complex fertilizer, 111 was the most favourable ratio, with which there was a maximum specific increase in grain production of 8.24 g per g fertilizer compared to the unfertilized control.

For sunflower crops, the specific increase in production using microencapsulated urea was 2.64 g seed per g fertilizer.

Regarding complex NPK fertilizers with various ratios of N, P and K, specific increases in seed production are also important. The complex NPK 111 led to an increase of 6.07 g of seeds per g of fertilizer.

The average production increase was calculated as the average of the two specific production increases. The employment of microencapsulated urea generated specific production increases comparable for the two cultures at the lowest cost price (this microencapsulated fertilizer being the cheapest).

CONCLUSIONS

All microencapsulated fertilizers studied meet the physical and chemical demands that facilitate superior storage, handling and differentiated fertilization depending on the content of the active substance. All samples of the tested mic-

roencapsulated fertilizers were characterized by gradual leaching, over a significantly longer period than the non-encapsulated mineral fertilizers, thus having a significant “slow- release” activity.

From the determination of the degree of leaching of water-soluble substances embedded in microencapsulated fertilizers, it could be concluded that they were greatly reduced compared with conventional fertilizers. As a result, the employment of this type of fertilizers ensures significant reduction in chemical pollution and a much higher proportion of the nutrients are taken up by the plants.

For all investigated fertilizers, an improved resistance to leaching of the nutrients was recorded, which resulted in significantly lower leaching degree. The explanation is that in the case of these fertilizers, the release of nutrients through leaching occurs over a longer period than from conventional mineral fertilizers (non-encapsulated). Thus, the plants benefit from improved nutrition for longer periods and higher production yields are ensured due to the higher ratio of the usage of the nutrients.

By supplementing the deficient nutrients in soil, in relation to the actual plant requirements, and by the influence they exert on the dynamics of the uptake of nutrients, encapsulated mineral fertilizers are an important means for directing plant nutrition and, thereby, influencing their growth and development throughout the vegetation period. When applied together, phosphorus and nitrogen have positive effects, each influencing the uptake of the other.[15–17]

Due to microencapsulation, the nutrients undergo leaching (nitrogen) or a downgrade (phosphorus) through chemical reactions that occur in soil to a significantly smaller extent than is the case with non-encapsulated mineral fertilizers. Thus, in tests conducted for nitrogen leaching for non-encapsulated urea and ammonium nitrate, the obtained values (42.4–44.6 %) were much higher than for the encapsulated fertilizers (28.03–34.11 %).

Regarding the dynamics of phosphorus, which leaches to a much lower extent than nitrogen, but suffers a downgrade into soluble forms within a few days, microencapsulated fertilizers ensure an extension of time periods for maintaining the monophosphate form, due to the slow and gradual release during plant vegetation.

The results for the dynamics of potassium leaching show a positive influence of encapsulation on the extended dissociation of potassium ions in the fertilizers and root uptake from a soil intensively fertilized.

The production increases that were obtained with the microencapsulated fertilizers are due to the fact that, in addition to intake of nutrients, such fertilizers in the soil give rise to a series of slow and longer chemical and biological reactions (enzyme-catalysed reactions, such as the hydrolytic decomposition of urea by the enzyme urease), through which the dynamics of many substances existing in soil are also influenced. The production increases provided by the

microencapsulated fertilizers in maize and sunflower grown in vermic chernozem, the soil prevalent in Romania, are high, ranging from 42.38 to 136.60 % compared to the control unfertilized maize, and between 68.97 to 188.64 % compared to the control in sunflowers. These production increases certify the superior quality of these new crop fertilizers that are to be used in sustainable agriculture, which is the main objective today.

Based on the outlined findings, these fertilizers could ensure high quality fertilization in terms of a greater degree of nutrient recovery, lower doses required to maintain high plant productivity and reduced chemical pollution of soil.

ИЗВОД

ЂУБРИВА У МИКРОКАПСУЛАМА ЗА БОЉУ ИСХРАНУ БИЉАКА

CIPRIAN TOLESCU[1], IRINA FIERASCU[2], CONSTANTIN NEAMTU[2], IULIA ANTON[3] и RADU CLAUDIU FIERASCU[2]

[1]Siemens S.R.L., Bucharest, Romania, [2]National R&D Insitute for Chemistry and Petrochemistry – ICECHIM Bucharest, Romania и [3]National R & D Institute for Soil Science Agro-Chemistry and Environment – ICPA, Bucharest, Romania

Да би се смањио утицај хемијских ђубрива на квалитет житарица за исхрану, пожељно је правити ђубрива у капсулама, у циљу постепеног и контролисаног отпуштања активних супстанци, омогућујући биљкама да их скоро у потпуности метаболишу. У овом раду су тестирана ђубрива инкапсулирана у полимерне структуре, а праћена је биолошка активност у кукурузу и сунцокрету, житарицама веома важним у пољопривреди. На основу добијених резултата, могло се закључити да се оваквим ђубривима постиже квалитетно ђубрење у смислу искористљивости хранљивих састојака, потребне су биле мање дозе ђубрива, није долазило до смањења производње житарица, а било је смањено загађење земљишта.

(Примљено 4. октобра, ревидирано 2. децембра, прихваћено 6. децембра 2013)

REFERENCES

1. S. Savci, *Int. J. Environ. Sci. Develop.* **3** (2012) 77
2. M. Kalani, R. Yunus, *Int. J. Nanomed.* **6** (2011) 1429
3. D. Poncelet, A. Picot, S. El Mafadi, *Innov. Food Technol.* **1** (2011) 32
4. A. Blandino, M. Macias, D. Cantero, *Appl. Biochem. Biotechnol.* **110** (2003) 53
5. P. Randall, S. Chattopadhyay, *J. Hazard. Mat.* **114** (2004) 211
6. X. Han, S. Chen, X. Hu, *Desalination* **240** (2009) 21
7. S. A. Riyajan, Y. Sasithornsonti, P. Phinyocheep, *Carbohyd. Polym.* **89** (2012) 251
8. P. A. Stiehl-Braun, D. S. Powlson, P. R. Poulton, P. A. Niklaus, *Soil Biol. Biochem.* **43** (2011) 1034
9. C. Tolescu, C. Neamtu, G. Raceanu, M. Popescu, H. Iovu, *Mater. Plast.* **46** (2009) 387
10. C. Tolescu, H. Iovu, *Univ. Polytech. Bucharest - Sci. Bull., B* **72** (2010) 3
11. C. Tolescu, C. Neamtu, M. Ghiurea, H. Iovu, *Environ. Eng. Manag. J.* **9** (2010) 553
12. J. B. Zhou, J. G. Xi, Z. J. Chen, S. X. Li, *Pedosphere* **16** (2006) 245
13. Official Journal of the European Union, http://eur-lex.europa.eu/LexUriServ/LexUriServ.do?uri=OJ:L:2003:304:0001:0001:EN:PDF (04.10.2013)
14. H. A. Marzouk, H. A. Kassem, *Sci. Hortic.* **127** (2011) 249

15. M. Karim, S. M. Rahman, F. Ahmed, S. U. Patwary, *Geoderma* **7** (1972) 121
16. J. A. Entry, R. E. Sojka, *J. Environ. Manag.* **87** (2008) 364
17. W. A. Ket, J. P. Schubauer-Berigan, C. B. Craft, *Aquat. Bot.* **95** (2011) 17.

Journal of the Serbian Chemical Society
JSCS-info@shd.org.rs • www.shd.org.rs/JSCS
J. Serb. Chem. Soc. 79 (6) 669–676 (2014)
JSCS–4617
UDC 546.482+547.53+547.476.2/.3:
541.64:548.7:535.37
Original scientific paper

A new cadmium(II) coordination polymer constructed from 2-(2-chloro-6-fluorophenyl)-1*H*-imidazo[4,5-*f*][1,10]phenanthroline and 1,3-benzenedicarboxylate: Synthesis, crystal structure, thermal behavior and luminescent properties

ZHI-GUO KONG*, SHENG-NAN GUO, YING-XUE ZHAO and DAN SONG

Key Laboratory for the Preparation and Application of Environmentally Friendly Materials, Ministry of Education, College of Chemistry, Jilin Normal University, Siping 136000, China

(Received 23 May, revised 15 September, accepted 19 November 2013)

Abstract: A new Cd(II) coordination polymer, namely, $[Cd_2(Cl)(1,3\text{-BDC})_{1.5}(L)_2]\cdot 1.25H_2O$ (**1**) (L = 2-(2-chloro-6-fluorophenyl)-1*H*-imidazo[4,5-*f*][1,10]phenanthroline and 1,3-benzenedicarboxylate (1,3-BDC) was synthesized under hydrothermal conditions. The crystal of **1** belongs to orthorhombic, space group *P* bcn with a = 31.3116(19) Å, b = 13.5485(8) Å, c = 22.9850(15) Å, α = 90°, β = 90°, γ = 90°, $C_{50}H_{28.5}Cd_2Cl_3F_2N_8O_{7.25}$, M_r = 1226.46, V = 9750.8(10) Å^3, Z = 8, D_{calc} = 1.671 g cm^{-3}, S = 1.038, μ(MoK$_\alpha$) = 1.106 mm^{-1}, F(000) = 4860, R = 0.0585 and wR = 0.1485. Compound **1** exhibits a 1D-ladder structure. Furthermore, neighboring 1D-ladders are joined together by $\pi\cdots\pi$ interactions to result in a 2D supramolecular layer. The thermal behavior of **1** was characterized. Furthermore, its luminescent properties were studied in the solid state at room temperature.

Keywords: crystal structure; 1,3-benzenedicarboxylate; luminescence; 2-(2-chloro-6-fluorophenyl)-1*H*-imidazo[4,5-*f*][1,10]phenanthroline.

INTRODUCTION

Coordination polymers comprised of metal ions and bridging ligands have received much attention because of their fascinating motifs and potential applications as functional materials, ranging from catalysis, gas absorption, molecular recognition, optics, *etc*.[1–3] The organic ligands play an important role in the construction of coordination polymers.[4–6] In this regard, carboxylic acids exhibit diverse coordination modes, especially multi-carboxylic acids, such as benzenedicarboxylates, when used in the preparation of various coordination polymers.[7–9] On the other hand, the intriguing structures of coordination polymers may be varied or tailored by incorporating different auxiliary ligands, in which conju-

* Corresponding author. E-mail: kongzhiguo1977@sohu.com
doi: 10.2298/JSC130523138K

gated polycarboxylates are bridging ligands.[10] 1,10-Phenanthroline (phen) and its various derivatives have become promising chelating ligands because of their potential ability to form supramolecular aggregates through π–π stacking interactions.[11,12] Herein, the hydrothermal synthesis, crystal structure, thermal behavior and luminescent properties of $[Cd_2(Cl)(1,3\text{-BDC})_{1.5}(L)_2]\cdot 1.25H_2O$ (**1**), in which L = 2-(2-chloro-6-fluorophenyl)-1*H*-imidazo[4,5-*f*][1,10]phenanthroline and 1,3-BDC = 1,3-benzenedicarboxylate.

EXPERIMENTAL

All the materials were of analytical reagent grade and used as received without further purification. The C, H and N elemental analysis were realized on a Perkin–Elmer 240C elemental analyzer. The crystalline structures of the as-synthesized products were investigated by X-ray diffraction analysis using CuK_α radiation (XRD, BRUKER, D8 ADVANCE, Germany). The thermal stability experiment was performed on a TG SDT2960 thermal analyzer from room temperature to 800 °C under a nitrogen atmosphere at a heating rate of 10 °C min^{-1}. The photoluminescent properties were measured on a Renishaw inVia Raman microscope at room temperature.

*General procedure for the synthesis of $[Cd_2(Cl)(1,3\text{-BDC})_{1.5}(L)_2]\cdot 1.25H_2O$ (**1**)*

A mixture of $CdCl_2\cdot 2H_2O$ (1 mmol, 0.192 g), L (1 mmol, 0.300 g) and 1,3-H_2BDC (1 mmol, 0.166 g) were dissolved in 10 mL distilled water, followed by the addition of triethylamine until the pH value of the system was adjusted to between 4.5 and 5.5. Then the mixture was transferred and sealed in a 25 mL teflon-lined stainless steel container. The container was heated to 438 K and the temperature was held for 6 d. After the mixture had been cooled to room temperature at a rate of 10 °C h^{-1}, crystals of **1** were obtained. Yield: 15 %. Anal. Calcd. for $C_{50}H_{28.5}Cd_2Cl_2F_2N_8O_{7.25}$: C, 48.96; H, 2.34; N, 9.14 %. Found: C, 48.52; H, 2.21; N, 8.93 %.

X-Ray crystallography

Single-crystal X-ray diffraction data for **1** was recorded on a Bruker-AXS Smart CCD diffractometer equipped with a graphite-monochromatized MoK_α (λ = 0.71073 Å) radiation by using an ω–ϕ scan method at 293(2) K. The structure was solved by direct methods using the SHELXS-97 program and refined with SHELXL-97 by full-matrix least-squares techniques on F^2.[13,14] Non-hydrogen atoms of the compound were refined with anisotropic temperature parameters. All H atoms were positioned geometrically (C–H = 0.93 Å) and refined as riding, with $U_{iso}(H) = 1.2U_{eq}$(carrier). The water H atoms were not included in the model. A summary of crystallographic data and structure analysis is given in Table I. Selected bond lengths and bond angles are listed in Table II.

TABLE I. Crystal data and structure refinement for **1**

Compound	$[Cd_2(Cl)(1,3\text{-BDC})_{1.5}(L)_2]\cdot 1.25H_2O$
Chemical formula	$C_{50}H_{28.5}Cd_2Cl_3F_2N_8O_{7.25}$
Formula weight	1226.46
Wavelength, Å	0.71073
Temperature, K	293(2)
Crystal system	Orthorhombic
Space group	*P* bcn

TABLE I. Continued

a / Å	31.3116(19)
b / Å	13.5485(8)
c / Å	22.9850(15)
α / °	90
β / °	90
γ / °	90
V / Å^3	9750.8(10)
Z	8
D_{calc} / g cm^{-3}	1.671
μ / mm^{-1}	1.106
F(000)	4860
(θ_{min}– θ_{max}) / °	1.30–25.05
Diffraction measured fraction, θ_{max}	25.05
Refined difference density, max/min	1.845/–0.514
Reflection collected/unique (R_{int})	48689/8624 (0.0762)
Data/restraints/parameters	8624/6/668
Goodness-of-fit on F^2	1.038
R indices (all data)	R_1 = 0.1000 , wR_2 = 0.1694
Final R indices ($I > 2\sigma(I)$)	R_1 = 0.0585 , wR_2 = 0.1485

TABLE II. Selected bond lengths and angles for **1**; symmetry transformations used to generate equivalent atoms: $^i x, y+1, z$

Bond lengths, Å			
Cd(2)–N(1)	2.319(6)	Cd(2)–N(2)	2.323(6)
Cd(1)–N(5)	2.326(6)	Cd(1)–N(6)	2.403(5)
Cd(1)–O(1)	2.340(5)	Cd(1)–O(2)	2.409(5)
Cd(1)–O(3)	2.253(5)	Cd(2)–O(4)	2.220(5)
Cd(1)–Cl(3)	2.546(2)	Cd(2)–Cl(3)	2.585(2)
Cd(2)–O(6)^i	2.221(5)	Cd(2)–O(5)^i	2.573(5)
Bond angles, °			
O(3)–Cd(1)–N(5)	84.5(2)	O(3)–Cd(1)–O(1)	83.0(2)
N(5)–Cd(1)–O(1)	120.0(2)	O(3)–Cd(1)–N(6)	139.58(19)
N(5)–Cd(1)–N(6)	70.4(2)	O(5) ^{i}–Cd(2)–Cl(3)	153.00(12)
O(3)–Cd(1)–O(2)	129.27(19)	O(6) ^{i}–Cd(2)–Cl(3)	99.49(13)
O(1)–Cd(1)–O(2)	54.59(17)	O(6) ^{i}–Cd(2)–O(5) ^{i}	53.88(17)
O(3)–Cd(1)–Cl(3)	92.17(16)	N(5)–Cd(1)–Cl(3)	142.52(16)
O(1)–Cd(1)–Cl(3)	96.48(16)	N(6)–Cd(1)–Cl(3)	89.54(15)
O(2)–Cd(1)–Cl(3)	116.56(13)	O(3)–Cd(1)–C(39)	106.8(2)
O(4)–Cd(2)–N(2)	155.8(2)	N(5)–Cd(1)–C(39)	108.8(2)
O(6) ^{i}–Cd(2)–N(2)	105.2(2)	O(1)–Cd(1)–C(39)	27.18(19)
N(1)–Cd(2)–N(2)	71.57(19)	N(6)–Cd(1)–C(39)	111.0(2)
O(4)–Cd(2)–O(5) ^{i}	96.6(2)	O(2)–Cd(1)–C(39)	27.41(18)
N(5)–Cd(1)–O(2)	93.4(2)	Cl(3)–Cd(1)–C(39)	107.89(17)
N(1)–Cd(2)–O(5) ^{i}	86.31(17)	O(4)–Cd(2)–O(6) ^{i}	99.0(2)
N(2)–Cd(2)–O(5) ^{i}	97.1(2)	O(4)–Cd(2)–Cl(3)	91.66(16)
N(6)–Cd(1)–O(2)	84.62(17)	N(1)–Cd(2)–Cl(3)	119.51(14)
O(1)–Cd(1)–N(6)	136.90(19)	N(2)–Cd(2)–Cl(3)	85.03(17)

*Deposition for complex **1***. CCDC-933986 (**1**) contains the supplementary crystallographic data for this paper. These data can be obtained free of charge from the Cambridge Crystallographic Data Centre *via* www.ccdc.cam.ac.uk/data_request/cif.

RESULTS AND DISCUSSION

*Crystal structure of **1***

The X-ray crystallographic analysis revealed that the asymmetric unit of **1** contains two Cd(II) atoms, two L ligands, one Cl anion, one and a half 1,3-BDC anions, and one and one fourth water molecules (Fig. 1).

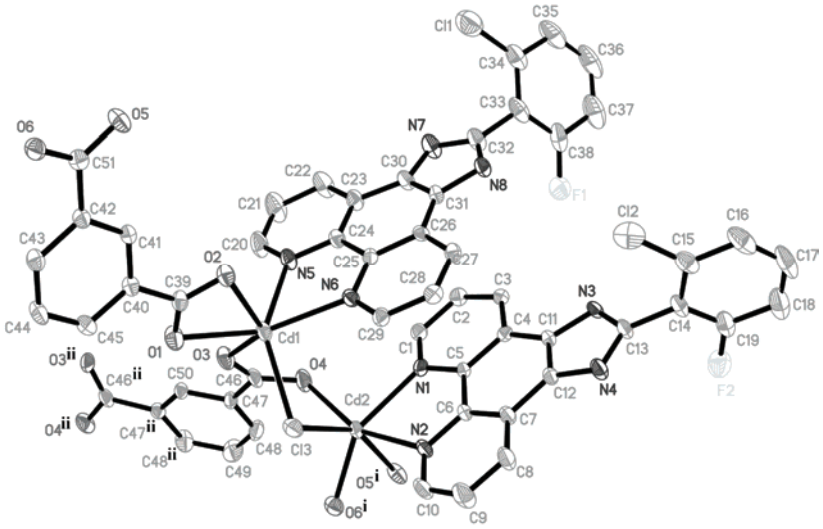

Fig. 1. View of the coordination environments of the Cd(II) atoms in complex **1**. All the hydrogen atoms have been omitted for clarity.

The two Cd(II) atoms show the same coordination geometries and coordination environments. Each Cd(II) atom is six-coordinated by three carboxylate oxygen atoms from two different 1,3-BDC anions, two nitrogen atoms from one L ligand, and one Cl anion in an octahedral sphere. The Cd–O and Cd–N distances of **1** (Table II) are very similar to those reported for another related complex $[Cd_2(NDC)_2(L')_2(H_2O)]\cdot 0.5DMF$ (NDC = 1,4-naphthalenedicarboxylate, L′ = pyrazino[2,3-*f*][1,10]phenanthroline and DMF = *N*,*N*-dimethylformamide).[10] It is noteworthy that one Cl anion bridges two Cd(II) atoms to furnish a $[Cd_2Cl]$ dimer with a Cd···Cd distance of 3.737 Å. Further, neighboring dimers are linked by 1,3-BDC anions in tridentate and tetradentate modes to give rise to a 1D ladder structure (Fig. 2). The L ligands are alternately attached on both sides of the ladders (Fig. 2). Interestingly, π–π stacking interactions among neighboring L ligands in adjacent ladders exist. These π–π stacking interactions extend the ladders into a 2D supramolecular layer (Fig. 3).

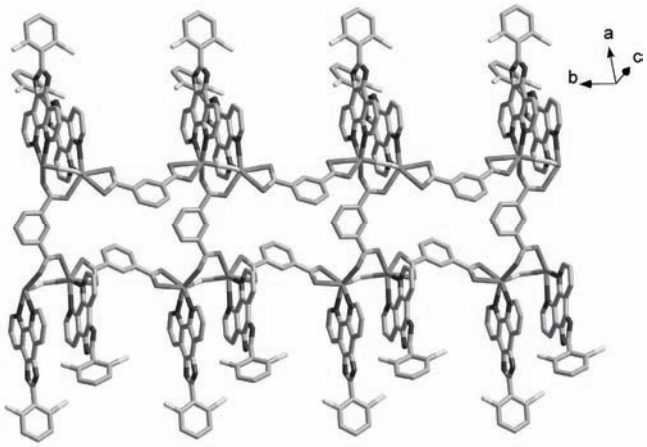

Fig. 2. View of the 1D ladder structure of **1**.

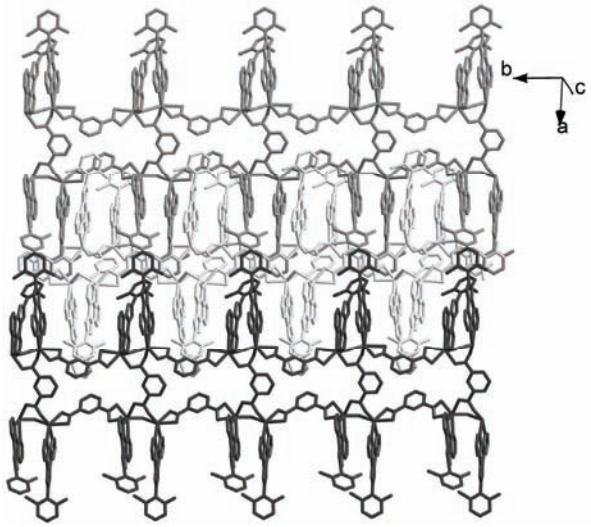

Fig. 3. View of the 2D supramolecular layer constructed by π–π interactions in **1**.

It should be stressed that some related complexes with phen derivatives have been reported.[15–20] However, the structure of complex **1** is different from the reported ones. For example, in the related known complex $[Cd_2(L)_2(1,3,5\text{-}BTC)(Cl)]\cdot H_2O$ (1,3,5-BTC = 1,3,5-benzenetricarboxylate anion),[15] each 1,3,5-BTC anion connects five Cd(II) atoms to form a double chain. These chains are further extended into 2D supramolecular networks through π–π interactions.

Powder X-ray diffraction and thermal behavior

The powder X-ray diffraction (PXRD) pattern for compound **1** was recorded at room temperature to confirm its phase purity (Fig. 4). The experimental PXRD

pattern corresponds well to the simulated one from the respective single-crystal data, indicating that the synthesized bulk materials and the measured single crystals are the same.

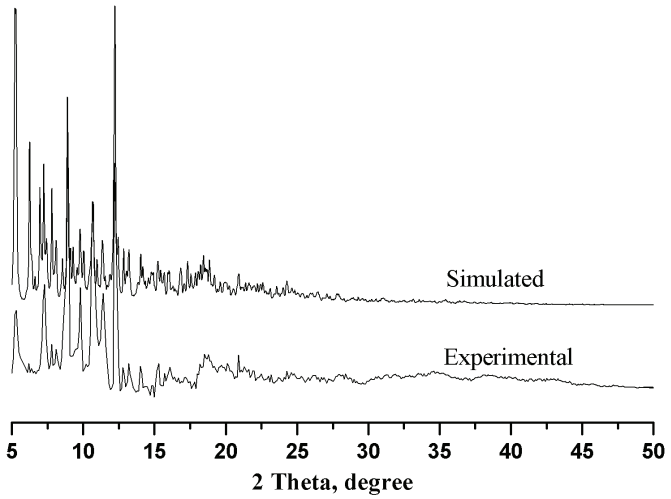

Fig. 4. Simulated and experimental powder X-ray diffraction patterns.

Thermogravimetric analysis of **1** was performed. The experiment was realized under a N_2 atmosphere at a heating rate of 10 °C min^{-1} in the temperature range 40 to 800 °C. As illustrated in Fig. 5, the first mass loss of 1.7 % between 54 and 178 °C corresponds to the loss of free water molecules (Calcd. 1.8 %). The second weight loss could be assigned to the decomposition of the 1,3-BDC ligand in the temperature range 245–353 °C (observed 19.2, Calcd. 20.1 %). The final weight loss from 371 to 644 °C may be attributed to the decomposition of L ligand (obsd 56.1 %, calcd. 56.9 %).

Luminescent properties

Coordination polymers with d^{10} metals have received intensive attention because of their various applications in photochemistry, chemical sensors, and electroluminescent (EL) displays.[12] In this work, the luminescent properties of the free organic ligands and compound **1** were investigated in the solid state at room temperature (Fig. 6). The free L and 1,3-H_2BDC showed emission bands centered at 404 nm (λ_{ex} = 325 nm) and 385 nm (λ_{ex} = 325 nm), respectively. As previously reported, these emissions can be attributed to the π*–n or π*–π transitions. Compound **1** showed an emission at about 538 nm (λ_{ex} = 325 nm). In comparison with the emission of 1,3-H_2BDC, a red shift was observed for compound **1**. The emission of **1** may be attributed to the synergetic contribution of a charge-transfer transition and the intraligand transition.[12]

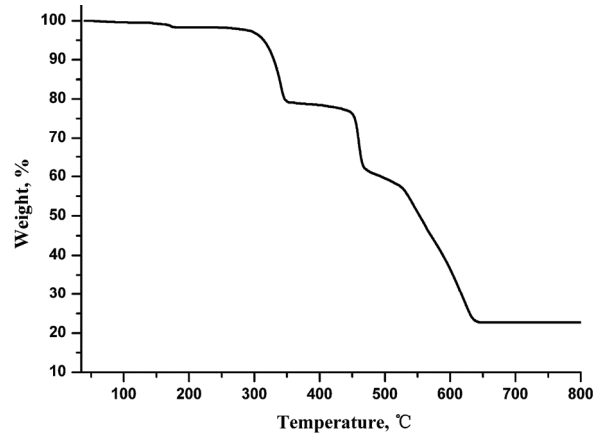

Fig. 5. TG curve of **1**.

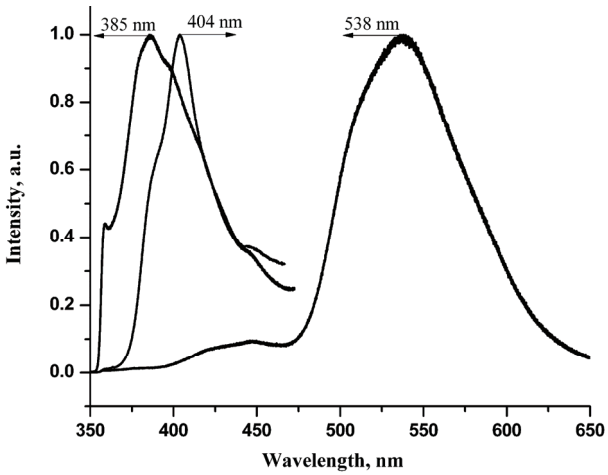

Fig. 6. Emission spectra of 1,3--H_2BDC, L and **1** (observed down the direction of increasing wavelength) in the solid state at room temperature.

CONCLUSION

A new Cd(II) coordination polymer was prepared from the phen derivative L and 1,3-benzenecarboxylate under hydrothermal condition. In compound **1**, the 1,3-BDC anions bridge the [Cd_2Cl] dimers to form a 1D-ladder structure. Furthermore, neighboring 1D-chains are joined together by π···π interactions to give a 2D supramolecular layer. In addition, compound **1** showed good luminescent properties in solid state at room temperature.

SUPPORTING INFORMATION

Crystallographic data can be obtained free of charge from the Cambridge Crystallographic Data Centre *via* www.ccdc.cam.ac.uk/data_request/cif.

Acknowledgement. This work was supported by a Science and Technology Research Project of the Education Committee of Jilin Province (No. 2013206).

И З В О Д

НОВИ КООРДИНАЦИОНИ ПОЛИМЕР КАДМИЈУМА(II) КОЈИ САДРЖИ 2-(2-ХЛОРО-6-ФЛУОРОФЕНИЛ)-1*H*-ИМИДАЗО[4,5-*f*][1,10]ФЕНАНТРОЛИН И 1,3-БЕНЗЕНДИКАРБОКСИЛАТ: СИНТЕЗА, КРИСТАЛНА СТРУКТУРА, ТЕРМИЧКО ПОНАШАЊЕ И ЛУМИНИСЦЕНТНА СВОЈСТВА

ZHI-GUO KONG, SHENG-NAN GUO, YING-XUE ZHAO и DAN SONG

Key Laboratory of Preparation and Application of Environmental Friendly Materials, Ministry of Education, College of Chemistry, Jilin Normal University, Siping 136000, China

У овом раду је синтетизован нови координациони полимер кадмијума(II), $[Cd_2(Cl)(1,3\text{-BDC})_{1,5}(L)_2]\cdot 1{,}25H_2O$ (**1**) (L = 2-(2-хлоро-6-флуорофенил)-1*H*-имидазо[4,5-*f*][1,10]фенантролин и 1,3-BDC = 1,3- бензендикарбоксилат). Полимер **1** кристалише у просторној групи *P* bcn орторомбичног кристалног система, при чему су параметри јединичне ћелије: a = 31,3116(19) Å, b = 13,5485(8) Å, c = 22,9850(15) Å, α = 90°, β = 90°, γ = 90°, $C_{50}H_{28,5}Cd_2Cl_3F_2N_8O_{7,25}$, M_r = 1226,46, V = 9750,8(10) Å^3, Z = 8, D_{calc} = 1,671 g cm^{-3}, S = 1,038, $\mu(MoK_\alpha)$ = 1,106 mm^{-1}, $F(000)$ = 4860, R = 0,0585 и wR = 0,1485. Полимер **1** има 1D структуру налик на лествице, при чему су суседни 1D мотиви повезани π···π интеракцијама у 2D супрамолекулске слојеве. Испитано је термичко понашање полимера **1**, као и његове луминисцентне особине у чврстом стању и на собној температури.

(Примљено 23. маја, ревидирано 15. септембра, прихваћено 19. новембра 2013)

REFERENCES

1. B. Moulton, M. J. Zaworotko, *Chem. Rev*. **101** (2001) 1629
2. V. A. Blatov, M. O'Keeffe, D. M. Proserpio, *CrystEngComm* **12** (2010) 44
3. N. Stock, S. Biswas, *Chem. Rev*. **112** (2012) 933
4. J. Yang, J. F. Ma, S. R. Batten, *Chem. Commun.* **48** (2012) 7899
5. C. Janiak, *Dalton Trans*. (2003) 2781
6. P. Lin, R. A. Henderson, R. W. Harrington, W. Clegg, C. D. Wu, X. T. Wu, *Inorg. Chem.* **43** (2004) 181
7. G. B. Gardner, S. Lee, Z. T. Xu, E. B. Lobkovsky, *J. Am. Chem. Soc.* **121** (1999) 8204
8. K. Kim, *Chem. Soc. Rev.* **31** (2002) 96
9. S. Kitagawa, R. Kitaura, S. I. Noro, *Angew Chem. Int. Ed.* **43** (2004) 2334
10. Z. G. Kong, X. Y. Wang, L. Carlucci, *Inorg. Chem. Commun.* **12** (2009) 691
11. Z. L. Xu, Y. He, S. Ma, X. Y. Wang, *Transition Met. Chem.* **36** (2011) 585
12. Z. G. Kong, X. R. Sun, L. Li, H. X. Wang, X. Y. Wang, S. W. Ng, *Transition Met. Chem.* **38** (2013) 449
13. G. M. Sheldrick, *SHELXS 97, Program for the Solution of Crystal Structure*, University of Göttingen, 1997
14. G. M. Sheldrick, *SHELXL 97, Program for the Refinement of Crystal Structure*, University of Göttingen, 1997
15. Z. G. Kong, Y. He, N. Xu, J. Guo, D. Li, *Z. Naturforsch.* **67b** (2012) 23
16. Z. G. Kong, M. Wang, Q. W. Wang, *Chin. J. Inorg. Chem.* **26** (2010) 537
17. X. Y. Wang, S. Ma, L. N. Zhao, Y. Chen, *Chin. J. Inorg. Chem.* **27** (2011) 2283
18. X. Y. Wang, Y. He, F. F. Liu, *Z. Naturforsch* **67b** (2012) 459
19. Z. G. Kong, X. R. Sun, X. M. Jin, B. Liu, W. W. Chen, *Chin. J. Struct. Chem.* **32** (2013) 1019
20. X. Y. Wang, Y. He, L. N. Zhao, Z. G. Kong, *Inorg. Chem. Commun.* **14** (2011) 1186.

Journal of the Serbian Chemical Society
JSCS-info@shd.org.rs • www.shd.org.rs/JSCS
J. Serb. Chem. Soc. *79* (6) 677–688 (2014)
JSCS–4618
UDC 544.6.076.2+546.135+519.87
Original scientific paper

Current efficiency in the chlorate cell process

MIROSLAV D. SPASOJEVIĆ[1], LENKA J. RIBIĆ-ZELENOVIĆ[1]*, PAVLE M. SPASOJEVIĆ[2] and BRANISLAV Ž. NIKOLIĆ[2#]

[1]*Faculty of Agronomy, University of Kragujevac, Cara Dušana 34, Čačak, Serbia and* [2]*Faculty of Technology and Metallurgy, University of Belgrade, Karnegijeva 4, Belgrade, Serbia*

(Received 23 October 2013, revised 14 January, accepted 16 January 2014)

Abstract: A mathematical model has been set up for current efficiency in a chlorate cell acting as an ideal electrochemical tubular reactor with a linear increase in hypochlorite concentration from the entrance to the exit. Good agreement was found between the results on current efficiency experimentally obtained under simulated industrial chlorate production conditions and the theoretical values provided by the mathematical model.

Keywords: chlorate; active chlorine; limiting diffusion current; current efficiency.

INTRODUCTION

During the electrolytic production of chlorate by the electrolysis of concentrated sodium chloride solution, chlorine is evolved at the anode by the anodic oxidation of chloride ions:

$$2Cl^- \rightarrow Cl_2 + 2e^- \quad (1)$$

The evolved elemental chlorine diffuses through the anodic diffusion layer towards the bulk solution where it is subject to hydrolysis. The hydrolysis reaction is fast and, therefore, at pH values of the solution above 6.0, almost all the dissolved chlorine hydrolyses near the anode:[1–13]

$$Cl_2 + H_2O \rightarrow HClO + H^+ + Cl^- \quad (2)$$

In the solution, equilibrium of the hypochlorous acid dissociation reaction is established:

$$HClO \rightarrow H^+ + ClO^- \quad (3)$$

* Corresponding author. E-mail: lenka@kg.ac.rs
# Serbian Chemical Society member.
doi: 10.2298/JSC131023004S

In the bulk solution, the resulting hypochlorous acid and hypochlorite (active chlorine) ions are converted to chlorate:

$$2HClO + ClO^- \rightarrow ClO_3^- + 2Cl^- + 2H^+ \quad (4)$$

Active chlorine diffuses into the anode, where it is oxidised to chlorate in an undesirable reaction:[1–13]

$$6ClO^- + 3H_2O \rightarrow 2ClO_3^- + 4Cl^- + 6H^+ + \frac{3}{2}O_2 + 6e^- \quad (5)$$

Maximum anodic current efficiency, η_a, is obtained if only reactions (1)–(4) occur. Reaction (5) in the diffusion-controlled electrochemical production of chlorate causes anodic current losses. Chlorine diffusion and hydrolysis, and active chlorine diffusion are determinants of the concentration profile of active chlorine in the anode diffusion layer. This profile determines the flux of active chlorine on the anode surface and, hence, the anodic current losses, which are additionally caused by water oxidation:[1–13]

$$2H_2O \rightarrow O_2 + 4H^+ + 4e^- \quad (6)$$

During chlorate production by the electrolysis of concentrated sodium chloride solutions, current losses due to the anodic oxidation of water are negligible.[1,11–14] The relatively high temperature of the solution, $t > 80$ °C, ensures a high rate of chemical conversion of active chlorine into chlorate (reaction (4)) and, hence, a relatively low steady-state concentration of active chlorine. In the chlorate production process, the pH of the solution, $6.1 < pH < 6.5$, ensures an optimal ratio of hypochlorous acid to hypochlorite ion concentrations for the maximum rate of the chemical conversion of active chlorine into chlorate.[1–13]

Hydrogen evolution is the primary reaction at the cathode:

$$4H_2O + 4e^- \rightarrow 2H_2 + 4OH^- \quad (7)$$

Apart from reaction (7), the reduction of active chlorine and chlorates may also occur at the cathode:

$$ClO^- + H_2O + 2e^- \rightarrow Cl^- + 2OH^- \quad (8)$$

$$ClO_3^- + 3H_2O + 6e^- \rightarrow Cl^- + 6OH^- \quad (9)$$

Cathodic current losses are completely prevented by the addition of 2 to 5 g dm^{-3} $Na_2Cr_2O_7$ to the solution.[1,2,6,7,16–22] Sodium dichromate plays multiple roles: a) it develops a thin layer of chromium oxide and hydroxide on the cathode surface, thus completely preventing the cathodic reduction of active chlorine and chlorite, b) it inhibits the corrosion of the steel cathode,[23] c) its buffering effect ensures an optimal pH for the chemical conversion of active chlorine into chlorate and d) it has a catalytic effect on the chemical conversion.[4,8]

Industrial systems for the electrolytic production of chlorates consist of cells and a holding tank, usually in a closed loop. Active chlorine is generated in the cells, and the chemical conversion of the active chlorine into chlorate occurs in the holding tank. During the production, a steady-state concentration of active chlorine is achieved in each volume element of the system ($\partial c_2 / \partial \tau = 0$). The anodic current efficiency ranges from 2/3 to 1 $\left(2/3 \leq \eta_a \leq 1\right)$.[1–6] The current efficiency can be lower than 2/3 only if the active chlorine concentration is higher than the steady-state concentration (non-steady-state conditions). In modern industrial chlorate plants, the current efficiency is only dependent on the ratio of the amount of chlorate resulting from the chemical conversion (reaction (4)) to the amount of chlorate produced by the electrochemical oxidation of active chlorine (reaction (5)). The contributions of the two reactions depend on the pH, temperature and volume of the solution, total current, current density, hydrodynamic electrolyte flow regime and electrochemical cell design.

The objective of this study was to set up a new mathematical model for current efficiency in the chlorate cell and experimentally verify the model in a laboratory chlorate plant.

EXPERIMENTAL

The experiment was conducted using laboratory apparatus composed of an electrochemical cell, a gas/liquid separator, a holding tank, a thermostat, a pump, a flow check valve and a flow metre (Fig. 1).

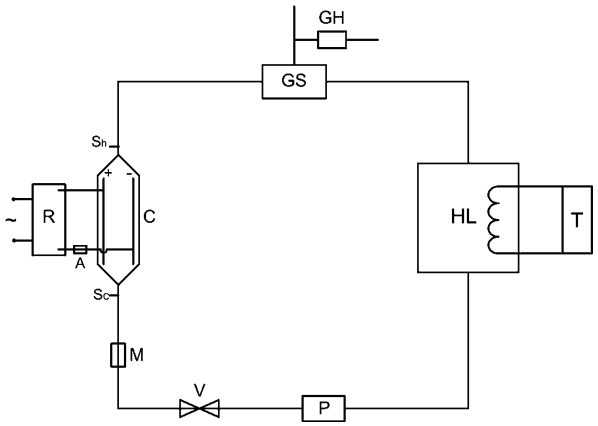

Fig. 1. Laboratory chlorate producing apparatus: C – electrochemical cell; GS – gas/liquid separator; GH – gas analyser; HL – holding tank; T – thermostat; P – pump; V – flow check valve; M – flow metre; R – rectifier; A – ammeter and SC; Sh – sampling valves.

The cell case, gas separator and the holding tank were made of Plexiglas and connected by polypropylene tubing. The holding tank contained 12.0 dm^3 of the solution. The total volume of the solution in the apparatus was 13.5 dm^3. The anode was a titanium plate activated by a catalytic 40 mol % RuO_2, 60 mol % TiO_2 (DSA) coating. A titanium plate-

-shaped cathode 200 cm^2 in surface area was placed parallel to the anode at a distance of 0.3 cm. Both electrodes were 0.3 cm in thickness. Three different electrochemical cells equipped with electrodes identical in surface area, but differing in height, *L*, and width, *b*, were used in the experiment: a) L = 25 cm, b = 8 cm; b) L = 50 cm, b = 4 cm and c) L = 100 cm, b = 2 cm. The electrolyte flow in the apparatus was controlled by both the pump P and valve V. The flow was adjusted in such a way as to ensure the same electrolyte velocity of 50 cm s^{-1} in the inter-electrode gap in all cells.

The solution temperature was 80±0.5 °C, and was adjusted by regulating the flow of water through a cooling coil. The pH of the solution was adjusted to within ±0.05 pH units by the addition of NaOH alkali or HCl acid to the solution using an automatic titrator.

The solution was composed of 300 g dm^{-3} NaCl and 3 g dm^{-3} $Na_2Cr_2O_7$. It was prepared using reagent-grade chemicals and triple-distilled water. The active chlorine concentration was determined by titration with sodium arsenite, and the current efficiency for chlorate formation was measured using the composition of the output gas mixture.[1,5,6] The composition of the mixture was determined by the gas chromatography. Measurements were conducted after reaching a steady state. The experimental values presented are the mean of ten measured values.

RESULTS AND DISCUSSION

The diffusion and hydrolysis of the chlorine generated at the anode and the diffusion of active chlorine can be described by the Danckwerts surface renewal model.[24,25] This model assumes that during turbulent mixing, the elements of the solution contact the anode surface and spend some time on it. During the electrolysis, some elements of the solution leave the anode surface and go into the bulk solution to be replaced by new fresh elements. The probability for an element of the solution to be replaced on a portion of the anode with another fresh element is not dependent on the length of its contact with the anode. Under steady-state conditions, the portion of the element surface that was in contact with the anode surface in the time interval from τ to $\tau+\mathrm{d}\tau$ is $S^{-S\tau}\mathrm{d}\tau$, where S denotes the portion of the anode surface on which the old element of the solution was replaced by the new one per unit time. If in an element of the solution brought into contact with the anode surface $c_1(x,\tau)$ – the concentration of chlorine is at a distance x from the anode surface after a time τ that elapsed from the initial contact with the anode, the average chlorine concentration for all elements of the solution on the anode surface at a distance x from the anode is equal to:

$$\overline{c_1} = S\int_0^\infty c_1(x,\tau)e^{-s\tau}\mathrm{d}\tau \qquad (10)$$

Equation (10) is the Laplace–Carlson transform of the function $c_1(x,\tau)$.

Assuming that chlorine hydrolysis is a first-order reaction, the diffusion and hydrolysis of chlorine in one element of the solution on the anode surface can be presented using the following equation for non-steady-state diffusion:

$$\frac{\partial c_1}{\partial \tau} = D_1 \frac{\partial^2 c_1}{\partial x^2} - k_1 c_1 \tag{11}$$

and Eq. (12) for the diffusion of active chlorine:

$$\frac{\partial c_2}{\partial \tau} = D_2 \frac{\partial^2 c_2}{\partial x^2} + k_1 c_1 \tag{12}$$

The initial and boundary conditions needed to solve the differential equations for chlorine are:

$$\text{for } \tau = 0,\ c_1 = 0 \tag{13}$$

$$\text{for } x = 0,\ -D_1 \frac{\mathrm{d}\bar{c}_1}{\mathrm{d}x} = \frac{j\eta_\mathrm{a}}{2F} \tag{14}$$

$$\text{for } x = \infty,\ c_1 \to 0 \tag{15}$$

and for active chlorine:

$$c_2 = 0, \text{ for } \tau = 0 \text{ and } x > 0 \tag{16}$$

$$c_2 = 0, \text{ for } \tau > 0 \text{ and } x = 0 \tag{17}$$

$$c_2 = c_0, \text{ for } \tau > 0 \text{ and } x \to 0 \tag{18}$$

Applying Laplace–Carlson transforms to Eqs. (11) and (12), as well to the initial and boundary conditions (Eqs. (13)–(18)) gives for chlorine:

$$D_1 \frac{\mathrm{d}^2 \bar{c}_1}{\mathrm{d}x^2} - \left(k_1 + S\right)\bar{c}_1 = 0 \tag{19}$$

$$\text{for } x = \delta_\mathrm{a},\ \bar{c}_1 = 0 \tag{20}$$

and

$$\text{for } x = 0,\ -D_1 \frac{\mathrm{d}\bar{c}_1}{\mathrm{d}x} = \frac{j\eta_\mathrm{a}}{2F} \tag{21}$$

and for active chlorine:

$$\frac{\mathrm{d}^2 \bar{c}_2}{\mathrm{d}x^2} - \frac{S}{D_2}\bar{c}_2 = -\frac{c_0}{D_2} S - \frac{k_1 \bar{c}_1}{D_2} \tag{22}$$

$$\text{for } x \to \infty,\ \bar{c}_2 = c_0 \tag{23}$$

and

$$\text{for } x \to 0,\ \bar{c}_2 = 0 \tag{24}$$

As in case with concentration $\bar{c}_1$, concentration $\bar{c}_2$ is defined using Eq. (10).

Solving Eqs. (19) and (22) results in the following expressions for the concentration profiles of chlorine (Eq. (25)) and active chlorine (Eq. (26)) in the anodic diffusion layer of the chlorate cell:

$$\bar{c}_1 = \frac{j\eta_\mathrm{a}}{2F} \frac{1}{K\left(1+M\right)^{0.5}} \exp\left(-\frac{K}{D_1}\left(1+M\right)^{0.5} x\right) \tag{25}$$

$$\bar{c}_2 = \frac{j\eta_a M}{2FK(1+M)^{0.5}\left[(1+M)\left(\frac{D_2}{D_1}-1\right)\right]} \times \{\exp\left[-\left(\frac{K^2}{D_1 D_2}\right)^{0.5} x\right] - \exp\left[-(1+M)^{0.5}\frac{K}{D_1}x\right] + c_0\left\{1-\exp\left[-\left(\frac{K^2}{D_1 D_2}\right)^{0.5} x\right]\right\}\} \quad (26)$$

where:

$$M = \left(\frac{k_1}{D_1}\right)^{0.5} \delta_a \quad (27)$$

and

$$K = (SD_1)^{0.5} = \frac{D_1}{\delta_a} \quad (28)$$

as according to [25]:

$$S = \frac{D_1}{\delta_a^2} \quad (29)$$

The flux of active chlorine at the anode surface defines the portion $(1-\eta_a)$ of the anodic current density that is consumed for the oxidation of active chlorine to chlorate (reaction (5)):

$$\frac{1-\eta_a}{F} = D_2 \frac{d\bar{c}_2}{dx}\Big|_{x=0} \quad (30)$$

Combining Eqs. (26) and (30) and solving for η_a gives a relatively simple expression for the anodic current efficiency:

$$\eta_a = \frac{1 - D_2\ c_0\ F\ (j\delta_a)^{-1}}{1.5 - 0.5\left(1+\frac{k_1}{D_1}\delta_a{}^2\right)^{-0.5}} \quad (31)$$

Equation (31) is valid for an ideal stirred electrochemical reactor, in which the active chlorine concentration is invariable within each element of the volume. The active chlorine concentration at the entrance to the cell, $c_{2,c}$ is identical to that at the exit from the cell, $c_{2,h}$.

Equation (31) was used to determine the theoretical dependence of the current efficiency on the steady-state concentration of active chlorine (Fig.2). The same dependence was also experimentally determined (Fig. 2). A cell equipped with a 25 cm high anode was used in the experiment. The desired steady-state

concentration of active chlorine was adjusted through changes in the solution pH. The difference between active chlorine concentration at the entrance to the cell and that at the exit was less than 2.6 % for $c_{2,c}$ = 0.1 mol dm^{-3}. The current efficiency presented in Fig. 1 was determined by the mean of the inlet and outlet concentrations. A difference of less than 0.1 % was found between the current efficiency calculated from the inlet concentration and that from the outlet concentration. This suggests that the electrochemical cell equipped with a 25 cm high anode acted practically as an ideal stirred reactor.

The diagram in Fig. 2 shows the agreement between the experimental values for current efficiency and the theoretical values calculated using Eq. (31), which confirms the validity of the mathematical model.

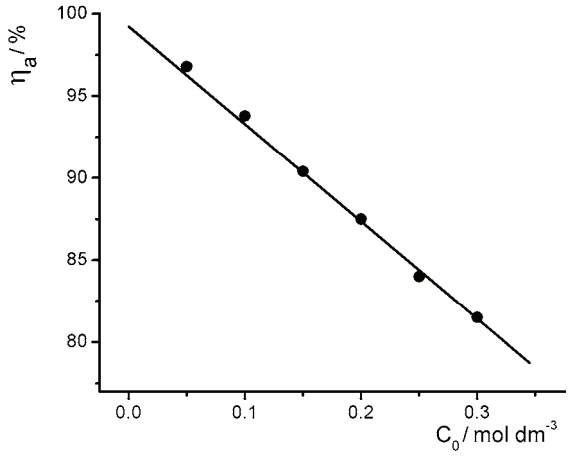

Fig. 2. Anodic current efficiency, η_a, as a function of active chlorine concentration c_0 (300 g dm^{-3} NaCl, 3 g dm^{-3} $Na_2Cr_2O_7$, t = 80 °C, j = = 300 mA cm^{-2}, v = 50 cm s^{-1}, L = = 25 cm): (—) theoretical values derived from Eq. (31) and ● – experimental values.

Industrial chlorate cells have considerably larger anodes. Therefore, the active chlorine concentration in these cells increases from the entrance through to the exit. Vogt[26] set up a mathematical model for the anodic current efficiency in the chlorate cell process, assuming that the hypochlorite bulk concentration in the cell exhibited a linear axial increase.

Later, Vogt[27] established the true axial concentration profile taking into account the interaction between the current density and gas volume fraction, the resulting variation in the flow velocity and the mass transfer of hypochlorite. The true profile was close to the linear profile, and it could be concluded that the linear profile assumption is a satisfactory model assumption.

The increase in the amount of gas bubbles of cathode-evolved hydrogen from the entrance to the exit decreases the local current density in the same direction.

In industrial cells under steady-state conditions, the local densities change by up to 5 %. In the current density range between 150 and 500 mA cm^{-2}, changes

in current density of 5 % have practically no effect on the current efficiency, as illustrated by Eq. (31).

The above considerations show that the axial concentration profile in a chlorate cell can be presented using the following equation:

$$c_{2,l} = \frac{c_{2,\mathrm{h}} - c_{2,\mathrm{c}}}{L} l + c_{2,\mathrm{c}} \tag{32}$$

Combining Eqs. (31) and (32) gives an expression for the current efficiency in the chlorate cell acting as the ideal tubular reactor, where the active chlorine concentration linearly increases from the entrance to the exit:

$$\eta_{\mathrm{a}} = \frac{1 - 0.5 D_2 F \left(j \delta_{\mathrm{a}} \right)^{-1} \left(c_{2,\mathrm{c}} + c_{2,\mathrm{h}} \right)}{1.5 - 0.5 \left(1 + \frac{k_1}{D_1} \delta_{\mathrm{a}}^2 \right)^{-0.5}} \tag{33}$$

Equation (33) was used to determine the theoretical dependences of the current efficiency of chlorate cells on the output concentration of active chlorine. Both the theoretical and experimental values for current efficiencies are presented in Fig. 3.

To ensure identical solution velocity between the electrodes and identical active chlorine production per unit time, four cells differing in anode size (cells a–d) were used in the experiments.

The diagrams in Fig. 3 indicate good agreement between the experimentally obtained values for the anodic current efficiency and the theoretical values calculated using Eq. (33), thus confirming the assumption that the chlorate cell serves as an ideal tubular reactor with a linear axial concentration profile of active chlorine.

Combining the expression for the solution flow rate in the cell:

$$q = vbg = \frac{vAg}{L} \tag{34}$$

and the expression for the amount of active chlorine evolved per unit time:

$$n = \frac{I\tau}{2F} \tag{35}$$

gives the expression for the output concentration of active chlorine:

$$c_{2,\mathrm{h}} = c_{2,\mathrm{c}} + \frac{n}{q} = c_{2,\mathrm{c}} + \frac{j\tau L}{2Fvq} \tag{36}$$

Replacing $c_{2,\mathrm{h}}$ in Eq. (33) with the expression for $c_{2,\mathrm{h}}$ defined by Eq. (36) results in the expression defining the anodic current efficiency as a function of anode height and solution velocity:

$$\eta_a = \frac{1 - D_2 F \left(j\delta_a \right)^{-1} \left[c_{2,c} + j\tau L \left(4Fvg \right)^{-1} \right]}{1.5 - 0.5 \left(1 + \frac{k_1}{D_1} \delta_a^2 \right)^{-0.5}} \quad (37)$$

Equation (37) was used to determine the theoretical dependences of current efficiency on anode height for different input concentrations of active chlorine. These theoretical dependences and the experimentally determined current efficiencies are presented in Fig. 4.

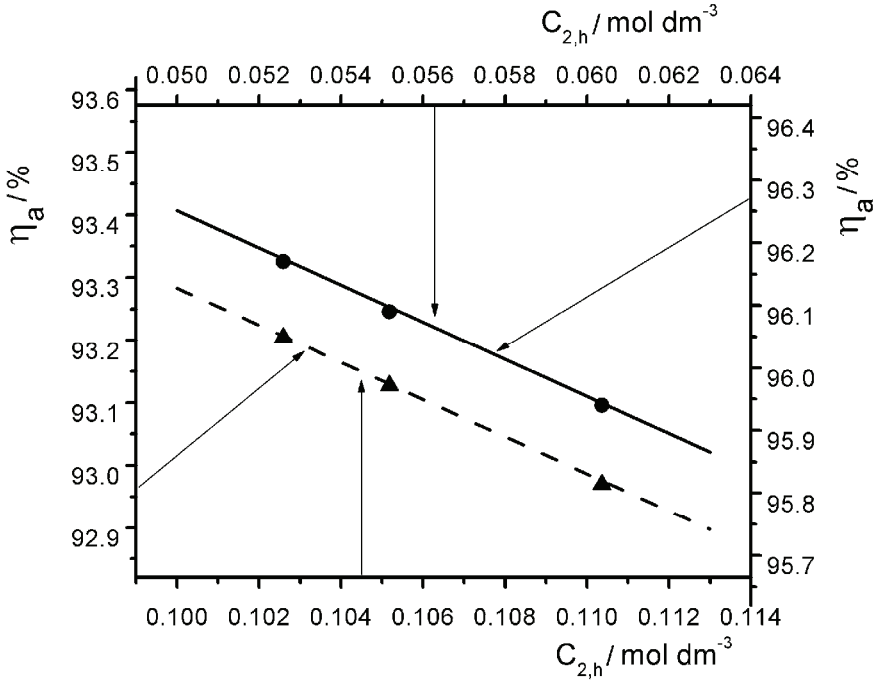

Fig. 3. Anodic current efficiency, η_a, as a function of the output concentration of active chlorine, $c_{2,h}$, for different input concentrations, $c_{2,c}$. Theoretical values derived from Eq. (33) for: $c_{2,c}$ = 0.05 mol dm^{-3} NaClO (—); $c_{2,c}$ = 0.10 mol dm^{-3} NaClO (– – –). Experimental values for: $c_{2,c}$ = 0.05 mol dm^{-3} NaClO (●); $c_{2,c}$ = 0.10 mol dm^{-3} NaClO (▲); (300 g dm^{-3} NaCl, 3 g dm^{-3} $Na_2Cr_2O_7$, t = 80 °C, j = 300 mA cm^{-2}, v = 50 cm s^{-1}).

The good agreement between the theoretical and experimental values for the current efficiency in the chlorate cell process suggests that the established mathematical models could be employed to determine the parameters for the optimisation of both the electrolyser and chlorate plant design.

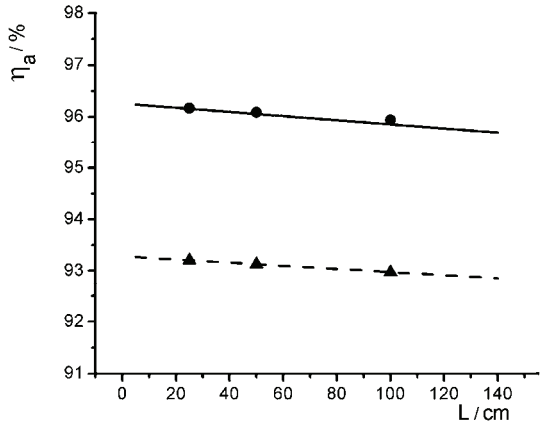

Fig. 4. Anodic current efficiency, η_a, as a function of anode height, L, for different input concentrations of active chlorine, $c_{2,c}$. Theoretical values values derived from Eq. (37) for: $c_{2,c}$ = 0.05 mol dm^{-3} NaClO (—); $c_{2,c}$ = 0.10 mol dm^{-3} NaClO (– – –). Experimental values for: $c_{2,c}$ = 0.05 mol dm^{-3} NaClO (●); $c_{2,c}$ = 0.10 mol dm^{-3} NaClO (▲); (300 g dm^{-3} NaCl, 3 g dm^{-3} $Na_2Cr_2O_7$, t = 80°C, j = 300 mA cm^{-2}, v = 50 cm s^{-1}).

CONCLUSIONS

New mathematical models have been developed to describe current efficiency in the chlorate cell process, both for cells serving as ideal stirred reactors and for those acting as ideal tubular reactors. It was experimentally determined that chlorate cells equipped with short anodes and exhibiting sufficient electrolyte velocity in the inter-electrode gap act as ideal stirred electrochemical reactors. Chlorate cells with a greater anode height behave as tubular reactors with an axial linear concentration profile of active chlorine. Good agreement was obtained between the current efficiency values determined by the established mathematical models and the experimental values.

NOMENCLATURE

c_1 – chlorine concentration, mol dm^{-3};
$\overline{c}_1$ – mean chlorine concentration, mol dm^{-3};
c_2 – active chlorine concentration, mol dm^{-3};
$\overline{c}_2$ – mean active chlorine concentration, mol dm^{-3};
c_0 – active chlorine concentration in the bulk of the solution. mol dm^{-3};
$c_{2,c}$ – active chlorine concentration at the entrance to the cell. mol dm^{-3};
$c_{2,h}$ – active chlorine concentration at the exit from the cell, mol dm^{-3};
$c_{2,l}$ – active chlorine concentration at the height l from the entrance to the cell mol dm^{-3}
D_1 – diffusion coefficient of chlorine, $D_1 = 1.86 \cdot 10^{-5}$ cm^2 s^{-1};
D_2 – diffusion coefficient of active chlorine, $D_2 = 1.86 \cdot 10^{-5}$ cm^2 s^{-1};
δ_a – thickness of anode diffusion layer, $\delta_a = 1.0 \cdot 10^{-2}$ cm;
F – Faraday constant, 96487 C mol^{-1};
n – amount of active chlorine;
k_1 – the rate constant for chlorine hydrolysis, $k_1 = 6.0 \cdot 10^{-3}$ s^{-1};

S – part of the anode surface where old elements of the solution are replaced by new ones per unit of time,
τ – time, s;
t – temperature, °C;
j_a – anodic current density, mA cm^{-2};
I – total current in the cell, mA;
L – anode height, cm;
l – coordinate in the flow direction, cm;
b – anode width, cm;
g – interelectrode distance, g = 0.3 cm;
A – anode surface area, A = 200 cm^2;
v – electrolyte flow velocity in the interelectrode gap;
q – volumetric flow rate of electrolyte in the interelectrode gap, cm^3 s^{-1};
η_a – anodic current efficiency.

Acknowledgement. The authors acknowledge the financial support from the Ministry of Education, Science and Technological Development of the Republic of Serbia, through Project Nos. 172057 and 172062.

И З В О Д

ИСКОРИШЋЕЊЕ СТРУЈЕ ХЛОРАТНОГ ЕЛЕКТРОЛИЗЕРА

МИРОСЛАВ Д. СПАСОЈЕВИЋ[1], ЛЕНКА Ј. РИБИЋ-ЗЕЛЕНОВИЋ[1] и БРАНИСЛАВ Ж. НИКОЛИЋ[2]

[1]*Аīрономски факулīеī, Универзиīеī у Краīујевцу, Цара Душана 34, Чачак и*
[2]*Технолошко–меīалуршки факузлīеī, Универзиīеī у Беоīраду, Карнеīијева 4, Беоīрад*

Постављен је математички модел за искоришћење струје хлоратног електролизера са равномерним транслаторним током раствора дуж анодне површине. Модел важи за електролизере у којима концентрација хипохлорита линерано расте од улаза до излаза. Установљено је добро слагање експериментално одређених вредности и вредности израчунатих на бази математичког модела.

(Примљено 23. октобра 2013, ревидирано 14. јануара, прихваћено 16. јануара 2014)

REFERENCES

1. N. Ibl, D. Landolt, *J. Electrochem. Soc.* **115** (1968) 713
2. D. Landolt, N. Ibl, *Electrochim. Acta* **15** (1970) 1165
3. A. Despić, M. Jakšić, B. Nikolić, *J. Appl. Electrochem.* **2** (1972) 337
4. M. Jakšić, A. Despić, B. Nikolić, *Elektrokhim.* **8** (1972) 1573
5. M. Jakšić, B. Nikolić, M. Spasojević, *Chem. Tech.* **27** (1975) 534
6. M. Jakšić, *Electrochim. Acta* **21** (1976) 1127
7. N. Ibl, H. Vogt, *Inorganic electrosynthesis*, in *Comprehensive treatise of electrochemistry*, J. O'M. Bockris, B. E. Conway, E. Yeager, R. E. White, Eds., Plenum, New York, USA, 1981, p. 167
8. M. Jakšić, *J. Electrochem. Soc.* **121** (1974) 70
9. M. Spasojević, N. Krstajić, M. Jakšić, *Surf. Technol.* **21** (1984) 19
10. D. M. Novak, B. V. Tilak, B. F. Conway, *Fundamental and Applied Aspects of Anodic Chlorine Production*, in *Modern Aspects of Electrochemistry*, J. O'M. Bockris, B. E. Conway, R. E. White, Eds., Pergamon Press, New York, USA, 1982, p. 195
11. N. Krstajić, M. Spasojević, M. Jakšić, *J. Mol. Catal.* **38** (1986) 81

12. M. Spasojević, L. Ribić-Zelenović, P. Spasojević, *Ceram. Int.* **38** (2012) 5827
13. M. Spasojević, T. Trišović, L. Ribić-Zelenović, P. Spasojević, *Hem. Ind.* **67** (2013) 313
14. S. Chen, Y. Zheng, S. Wang, X. Chen, *Chem. Eng. J.* **172** (2011) 47
15. N. Krstajić, V. Nakić, M. Spasojević, *J. Appl. Electrochem.* **21** (1991) 637
16. A. Djordjević, B. Nikolić, I. Kadija, A. Despić, M. Jakšić, *Electrochim. Acta* **18** (1973) 465
17. M. Jakšić, *J. Appl. Electrochem.* **3** (1973) 219
18. U. Č. Lačnjevac, B. M. Jović, Lj. M. Gajić-Krstajić, J. Kovač, V. D. Jović, N. V. Krstajić, *Electrochim. Acta* **96** (2013) 34
19. G. Lindbergh, D. Simonsson, *J. Electrchem. Soc.* **137** (1990) 3094
20. A. Tidblad, G. Lindbergh, *Electrochim. Acta* **36** (1991) 1605
21. A. A. Tidblad, J. Martensson, *Electrochim. Acta* **42** (1997) 389
22. J. Wulff, A. Cornell, *J. Appl. Electrochem.* **37** (2007) 181
23. K. Viswanathan, B. V. Tilak, *J. Elctrochem. Soc* **131** (1984) 1551
24. P. W. Danckwerts, *Ind. Eng. Chem.* **43** (1951) 1460
25. P. W. Danckwerts, *Gas–Liquid Reactions*, McGraw Hill, New York, USA, 1970, p. 247
26. H. Vogt, *J. Appl. Electrochem.* **22** (1992) 1185
27. H. Vogt, *Electrochim. Acta* **39** (1994) 2173.

Journal of the Serbian Chemical Society
JSCS-info@shd.org.rs • www.shd.org.rs/JSCS
J. Serb. Chem. Soc. 79 (6) 689–706 (2014)
JSCS–4619
UDC 546.562'472+547.979.7+541.144.7:
543.51+543.544.5.068.7
Original scientific paper

Electrospray ionization mass spectrometry combined with ultra high performance liquid chromatography in the analysis of *in vitro* formation of chlorophyll complexes with copper and zinc

JELENA B. ZVEZDANOVIĆ[1], SANJA M. PETROVIĆ[1], DEJAN Z. MARKOVIĆ[1]*, TATJANA D. ANDJELKOVIĆ[2#] and DARKO H. ANDJELKOVIĆ[3]

[1]*University of Niš, Faculty of Technology, Bulevar Oslobodjenja 124, Leskovac, Serbia,* [2]*University of Niš, Faculty of Science, Department of Chemistry, Višegradska 33, Niš, Serbia and* [3]*JKP Naissus, Kneginje Ljubice 1/1, Niš, Serbia*

(Received 18 September 2013, revised 22 January, accepted 23 January 2014)

Abstract: The aim of this study was to obtain a more accurate insight into the interaction of the major photosynthesis pigment, chlorophyll (Chl), with copper(II) and zinc(II) in solution using flow injection analysis combined with electrospray ionization mass spectrometry (FIA–ESI-MS), as well as combined with ultra high performance liquid chromatography with DAD detection (UHPLC-DAD). These interactions may potentially, but not necessarily, lead to the formation of Cu–Chl and Zn–Chl complexes of two different types, which has a large number, at least, disfunctional implications in the plant world. The results based on analysis of full-scan and MS/MS spectra, with and without UHPLC chromatograms, confirmed the formation of a "central type" Cu–Chl complex and a "central type" Zn–Chl complex, as well as proved the formation of a "peripheral" Zn–Chl complex, the latter one originating from a very weak coordinative interaction at the edge of the Chl structure. The employed techniques appeared to be efficient and reliable tools for studying the formation and stability of heavy metals complexes with chlorophyll, at least *in vitro*, with a considerable possibility for an assessment of real bioenvironmental behavior.

Keywords: chlorophyll; heavy metals; complexes; mass spectrometry; UHPLC.

INTRODUCTION

Plants and algae easily absorb toxic heavy metals; in the case of high metal concentrations, plants become their hyperaccumulator, such as in the case of cadmium and zinc[1] or nickel.[2] In lower concentrations, many heavy metals, such as copper and zinc, are essential micronutrients for higher plants and algae, and

* Corresponding author. E-mail: dejan_markovic57@yahoo.com
# Serbian Chemical Society member.
doi: 10.2298/JSC130918009Z

furthermore, a small Cu-protein, plastocyanin, is one of the integrative part of the electron-transport chain (ECL) of the photosynthetic apparatus of plants, connecting the photosystems I and II;[3] on the other hand zinc-porphyrins are formed during chlorophyll biosynthesis.[4] However, high external concentrations of copper and zinc may lead to many damaging effects. Zinc may be included in degradation of stromal proteins of chloroplasts.[5] Copper may affect all kinds of photosynthetic activities, such as electron transport and ATP production,[6,7] and oxygen evolution.[8] Other disrupting or toxic effects of zinc and copper on plants (and other heavy metals) were reviewed by Nagajyoti *et al.*[9] *In vivo* experiments showed that the substitution of the central magnesium (Mg) atom in chlorophyll (Chl), a major photosynthesis pigment, by heavy metals (already observed *in vitro*) may be one of the principal causes for their permanent damaging effects on the photosynthesis apparatus. Thus, the formation of chlorophyll–heavy metal complexes (Chl–HMS), even in minor proportions relative to the total Chl content, may inhibit photosynthesis completely.[10] The consequences of Chl–HMS for higher plants and green algae were discussed in details by Küpper *et al.*[10–13]

In two previous reports, the formation of copper and zinc complexes with chlorophyll *in vitro* (*i.e.*, Cu(II)–Chl and Zn(II)–Chl complexes, respectively) was proven by Vis, FTIR and fluorescence spectroscopy,[14] as well as the formation of Cu–Chl complexes in isolated photosynthetic organelles, chloroplasts, and sub-organelles, thylakoids (*ex vivo*), while the formation of the Zn–Chl counterpart was sterically prevented.[15] In a recent study, the stability of these two complexes to UV-B radiation was investigated *in vitro* and compared to those obtained with pheophytin and mesoporphyrin.[16] The higher stability of the Cu–Chl (compared to Zn–Chl) obtained confirmed the conclusions from a previous report,[14] *i.e.*, that copper forms a relatively stable "central type" of complex with Chl, with Cu(II) replacing Mg(II) in the center of the porphyrin nucleus. On the other hand, based on existing FTIR data,[14] the possible formation of a very unstable Zn–Chl chelate complex in an excess of Zn(II) ions could only be supposed, as the consequence of Zn-coordinative interactions at the edge of the Chl isocyclic cyclopentanone ring (Fig. 1), between the position of C-13^1 and C-13^3. The "central" complexes are thermodynamically favored, but the "peripheral step" may occur before their formation, and this is more enhanced in the case of Zn–Chl than in the case of Cu–Chl.[17]

Confirmation concerning the formation of Cu–Chl and Zn–Chl complexes are still rare. In the present study, the electrospray ionization mass spectrometry (ESI-MS) method was employed to provide additional proof for the formation of complexes, which should provide a deeper insight into the stabilities of the two complexes.

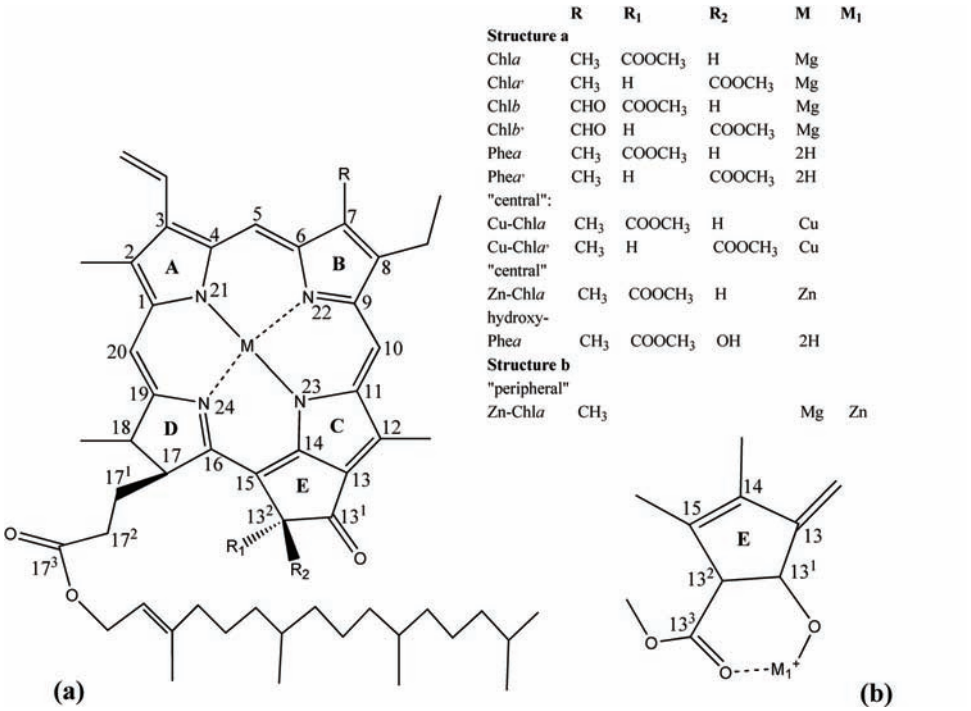

	R	R_1	R_2	M	M_1
Structure a					
Chl*a*	CH_3	$COOCH_3$	H	Mg	
Chl*a*′	CH_3	H	$COOCH_3$	Mg	
Chl*b*	CHO	$COOCH_3$	H	Mg	
Chl*b*′	CHO	H	$COOCH_3$	Mg	
Phe*a*	CH_3	$COOCH_3$	H	2H	
Phe*a*′	CH_3	H	$COOCH_3$	2H	
"central":					
Cu-Chl*a*	CH_3	$COOCH_3$	H	Cu	
Cu-Chl*a*′	CH_3	H	$COOCH_3$	Cu	
"central"					
Zn-Chl*a*	CH_3	$COOCH_3$	H	Zn	
hydroxy-					
Phe*a*	CH_3	$COOCH_3$	OH	2H	
Structure b					
"peripheral"					
Zn-Chl*a*	CH_3			Mg	Zn

Fig. 1. Structures of some of the main chlorophyll derivatives considered in this paper.

Recently, the employment of the ESI-MS method for a study of the interactions of chromium(III) with a series of *O*-donor humic ligands in solution was reported as informative and proved the advantages of this method for investigations of metal–ligand interactions.[18] Pursuing this goal, in the present study an attempt was made to obtain deeper insight into the formation and stability of Cu–Chl and Zn–Chl complexes using the same method.

EXPERIMENTAL

The formation of heavy metal complexes of chlorophyll, Chl–HMS, may occur under low light (“shade reaction”) and under high light conditions (“sun reaction”).[13] Since only just a minority of antenna chlorophylls (*in vivo*) is accessible to Chl–HMS formation under high light conditions,[13] the experimental procedure described below was performed under shade conditions as much as possible, inside vessels and equipment covered with aluminum foil or black cloth.[19]

Isolation of chlorophylls

Extraction of plant pigments from spinach leaves, *Spinacia oleracea* L. (from the local market), was performed using a previously published method,[20] by extraction with a mixture of methanol and petroleum ether in a 2:1 volume ratio, and a petroleum ether and diethyl ether (1:1 volume ratio) mixture used for re-extraction. The final extract was a mixture of pigments containing large amounts of various chlorophyll forms, as well as accessory pigments and carotenoids (carotenes and xanthophylls).[20] The chlorophyll fraction, a purified mixture of

various chlorophyll forms (predominantly Chl*a* and Chl*b*), was isolated from the pigment extract using open column chromatography with silica gel as the adsorbent (silica gel 60, Merck, 0.063–0.200 mm) and an *n*-hexane/acetone mixture as the eluent.[21] The chlorophyll fraction eluted at an eluent composition of 10:1 (*n*-hexane/acetone, v/v, respectively).[21] The total Chl content (Chl*a* + Chl*b*) in the isolated Chl-fraction was calculated as reported.[22]

Copper and zinc interaction with chlorophyll – preparation of the complexes (Cu–Chl and Zn–Chl)

Heavy metal complexes with chlorophyll, HMS–Chl (Cu–Chl and Zn–Chl), were prepared using an already published method.[16] The solvent was removed from the Chl-fraction at room temperature and the remaining solid was dissolved in ethanol/water mixture (95:5 volume ratio), to which a solution of $CuSO_4$, or $ZnSO_4$, was added. The final reaction mixture, Cu-treated or Zn-treated chlorophyll fraction, contained 5.0 mM of $CuSO_4$, or $ZnSO_4$, respectively, and 5 μM of chlorophylls (Chl*a* and Chl*b*). The reaction of the Chl molecules with Zn(II), or Cu(II) was performed by heating the reaction mixture in a reflux apparatus for 1 h at 40 °C, followed by 24 h at room temperature. The Cu-treated and Zn-treated Chl--fractions as the final solutions contained Cu–Chl and Zn–Chl complexes, as well as remaining chlorophylls and degradation products of the chlorophyll.[1,2] These solutions were used for the analyses following the hereinafter described procedures. The chlorophyll-fraction was analyzed in acetonitrile solution.

Flow injection electrospray ionization mass spectrometry analysis

Flow injection ESI-MS and MS/MS experiments were performed on an LCQ Deca ion trap mass spectrometer (Thermo Finnigan, USA) operating in the positive ion mode by introducing the samples directly into the ion source *via* a syringe pump using the following conditions: applied flow rate, 5 μl min^{-1}; capillary voltage, 24 V; capillary temperature, 200 °C; tube lens voltage, 15 V; sheath gas flow (N_2), 18 (arbitrary units). The MS-spectra were acquired by full range covering the scale *m*/*z* 100–1000. For the fragmentation study, MS/MS experiments were performed by deploying collision-induced dissociation (CID) with the normalized collision energy of the collision-induced dissociation set at 30 and 35 eV.

Ultra high performance liquid chromatography-diode array-electrospray ionization mass spectrometry analysis

The liquid chromatography (ultra high performance chromatography – UHPLC) runs were realized using a Dionex Ultimate 3000 UHPLC+ system equipped with a diode array (DAD) detector and connected with LCQ Fleet Ion Trap Mass Spectrometer, Thermo Fisher Scientific, Germany. The separations were performed on a Hypersil gold C18 column (50×2.1 mm, 1.9 μm) from the same producer, at a 25 °C temperature. The mobile phase consisted of (A) methanol and (B) acetonitrile. A linear gradient program at a flow rate of 0.200 ml min^{-1} consisting of 0–0.75 min from 10 to 40 % (B), followed by 0.75–1.5 min to 50 % (B), 5–6 min from 50 to 10 % (B) and finishing with 10 % (B) for 4 min. An injection volume of 5 μl was used.

UV–Vis spectra were recorded on DAD-detector (with total range between 200 and 800 nm), set at two detection wavelengths, λ_{det}, 430 and 660 nm, simultaneously. The mass spectrometric analysis was performed using a LCQ 3D-ion trap mass spectrometer with electrospray ionization (ESI) operating in positive ion mode as the method of identification. The ESI-source parameters were as follows: source voltage, 4 kV; capillary voltage, 37 V; tube lens voltage, 110 V; capillary temperature, 200 °C; sheath and auxiliary gas flow (N_2), 18 and 8 (arbitrary units), respectively. The MS-spectra were acquired by full range acquisition in the

m/*z* range 100–1000. For fragmentation study, a data dependant scan was performed deploying collision-induced dissociation (CID). The normalized collision energy of the CID cell was set at 35 eV.

The cone voltage, applied to the source, can have a considerable impact on the fragmentation pattern of an ionized molecule; common ESI-MS findings of sodium (Na) or potassium (K) ion adducts with the molecules, giving shift in the corresponding peaks by 23 or 39 units, respectively, were observed together with the major fragmentation ions.[23,24] It is also common to see addition of one or more protons to the molecular ions and the corresponding Na or K adducts.[23] In some reports on fast atom bombardment (FAB) in combination with MS/MS investigations, the same effects were observed.[25]

Complexes of chlorophyll with copper and zinc were identified according to their mass spectra, and characteristic ion fragmentation within selected peaks from the corresponding UHPLC chromatogram. Xcalibur software (version 2.1) was used for instrument control, data acquisition and data analysis, as well as for the simulation of some MS spectra.

All solvents used in the experiments were of HPLC or LC–MS grade. Methanol and acetonitrile used in UHPLC–MS experiments (LC–MS grade) were purchased from Baker, The Netherlands and Fisher Scientific, UK, respectively. Crystalline copper(II) sulfate pentahydrate and zinc sulfate heptahydrate were purchased from Sigma–Aldrich, Germany.

RESULTS AND DISCUSSION

The full scan mass spectra (obtained by the flow injection technique) of the investigated Chl-fraction, and the Cu- and the Zn-treated Chl-fractions are shown in Fig. 2a, b and c, respectively; the full list of the main compounds found in the chlorophyll, Cu- and Zn-treated Chl-fractions with their assignments, as well as the MS/MS spectra are given in Table I.

Chromatogram of the Cu-treated Chl-fraction, obtained from the DAD signal at a detection wavelength, $\lambda_{det.}$ = 430 nm, is shown in Fig. 3a; the corresponding Vis spectrum of the main observed peak in the chromatogram, assigned as the "central" Cu–Chl*a* complex is shown in Fig. 3b. The MS/MS spectrum of the peak belonging to the anticipated "central" Cu–Chl*a* complex, with a retention time, $t_{ret.}$ = 4.77 min, is shown in Fig. 3c; the proposed fragmentation pattern for this complex is shown in Fig. 4.

The chromatogram of the Zn-treated Chl-fraction, obtained from the DAD signal at a detection wavelength, $\lambda_{det.}$ = 430 nm, is shown in Fig. 5.

The main identified Chl-derivatives with their full chromatographic ($t_{ret.}$), Vis spectroscopic (λ_{max}) and MS (*m*/*z*) parameters found using UHPLC-DAD–MS/MS data are listed in Table II. The information from the spectral data agrees basically with the published data (given in Table II).

The Chl derivatives containing magnesium, zinc, copper could be mutually distinguished by molecular weight and by the isotope pattern of the molecular ions. If no metal was present, the molecular weight was lower and the isotope pattern was simpler than that of the derivatives containing metals. As copper has two natural isotopes, ^{63}Cu (69.17 %) and ^{65}Cu (30.83 %) and magnesium has three natural isotopes, ^{24}Mg (79.0 %), ^{25}Mg (10.0 %), and ^{26}Mg (11.0 %), whereas

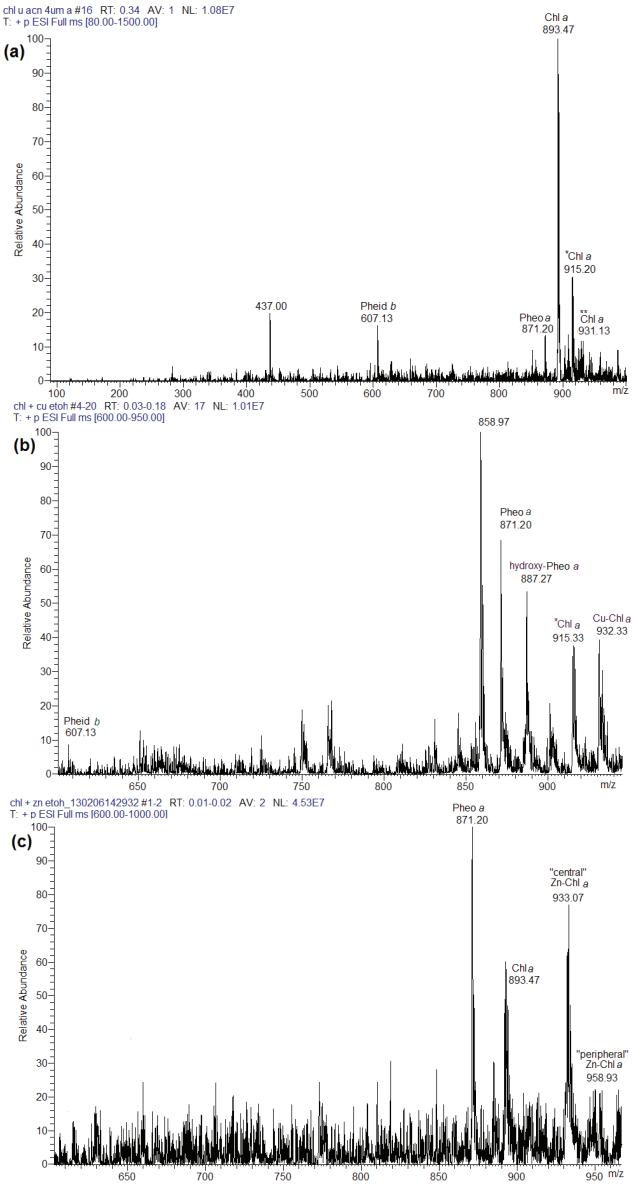

Fig. 2. Full scan MS spectra of the Chl-fraction (a), the Cu-treated Chl-fraction (b) and the Zn-treated Chl-fraction (c) obtained in the flow injection ESI-MS experiments. The main observed peaks correspond to molecular ions assigned as various Chl-derivatives. Molecular ions representing adduct-ions of Chl*a* with Na and K (at *m*/*z* 915 and 931, labeled as * and **, respectively) were observed in the full scan MS spectrum of the Chl-fraction (a); a similar situation was also observed in the Cu-treated Chl-fraction (b). A full list of the corresponding ESI-MS/MS data chosen for some of the main peaks found in the full scan MS are listed in Table I.

TABLE I. Flow injection ESI-MS/MS data of the main compounds found in the Chl-fraction, and the Cu- and Zn-treated Chl-fraction in ethanol

Compound	$[M]^+$	$[M]^+$	Main observed fragment-ions *m*/*z*	Proposed structure of the fragment-ions[b]
	Found MW/(*m*/*z*)	Average calculated MW/(*m*/*z*)[a]		
Chlorophyll *a*	893.47 (100 %)	893.50	615 $[M–278]^+$	$[M–C_{20}H_{38}]^+$
			555 $[M–338]^+$	$[M–C_{20}H_{39}CO_2CH_3]^+$
Pheophytin *a*	871.20 (100 %)	871.21	839 $[M–32]^+$	$[M–CH_3OH]^+$
			811 $[M–60]^+$	$[M–HCO_2CH_3]^+$
			593 $[M–278]^+$	$[M–C_{20}H_{38}]^+$
			533 $[M–338]^+$	$[M–C_{20}H_{39}CO_2CH_3]^+$
Pheophorbide *b*	606.39 (100 %)	606.67	574 $[M–32]^+$	$[M–CH_3OH]^+$
			548 $[MH–59]^+$	$[MH–CO_2CH_3]^+$
“Central” Cu–Chl*a*	932.33	932.74	900 $[M–32]^+$	$[M–CH_3OH]^+$
			654 $[M–278]^+$ (100 %)	$[M–C_{20}H_{38}]^+$
			593 $[M–339]^+$	$[M–C_{20}H_{39}CO_2CH_3–H]^+$
			521 $[M–411]^+$	$[M–C_{20}H_{39}CO_2CH_2CH_2––CO–HOCH_3]^+$
„Central“ Zn–Chl*a*	934.13	934.58	902 $[M–32]^+$	$[M–CH_3OH]^+$
			656 $[M–278]^+$ (100 %)	$[M–C_{20}H_{38}]^+$
„Peripheral“ Zn–Chl*a*	958.60	957.875	900 $[M–59]^+$ (100 %)	$[M–CO_2CH_3]^+$
			681 $[M–278]^+$	$[M–C_{20}H_{38}]^+$

[a]The calculated molecular masses are average values bearing in mind the isotopic abundances of each element in the proposed formula; [b]structures of the proposed fragments obtained from the literature.[25-32]

there are five isotopes of zinc, ^{64}Zn (48.6 %), ^{66}Zn (27.9 %), ^{67}Zn (4.1 %), ^{68}Zn (18.8 %) and ^{70}Zn (0.6 %), the molecular ion (M^+) of Zn–Chl derivatives was significantly broader than those of the corresponding Cu- or Mg- derivatives.[26] Software simulated spectra were compared with the experimental spectra to confirm, relativize or to reject the isotope distribution of the M^+ peaks in the full-MS experimental spectra, both flow injection and UHPLC-MS. Good agreement was found for all the investigated compounds (not shown). For example, for M^+ of “central” Cu–Chl*a* complex, a mass distribution in the *m*/*z* range 931.48 to 936.49 was found by simulation, and in flow injection MS/MS experiment, an M^+ ion at *m*/*z* 932.33 was detected.

Positive mode MS-fragmentation of the chlorophylls – a general pattern

The most abundant fragment ions in the positive mode MS/MS spectra of the different Chls usually originated from fragmentation at the C-17 and C-13 positions (Fig. 1). The former one results either in a loss of a phytyl chain (the phytadiene structure, $C_{20}H_{38}$) or in the loss of the whole $C_{20}H_{39}CO_2CH_3$ group, which

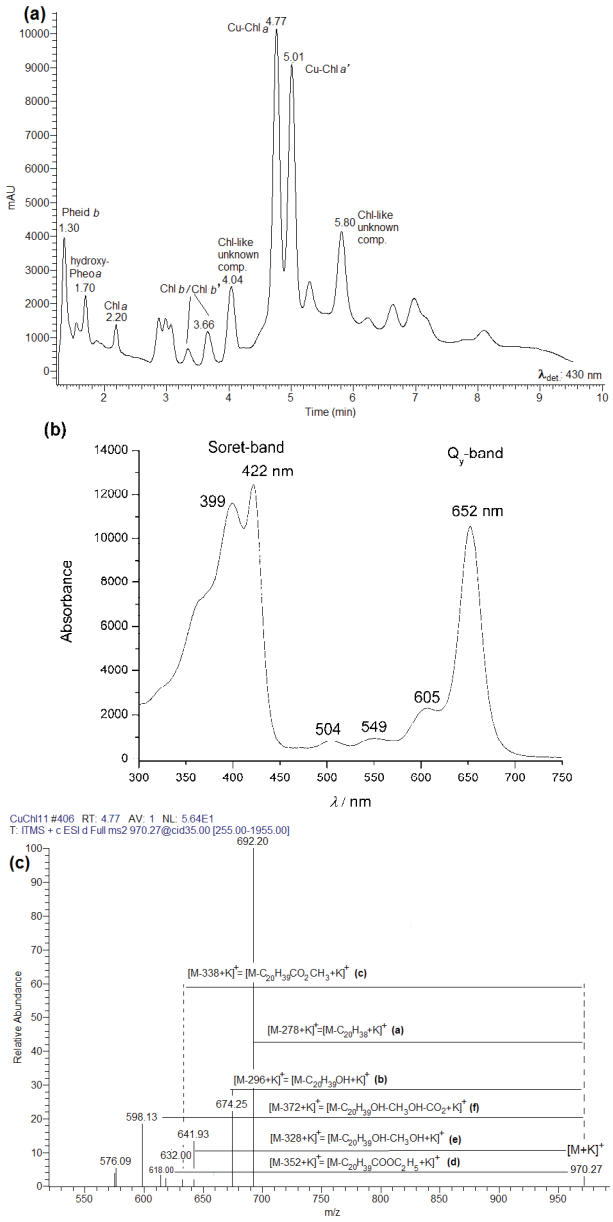

Fig. 3. Chromatogram of the Cu-treated Chl-fraction obtained from the UHPLC-DAD signal at 430 nm (a). The corresponding UV–Vis spectrum (taken from the DAD-signal (b) and the MS/MS spectrum (obtained from the UHPLC-ESI/MS measurements) by CID fragmentation of the main product, $t_{ret.}$ = 4.77 min, assigned as the "central" Cu–Chl*a* complex (c). The corresponding structure assignments are shown in Fig. 1. A possible scheme of the fragmentation pattern (linked to Fig. 3c) is shown in Fig. 4. The remaining chromatographic, UV–Vis and MS data are given in Table II.

TABLE II. UHPLC-DAD-ESI-MS/MS characterization of the main compounds found in the Chl-fraction and Cu- and Zn-treated Chl-fractions in ethanol

Assignment of the peaks	t_{ret} min	Absorbance maxima in the mobile phase[a], nm			$[M]^+$ Found MW/(*m/z*)	$[M]^+$ Average calculated[b] MW/(*m/z*)	Main observed fragment-ions in MS/MS spectra	
		I	Soret II	Q_y III			*m/z*	Proposed structure of the fragment-ions[c]
Pheophorbide *b*	1.30	–	407	665	$[MH]^+$ 607.31	606.67	575 $[MH-32]^+$ 547 $[M-59]^+$ (100%)	$[MH-CH_3OH]^+$ $[M-CO_2CH_3]^+$
Hydroxy-pheophytin *a*	1.70	–	446	650	887.20	887.21[d]	469 $[M-418]^+$	–
Chlorophyll *a* Chlorophyll *a*'	2.20 2.37	411	431	665	893.47	893.50	615 $[M-278]^+$ (100%) 555 $[M-338]^+$	$[M-C_{20}H_{38}]^+$ $[M-C_{20}H_{39}CO_2CH_3]^+$
Chlorophyll *b* Chlorophyll *b*'	3.36 3.66	–	435	654	907.37	907.50	553 $[M-354]^+$ (100%)	$[M-C_{20}H_{39}CO_2CH_3-CH_3-H]^+$
Pheophytin *a* Pheophytin *a*'	4.58 5.06	–	408	666	871.53	871.21	839 $[M-32]^+$ 811 $[M-60]^+$ 593 $[M-278]^+$ (100%) 533 $[M-338]^+$ 460 $[M-411]^+$	$[M-CH_3OH]^+$ $[M-CO_2CH_3-H]^+$ $[M-C_{20}H_{38}]^+$ $[M-C_{20}H_{39}CO_2CH_3]^+$ $[M-C_{20}H_{39}CO_2CH_2CH_2-CO-HOCH_3]^+$

TABLE II. Continued

Assignment of the peaks	$t_{ret.}$ min	Absorbance maxima in the mobile phase[a], nm			$[M]^+$ Found MW/(m/z)	$[M]^+$ Average calculated[b] MW/(m/z)	Main observed fragment-ions in MS/MS spectra	
		I	Soret II	Q_y III			m/z	Proposed structure of the fragment-ions[c]
„Central“								
Cu-Chlorophyll *a*	4.77	399	422	652	$[M+K]^+$[e]	$[M+K]^+$	692 $[M-278+K]^+$	$[M-C_{20}H_{38}+K]^+$
Cu-Chlorophyll *a*'	5.01				970.27	971.87	(100%)	
							674 $[M-296+K]^+$	$[M-C_{20}H_{39}OH+K]^+$
							642 $[M-328+K]^+$	$[M-C_{20}H_{39}OH-CH_3OH+K]^+$
						$[M]^+$	632 $[M-338+K]^+$	$[M-C_{20}H_{39}CO_2CH_3+K]^+$
						932.74	618 $[M-352+K]^+$	$[M-C_{20}H_{39}CO_2C_2H_5+K]^+$
							598 $[M-372+K]^+$	$[M-C_{20}H_{39}OH-CH_3OH-CO_2+K]^+$
“Central“[f]								
Zn-Chlorophyll *a*	2.80	410	426	658	$[M+Na]^+$	$[M+Na]^+$	677 $[M-278+Na]^+$	$[M-C_{20}H_{38}+Na]^+$
					955.25	957.57	645 $[M-310+Na]^+$	$[M-C_{20}H_{39}-CH_3O+Na]^+$
					$[M]^+$	$[M]^+$	601 $[M-354+Na]^+$	$[M-C_{20}H_{39}CO_2CH_3-CH_3-H+Na]^+$
					933.33	934.58	(100%)	
„Peripheral“								
Zn-Chlorophyll *a*	5.85	402	423	652	957.95	957.875	679 $[M-279]^+$	$[M-C_{20}H_{38}-H]^+$
							(100%)	
							603 [M-355]+	

[a]Absorbance maxima wavelengths were compared with the ones given in the literature;[29,36,38,40,41] [b]calculated molecular masses are average values keeping in mind isotopic abundances of each element in the proposed formula; [c]structures of the proposed fragments taken from the literature;[25–28,30,32] [d]literature value;[7] [e]MS/MS spectra of the molecular ion peaks at m/z 971.2 were also recorded, but are not shown in this table due to the poor fragmentation found; [f]the presence of m/z 933 and 970 peaks in the full-MS at $t_{ret.}$ = 2.8 min is typical for the “central” Zn-Chl*a* and Zn-Chl*a*–dihydrate complexes, respectively.[40] Species at m/z 955, considered as “central” Zn–Chl*a* adducts with Na, were also found. The CID-fragmentation was found only for m/z 955 species

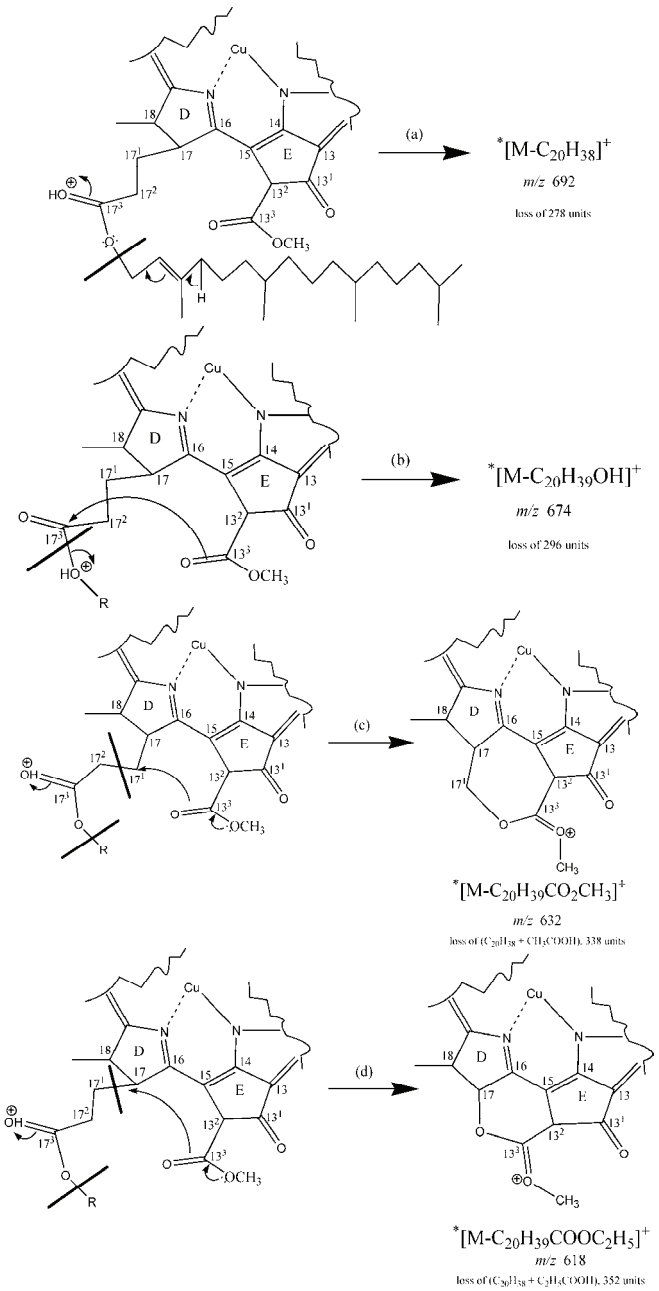

Fig 4. A proposed fragmentation pattern for the main observed compound in the Cu-treated Chl-fraction assigned as the "central" Cu–Chl*a* complex (Cu–Chl*a* and Cu–Chl*a*′), found at $t_{ret.}$ = 4.77 and 5.01 min, respectively, in the UHPLC chromatogram, based on DAD and MS/MS data. *The molecular-ion and the peaks of the fragment-ions correspond to adducts of Chl*a* with K (the corresponding masses are 39 mass units higher).

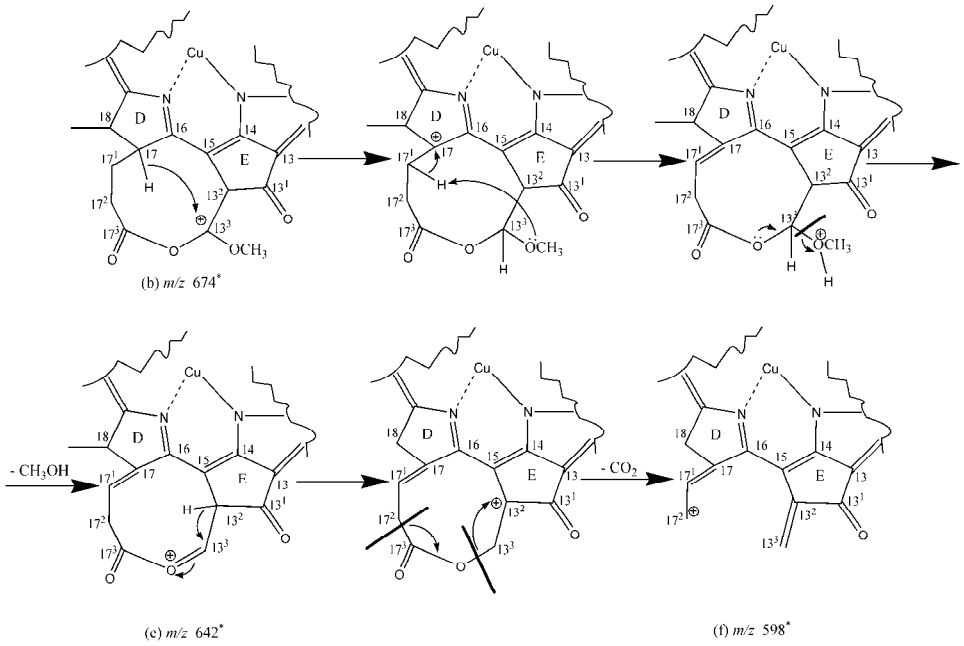

Fig 4. (Continued) A proposed fragmentation pattern for the main observed compound in the Cu-treated Chl-fraction assigned as the "central" Cu–Chl*a* complex (Cu–Chl*a* and Cu–Chl*a*′), found at $t_{ret.}$ = 4.77 and 5.01 min, respectively, in the UHPLC chromatogram, based on DAD and MS/MS data. *The molecular-ion and the peaks of the fragment-ions correspond to adducts of Chl*a* with K (the corresponding masses are 39 mass units higher).

appears in the MS/MS spectrum at *m*/*z* values corresponding to $[M–C_{20}H_{38}]^+$ = = $[M–278]^+$ and $[M–C_{20}H_{39}CO_2CH_3]^+$ = $[M–338]^+$, respectively.[27] The latter one (C-13 position) is result of a loss of CH_3OH (in the C-13^3 position) or, of the whole ester-group ($COOCH_3$ in the C-13^2 position, Fig.1), which appears in the spectrum at *m*/*z* values corresponding to $[M–CH_3OH]^+$ = $[M–32]^+$ and $[M–COOCH_3]^+$ = $[M–59]^+$, respectively.[28] The list of the obtained data presented in Tables I and II, includes, among all, the peaks resulting from a loss of 278, 338, 32 and 59 fragments.

Flow injection ESI-MS/MS spectra of Chl-, Cu- and Zn-treated Chl-fraction

Peaks at the *m*/*z* values corresponding to the molecular weights of the different Chls, such as chlorophyll *a* (Chl*α*, at 893.47) and pheophytin *a* (Pheo*a*, at 871.20), were observed in the full-MS spectra of all three samples, Chl-fraction, Cu-treated and Zn-treated Chl-fraction, as shown in Fig. 2a–c, respectively; pheophorbide *b* (Pheid*b*, at 607.13) was observed in the Chl-fraction and the Cu-treated Chl-fraction, as shown in Fig. 2a and b, respectively. On the other hand, several other peaks were also observed at *m*/*z* 858.97, 887.27, 932.33 in the Cu-treated, and at *m*/*z* 933.07, 958.93 in the Zn-treated Chl-fraction (Fig. 2b and

c, respectively). These peaks belong to hydroxy-Pheo*a* (887.27) and the "central" Cu–Chl*a* complex (932.33) in the Cu-treated Chl-fraction; the peak at *m*/*z* 858.97 (not assigned) belongs to an unknown compound (Fig. 2b). Peaks at *m*/*z* 933.07 and 958.93 found in the Zn-treated Chl-fraction (Fig. 2c) could belong to the "central" and "peripheral" chelate Zn–Chl*a* complexes, respectively. The peaks at 915 (Fig. 2a and b) and *m*/*z* 931 (Fig. 2a) are assigned as "cluster" or "adduct" ion peaks, *i.e.*, M^+ peaks of Chl*a* with metals such as Na and K, respectively.[23,24]

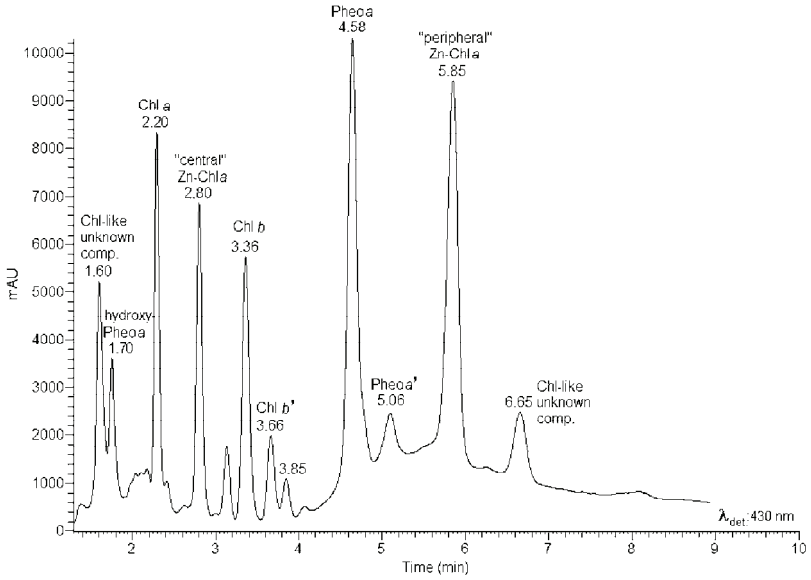

Fig. 5. Chromatogram of the Zn-treated Chl-fraction, obtained from the UHPLC-DAD signal at 430 nm. The remaining chromatographic, UV–Vis and MS data are listed in Table II.

The data taken from corresponding MS/MS spectra of the compounds found by the flow injection ESI-MS in the full scan MS spectra (given in Table I) implies fragmentation which is in agreement with the loss of groups from the C-17 and C-13 positions in the basic Chl structure shown in Fig. 1.[26–30] For example the MS/MS spectrum of *m*/*z* 893.47 (M^+) yielded fragments at 615 and 555, among the most abundant ones (Table I). The two peaks correspond to the fragmentation of the Chl*a* molecule in the C-17 position (shown in Fig. 1) with the loss of $C_{20}H_{38}$ ($[M–278]^+$) and $C_{20}H_{39}CO_2CH_3$ ($[M–338]^+$), respectively, which is in agreement with other reports.[27] On the other hand, the peak at *m*/*z* 932.33 from the Cu-treated Chl-fraction gave as the most abundant fragment in the MS/MS spectrum an ion at *m*/*z* 654 (Table I): the loss of 278 units corresponds to phytadiene, $C_{20}H_{38}$, in the C-17[3] position of the "central" Cu–Chl complex (structure shown in Fig. 1a), proving its formation in the fraction. In addi-

tion, a similar group of fragments was previously found, but in the negative mode MS/MS spectrum, originating from the molecular ion M^- at *m*/*z* 931.5, assigned as the "central" Cu–Chl*a* complex, in the extract of bright green table olives (which is called "Cu–pheophytin *a*").[29]

The peaks at *m*/*z* 933.07 and 958.93 found in Zn-treated Chl-fraction were assigned as the "central" and "peripheral" Zn–Chl*a* complexes (full-MS spectrum is given in Fig. 2c). The corresponding MS/MS fragments of the peak at *m*/*z* 934.13 (the "central" Zn–Chl*a*), 902 ($[M–32]^+ = [M–CH_3OH]^+$) and, as the most abundant, at 656 ($[M–278]^+ = [M–C_{20}H_{38}]^+$), as shown in Table I, are similar to the one found (for the Zn–Chl*a* complex) in Chl solutions subjected to FAB (fast atom bombardment)[26] as well as to APCI (atmospheric pressure chemical) ionization combined with collision activation and tandem mass spectrometry,[30] (marked as Zn–pheophytin *a* in the related papers).[26,30] On the other hand, the corresponding MS/MS fragments of the peak at *m*/*z* 958.60 (the "peripheral" Zn–Chl*a* complex) were found at *m*/*z* 900 ($[M–59]^+ = [M–CO_2CH_3]^+$), the most abundant one, and at *m*/*z* 681 ($[M–278]^+ = [M–C_{20}H_{38}]^+$) (Table I). No supporting MS-report was found to date that deals with MS and/or MS/MS fragmentation patterns that could be related to the "peripheral" heavy metal complexes of chlorophyll. However, the possibility for the formation of "peripheral" HMS complexes was already proven in other, not MS-related reports with magnesium[17] and zinc,[14] based on FTIR data.

UHPLC-DAD–ESI-MS/MS experiments

Results of chromatographic analysis (coupled with UV–Vis and MS/MS detection systems) of the investigated samples (Chl-fraction, Cu- and Zn-treated Chl-fractions) generally confirmed the results obtained by above discussed, flow injection ESI-MS/MS analysis (the chromatogram of Cu-treated Chl-fraction shown in Fig. 3a and the other data shown in Table II). The interactions of chlorophyll with zinc and copper were clearly proven.

The most intense peaks in the chromatogram of the Chl-fraction belong to Chl*a* (t_{ret} = 2.20 min), and to Chl*a*′ (Epimer*, $t_{ret.}$ = 2.37 min). The corresponding data from the MS/MS and UV-Vis spectra are presented in Table II. On the other hand, the most intense peaks in the chromatogram of the Cu-treated Chl-fraction (shown in Fig. 3a) found at $t_{ret.}$ = 4.77 and 5.01 min, were assigned to the "central" Cu–Chl*a* and Cu–Chl*a*′ complexes**. The corresponding Vis

* Epimers of chlorophylls (Chls') are almost always present in preparations of chlorophyll and its derivatives and they are naturally present in small amounts in photosynthetic organisms.[22,33] On the other hand, chlorophylls can be, in small amount, converted to the 13^2-epimers (Chls′, Fig. 1a) during the extraction processes.[33-35] Epimers of chlorophylls showed almost identical UV–Vis absorption as well as MS spectral behavior; they could be only separated by chromatography and then identified.[33]

** Epimers of Cu-chlorophyll showed identical UV–Vis absorption and MS spectra (Table II).

spectrum of the compound at $t_{ret.}$=4.77 min is shown in Fig. 3b, which is supported by the available reports.[36–38] A notable hypsochromic effect of the Q_y-band belonging to the "central" Cu–Chl*a* complex ($\lambda_{Qy\text{-}max.}$ = 652 nm, Table II) can be compared to the same band observed for Chl*a* ($\lambda_{Qy\text{-}max.}$ = 665 nm, Table II) already documented in earlier papers.[14–16,39] In addition, the MS/MS spectrum of the compound found at $t_{ret.}$= 4.77 min with mass found at *m*/*z* 970.27 ("central" Cu–Chl*a* complex, the M^+-adduct with potassium, K) is shown in Fig. 3c. The assignment of the fragments as well as a proposed pattern of MS/MS collision-induced fragmentation is shown in Fig. 4. The labels a–f in Fig. 3c correspond to the same labels of different fragmentation steps shown in Fig. 4. It is important to stress the presence of K in both molecular ions as well as in the corresponding fragments peaks in the MS/MS spectrum (Figs. 3c and 4). A major fragment at *m*/*z* 692 ($[M–278+K]^+$), corresponds to the loss of the phytyl moiety, $C_{20}H_{38}$ (Fig. 4a – fragmentation, Fig. 3c – MS/MS).[26,30] The second fragment at *m*/*z* 674 ($[M–296+K]^+$), represents phytyl chain loss at C-17[3] – in a form of phytol, $C_{20}H_{39}OH$ (Fig. 4b – fragmentation, Fig. 3c – MS/MS). The next two fragments (e, *m*/*z* 642 and f, *m*/*z* 598) are formed through a rearrangement of fragment b followed by a loss of CH_3OH and CH_3OH+CO_2, respectively (Fig. 4e and f, Fig. 3c – MS/MS spectrum). The fragment at *m*/*z* 632 ($[M–338+K]^+$) belongs to the loss of the phytyl chain, $C_{20}H_{38}$, and CH_3COOH from the C-17[1] position (Fig. 4c). The fragment at *m*/*z* 618 ($[M–352+K]^+$), corresponds to loss of $C_{20}H_{38}$ and C_2H_5COOH from the C-17 position (Fig. 4d – fragmentation, Fig. 3c – MS/MS). The fragments are also presented in Table II.

The peaks at $t_{ret.}$ = 2.20, 2.80, 3.36, 3.66, 4.58, 5.06 and 5.85 min, belonging to Chl*a*, the "central" Zn–Chl*a* complex, Chl*b*, Chl*b*′, Pheo*a*, Pheo*a*′ and the "peripheral" Zn–Chl*a* complex, respectively, are found in the chromatogram obtained from the Zn-treated Chl-fraction (Fig. 5). The three most abundant peaks at *m*/*z* 933.33, 955.25 and 970.50 dominate in the full scan MS spectrum obtained from the peak at $t_{ret.}$ = 2.80 min; they are assigned to the "central" Zn–Chl*a* complex, $[M]^+$, the $[M+Na]^+$-adduct and $[M·2H_2O]^+$ peaks, respectively. The presence of *m*/*z* 933 and 970 peaks is typical for the "central" Zn–Chl*a* and Zn–Chl*a*-dihydrate complexes, respectively (marked as Zn–pheophytin *a* and Zn–pheophytin *a* dihydrate in the paper by Nurhayati and Suendo.[40] The intensity of the *m*/*z* 970.50 peak is higher than that of the *m*/*z* 933.33 peak, probably due to more preferable existence of the "central" Zn–Chl*a*-dihydrate with coordination number 6, compared to the "central" Zn–Chl*a* complex with coordination number 4.[40] The corresponding MS/MS spectrum of the $[M+Na]^+$ adduct (*m*/*z* 955.25) is related to the peak with $t_{ret.}$ = 2.80 min, and consisted of fragments characterized by the loss of the phytyl chain from the C-17[3] position (Table II, Fig. 1a). On the other hand, the MS/MS spectrum of the anticipated "peripheral" Zn–Chl*a* complex,[14,17] with an M^+ of *m*/*z* 957.95, found at $t_{ret.}$ = 5.85 min,

consisted of two peaks, one at 679 $[M–279]^+$, the most abundant one, and at *m*/*z* 603 $[M–355]^+$ (Table II). The former one obviously originates from separation of a phytyl tail.

CONCLUSIONS

The *in vitro* formation of Cu– and Zn–Chl*a* complexes of both types (the "central" as well as the "peripheral") was confirmed by the UHPLC–ESI-MS method. This is a significant step forward because the formation of "central" Zn–Chl complexes could not be proven by Vis and FTIR spectrometry in earlier reports.[14,15,39] It should not be forgotten that the formation and stability of these complexes under *in vitro* circumstances certainly differs from those existing in *in vivo* plants and algae environments. From this point of view, the probability for the formation of "peripheral" Zn–Chl complexes seems almost negligible, taking into account the aggregated "network" of Chl molecules (both Chl*a* and Chl*b*) inside the antennas of the two photosystems, PSII and PSI.[33] Still, the reliability and high sensitivity of this method makes it an efficient tool to detect not only the formation and existence of complexes but also to study other related processes (stability, dynamics, thermodynamics, *etc*).

Acknowledgements. This work was supported under Projects of the Ministry of Education, Science and Technological development of the Republic of Serbia, Projects No. TR-34012 and OI-172044.

И З В О Д

ЕЛЕКТРОСПРЕЈ ЈОНИЗАЦИОНА МАСЕНА СПЕКТРОМЕТРИЈА КОМБИНОВАНА СА ТЕЧНОМ ХРОМАТОГРАФИЈОМ ВИСОКИХ МОГУЋНОСТИ У АНАЛИЗИ ФОРМИРАЊА КОМПЛЕКСА ХЛОРОФИЛА СА БАКРОМ И ЦИНКОМ, *IN VITRO*

ЈЕЛЕНА Б. ЗВЕЗДАНОВИЋ[1], САЊА М. ПЕТРОВИЋ[1], ДЕЈАН З. МАРКОВИЋ[1], ТАТЈАНА Д. АНЂЕЛКОВИЋ[2] и ДАРКО Х. АНЂЕЛКОВИЋ[3]

[1]*Универзитет у Нишу, Технолошки факултет, Булевар Ослобођења 124, Лесковац,* [2]*Универзитет у Нишу, Природно–математички факултет, Одсек за хемију, Вишеградска 33, Ниш и* [3]*ЈКП Наисус,Кнеginье Љубице 1/1, Ниш*

Циљ овог рада је постизање бољег увида у интеракције хлорофила (Chl), најважнијег фотосинтетског пигмента, са бакром (II) и цинком (II), у раствору, користећи методу јонизационе масене спектрометрије комбиноване са методом течне хроматографије високих могућности са UV–Vis детекцијом (UHPLC-DAD). Ове интеракције могу потенцијално, али не и нужно, довести до формирања два различита типа комплекса хлорофила са бакром и цинком, Cu–Chl и Zn–Chl, редом, које доводе до бројних дисфункција у биљном свету. Резултати овог рада (базирани на анализи спектара добијених методом масене спектрометрије, са применом UHPLC хроматографије и без ње) потврђују формирање „централног типа" Cu–Chl комплекса, као и "централног типа" Zn–Chl комплекса, заједно са доказом о формирању и "периферног типа" Zn–Chl комплекса, који потиче од веома слабе координативне интеракције на ободу структуре молекула хлорофила. Примењен метод се показао као поуздано средство за проучавање формирања и стабилности комплекса тешких метала са хлорофилом, пре свега *in vitro*, али и са значајном могућношћу примене у реалним условима био-окружења.

(Примљено 18. септембра 2013, ревидирано 22. јануара, прихваћено 23. јануара 2014)

REFERENCES

1. H. Küpper, E. Lombi, F. J. Zhao, S. P. McGrath, *Planta* **212** (2000) 75
2. H. Küpper, E. Lombi, F. J. Zhao, G. Wieshammer, S. P. McGrath, *J. Exp. Bot.* **52** (2001) 2291
3. M. Barón, J. B. Arellano and J.L. Gorgé, *Physiol. Plant.* **94** (1995) 174
4. C. A. Rebeiz, P. A. Castelfranco, *Annu. Rev. Plant Physiol.* **24** (1973) 129
5. S. Roulin, U. Feller, *Planta* **205** (1998) 297
6. J. L. Stauber, T. M. Florence, *Mar. Biol*. **94** (1987) 511
7. I. Yruela, G. Montoya, R. Picorel, *Photosynth. Res*. **33** (1992) 227
8. M. Uchimura, A. Rival, A. Nato, R. Sandeaux, J. Sandeaux, J. C. Baccou, *J. Appl. Phycol*. **12** (2000) 15
9. C. Nagajyoti, K. D. Lee, T. V. M. Sreekanth, *Environ. Chem. Lett*. **8** (2010) 199
10. H. Küpper, F. Küpper, M. Spiller, *J. Exp. Bot*. **47** (1996) 259
11. H. Küpper, F. Küpper, M. Spiller, *Photosynth. Res*. 58 (1998) 125
12. H. Küpper, I. Šétlik, M. Spiller, F. C. Küpper, O. Prášil, *J. Phycol*. **38** (2002) 429
13. H. Küpper, F. C. Küpper, M. Spiller, in *Advances in Photosynthesis and Respiration – Chlorophylls and Bacteriochlorophylls*, Vol. 25, B. Grimm, R. Porra, W. Rudigger, H. Scheer, Eds., Springer, Dordrecht, 2006, p. 67
14. J. B. Petrović, G. Nikolić, D. Marković, *J. Serb. Chem. Soc*. **71** (2006) 501
15. J. B. Zvezdanović, G. Nikolić, D. Marković, *J. Serb. Chem. Soc*. **72** (2007) 1053
16. J. B. Zvezdanović, D. Z. Marković, S. M. Milenković, *J. Serb. Chem. Soc*. **77** (2012) 187
17. H. Scheer, J. J. Katz, *J. Am. Chem. Soc*. **100** (1978) 561
18. D. H. Anđelković, R. Nikolić, D. Marković, T. Anđelković, G. Kocić, Z. Todorović, A. Bojić, *J. Serb. Chem. Soc*. **78** (2013) 137
19. P. H. Hynninen, in *Chlorophylls*, H. Scheer, Ed., CRC-Press, Boca Raton, FL, 1991, p. 145
20. W. A. Svec, in *Chlorophylls*, H. Scheer, Ed., CRC-Press, Boca Raton, FL, 1991 p. 89
21. J. B. Zvezdanović, T. Cvetić, S. Veljović-Jovanović , D. Marković, *Radiat. Phys. Chem*. **78** (2009) 25
22. H. K. Lichtenthaler, *Meth. Enzym*. **148** (1987) 350
23. K. D. Zissis, R. G. Brereton, S. Dunkerley, *Rapid. Commun. Mass Spectrom*. **13** (1999) 1755
24. K. D. Zissis, S. Dunkerley, R. G. Brereton, *Analyst* **124** (1999) 971
25. R. P. Grese, R. L. Cerny, M. L. Gross, M. Senge, *J. Am. Soc. Mass Spectrom*. **1** (1990) 72
26. R. B. van Breemen, F. L. Canjura, S. J. Schwartz, *J. Agric. Food Chem*. **39** (1991) 1452
27. C.K. Lim, in *Methods in Chromatography – High-Performance Liquid Chromatography and Mass Spectrometry of Porphyrins, Chlorophylls and Bilins*, C. K. Lim, Ed., World Scientific Publishing Co., Singapore, 2009, p. 177
28. J. M. E. Quirke, in *The Porphyrin Handbook – Theoretical and physical characterization*, Vol. 7, K. M. Kadish, K. M. Smith, R. Guilard, Eds., Academic Press, San Diego, CA, 2000, p. 371
29. R. Aparicio-Ruiz, K. M. Riedl, S. J. Schwartz, *J. Agric. Food Chem*. **59** (2011) 11100
30. A. Gauthier-Jaques, K. Bortlik, J. Hau, L. B. Fay, *J. Agric. Food Chem*. **49**, (2001) 1117
31. C. Jie, J. S. Walker, B .J. Keely, *Rapid Commun. Mass Spectrom*. **16** (2002) 473
32. K. Hyvärinen, P. H. Hynninen, *J. Chromatogr*., *A* **837** (1999) 107
33. H. Scheer, in *Chlorophylls*, H. Scheer, Ed., CRC-Press, Boca Raton, FL, 1991, p. 1

34. A. Khalyfa, S. Kermasha, I. Alli, *J. Agric. Food Chem.* **40** (1992) 215
35. S. J. Schwartz, S. L. Woo, J. H. von Elbe, *J. Agric. Food Chem.* **29** (1981) 533
36. L. J. Boucher, J. J. Katz, *J. Am. Chem. Soc*. **89** (1967) 4703
37. S. Liu, F.-Q. Dong, C.-H. Yang, C.-Q. Tang, T.-Y. Kuang, *J. Integr. Plant Biol*. **48** (2006) 1330
38. M. Roca, L. Gallardo-Guerrero, M. I. Míngues-Mosquera, B. G. Rojas, *J. Agric. Food. Chem*. **58** (2010) 51
39. J. B. Zvezdanović, D. Marković, *Russ. J. Phys. Chem. A* **83** (2009) 1542
40. Nurhayati, V. Suendo, *Jurnal Matematika Sains* **16** (2011) 65
41. S. W. Jeffrey, R. F. C. Mantoura, S. W. E. Wright, *Phytoplankton Pigments in Oceanography: Guidelines to Modern Methods.* UNESCO Publishing, Paris, 1996.

Journal of the Serbian Chemical Society
JSCS-info@shd.org.rs • www.shd.org.rs/JSCS
J. Serb. Chem. Soc. *79* (6) 707–718 (2014)
JSCS–4620
UDC 541.123.2.004.12:541.25:544.351–145.82:621.78.063:535.327
Original scientific paper

Prediction of excess molar volumes of selected binary mixtures from refractive index data

JELENA M. VUKSANOVIĆ[#], DIVNA M. BAJIĆ[#], GORICA R. IVANIŠ[#], EMILA M. ŽIVKOVIĆ[#], IVONA R. RADOVIĆ[#], SLOBODAN P. ŠERBANOVIĆ[#] and MIRJANA LJ. KIJEVČANIN[#]*

Faculty of Technology and Metallurgy, University of Belgrade, Karnegijeva 4, 11120 Belgrade, Serbia

(Received 13 August, accepted 7 November 2013)

Abstract: The excess molar volumes of twenty two binary mixtures containing various groups of organic compounds: alcohols (ethanol, 1-propanol, 1,2-propanediol, 1,3-propanediol and glycerol), ketone (acetone), ester (butyl lactate), lactam (*N*-methyl-2-pyrrolidone), polyethylene glycol (PEG 200 and PEG 400) and aromatics (benzene, toluene and pyridine) were predicted from the refractive index data, using three types of equations coupled with several mixing rules for refractive index calculations: the Lorentz–Lorenz, Dale––Gladstone, Eykman, Arago–Biot, Newton and Oster. The obtained results were analysed in terms of the applied equation and mixing rule and the nature of the interactions between the components of the mixtures.

Keywords: excess molar volume; mixing rules; prediction; organic solvents.

INTRODUCTION

Knowledge of the thermophysical properties (volumetric properties, refractive index, viscosity, *etc*.) of pure organic compounds and their mixtures as a function of composition and temperature is of considerable interest for industrial applications. It is necessary for the investigation of non-ideality of mixtures, caused by molecular interactions and intermolecular forces between the components of a mixture, as well as for the design of processes and process equipment.

This work represents the results obtained for excess molar volume V^E prediction from refractive index n_D data for 22 binary mixtures in the temperature range 288.15–323.15 K (in some cases 288.15–333.15 K) and at atmospheric pressure. Binary systems containing alcohols (ethanol, 1-propanol, 1,2-propane-

* Corresponding author. E-mail: mirjana@tmf.bg.ac.rs
# Serbian Chemical Society member.
doi: 10.2298/JSC130813127V

diol, 1,3-propanediol, and glycerol), ketone (acetone), ester (butyl lactate), lactam (*N*-methyl-2-pyrrolidone), polyethylene glycol (PEG 200 and PEG 400) and aromatics (benzene, toluene and pyridine) were chosen, due to their: *i*) structural variety causing non-ideal behaviour in the mixtures (mixtures exhibiting positive, negative and S-shaped V^E and Δn_D *vs*. composition curves) and *ii*) industrial importance.

The alcohols examined in this work are colourless liquids miscible with water and are mainly used as solvents. In addition, ethanol is a potential clean fuel to substitute for petroleum fuels due to its low emissions, particularly the significantly low level of soot.[1–3] 1-Propanol is an important industrial chemical that has been used in various industrial products, such as paints and cosmetics,[4] and is considered a better biofuel than ethanol. One of the major uses of 1,2-propanediol is as an industrial antifreeze due to lower toxicity than ethylene glycol.[5,6] 1,3-Propanediol can be used in the production of polymers, cosmetics, lubricants or drugs.[7–9] 1,3-Propanediol-based polymers have better properties and greater stability in comparison to polymers produced from 1,2-propanediol, butanediols or ethylene glycol.[10] Glycerol is used in foods and cosmetics, tobacco, wrapping and packaging materials, lubricants, urethane polymers, cleaning materials, detergents, wetting agents, emulsifiers, skin protectives, as well as in the pulp and paper, and leather and textile industries.[11,12]

Acetone is a colourless, mobile, flammable liquid, and is the simplest ketone. The main application of this compound is as a solvent, also as an intermediate to produce many important chemical substances, such as methyl methacrylate (MMA), bisphenol-A (BPA) and methacrylic acid, and in cosmetics.

Lactate esters are non-toxic and biodegradable, with excellent solvent properties, such as the ability to dissolve organic compounds, *e.g*., nitro and ethyl cellulose, gums, oils, dyes, polymers and paints, and as high-boiling solvents.[13] As a "green" solvent, butyl lactate is an excellent candidate to replace halogenated solvents, such as ozone-depleting chlorofluorocarbons (CFCs), carcinogenic methylene chloride, toxic ethylene glycol ethers, and chloroform.[14]

N-Methyl-2-pyrrolidone (NMP) is a widely used compound due to its strong and selective power as a solvent.[15] For example, NMP is used in the petrochemical industry, in the microelectronics fabrication industry and in the manufacture of various compounds, such as pigments, cosmetics, drugs and pesticides.[16]

Polyethylene glycol is a non-toxic, highly biodegradable polymer.[17] PEG is well known as a food-additive[18,19] and is used for various biological and biomedical applications in aqueous solutions with biological macromolecules.[20]

Aromatics were analysed as a last class of chemical compounds in this work. Pyridine, as an industrial solvent and raw material in herbicide synthesis, is widely used in the chemical, pharmaceutical and oil industries.[21] Considering its

toxicity, there is a constant effort to find a way to remove this substance from wastewater and environment. Benzene is one of the basic petrochemicals, which is usually used as an intermediate in the processing of other substances. A large proportion of benzene is used in the production of three chemicals, cyclohexane,[22] cumene[23] and ethylbenzene.[24] Toluene has wide industrial application as a feedstock and as a solvent able not only to dissolve paints, rubber, adhesives and lacquers, but also some inorganic chemicals. It is much less toxic than benzene; hence it represents a good replacement for benzene as a solvent in industry. A number of works consider its removal from industrial wastewaters,[25] the treatment of toluene vapours[26,27] and the removal of toluene from air.[28]

For the prediction of V^E from n_D data, three types of equations were tested: *i*) the equation proposed by Nakata and Sakurai,[29] based on the use of mass fraction-based mixing functions, was applied for the first time in the work of Arancibia and Katz[30] (Model I), *ii*) the equation obtained by the first order expansion of Model I[29] (Model II) and *iii*) a particular case of Model II developed for iso-refractive mixtures[29] (Model III), coupled with different mixing rules for refractive indices, *i.e.*, the Lorentz–Lorenz, Dale–Gladstone, Eykman, Arago–Biot, Newton and Oster[31] rules.

THEORETICAL

The different mixing rules used in this paper for refractive indices calculation are presented by the following equations:

Lorentz–Lorenz (L–L):[32,33]

$$\frac{n_{Di}^2-1}{n_{Di}^2+2}=\sum_{i=1}^{N}\left[\varphi_i\left(\frac{n_{Di}^2-1}{n_{Di}^2+2}\right)\right] \tag{1}$$

Dale–Gladstone (D–G):[34]

$$n_{Di}-1=\sum_{i=1}^{N}\left[\varphi_i(n_{Di}-1)\right] \tag{2}$$

Eykman (Eyk):[35]

$$\frac{n_{Di}^2-1}{n_{Di}^2+0.4}=\sum_{i=1}^{N}\left[\varphi_i\left(\frac{n_{Di}^2-1}{n_{Di}^2+0.4}\right)\right] \tag{3}$$

Arago–Biot (A–B):[34]

$$n_D=\sum_{i=1}^{N}\left[\varphi_i(n_{Di})\right] \tag{4}$$

Newton (New):[36]

$$n_D^2-1=\sum_{i=1}^{N}\left[\varphi_i(n_{Di}^2-1)\right] \tag{5}$$

Oster (Ost):[37]

$$\frac{(n_D^2-1)(2n_D^2+1)}{n_D^2}=\sum_{i=1}^{N}\left[\varphi_i\left(\frac{(n_{Di}^2-1)(2n_{Di}^2+1)}{n_{Di}^2}\right)\right] \tag{6}$$

In the above equations, φ_i represents the volume fraction of the component in the mixture:

$$\varphi_i=\frac{x_iV_i}{\sum_{i=1}^{N}x_iV_i} \tag{7}$$

where V_i is the molar volume of component i, and x_i is its mole fraction.

The first type of equation (Model I), establishing the relation between the V^E and n_D data of the mixtures is based on the employment of a mass fraction-based mixing function for the specific refraction $f(n_D)/\rho$:

$$\frac{f(n_D)}{\rho}=\sum_{i=1}^{2}\omega_i\frac{f(n_{Di})}{\rho_i} \tag{8}$$

and the definition of the excess molar volume (Model I) could be written as:

$$V^E=\sum_{i=1}^{2}\left[\left(f(n_{Di})-f(n_D)\right)\left(\frac{x_iV_i}{f(n_D)}\right)\right] \tag{9}$$

where w_i, ρ_i, n_{Di} and x_i are the mass fraction, density, refractive index, and mole fraction of component i, respectively, $f(n_{Di})$ and $f(n_D)$ represent functions of the refractive index of pure component i and of a mixture, respectively, and V_i is the pre-mixing molar volume of component i.

Typical $f(n_D)$ equations for the refractive index calculations are given by Eqs. (1)–(6).

Considering V^E in Eq. (9) as a function of n_D and expanding to the first order at $n_{D\varphi}=n_{D1}\varphi_1+n_{D2}\varphi_2$ provides the second type of equation (Model II) for the calculation of the excess molar volume:

$$V^E=\sum_{i=1}^{2}x_iV_i\left(\frac{f(n_{Di})}{f(n_{D\varphi})}-1\right)-\Delta_\varphi n_D\left[\frac{f'(n_{D\varphi})}{f^2(n_{D\varphi})}\sum_{i=1}^{2}x_iV_i f(n_{Di})\right] \tag{10}$$

where $f(n_{D\varphi})$ is the function of the refractive index of a mixture as in Eq. (9), $f'(n_{D\varphi})$ denotes the value of the first derivative of $f(n_{D\varphi})$ and $\Delta_\varphi n_D$ represents the deviation of the refractive index values of a binary mixture from the ideal binary mixture

$$\Delta_\varphi n_D=n_D-(n_{D1}\varphi_1+n_{D2}\varphi_2) \tag{11}$$

where n_{D1} and n_{D2} are the refractive indices, and φ_1 and φ_2 are the components volume fractions based on the molar volumes of the pure components.

The third type of equation (Model III) is related to iso-refractive mixtures; when $n_{D1}=n_{D2}$, Eq. (10) is reduced to:

$$V^{\mathrm{E}} = -\Delta_{\varphi} n_{\mathrm{D}} \left[\frac{f'(n_{\mathrm{D1}})}{f^2(n_{\mathrm{D1}})} \sum_{i=1}^{2} x_i V_i \right] \tag{12}$$

where $f(n_{D1})$ represents the function of the refractive index and $f'(n_{D1})$ denotes the value of the $f(n_{D1})$ derivative, as in the above equations.

RESULTS AND DISCUSSION

The predictions of V^{E} from n_{D} data in the temperature range 288.15–323.15 K (or 288.15–333.15 K) and at atmospheric pressure for 22 binary systems (the experimental data were taken from the literature[38–42] and from ongoing investigations) were realised using the three chosen Models I–III with incorporated L–L, D–G, Eyk, A–B, New and Ost mixing rules for the determination the refractive index. The results of V^{E} calculation were assessed by the absolute maximum percentage average deviation $PD_{\max}$:

$$PD_{\max} = \frac{100}{N} \sum_{i=1}^{N} \left| \frac{V^{\mathrm{E}}_{\mathrm{exp}} - V^{\mathrm{E}}_{\mathrm{cal}}}{\left(V^{\mathrm{E}}_{\mathrm{exp}}\right)_{\max}} \right|_i \tag{13}$$

where $V^{\mathrm{E}}_{\mathrm{exp}}$ and $V^{\mathrm{E}}_{\mathrm{cal}}$ represent the experimental and calculated V^{E} values, respectively, N is the number of experimental data points, while $(V^{\mathrm{E}}_{\mathrm{exp}})_{\max}$ denotes the absolute maximum of the experimental V^{E} value.

The results are summarized in Table S-1 of the Supplementary material to this paper and are graphically presented in Figs. 1–4.

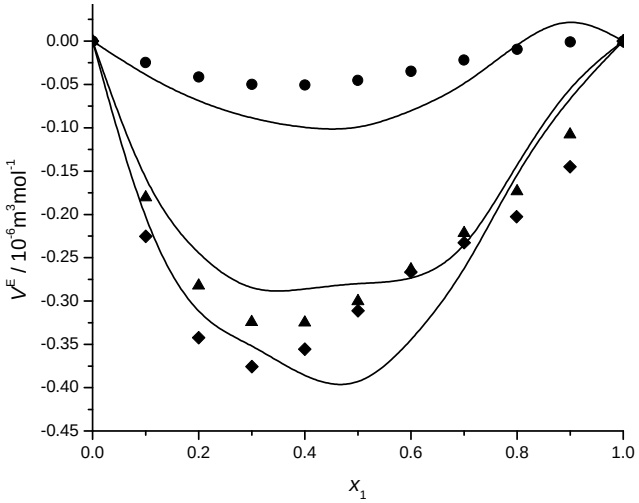

Fig. 1. Graphical presentation of the results obtained for the prediction of V^{E} from n_{D} at 298.15 K for the systems 1-propanol with: acetone (●),pyridine (▲) and NMP (♦), in which the symbols represent the experimental values and lines the predictions obtained using the appropriate Eykman mixing rule in combination with the Model I.

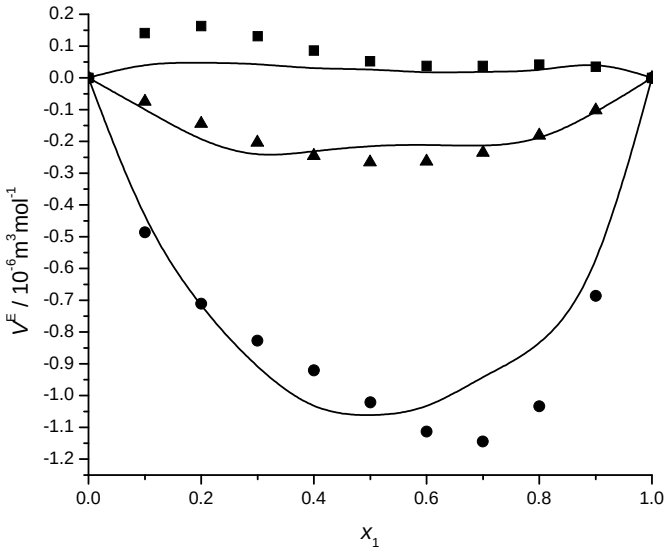

Fig. 2. Graphical presentation of the results obtained for the prediction of V^E from n_D at 298.15 K for the systems 1,2-propanediol with: (■) butyl lactate, (▲) pyridine and (●) acetone, in which the symbols represent the experimental values and the lines the predictions obtained using the appropriate Dale–Gladstone mixing rule in combination with the Model II.

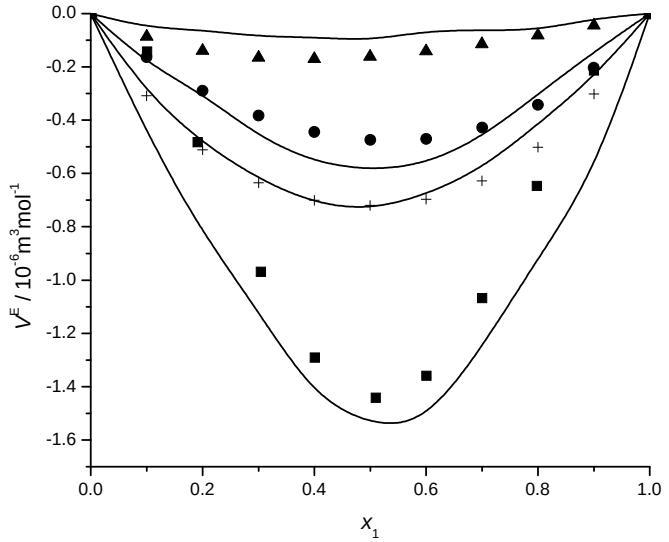

Fig. 3. Graphical presentation of the results obtained for the prediction of V^E from n_D at 313.15 K for the systems 1,3-propanediol with: (+) PEG200, (▲) pyridine, (■) butyl lactate and (●) acetone, in which the symbols represent the experimental values and lines the predictions obtained using the appropriate Newton mixing rule in combination with the Model III.

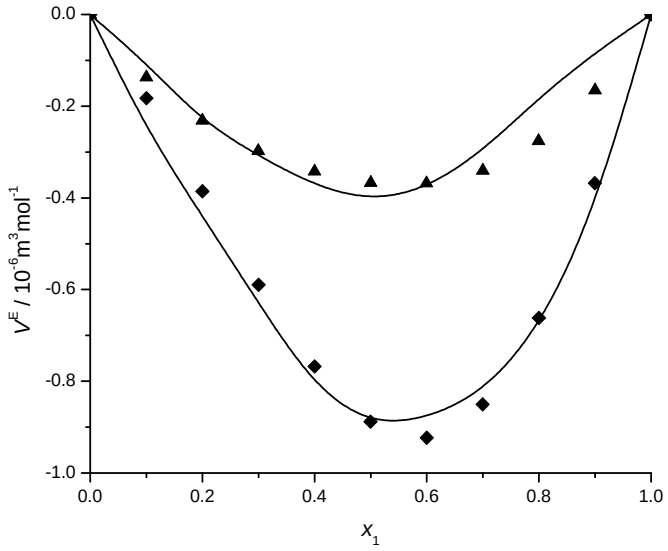

Fig. 4. Graphical presentation of the results obtained for the prediction of V^E from n_D at 323.15 K for the systems glycerol with: NMP (♦) and pyridine (▲), in which the symbols represent the experimental values and lines the predictions obtained using the appropriate Lorentz–Lorenz mixing rule in combination with the Model III.

For easier analysis, the investigated systems are classified in six groups of binary mixtures: acetone + alcohols, butyl lactate + alcohols, *N*-methyl-2-pyrrolidone + alcohols, PEGs + alcohols, pyridine + alcohols and PEGs + aromatics.

Acetone +alcohols

Three binary systems were investigated in this group. For the acetone+1-propanol binary mixture (Fig. 1) both V^E–x_1 and Δn_D–x_1 were S-shaped with the difference that the excess molar volume changed from negative to positive in the acetone rich region while the refractive index deviation was positive for lower and negative for higher acetone mole fractions.[38] For this system, it was observed (Table S-I of the Supplementary material) that the mixing rule influenced the quality of the results more than the chosen excess molar volume equation did. The best, but still unsatisfactory, fit of the experimental data was obtained using the Arago–Biot mixing rule with maximum percentage deviations ranging from 18 to 42 %, depending on the temperature. The reason for such poor prediction results could be the very small absolute V^E values and sigmoid shape of the V^E–x_1 and Δn_D–x_1 curves.

For the remaining two systems in this group, the changes in the refractive indices were positive, while the excess molar volumes were negative over the whole temperature and composition ranges. The best results for the acetone+ +1,2-propanediol binary mixture (Fig. 2), with values of PD_{max} below 10 % at

all temperatures, were obtained with Model II in combination with the Dale–Gladstone mixing rule and with Model I in combination with the Newton mixing rule. For the acetone+1,3-propanediol mixture (Fig. 3), Model I in combination with the Oster mixing rule gave the best prediction results.

Butyl lactate+alcohols

The binary systems analyzed in this group were butyl lactate+1-propanol, butyl lactate+1,2-propanediol and butyl lactate+1,3-propanediol.[39]

For the butyl lactate+1-propanol mixture, similar results were obtained with all three types of equations and different mixing rules with the exception of the Arago–Biot mixing rule, which again gave higher values of PD_{max}. None of the relations considered could be generally emphasized as superior since the prediction results varied with temperature. At lower temperatures, the best results were obtained using the Newton mixing rule in combination with Model II and at higher temperatures, the most successful was the Lorentz–Lorenz mixing rule coupled with Model I. The butyl lactate+1,2-propanediol binary mixture (Fig. 2) is characterized with small absolute V^E values and S-shaped V^E *vs*. composition curves, which is probably the reason for unsatisfactory results obtained with all applied mixing rules and models for the calculation of V^E. The possible explanation of the better results achieved for the butyl lactate+1,3-propanediol mixture (Fig. 3) in comparison with the other systems from this group might be because this system yielded the most symmetric curve V^E–x_1 and positive values of both the excess molar volumes and the changes in the refractive indices. The best fit of the experimental data was obtained with the Newton mixing rule coupled with Model III or, at higher temperatures, with Model I.

N-*Methyl-2-pyrrolidone+ alcohols*

The systems consisting of *N*-methyl-2-pyrrolidone with mono-, di- and trihydroxyl alcohols, from ongoing research, showed negative excess molar volume data and positive experimental changes in the refractive indices with relatively symmetric Δn_D curves. For systems with ethanol or 1,3-propanediol, none of the applied mixing rules and equations for the calculation of V^E gave satisfactory prediction results. Better fits of the experimental data for the system *N*-methyl-2--pyrrolidone+1-propanol (Fig. 1) were obtained with the Dale–Gladstone mixing rule in combination with Model III. For system with glycerol, the Lorentz–Lorenz mixing rule in combination with Model III showed the best prediction capability at all the investigated temperatures.

PEGs+alcohols

Experimental changes of the refractive indices were positive for all systems in this group[41], while the V^E–x_1 curves were negative for the systems with PEG 400 and S-shaped with very small absolute values of excess molar volume for

systems with PEG 200. The prediction of V^E from the refractive index data was unsatisfactory irrespective of the excess molar volume equation and the mixing rule applied, where for the systems PEGs+1,2-propanediol, PD_{max} had the highest values, for all models above 100 %.

Pyridine+alcohols

Systems containing pyridine[40] showed negative excess molar volume data and positive experimental changes in the refractive indices with relatively symmetric Δn_D curves. In the case of the pyridine+1-propanol mixture (Fig. 1), the best results at all temperatures were achieved with the Eykman mixing rule in combination with Model I or III. At some temperatures, a relatively good fit of the experimental data was also obtained with the Dale–Gladstone mixing rule coupled with Model I or the Newton mixing rule and Model II. For the remaining binary systems in this group, the Eykman mixing rule usually coupled with Model II in general gave somewhat better results than the other equations and mixing rules. In some cases, the Dale–Gladstone and the Lorentz–Lorenz mixing rule also showed satisfactory fits of the experimental data. Similar to the previous groups, the obtained results were more influenced by the mixing rule than by the equation for the calculation of the excess molar volume.

PEGs+aromatics

In this group, four systems consisting of benzene or toluene with PEG 200 or PEG 400 were included.[42] All of the analyzed systems showed negative excess molar volumes V^E and negative Δn_D values. For benzene+PEG 200 binary mixture, all the mixing rules and equations for the calculation of the excess molar volume showed unsatisfactory fits of the experimental data. In the case of benzene+PEG 400 and toluene+PEG 200 mixtures the best results at most of the investigated temperatures were obtained with Newton mixing rule coupled with Model II. At higher temperatures, satisfactory prediction results for both systems were also achieved with the Dale–Gladstone mixing rule in combination with Model I. For the toluene+PEG 400 binary system, Dale–Gladstone mixing rule in combination with Model II or III and the Eykman mixing rule coupled with Model I or III showed the best prediction capabilities, especially at higher temperatures.

Graphical presentations of the results obtained at 298.15 K for the systems with 1-propanol using the Eykman mixing rule and Model I are shown in Fig. 1. It could be seen that satisfactory fits of the experimental data were not achieved for any of the presented systems. A slightly better result than the presented ones was obtained only for the *N*-methyl-2-pyrrolidone+1-propanol mixture using the Dale–Gladstone mixing rule.

Results obtained at 298.15 K for the systems with 1,2-propanediol using the Dale–Gladstone mixing rule and Model II are given at Fig. 2. Both PEGs (PEG 200 and PEG 400) showed very poor prediction results and were omitted from Fig. 2. From the remaining three systems, the best result was obtained for the acetone+1,2-propanediol mixture with values of the percentage deviation PD_{max} of around 7 %.

The values of the excess molar volume for the systems with 1,3-propanediol at 313.15 K, calculated from the experimental data and using the Newton mixing rule coupled with Model III are presented in Fig. 3. The best result in this case was obtained for system with butyl lactate with a value of the percentage deviation PD_{max} of below 5 %. For the pyridine+1,3-propanediol mixture, a better fit of the experimental data than the one presented was achieved with the Eykman mixing rule, while for the acetone+1,3-propanediol binary system, the Oster mixing rule was the most appropriate.

The results presented in Fig. 4 for the systems with glycerol, obtained at 323.15 K using the Lorentz–Lorenz mixing rule in combination with Model III show that quite good fits of the experimental data were achieved for both analyzed systems.

CONCLUSIONS

Conclusions reached in a previous paper[43] were confirmed by the investigations presented in this work:

1) unsatisfactory fit of experimental data was achieved for systems exhibiting asymmetric or S-shaped experimental V^E *vs.* composition curves and for systems with very small absolute V^E values;

2) the obtained results were more influenced by the mixing rule employed for refractive index determination than by the model used for excess molar volume calculation;

3) although none of the relations considered could be generally considered as being superior, the Arago–Biot mixing rule offered the worst experimental data fit for most of the investigated systems.

SUPPLEMENTARY MATERIAL

Results, of the V^E prediction of the binary liquid mixtures are available electronically from http://www.shd.org.rs/JSCS/, or from the corresponding author on request.

Acknowledgements. The authors gratefully acknowledge the financial support received from the Research Fund of Ministry of Education, Science and Technological Development of the Republic of Serbia and the Faculty of Technology and Metallurgy, University of Belgrade (Project No. 172063).

ИЗВОД

ПРЕДВИЂАЊЕ ДОПУНСКИХ МОЛАРНИХ ЗАПРЕМИНА ИЗАБРАНИХ БИНАРНИХ СМЕША ИЗ ПОДАТАКА ЗА ИНДЕКСЕ РЕФРАКЦИЈЕ

ЈЕЛЕНА М. ВУКСАНОВИЋ, ДИВНА М. БАЈИЋ, ГОРИЦА Р. ИВАНИШ, ЕМИЛА М. ЖИВКОВИЋ, ИВОНА Р. РАДОВИЋ, СЛОБОДАН П. ШЕРБАНОВИЋ и МИРЈАНА Љ. КИЈЕВЧАНИН

Технолошко–металуршки факултет, Универзитет у Београду, Карнегијева 4, 11120 Београд

Предвиђање допунских моларних запремина 22 бинарне смеше које садрже различите групе органских једињења: алкохоле (етанол, 1-пропанол, 1,2-пропандиол, 1,3-пропандиол и глицерол), кетон (ацетон), естар (бутил-лактат), лактам (*N*-метил-2-пиролидон), полимере од етилен-гликола (PEG 200 и PEG 400), као и ароматична једињења (бензен, толуен и пиридин) извршено је коришћењем података о индексима рефракције, уз примену три типа модела за прорачун допунских моларних запремина, комбинованих са правилима мешања за израчунавање индекса рефракције: Lorentz–Lorenz, Dale–Gladstone, Eykman, Arago–Biot, Newton и Oster. Добијени резултати су анализирани у зависности од примењеног модела и правила мешања, као и од природе интеракција између компонената смеша.

(Примљено 13. августа, прихваћено 7. новембра 2013)

REFERENCES

1. C. Beatrice, C. Bertoli, N. D. Giacomo, *Combust. Sci. Technol.* **137** (1998) 31
2. K. H. Song, P. Nag, T. A. Litzinger, D. C. Haworth, *Combust. Flame* **135** (2003) 341
3. C. Esarte, Á. Millera, R. Bilbao, M. U. Alzueta, *Ind. Eng. Chem. Res.* **49** (2010) 6772
4. C. R. Shen, J. C. Liao, *Metab. Eng.* **10** (2008) 312
5. E. Jeon, S. Lee, D. Kim, H. Yoon, M. Oh, C. Park, J. Lee, *Enzyme Microb. Tech.* **45** (2009) 42
6. D. C. Cameron, N. E. Altaras, M. L. Hoffman, A. J. Shaw, *Biotechnol. Prog.* **14** (1998) 116
7. H. Biebl, K. Menzel, A. P. Zeng, W. D. Deckwer, *Appl. Microbiol. Biotechnol.* **52** (1999) 289
8. A. P. Zeng, H. Biebl, *Adv. Biochem. Eng. Biotechnol.* **74** (2002) 239
9. M. Sauer, H. Marx, D. Mattanovich, *Rec. Pat. Biotechnol.* **2** (2008) 191
10. J. V. Kurian, *J. Polym. Environ.* **13** (2005) 159
11. R. L. Morrison, *Glycerol.* In *Encyclopedia of chemical technology*, Wiley, New York, USA, 1994, p. 681
12. Z. Wang, J. Zhuge, H. Fang, B. A. Prior, *Biotechnol. Adv.* **19** (2001) 201
13. J. J. Clary, V. J. Feron, J. A. van Velthuijsen, *Regul. Toxicol. Pharm.* **27** (1998) 88
14. V. T. Dung, L. T. Carl, A. S. Navinchandra, K. K. Aspi, M. J. Dennis, *J. Chem. Eng. Data* **51** (2006) 1220
15. M. A. Carnerup, A. M. Saillenfait, B. A. G. Jönsson, *Food Chem. Toxicol.* **43** (2005) 1441
16. *International Program on Chemical Safety (IPCS) No. 35. N-methyl-2-pyrrolidone*. World Health Organization, Geneva, 2001
17. J. Liang, J. Lv, J. Fan, Z. Shang, *Synth. Commun.* **39** (2009) 2822
18. *Toxicological Evaluation of Certain Food Additives, Food Additives Series 14*, World Health Organization, Geneva, 1979
19. Code of Federal Regulations, Title 21, Vol. 3, CITE 21CFR172.820, FDA, Washington DC, 2001

20. J. M. Harris, in *Poly(Ethylene Glycol) Chemistry: Biotechnical and Biomedical Applications*, J. M. Harris, Ed., Plenum Press, New York, 1992, p. 7
21. L. Qiao, J.-L. Wang, *J. Hazard. Mater.* **176** (2010) 220
22. J. P. G. Villaluenga, A. Tabe-Mohammadi, *J. Membrane Sci.* **169** (2000) 159
23. V. V. Bokade, U. K. Kharul, *Chem. Eng. J.* **147** (2009) 97
24. M. C. Al-Kinany, B. Y. Jibril, S. H. Al-Khowaiter, M. A. Al-Dosari, H. A. Al-Megren, S. M. Al-Zahrani, K. I. Al-Humaizi, *Chem. Eng. Process.* **44** (2005) 841
25. N. G. Asenjo, P. Álvarez, M. Granda, C. Blanco, R. Santamaría, R. Menéndez, *J. Hazard. Mater.* **192** (2011) 1525
26. E. R. Rene, D. V. S. Murthy, T. Swaminathan, *Process Biochem.* **40** (2005) 2771
27. A. Vergara-Fernández, L. L. Molina, N. A. Pulido, G. Aroca, *J. Environ. Manag.* **84** (2007) 115
28. M.-C. Delhoménie, L. Bibeau, N. Bredin, S. Roy, S. Broussau, R. Brzezinski, J. L. Kugelmass, M. Heitz, *Adv. Environ. Res.* **6** (2002) 239
29. M. Nakata, M. Sakurai, *J. Chem. Soc., Faraday Trans. I* **83 (**1987**)** 2449
30. L. E. Arancibia, M. Katz, *Phys. Chem. Liq*. **26** (1993) 107
31. Á. Piñeiro, P. Brocos, A. Amigo, M. Pintos, R. Bravo, *J. Chem. Thermodyn.* **31** (1999) 931
32. H. A. Lorentz, *Wied. Ann.* **9** (1880) 641
33. L. Lorenz, *Wied. Ann.* **11** (1880) 70
34. W. J. Heller, *J. Phys. Chem.* **69** (1965) 1123
35. A. Piñeiro, P. Brocos, A. Amigo, M. Pintos, R. Bravo, *J. Chem. Thermodyn.* **31** (1999) 931
36. J. R. Partington, *An advanced Treatise on Physical Chemistry*, Vol. 4, Sec. X, Longmans & Green, London, 1953
37. G. Oster, *Chem. Rev*. **43** (1948) 319
38. M. Lj. Kijevčanin, B. D. Djordjević, I. R. Radović, E. M. Živković, A. Ž. Tasić, S. P. Šerbanović, *Modeling of Volumetric Properties of Organic Mixtures Based on Molecular Interactions*, in *Molecular Interaction*, Aurelia Meghea, Ed., InTech, Rijeka, 2012, p. 1
39. D. M. Bajić, E. M. Živković, S. P. Šerbanović, M. Lj. Kijevčanin, *Thermochim. Acta* **562** (2013) 42
40. M. Lj. Kijevčanin, E. M. Živković, B. D. Djordjević, I. R. Radović, J. Jovanović, S. P. Šerbanovic, *J. Chem. Thermodyn.* **56** (2013) 49
41. D. M. Bajić, G. R. Ivaniš, Z. P. Višak, E. M. Živković, S. P. Šerbanović, M. Lj. Kijevčanin, *J. Chem. Thermodyn.* **57** (2013) 510
42. J. M. Vuksanović, E. M. Živković, I. R. Radović, B. D. Djordjević, S. P. Šerbanović, M. Lj. Kijevčanin, *Fluid Phase Equilib.* **345** (2013) 28
43. I. R. Radović, M. Lj. Kijevčanin, M. Z. Gabrijel, S. P. Šerbanović, B. D. Djordjević, *Chem. Pap.* **62** (2008) 302.

Journal of the Serbian Chemical Society
JSCS@tmf.bg.ac.rs • www.shd.org.rs/JSCS
J. Serb. Chem. Soc. 79 (6) S60–S73 (2014) *Supplementary material*

SUPPLEMENTARY MATERIAL TO

Prediction of excess molar volumes of selected binary mixtures from refractive index data

JELENA M. VUKSANOVIĆ, DIVNA M. BAJIĆ, GORICA R. IVANIŠ, EMILA M. ŽIVKOVIĆ, IVONA R. RADOVIĆ, SLOBODAN P. ŠERBANOVIĆ and MIRJANA LJ. KIJEVČANIN*

Faculty of Technology and Metallurgy, University of Belgrade, Karnegijeva 4, 11120 Belgrade, Serbia

J. Serb. Chem. Soc. 79 (6) (2014) 707–718

TABLE S-I. Results, PD_{max} (%), of the V^E prediction of the binary liquid mixtures; hv – high value (above 100 %)

T / K	Model	Model					
		L–L	D–G	Eyk	A–B	New	Ost
Acetone (1) + 1-propanol (2)							
288.15	I	58.23	62.03	58.57	32.11	70.07	41.19
	II	54.42	67.13	60.66	31.74	86.13	46.86
	III	58.06	61.85	58.40	32.13	69.86	62.14
293.15	I	58.86	61.61	58.72	32.57	67.51	39.40
	II	54.15	66.64	60.25	32.21	85.37	45.88
	III	58.73	61.47	58.59	32.59	67.34	60.80
298.15	I	68.52	71.02	68.32	30.76	75.86	45.72
	II	63.04	76.39	69.53	30.39	96.46	53.29
	III	68.40	70.89	68.19	30.77	75.71	69.47
303.15	I	84.17	84.88	82.33	24.88	88.58	55.27
	II	76.14	90.85	83.25	24.47	hv [1]	64.34
	III	84.05	84.75	82.21	24.89	88.43	82.41
308.15	I	98.42	98.38	96.29	21.36	hv	64.73
	II	89.04	hv	96.57	20.99	hv	75.35
	III	98.32	98.27	96.18	21.36	99.90	94.72
313.15	I	hv	hv	hv	18.24	hv	95.71
	II	hv	hv	hv	18.08	hv	hv
	III	hv	hv	hv	18.24	hv	hv
318.15	I	hv	hv	hv	32.37	hv	hv
	II	hv	hv	hv	32.60	hv	hv
	III	hv	hv	hv	32.36	hv	hv
323.15	I	hv	hv	hv	41.44	hv	hv

* Corresponding author. E-mail: mirjana@tmf.bg.ac.rs

TABLE S-I. Continued

T / K	Model	Model					
		L–L	D–G	Eyk	A–B	New	Ost
Acetone (1) + 1-propanol (2)							
323.15	II	hv	hv	hv	42.06	hv	hv
	III	hv	hv	hv	41.42	hv	hv
Acetone (1) + 1,2 propanediol (2)							
288.15	I	12.66	11.12	12.20	55.17	8.98	19.11
	II	11.81	9.38	9.91	54.72	11.62	15.31
	III	13.20	11.51	12.66	55.22	9.23	11.56
293.15	I	12.23	10.17	11.73	55.09	7.17	19.36
	II	10.92	7.39	8.35	54.64	9.87	15.54
	III	12.92	10.79	12.30	55.14	7.68	10.85
298.15	I	10.43	8.55	9.89	54.64	6.45	18.08
	II	9.35	7.17	7.62	54.17	10.97	14.12
	III	11.06	9.00	10.50	54.69	6.81	9.07
303.15	I	8.33	6.80	7.98	53.94	6.47	16.02
	II	7.68	7.04	6.99	53.46	12.88	11.92
	III	8.78	7.29	8.44	54.00	6.46	7.38
308.15	I	6.73	6.33	6.47	53.37	6.58	14.37
	II	6.77	7.82	6.52	52.87	15.58	10.12
	III	7.20	6.32	6.88	53.43	6.57	6.46
313.15	I	7.42	7.74	7.59	52.38	8.67	11.92
	II	7.67	10.83	8.53	51.85	20.57	8.76
	III	7.38	7.70	7.55	52.45	8.30	7.85
318.15	I	10.41	9.29	10.33	54.67	7.94	18.28
	II	8.27	6.30	6.99	54.19	10.91	14.44
	III	10.96	9.90	10.90	54.73	8.40	10.27
323.15	I	12.00	11.16	12.06	54.20	9.58	18.65
	II	9.67	7.11	8.04	53.73	11.46	14.93
	III	12.52	11.74	12.60	54.26	10.27	12.23
Acetone (1) + 1,3 propanediol (2)							
288.15	I	11.90	15.44	13.03	40.60	21.01	5.20
	II	14.99	23.89	19.35	39.95	37.20	9.69
	III	10.93	14.36	12.02	40.69	19.72	14.65
293.15	I	12.29	15.67	13.33	39.98	21.05	5.37
	II	15.40	24.21	19.73	39.32	37.35	9.65
	III	11.30	14.57	12.30	40.07	19.73	14.79
298.15	I	12.25	15.46	13.19	39.71	20.61	5.73
	II	15.48	24.08	19.66	39.06	37.03	9.19
	III	11.24	14.35	12.15	39.80	19.28	14.48
303.15	I	11.65	14.71	12.50	40.31	19.67	5.88
	II	14.93	23.43	19.04	39.66	36.25	8.11
	III	10.63	13.58	11.44	40.40	18.32	13.63
308.15	I	11.77	14.68	12.53	39.87	19.42	6.76

TABLE S-I. Continued

T / K	Model	Model					
		L–L	D–G	Eyk	A–B	New	Ost
Acetone (1) + 1,3 propanediol (2)							
308.15	II	15.11	23.45	19.12	39.22	36.08	7.81
	III	10.73	13.53	11.46	39.96	18.06	13.50
313.15	I	10.60	13.00	11.02	38.63	17.30	9.83
	II	13.62	21.43	17.36	38.01	33.31	8.85
	III	10.01	11.89	10.35	38.71	15.98	11.78
318.15	I	11.42	13.73	11.78	38.15	17.94	10.74
	II	14.59	22.36	18.29	37.62	34.21	9.96
	III	10.80	12.59	11.12	38.24	16.59	12.43
323.15	I	13.24	14.85	13.56	37.47	18.62	12.99
	II	15.63	23.26	19.24	36.96	34.93	12.40
	III	12.82	14.14	12.97	37.56	17.25	13.96
Butyl lactate (1) + 1-propanol (2)							
288.15	I	11.49	10.99	11.71	56.15	11.08	17.21
	II	18.60	12.26	14.63	56.34	9.19	14.11
	III	11.55	11.02	11.77	56.16	11.12	11.81
293.15	I	11.30	10.89	11.52	56.07	10.96	16.81
	II	17.93	12.07	21.38	56.26	9.44	14.11
	III	11.36	10.93	11.58	56.09	11.00	11.71
298.15	I	11.82	11.49	12.07	56.47	11.63	17.69
	II	18.48	12.64	14.99	56.65	9.27	14.83
	III	11.88	11.52	12.14	56.48	11.67	12.33
303.15	I	12.91	12.73	13.26	56.93	13.11	19.43
	II	19.78	13.84	16.11	57.11	10.33	16.14
	III	12.97	12.76	13.32	56.95	13.14	13.64
308.15	I	10.73	11.01	11.28	56.35	11.14	17.18
	II	17.37	12.16	13.94	56.53	9.78	14.15
	III	10.78	11.04	11.31	56.37	11.18	11.85
313.15	I	9.42	14.03	9.93	56.04	9.58	16.13
	II	16.00	10.81	12.46	56.22	9.73	12.88
	III	9.45	9.64	9.96	56.05	9.63	10.42
318.15	I	8.41	8.55	8.90	55.89	8.96	15.52
	II	15.02	9.81	11.78	56.07	9.27	12.42
	III	8.45	8.59	8.94	55.90	8.94	9.37
323.15	I	7.37	7.50	7.87	55.60	8.25	14.51
	II	13.61	8.79	10.46	55.79	9.98	11.32
	III	7.41	7.54	7.91	55.61	8.22	8.33
Butyl lactate (1) + 1,2-propanediol (2)							
288.15	I	29.96	26.52	27.99	44.36	22.24	26.70
	II	28.88	26.24	27.45	44.33	22.77	27.19
	III	29.95	26.51	27.98	44.35	22.23	24.74
293.15	I	31.59	28.50	29.80	43.67	24.25	28.53

TABLE S-I. Continued

T / K	Model	Model					
		L–L	D–G	Eyk	A–B	New	Ost
Butyl lactate (1) + 1,2-propanediol (2)							
293.15	II	30.42	28.24	29.24	43.65	25.18	29.10
	III	31.58	28.49	29.79	43.67	24.24	26.87
298.15	I	34.22	31.50	32.62	43.31	27.78	31.31
	II	32.93	31.27	32.04	43.29	28.94	31.99
	III	34.21	31.50	32.61	43.31	27.78	30.02
303.15	I	35.25	32.78	33.77	42.80	29.42	32.39
	II	33.83	32.56	33.16	42.78	30.77	33.16
	III	35.25	32.78	33.76	42.80	29.41	31.39
308.15	I	37.13	34.29	35.42	42.06	30.93	33.84
	II	35.47	34.10	34.74	42.04	32.51	34.80
	III	37.12	34.29	35.42	42.06	30.92	32.68
313.15	I	41.20	39.05	39.84	41.97	36.15	38.13
	II	39.44	38.92	39.16	41.96	38.18	39.20
	III	41.20	39.05	39.84	41.97	36.15	37.71
318.15	I	47.13	45.87	46.22	42.34	44.24	44.23
	II	45.21	45.79	45.52	42.33	46.62	45.45
	III	47.13	45.86	46.21	42.34	44.24	44.88
323.15	I	48.73	47.87	48.01	40.86	46.84	45.76
	II	46.68	47.85	47.29	40.86	49.51	47.11
	III	48.72	47.87	48.00	40.86	46.83	47.03
Butyl lactate (1) + 1,3-propanediol (2)							
288.15	I	23.81	16.71	20.02	59.06	6.79	13.55
	II	23.60	16.47	19.80	59.03	6.51	18.92
	III	23.27	15.56	19.12	58.95	5.54	18.34
293.15	I	23.09	15.98	19.31	58.92	6.07	12.84
	II	22.86	15.73	19.08	58.90	5.99	18.45
	III	22.52	14.76	18.35	58.81	5.50	17.83
298.15	I	22.56	15.47	18.81	58.91	5.80	12.36
	II	22.33	15.20	18.56	58.89	5.72	18.21
	III	21.97	14.17	17.79	58.79	5.28	17.55
303.15	I	21.61	14.50	17.86	58.61	5.37	11.40
	II	21.36	14.22	17.60	58.59	5.30	17.53
	III	20.99	13.12	16.78	58.49	4.98	16.82
308.15	I	20.90	13.82	17.19	58.41	4.58	10.76
	II	20.64	13.53	16.92	58.38	4.49	17.13
	III	20.26	12.37	16.06	58.28	4.51	16.39
313.15	I	20.48	13.46	16.81	58.31	4.43	10.45
	II	20.21	13.16	16.54	58.28	4.35	17.04
	III	19.82	11.94	15.64	58.17	4.32	16.26
318.15	I	18.99	11.88	15.29	57.91	3.70	8.86
	II	18.70	11.56	15.00	57.88	3.73	15.81

TABLE S-I. Continued

T / K	Model	Model					
		L–L	D–G	Eyk	A–B	New	Ost
Butyl lactate (1) + 1,3-propanediol (2)							
318.15	III	18.28	10.25	14.03	57.77	4.97	14.98
323.15	I	19.98	14.28	17.04	55.21	10.71	11.89
	II	19.72	13.99	16.77	55.17	11.03	17.57
	III	19.19	12.61	15.72	55.05	13.08	16.75
NMP (1) + ethanol (2)							
288.15	I	29.72	21.25	22.46	44.87	24.20	19.47
	II	15.71	17.62	15.79	45.65	26.24	19.27
	III	29.21	20.83	21.93	44.92	23.84	20.60
293.15	I	29.18	21.04	21.77	45.13	24.39	19.94
	II	16.03	14.41	15.83	45.90	25.73	18.90
	III	28.68	20.63	21.25	45.18	24.03	20.75
298.15	I	27.11	19.77	20.01	45.64	23.92	20.63
	II	16.55	16.44	15.59	46.40	23.96	17.59
	III	26.64	19.37	19.61	45.69	23.72	20.33
303.15	I	27.61	19.94	20.29	45.24	40.21	20.01
	II	15.93	16.48	15.21	46.00	24.18	17.60
	III	27.13	19.54	19.89	45.28	23.32	20.05
308.15	I	24.53	17.26	16.99	46.58	26.57	22.78
	II	18.21	17.18	17.42	47.30	20.57	17.52
	III	24.10	17.04	16.66	46.62	26.44	21.23
313.15	I	27.65	19.99	20.47	45.64	23.37	20.23
	II	16.04	16.42	15.09	46.40	24.20	17.31
	III	27.17	19.58	20.06	45.69	23.29	19.38
318.15	I	28.36	19.93	20.74	45.79	34.96	19.61
	II	15.41	16.16	14.80	46.52	24.68	17.01
	III	27.89	19.53	20.33	45.83	22.74	18.15
323.15	I	35.37	24.40	26.68	44.21	23.12	19.01
	II	15.33	20.14	17.35	44.98	30.26	20.90
	III	34.82	23.94	26.11	44.26	22.75	20.29
NMP (1) + 1-propanol (2)							
288.15	I	17.85	12.78	13.11	50.16	14.61	15.95
	II	15.53	13.32	14.02	50.80	15.36	13.59
	III	17.61	12.68	13.01	50.18	14.73	12.53
293.15	I	17.07	12.35	12.54	50.71	15.87	17.00
	II	16.22	13.66	14.34	51.34	14.81	13.39
	III	16.83	12.29	12.48	50.73	15.98	13.56
298.15	I	16.43	12.46	12.66	51.34	17.31	18.72
	II	17.03	14.12	14.90	51.95	14.89	13.75
	III	16.21	12.40	12.60	51.36	15.50	14.58
303.15	I	16.89	12.68	12.87	51.83	18.52	20.09
	II	17.62	14.51	15.31	52.44	15.17	14.19

TABLE S-I. Continued

T / K	Model	Model					
		L–L	D–G	Eyk	A–B	New	Ost
NMP (1) + 1-propanol (2)							
303.15	III	16.67	12.62	12.82	51.85	18.83	15.11
308.15	I	16.79	14.20	14.33	52.37	20.36	21.60
	II	18.79	15.76	16.35	52.96	16.71	15.51
	III	16.60	14.14	14.27	52.39	20.66	16.52
313.15	I	16.64	13.68	13.84	52.62	21.02	22.16
	II	18.6	15.21	15.78	53.21	16.06	14.99
	III	16.45	13.61	13.78	52.64	21.32	15.44
318.15	I	15.59	11.86	12.14	53.50	24.23	24.83
	II	20.49	14.24	15.98	54.06	14.06	13.90
	III	15.42	11.81	12.09	53.52	24.50	17.47
323.15	I	14.87	13.55	13.39	54.78	28.89	28.53
	II	23.28	17.33	19.22	55.30	15.23	16.91
	III	14.76	13.65	13.34	54.80	29.13	21.48
NMP (1) + 1,3-propanediol (2)							
288.15	I	31.71	44.71	38.53	40.00	62.56	44.31
	II	24.19	41.34	33.98	40.33	64.31	46.46
	III	31.30	44.24	38.10	40.04	61.99	49.69
293.15	I	33.27	46.50	40.22	39.49	64.69	45.78
	II	25.85	43.15	35.70	39.82	66.37	47.88
	III	32.86	46.04	39.79	39.53	64.13	51.59
298.15	I	31.60	44.53	38.38	39.90	62.33	43.48
	II	24.45	41.34	34.05	40.21	64..04	45.53
	III	31.22	44.09	37.97	39.94	61.80	49.51
303.15	I	30.34	43.06	37.00	40.13	60.60	41.71
	II	23.48	40.02	32.86	40.43	62.31	43.71
	III	29.98	42.64	36.62	40.17	60.09	47.97
308.15	I	29.05	41.56	35.60	40.34	58.83	39.94
	II	22.50	38.69	31.66	40.62	60.54	41.87
	III	28.71	41.17	35.24	40.38	58.36	46.41
313.15	I	32.97	46.03	39.82	38.65	64.09	44.14
	II	26.52	43.16	35.91	38.93	65.66	46.00
	III	32.60	45.62	39.44	38.68	63.59	51.14
318.15	I	30.13	42.57	36.59	39.37	59.96	40.43
	II	24.94	39.93	33.26	39.63	61.63	42.26
	III	29.81	42.20	36.24	39.41	59.50	47.48
323.15	I	34.94	48.21	41.90	37.53	66.59	45.72
	II	28.85	45.50	38.20	37.79	68.10	47.48
	III	34.59	47.81	41.53	37.57	66.10	53.42
NMP (1) + glycerol (2)							
288.15	I	14.04	17.76	15.26	49.62	27.29	19.76
	II	14.15	17.99	15.43	49.59	27.60	19.82

TABLE S-I. Continued

T / K	Model	Model					
		L–L	D–G	Eyk	A–B	New	Ost
NMP (1) + glycerol (2)							
288.15	III	13.95	17.54	15.07	49.66	26.93	20.58
293.15	I	13.89	18.79	16.10	48.31	29.49	20.72
	II	14.03	19.08	16.37	48.27	29.89	20.80
	III	13.79	18.55	15.87	48.35	29.11	21.65
298.15	I	12.82	18.05	15.38	48.25	29.19	19.85
	II	12.99	18.40	15.71	48.20	29.69	19.95
	III	12.73	17.82	15.16	48.27	28.81	21.24
303.15	I	12.30	18.09	15.40	47.95	29.77	19.96
	II	12.50	18.50	15.78	47.90	30.36	20.12
	III	12.21	17.85	15.18	47.98	29.38	21.73
308.15	I	12.69	18.09	15.64	49.01	29.93	19.87
	II	13.03	18.57	15.99	48.95	30.63	20.05
	III	12.49	17.85	15.43	49.05	29.54	21.82
313.15	I	12.55	17.76	15.50	49.32	29.92	19.62
	II	12.92	18.29	15.89	49.26	30.74	19.84
	III	12.34	17.53	15.28	49.36	29.53	21.76
318.15	I	12.65	17.85	15.59	50.10	29.35	19.32
	II	13.05	18.34	16.01	50.03	30.26	19.53
	III	12.44	17.62	15.37	50.14	28.95	21.37
323.15	I	10.63	15.91	13.43	49.92	26.99	17.22
	II	11.04	16.51	13.88	49.84	28.00	17.45
	III	10.43	15.61	13.22	49.95	26.61	19.37
PEG200 (1) + 1,3-propanediol (2)							
288.15	I	37.93	36.43	37.50	60.85	34.18	38.38
	II	41.87	37.02	39.13	60.91	30.47	36.18
	III	37.95	36.45	37.52	60.85	34.21	36.44
293.15	I	37.69	36.12	37.21	60.77	33.77	38.13
	II	41.57	36.70	38.83	60.83	30.11	35.97
	III	37.71	36.14	37.23	60.78	33.79	36.08
298.15	I	37.90	36.30	37.40	60.91	33.90	38.36
	II	41.70	36.87	38.98	60.96	30.31	36.24
	III	37.92	36.32	37.42	60.91	33.93	36.24
303.15	I	38.36	36.80	37.88	61.06	34.46	38.92
	II	42.09	37.35	39.43	61.11	30.92	36.84
	III	38.38	36.82	37.90	61.06	34.48	36.75
308.15	I	37.73	36.04	37.18	60.88	33.52	38.23
	II	41.42	36.59	38.71	60.94	30.03	36.18
	III	37.75	36.06	37.20	60.89	33.55	35.92
313.15	I	39.51	38.06	39.08	61.55	35.87	40.30
	II	43.10	38.57	40.57	61.60	32.38	38.28
	III	39.53	38.08	39.10	61.55	35.89	38.04

TABLE S-I. Continued

T / K	Model	Model					
		L–L	D–G	Eyk	A–B	New	Ost
PEG200 (1) + 1,3-propanediol (2)							
318.15	I	36.33	34.38	35.62	60.37	31.49	36.68
	II	39.90	34.90	37.11	60.42	28.08	34.70
	III	36.35	34.40	35.64	60.37	31.52	34.12
323.15	I	37.55	35.75	36.92	60.94	33.08	38.14
	II	41.07	36.25	38.39	60.99	29.67	36.17
	III	37.57	35.77	36.94	60.94	33.10	35.56
328.15	I	36.43	34.46	35.71	60.52	31.55	36.94
	II	39.92	34.97	37.17	60.57	28.18	35.00
	III	36.45	34.48	35.73	60.52	31.57	34.19
333.15	I	34.12	31.83	33.23	59.67	28.48	34.45
	II	37.63	32.37	34.71	59.72	25.15	32.52
	III	34.14	31.86	33.25	59.67	28.51	31.41
PEG400 (1) + 1,3-propanediol (2)							
288.15	I	26.09	23.69	24.72	56.10	21.29	24.80
	II	29.85	24.21	26.24	56.17	18.94	23.14
	III	26.16	23.74	24.77	56.11	21.36	23.47
293.15	I	27.23	24.22	25.90	56.86	21.70	25.41
	II	30.91	24.80	27.45	56.92	19.01	23.60
	III	27.29	24.29	25.96	56.87	21.77	23.83
298.15	I	28.01	25.11	26.74	57.06	22.46	26.43
	II	31.64	25.69	28.27	57.12	19.83	24.44
	III	28.06	25.17	26.80	57.07	22.52	24.53
303.15	I	31.18	28.73	30.17	58.50	25.23	30.22
	II	34.73	29.28	31.65	58.56	22.50	28.24
	III	31.23	28.79	30.22	58.51	25.30	28.24
308.15	I	33.54	31.51	32.76	59.39	28.57	33.12
	II	37.00	32.01	34.19	59.44	25.26	31.18
	III	33.59	31.56	32.81	59.39	28.63	31.20
313.15	I	40.08	38.52	39.58	62.21	36.20	40.34
	II	43.64	38.95	41.00	62.25	32.59	38.26
	III	40.12	38.56	39.62	62.21	36.25	38.46
318.15	I	45.88	45.25	45.90	64.27	44.18	47.23
	II	49.37	45.62	47.26	64.31	40.55	45.16
	III	45.91	45.28	45.93	64.28	44.22	45.63
323.15	I	48.38	48.15	48.62	65.09	47.64	50.22
	II	51.81	48.50	49.96	65.13	44.01	48.17
	III	48.40	48.18	48.65	65.10	47.68	48.72
328.15	I	48.07	47.75	48.26	65.16	47.10	49.87
	II	51.49	48.10	49.59	65.20	43.50	47.84
	III	48.10	47.78	48.29	65.16	47.14	48.27
333.15	I	50.49	50.57	50.90	65.98	50.47	52.78

TABLE S-I. Continued

T / K	Model	Model					
		L–L	D–G	Eyk	A–B	New	Ost
PEG400 (1) + 1,3-propanediol (2)							
333.15	II	53.89	50.93	52.24	66.01	46.89	50.76
	III	50.52	50.60	50.93	65.98	50.51	51.28
Pyridine (1) + 1-propanol (2)							
288.15	I	21.11	19.27	9.45	57.46	68.66	51.44
	II	34.16	26.65	29.70	58.21	16.99	21.35
	III	20.98	19.42	9.52	57.47	68.84	47.60
293.15	I	21.30	19.07	9.43	57.54	68.99	51.58
	II	33.93	26.41	29.48	58.28	17.06	21.30
	III	21.16	19.22	9.49	57.55	69.17	47.57
298.15	I	22.24	17.82	9.01	57.20	68.11	50.67
	II	32.87	25.22	28.35	57.95	16.13	20.21
	III	22.11	17.97	9.08	57.21	68.30	46.43
303.15	I	22.79	17.21	9.46	57.11	68.07	50.41
	II	32.27	24.55	27.73	57.85	16.14	19.90
	III	22.66	17.36	9.52	57.13	68.26	46.02
308.15	I	31.96	9.75	7.88	54.01	56.76	40.87
	II	24.54	16.01	19.22	54.88	9.69	12.55
	III	31.77	9.81	7.71	54.02	57.01	35.37
313.15	I	34.23	7.59	8.30	53.42	55.76	39.74
	II	23.04	14.67	17.64	54.29	8.04	11.13
	III	34.04	7.68	8.12	53.44	56.02	33.93
318.15	I	39.38	5.71	11.96	52.06	50.34	35.13
	II	19.06	11.97	13.82	52.99	7.28	9.56
	III	39.17	5.82	11.74	52.09	50.63	28.66
323.15	I	17.46	24.99	12.74	59.82	80.44	59.94
	II	37.86	31.35	34.07	60.43	22.78	27.99
	III	17.36	25.09	12.79	59.83	80.56	55.35
Pyridine (1) + 1,2-propanediol (2)							
288.15	I	15.59	14.61	13.91	47.44	19.23	16.61
	II	15.75	13.82	14.25	48.05	16.41	13.74
	III	15.45	14.61	13.85	47.46	19.24	17.40
293.15	I	15.97	14.47	14.26	47.16	18.67	16.22
	II	15.31	13.58	14.03	47.77	17.22	13.94
	III	15.84	14.43	14.20	47.18	18.69	16.97
298.15	I	16.11	13.80	13.63	46.65	16.39	14.41
	II	14.29	12.50	12.52	47.26	17.25	13.52
	III	15.96	13.74	13.57	46.68	16.40	14.98
303.15	I	17.45	14.33	14.36	46.09	16.37	14.44
	II	12.82	12.58	12.59	46.70	18.73	14.71
	III	17.29	14.21	14.25	46.11	16.38	14.98
308.15	I	20.66	16.18	16.06	44.59	16.31	14.47

TABLE S-I. Continued

T / K	Model	Model					
		L–L	D–G	Eyk	A–B	New	Ost
Pyridine (1) + 1,2-propanediol (2)							
308.15	II	12.75	13.05	12.71	45.21	23.11	16.45
	III	20.43	16.05	15.94	44.61	16.33	14.99
313.15	I	24.68	19.18	19.29	42.99	16.57	14.12
	II	11.70	14.34	12.71	43.64	28.75	19.59
	III	24.42	18.96	19.08	43.02	16.55	15.78
318.15	I	28.06	22.66	22.78	41.54	18.73	15.91
	II	12.35	16.68	14.34	42.20	33.62	23.46
	III	27.77	22.34	22.49	41.58	18.64	17.65
323.15	I	38.32	34.87	34.19	37.62	31.26	24.24
	II	14.73	27.73	21.55	38.35	47.20	35.36
	III	37.97	34.47	33.82	37.66	30.78	28.93
Pyridine (1) + 1,3-propanediol (2)							
288.15	I	10.62	11.41	11.06	52.18	12.50	11.78
	II	20.12	11.45	14.84	52.71	13.42	11.13
	III	10.55	11.35	11.00	52.21	12.41	11.72
293.15	I	10.71	11.47	11.13	51.59	12.98	11.22
	II	18.96	10.80	13.70	52.12	14.47	11.41
	III	10.65	11.40	11.06	51.62	12.75	11.75
298.15	I	9.42	10.41	9.69	51.28	11.92	9.43
	II	17.08	9.06	11.66	51.80	14.06	10.27
	III	9.36	10.22	9.63	51.31	11.68	10.11
303.15	I	8.38	9.35	8.61	50.91	10.80	7.88
	II	15.71	7.25	9.38	51.42	14.26	9.19
	III	8.21	9.15	8.43	50.94	10.57	9.05
308.15	I	8.07	9.11	8.16	50.35	11.67	7.41
	II	13.75	6.62	7.82	50.87	15.07	9.31
	III	7.84	8.86	7.98	50.40	11.23	8.65
313.15	I	8.62	10.39	8.86	49.53	13.91	8.37
	II	11.44	7.34	6.48	50.05	16.84	10.65
	III	8.37	10.00	8.65	49.57	13.44	9.92
318.15	I	7.59	10.16	8.34	49.02	14.07	7.95
	II	9.76	6.74	5.37	49.54	18.08	10.18
	III	7.33	9.76	7.97	49.07	13.51	9.78
323.15	I	9.20	13.14	10.47	47.27	19.58	10.47
	II	5.54	8.59	5.50	47.80	23.75	13.85
	III	8.81	12.61	9.99	47.33	18.91	13.26
Pyridine (1) + glycerol (2)							
288.15	I	10.76	13.75	11.04	36.84	26.84	18.91
	II	10.34	11.65	9.65	37.07	26.20	19.43
	III	10.88	13.11	10.85	36.91	26.05	17.84
293.15	I	10.48	14.14	11.15	36.97	27.53	19.21

TABLE S-I. Continued

T / K	Model	Model					
		L–L	D–G	Eyk	A–B	New	Ost
Pyridine (1) + glycerol (2)							
293.15	II	10.07	11.97	9.61	37.23	26.77	19.63
	III	10.61	13.47	10.94	37.04	26.70	18.33
298.15	I	10.16	16.07	12.06	36.23	29.86	21.08
	II	9.75	13.77	10.45	36.44	28.99	21.41
	III	10.28	15.37	11.71	36.30	28.99	20.39
303.15	I	9.93	16.35	12.05	36.04	30.32	21.20
	II	9.43	14.14	10.54	36.25	29.36	21.46
	III	9.95	15.62	11.71	36.12	29.41	20.71
308.15	I	8.76	17.19	12.49	36.70	31.67	21.98
	II	7.99	15.03	10.10	36.93	30.63	22.18
	III	8.75	16.40	11.76	36.78	30.70	21.70
313.15	I	7.49	16.85	12.07	37.75	31.60	21.50
	II	6.81	14.78	9.80	37.98	30.52	21.64
	III	7.53	16.03	11.31	37.84	30.59	21.43
318.15	I	6.25	15.87	11.03	39.28	30.83	20.35
	II	5.42	13.88	8.87	39.49	29.71	20.44
	III	6.10	15.03	10.25	39.37	29.78	20.49
323.15	I	4.69	15.03	10.12	40.78	30.21	19.33
	II	3.65	13.13	8.07	40.98	29.08	19.38
	III	4.45	14.15	9.30	40.88	29.13	19.69
Benzene (1) + PEG200 (2)							
288.15	I	52.13	54.66	54.24	68.05	57.78	57.42
	II	58.48	55.56	56.76	68.15	51.75	53.71
	III	52.15	54.69	54.26	68.06	57.81	57.14
293.15	I	48.68	49.94	49.99	66.65	51.38	52.13
	II	54.69	51.08	52.57	66.77	46.37	48.93
	III	48.71	49.93	50.02	66.65	51.42	51.65
298.15	I	44.54	44.54	45.06	64.76	44.32	46.23
	II	50.24	45.92	47.71	64.90	40.27	43.48
	III	44.59	44.59	45.11	64.76	44.38	45.52
303.15	I	40.52	39.31	40.29	63.16	37.48	40.57
	II	45.96	40.91	43.01	63.33	34.28	38.22
	III	40.58	39.37	40.35	63.17	37.56	39.60
308.15	I	37.88	35.74	37.07	62.04	32.69	36.70
	II	42.96	37.45	39.75	62.22	30.17	34.69
	III	37.95	35.83	37.15	62.05	32.79	35.50
313.15	I	35.62	32.69	34.32	61.05	28.58	33.41
	II	40.36	34.46	36.94	61.24	26.66	31.72
	III	35.71	32.79	34.41	61.06	28.70	31.98
318.15	I	32.70	28.92	30.88	59.92	23.67	29.45
	II	37.17	30.78	33.48	60.12	22.29	28.03

TABLE S-I. Continued

T / K	Model	Model					
		L–L	D–G	Eyk	A–B	New	Ost
Benzene (1) + PEG200 (2)							
318.15	III	32.81	29.04	30.99	59.94	23.82	27.75
323.15	I	31.67	27.38	29.52	59.46	21.46	27.81
	II	35.77	29.20	31.99	59.65	20.47	26.62
	III	31.79	27.52	29.65	59.48	21.63	25.92
328.15	I	29.34	24.37	26.78	58.61	17.52	24.72
	II	33.17	26.22	29.18	58.79	16.94	23.74
	III	29.48	24.53	26.92	58.62	17.71	22.53
333.15	I	20.35	13.68	16.81	55.37	9.09	13.87
	II	24.22	15.82	19.41	55.59	8.67	13.14
	III	20.56	13.92	17.03	55.39	9.04	11.06
Benzene (1) + PEG400 (2)							
288.15	I	22.04	18.62	20.26	52.66	14.40	18.63
	II	27.90	20.86	23.44	52.93	13.31	17.21
	III	22.14	18.70	20.33	52.67	14.50	17.77
293.15	I	19.35	15.00	16.93	51.54	9.76	14.76
	II	24.91	17.34	20.20	51.82	9.16	13.59
	III	19.46	15.09	17.02	51.55	9.86	13.71
298.15	I	15.86	11.02	13.26	50.01	7.40	10.57
	II	21.18	13.46	16.27	50.30	7.33	9.63
	III	16.00	11.13	13.37	50.03	7.41	9.36
303.15	I	14.17	8.83	11.22	49.46	6.68	8.31
	II	19.17	11.22	14.16	49.75	6.67	7.59
	III	14.33	8.96	11.34	49.48	6.69	7.21
308.15	I	13.61	8.25	10.71	49.15	7.30	7.93
	II	18.12	10.53	13.50	49.42	7.29	7.70
	III	13.74	8.38	10.84	49.17	7.30	7.35
313.15	I	13.99	8.51	10.98	49.26	6.40	8.48
	II	18.00	10.63	13.58	49.52	6.46	8.21
	III	14.12	8.57	11.12	49.28	6.41	7.11
318.15	I	14.02	8.16	10.50	49.44	5.96	8.12
	II	17.88	9.96	12.95	49.69	6.06	7.92
	III	14.22	8.22	10.65	49.46	5.87	6.66
323.15	I	13.63	7.44	9.82	49.47	6.63	7.41
	II	17.19	9.11	12.14	49.70	6.46	7.28
	III	13.84	7.51	9.99	49.49	6.43	6.06
328.15	I	12.06	5.78	7.87	48.85	7.72	5.76
	II	15.37	7.34	10.12	49.08	7.00	5.69
	III	12.29	5.86	8.05	48.88	7.43	4.77
333.15	I	12.73	7.93	9.67	49.14	9.13	8.16
	II	15.51	9.32	11.24	49.35	8.84	8.18
	III	12.92	8.01	9.74	49.17	8.86	7.32

TABLE S-I. Continued

T / K	Model	Model					
		L–L	D–G	Eyk	A–B	New	Ost
Toluene (1) + PEG200 (2)							
288.15	I	29.73	27.03	28.83	64.72	23.14	28.36
	II	37.96	29.94	33.26	65.03	19.44	25.25
	III	29.82	27.13	28.93	64.73	23.26	26.95
293.15	I	21.01	17.44	19.29	61.46	13.02	18.25
	II	29.43	19.94	23.88	61.83	10.67	15.79
	III	21.13	17.56	19.40	61.47	13.17	16.93
298.15	I	16.90	12.79	15.02	59.75	8.87	13.38
	II	25.09	15.42	19.17	60.14	7.05	11.20
	III	17.04	12.93	15.15	59.77	8.96	11.76
303.15	I	14.06	9.21	11.74	58.43	8.01	9.66
	II	21.40	11.94	15.49	58.83	6.93	7.73
	III	14.21	9.37	11.89	58.45	7.95	7.87
308.15	I	12.23	6.78	9.54	57.90	6.74	7.17
	II	19.80	9.54	13.49	58.28	6.12	5.45
	III	12.41	6.96	9.70	57.92	6.69	5.32
313.15	I	12.16	5.35	8.44	57.83	6.03	5.69
	II	19.29	8.41	13.00	58.20	6.00	4.32
	III	12.34	5.50	8.63	57.85	5.88	4.26
318.15	I	10.51	2.69	6.46	57.21	8.23	3.17
	II	17.32	6.19	10.91	57.58	8.58	1.87
	III	10.70	2.86	6.66	57.24	7.96	2.55
323.15	I	11.37	3.38	7.23	57.46	8.09	4.00
	II	17.72	6.77	11.43	57.81	8.44	2.69
	III	11.57	3.60	7.44	57.49	7.83	2.18
328.15	I	7.84	2.31	3.22	56.18	13.08	1.88
	II	13.97	2.48	7.38	56.53	12.85	2.87
	III	8.07	2.06	3.46	56.20	12.76	5.20
333.15	I	5.57	16.62	11.46	51.04	31.80	16.01
	II	3.11	12.68	6.90	51.44	30.75	16.85
	III	5.24	16.25	11.12	51.08	31.35	21.05
Toluene (1) + PEG400 (2)							
288.15	I	22.21	20.74	21.56	52.68	20.73	20.97
	II	26.00	21.90	23.14	52.92	20.57	20.58
	III	22.24	20.77	21.59	52.69	20.67	20.45
293.15	I	20.15	18.25	19.24	51.10	19.51	18.40
	II	22.86	19.54	20.92	51.36	19.66	17.92
	III	20.17	18.27	19.27	51.12	19.36	17.64
298.15	I	15.45	13.41	14.02	49.27	19.87	14.12
	II	18.24	14.14	15.85	49.54	19.79	14.41
	III	15.50	13.35	14.06	49.29	19.61	14.66
303.15	I	10.73	10.97	9.82	48.69	19.53	12.19

TABLE S-I. Continued

T / K	Model	Model					
		L–L	D–G	Eyk	A–B	New	Ost
Toluene (1) + PEG400 (2)							
303.15	II	14.92	10.44	11.02	48.97	19.30	12.67
	III	10.80	10.86	9.80	48.71	19.27	13.07
308.15	I	9.60	9.05	7.81	48.42	17.65	10.11
	II	13.70	8.41	9.32	48.69	17.34	10.55
	III	9.75	8.90	7.74	48.45	17.38	11.07
313.15	I	9.00	7.10	6.74	48.49	15.31	8.01
	II	12.84	6.77	8.60	48.75	14.95	8.40
	III	9.12	6.96	6.81	48.52	15.05	9.03
318.15	I	9.67	6.06	6.38	49.48	12.85	6.28
	II	13.74	5.82	8.56	49.73	12.42	6.41
	III	9.86	6.02	6.47	49.51	12.60	6.77
323.15	I	10.11	7.16	7.17	49.31	13.03	7.33
	II	13.83	6.85	9.04	49.55	12.26	7.29
	III	10.22	7.11	7.21	49.34	12.79	7.66
328.15	I	9.05	7.89	7.34	48.72	15.98	8.07
	II	12.07	7.59	7.82	48.95	15.10	8.03
	III	9.17	7.83	7.29	48.74	15.72	9.53
333.15	I	7.55	13.36	9.80	45.66	26.50	14.21
	II	8.91	11.59	8.83	45.90	25.51	14.45
	III	7.46	13.06	9.59	45.69	26.11	17.43

Journal of the Serbian Chemical Society
JSCS-info@shd.org.rs • www.shd.org.rs/JSCS
J. Serb. Chem. Soc. 79 (6) 719–727 (2014)
JSCS–4621
UDC 546.32'264+547.466.22+54–145.2:
532.13/.14:535.327
Original scientific paper

Physical properties of aqueous solutions of potassium carbonate+glycine as a solvent for carbon dioxide removal

MUHAMMAD SHUAIB SHAIKH, AZMI M. SHARIFF*, MOHD A. BUSTAM and GHULAM MURSHID

Research Center for CO_2 Capture ($RCCO_2C$), Department of Chemical Engineering, Universiti Teknologi PETRONAS, 31750 Tronoh, Perak, Malaysia

(Received 18 August, revised 16 October, accepted 13 November 2013)

Abstract: The physical properties, such as densities, viscosities, and refractive indices, of aqueous solutions of potassium carbonate (PC) blended with glycine (Gly) as solvent blends for CO_2 capture were measured. The properties were measured at ten different temperatures from (298.15 to 343.15) K. The mass fractions (w_1+w_2) of the (PC+Gly) blends were 0.05+0.01, 0.10+0.02, 0.15+0.03, 0.20+0.04, 0.25+0.05, 0.30+0.06, 0.35+0.07 and 0.40+0.08 %, respectively. An analysis of the experimental results showed that the densities, viscosities, and refractive indices of the aqueous (PC+Gly) blends increase with increasing concentration of potassium carbonate and glycine, and decrease with increasing the temperature. The experimental data of density, viscosity and refractive index were correlated by a least-squares method as a function of temperature. The predicted data were estimated from coefficients of correlation equations for all the measured properties, and reported with standard deviation (*SD*). The experimental data were consistent with the predicted data.

Keywords: density; viscosity; refractive index; potassium carbonate; glycine; CO_2 capture.

INTRODUCTION

The concern of researchers to overcome the climate change issue is increasing with increasing level of carbon dioxide (CO_2) in the atmosphere. At present, the concentration of CO_2 in the atmosphere is 396.80 ppm, which is more than the acceptable limit (350 ppm). The CO_2 concentration is expected to grow further above 400 ppm by 2015.[1,2] The main causes of the increase in the CO_2 level are the rapid growth of industry and transport, mechanization of agricultural activities, the energy sector and domestic sources.[3,4] The major reasons of the endeavors undertaken to overcome the CO_2 issues are the appalling effects of this

* Corresponding author. E-mail: azmish@petronas.com.my
doi: 10.2298/JSC130818133S

greenhouse gas on the global environment and its inhabitants.[5] In continuation of these endeavors; various technologies have been developed to mitigate CO_2 emission. These technologies include absorption, adsorption, membrane and cryogenic processes. These technological options are in operation to capture CO_2 but efforts are being undertaken to improve these techniques.[6,7] The most developed and functioning technique is the absorption process by chemical solvents.[8]

The solvents that are very common and commercially proven are amine--based solvents, such as monoethanolamine, diethanolamine, triethanolamine, methyldiethanolamine and 2-amino-2-methyl-1-propanol, *etc*.[9–11] These amine--based solvents have been widely used for years on the commercial scale, but some issues were identified and reported in the literature, including, the short life of the solvent due to thermal and oxidative degradation, corrosiveness, volatility, and high-energy consumption during regeneration.[12–15] An aqueous solution of potassium carbonate has also been used as a CO_2 capture agent since it has a lower rate of degradation and lower cost as compared to amines.[16,17] However, the use of this solvent is limited due to the low rate of CO_2 absorption. One of the promising solutions is the addition of suitable promoters in order to remove the acid gases effectively from various gas streams. A varieties of promoters are used nowadays with potassium carbonate, such as monoethanolamine, diethanolamine and piperazine, *etc*.[17,18] Potassium carbonate promoted with these additives offers better CO_2 removal; however, the identified drawbacks of amines restrict the use of these promoters with potassium carbonate. The challenge is to search for the most appropriate promoter to overcome the drawback of amines. One of the potential promoters is an amino acid, such as sarcosine, which has been used for this purpose.[18] This is due to their benefits of having very low degradation, negligible volatility, able to be regenerate, environmental friendly and commercially available.[19–22] These prospective merits of amino acids have encouraged us to investigate another type of potential amino acid, *i.e*., glycine as a promoter.

Physical properties, such as density, viscosity and refractive index, are crucial for the practical development, design and implementation of a solvent.[23,24,35–37] Knowledge of the density and viscosity are a key requirement to establish rate modeling and to determine the constants of the reaction rate.[25] Refractive index data are important to calculate the molar refraction, which is useful for a detailed understanding of the molecular interaction of a solvent.[26–28] In this study, the density, viscosity, and refractive index of aqueous solutions of potassium carbonate (PC) blended with glycine (Gly) were determined and are reported. The concentration variations of the blends were selected in order to investigate their impact on the CO_2 removal performance.

EXPERIMENTAL

Materials

Potassium carbonate (≥99 % pure), glycine (≥99 % pure), and methyldiethanolamine (≥99 % pure) were purchased from Merck Sdn. Bhd, Malaysia. The additional information about the chemicals used in this study is specified in Table I. All the chemicals were used without further purification. Double distilled water was used to prepare all the solutions. The aqueous blends of potassium carbonate (PC) and glycine (Gly) were prepared in mass. An electronic analytical balance (Sartorius, model BSA-224S-CW) with the measurement accuracy of $\pm 1\times10^{-4}$ g was used. The different mass fractions (w_1+w_2) of the (PC+Gly) blends were 0.05+0.01, 0.10+0.02, 0.15+0.03, 0.20+0.04, 0.25+0.05, 0.30+0.06, 0.35+0.07 and 0.40+0.08 %. Furthermore, the uncertainty in the mass fraction was determined to be $\pm 1\times10^{-3}$. All the properties were measured within the temperature range of 298.15 to 343.15 K. The maximum mass fraction in the blend was kept at 0.40 for potassium carbonate, and 0.08 for glycine, which are as per the commercial suitability of the solvent.

TABLE I. Specifications of the chemicals

Name of chemical	Chemical formula	Purity	Method of purification	Source
Glycine	H_2NCH_2COOH	≥ 99 % pure	None	Merck
Potassium carbonate	K_2CO_3	≥ 99 % pure	None	Merck
Methyldiethanolamine	$CH_3N(C_2H_4OH)_2$	≥ 99 % pure	None	Merck
Double distilled water	H_2O	99 % pure	Distillation	–

Apparatus and procedure

The density of different aqueous (PC+Gly) blends was measured using a digital densimeter (Anton Par, model, DMA-4500M) with an accuracy of $\pm 5\times10^{-5}$ g·cm^{-3}. The apparatus was calibrated each time before and after the measurement in order to obtain accurate results. Standard water of Millipore quality was used in the calibration process. Each experiment was performed in triplicate, and the data reported are the average values. The density and temperature uncertainty was $\pm 6\times10^{-5}$ g·cm^{-3} and ±0.01 K, respectively. A digital rolling ball microviscometer (Anton Par, model Lovis-2000M / ME) with an accuracy of up to 0.5 % was used to measure the viscosity of the aqueous (PC+Gly) blends. Before filling the sample in a suitable capillary, the capillary was properly washed with acetone, and air-dried to avoid any error in the reading. Before and after each experiment, the viscometer was carefully calibrated with Millipore water. For the measurement, the capillary was filled with the sample by the help of the syringe, kept inside the viscometer until the set temperature was achieved, and finally, the measurement was started. Each experiment was repeated three times, and the average values of the viscosity are reported. The uncertainties in the viscosity and temperature were estimated to be $\pm 7\times10^{-3}$ mPa·s and ±0.02 K, respectively. For measurement of the refractive index of the aqueous blends of (PC+Gly), a digital Abbemat automatic refractometer (Anton Par, model WR), with an accuracy of $\pm 4\times10^{-5}$ n_D, was used. In order to obtain accurate readings, the refractometer was calibrated with water of Millipore quality each time the sample was changed. Before pouring the sample into the sample mould, the prism face was carefully cleaned with acetone and dried to prevent any disturbance in the results because of possible minute sediments on the prism face. Measurement was started after pouring the sample into the sample mould and setting the required temperature. Each experiment was

conducted three times and the average value is reported. The uncertainties in the refractive index and temperature were $\pm 5\times10^{-5}$ n_D and ±0.03 K, respectively.

RESULTS AND DISCUSSION

The experimental results for pure methyldiethanolamine (MDEA) were compared with the corresponding literature data in order to validate the results. The comparison results for density, viscosity and refractive index of pure MDEA are given in Table II. The % average absolute deviations (% *AAD*) reported in Table II were calculated using Eq. (1):[32]

$$\%\ AAD = \frac{1}{n}\sum\left|\frac{X_{\text{exp}} - X_{\text{lit}}}{X_{\text{lit}}}\right|\times 100 \quad (1)$$

where X_{exp} is experimental values of density, ρ, viscosity, η, and refractive index, n_D, whereas X_{lit} denotes the literature data of density, viscosity and refractive index, and n is the number of data points. The deviation values show that there was good consistency of experimental and literature data.

TABLE II. Comparison of experimental data of density, ρ, viscosity, η, and refractive index, n_D, of pure methyl diethanolamine with literature data

T/ K	Present work	Literature data[34]	*AAD* / %
	ρ / g·cm^{-3}		
303.15	1.03356	1.03325	0.02085
313.15	1.02553	1.02565	
	η / mPa s		
303.15	59.756	59.76	0.021
313.15	37.886	37.9	
	n_D		
303.15	1.46728	1.46796	0.03716
313.15	1.46397	1.46438	

The measured values of the density of the aqueous blends of (PC+Gly) at various temperatures from 298.15 to 343.15 K are presented in Table III. It was found that with increasing mass fraction of potassium carbonate and glycine in the blend, the density increased; however, the density decreased with increasing temperature. This could be due to the wider spaces between the blend molecules at higher temperatures.[23] This density trend is similar to that previously reported work.[29,30]

The investigated data for the viscosity of different concentrations of aqueous (PC+Gly) blends in the temperature range of 298.15 to 343.15 K are listed in Table IV. After analysis of results, it was noticed that the viscosity decreased with increasing temperature. This could be due to a decrease in the internal resistance of the molecules with increasing temperature, which allows the solution molecules to flow easily, thereby reducing the viscosity.[30,31] However, with

increasing concentration of potassium carbonate and glycine in the aqueous solutions, the viscosity tended to increase. The higher concentrated solutions had a higher viscosity than the lower ones, which may be due to the increased molecular resistance in the more concentrated solutions.[30,31] The trends of the variation in viscosity values with changing concentration and temperature were the same as those found in published studies.[30,31]

TABLE III. Density, ρ / g cm^{-3}, of aqueous blends of potassium carbonate (1)+ glycine(2)

T / K	(w_1+w_2) / %							
	0.05+0.01	0.10+0.02	0.15+0.03	0.20+0.04	0.25+0.05	0.30+0.06	0.35+0.07	0.40+0.08
298.15	1.04219	1.08767	1.13833	1.18964	1.24263	1.29839	1.35564	1.41943
303.15	1.04044	1.08565	1.13608	1.18721	1.24006	1.29570	1.35286	1.41656
308.15	1.03854	1.08351	1.13373	1.18470	1.23743	1.29298	1.35005	1.41367
313.15	1.03648	1.08125	1.13129	1.18213	1.23475	1.29021	1.34721	1.41078
318.15	1.03427	1.07887	1.12876	1.17948	1.23200	1.28739	1.34433	1.40784
323.15	1.03193	1.07637	1.12614	1.17675	1.22919	1.28451	1.34140	1.40487
328.15	1.02944	1.07377	1.12342	1.17395	1.22632	1.28158	1.33843	1.40185
333.15	1.02684	1.07108	1.12062	1.17109	1.22340	1.27862	1.33541	1.39880
338.15	1.02410	1.06827	1.11774	1.16816	1.22042	1.27561	1.33237	1.39573
343.15	1.02126	1.06537	1.11478	1.16517	1.21739	1.27256	1.32930	1.39265

TABLE IV. Viscosity, η / mPa s, of aqueous blends of potassium carbonate (1)+glycine (2)

T / K	(w_1+w_2) / %							
	0.05+0.01	0.10+0.02	0.15+0.03	0.20+0.04	0.25+0.05	0.30+0.06	0.35+0.07	0.40+0.08
298.15	0.993	1.164	1.372	1.590	2.014	2.567	3.541	5.010
303.15	0.891	1.048	1.236	1.431	1.788	2.292	3.128	4.387
308.15	0.806	0.954	1.120	1.297	1.613	2.063	2.813	3.879
313.15	0.733	0.869	1.021	1.183	1.458	1.870	2.540	3.464
318.15	0.672	0.795	0.937	1.083	1.331	1.705	2.306	3.111
323.15	0.619	0.733	0.863	1.005	1.222	1.562	2.103	2.816
328.15	0.572	0.682	0.799	0.923	1.112	1.439	1.931	2.583
333.15	0.532	0.634	0.743	0.857	1.045	1.331	1.780	2.367
338.15	0.496	0.594	0.693	0.800	0.972	1.237	1.648	2.179
343.15	0.464	0.555	0.648	0.749	0.911	1.152	1.531	2.017

The experimental data for the refractive index of the aqueous solutions of (PC+Gly) in the temperature range 298.15 to 343.15 K are reported in Table V. From experimental values, it was observed that the refractive index increased with increasing concentration of the blends but decreased slightly with increasing temperature. The decrease in refractive index with increasing temperature could be due to an increase in the speed of the particles in the aqueous (PC+Gly) blends, causing the light to strike fewer molecules, thereby reducing the refractive index. In case of concentration, since additional molecules were present in the solution, the chances of light striking the molecules was greater, thereby increasing the refractive index.[38] The manner in which the refractive index

decreased with temperature and increased with increasing concentration was same as reported in the literature.[32,33]

TABLE V. Refractive index, n_D, of aqueous blends of potassium carbonate (1)+glycine (2)

T / K	(w_1+w_2) / %							
	0.05+0.01	0.10+0.02	0.15+0.03	0.20+0.04	0.25+0.05	0.30+0.06	0.35+0.07	0.40+0.08
298.15	1.34158	1.35042	1.36001	1.36994	1.37893	1.38850	1.39801	1.40815
303.15	1.34091	1.34969	1.35921	1.36861	1.37817	1.38763	1.39714	1.40727
308.15	1.34020	1.34892	1.35843	1.36788	1.37733	1.38674	1.39626	1.40639
313.15	1.33951	1.34819	1.35776	1.36710	1.37654	1.38596	1.39542	1.40553
318.15	1.33876	1.34754	1.35717	1.36660	1.37592	1.38528	1.39464	1.40470
323.15	1.33800	1.34667	1.35680	1.36636	1.37540	1.38468	1.39402	1.40399
328.15	1.33727	1.34597	1.35657	1.36596	1.37495	1.38430	1.39361	1.40334
333.15	1.33662	1.34511	1.35601	1.36557	1.37453	1.38398	1.39323	1.40288
338.15	1.33602	1.34421	1.35583	1.36550	1.37445	1.38355	1.39311	1.40277
343.15	1.33546	1.34347	1.35536	1.36541	1.37421	1.38302	1.39282	1.40270

Experimentally measured data for density were converted into graphical form with respect to temperature, and based on various series of concentrations, the best fit was found by the least-squares method. The following equation was used to report the correlation coefficients for density:

$$\rho = P_0 + P_1(T / K) + P_2(T / K)^2 \quad (2)$$

where ρ represents the density, P_0, P_1 and P_2 are the optimized correlation parameters and T is the temperature. These fitting parameters are listed in Table VI along with the *SD* calculated using Eq. (3), as also mentioned in literature:[23]

$$SD = \left[\frac{\sum_{i=1}^{n} (X_{\text{exp},i} - X_{\text{calc}},i)^2}{n} \right]^{0.5} \quad 3)$$

where *SD* is the standard deviation, X_{exp} is the experimental value of the density, ρ, viscosity, η, or refractive index, n_D, X_{cal} is the calculated value of the same property, and n is the number of data points.

Measured viscosity data was transformed into graphical form with respect to the temperature. The fittings were conducted by the least- squares method using an exponential function. The following equation was used to correlate the viscosity data:

$$\eta = Q_0 \exp\left(-Q_1 T / K\right) \quad (4)$$

where η is the viscosity, Q_0 and Q_1 are the optimized coefficients, and T is the temperature. The optimized parameters of the correlation equation are reported in Table VII with the SD calculated using Eq. (3).

TABLE VI. Correlation Eq. (2) parameters and *SD* for the density, ρ / g·cm^{-3}, of aqueous blends of potassium carbonate (1)+glycine (2)

(w_1+w_2) / %	P_0	10^4P_1	10^6P_2	R^2	10^3SD
0.05+0.01	0.89973	12.982	–2.751	0.999	0.075
0.10+0.02	1.01042	9.155	–2.201	0.999	0.013
0.15+0.03	1.11189	6.208	–1.784	0.999	0.073
0.20+0.04	1.20693	3.643	–1.416	0.999	0.006
0.25+0.05	1.29024	1.890	–1.169	0.999	0.009
0.30+0.06	1.37268	0.331	–0.946	0.999	0.008
0.35+0.07	1.44956	–0.801	–0.787	0.999	0.009
0.40+0.08	1.53266	–1.928	–0.627	0.999	0.012

TABLE VII. Correlation Eq. (3) parameters and *SD* for the viscosity, η / mPa s, of aqueous blends of potassium carbonate (1)+glycine (2)

(w_1+w_2) / %	Q_0	Q_1	R^2	*SD*
0.05+0.01	143.793	–0.016	0.992	0.014
0.10+0.02	146.897	–0.016	0.994	0.015
0.15+0.03	185.701	–0.016	0.994	0.017
0.20+0.04	221.242	–0.016	0.992	0.050
0.25+0.05	361.613	–0.017	0.995	0.033
0.30+0.06	483.578	–0.017	0.994	0.036
0.35+0.07	837.945	–0.018	0.994	0.053
0.40+0.08	1884.389	–0.020	0.994	0.092

TABLE VIII. Correlation Eq. (2) parameters and *SD* for refractive index, n_D, of aqueous blends of potassium carbonate (1)+glycine (2)+water (3)

(w_1+w_2) / %	P_0	10^4P_1	10^6P_2	R^2	10^2SD
0.05+0.01	1.41254	–3.236	0.287	0.999	0.005
0.10+0.02	1.36221	0.602	–0.334	0.999	0.004
0.15+0.03	1.52877	–9.723	1.362	0.995	0.010
0.20+0.04	1.64353	–16.343	2.401	0.992	0.012
0.25+0.05	1.60404	–13.181	1.889	0.998	0.005
0.30+0.06	1.58081	–11.031	1.536	0.997	0.009
0.35+0.07	1.65388	–15.021	2.160	0.998	0.006
0.40+0.08	1.67178	–15.405	2.203	0.996	0.011

Likewise, the experimentally measured refractive index data were plotted in the form of its relationship *vs.* temperature followed by the series of different concentrations of (PC+Gly) blends. In order to predict the refractive index data, the same correlation Eq. (2) was used as for the density prediction. The parameters of the refractive index fitting equation are presented in Table VIII together with the *SD* estimated using Eq. (3).

After the analysis of the predicted density, viscosity, and refractive index data obtained from the correlation equations, it was observed that the predicted data were in good agreement with the experimental data.

CONCLUSIONS

The physical properties of aqueous (PC+Gly) blends such as density, viscosity, and refractive index were measured at a range of temperature from 298.15 to 343.15 K. The measured properties were observed to increase with increasing concentration of potassium carbonate and glycine in the solution. However, all properties tended to decrease with increasing temperature. The same trend was reported in the available literature. All experimental data were correlated by least-squares fitting to mathematical equations in order to calculate the predicted data. Based on the deviations calculated between the experimental and predicted data, good agreement was found. Hence, the developed correlations are acceptable and could be used in design calculations of future CO_2 removal systems.

Acknowledgement. The authors are thankful to $RCCO_2C$, Universiti Teknologi Petronas for financial and technical support in the completion of this research study.

И З В О Д

ФИЗИЧКА СВОЈСТВА ВОДЕНИХ РАСТВОРА КАЛИЈУМ-КАРБОНАТА СА ГЛИЦИНОМ КАО РАСТВАРАЧА ЗА УКЛАЊАЊЕ УГЉЕН-ДИОКСИДА

MUHAMMAD SHUAIB SHAIKH, AZMI M.SHARIFF, MOHD A. BUSTAM и GHULAM MURSHID

Research Center for CO_2 Capture ($RCCO_2C$), Department of Chemical Engineering, Universiti Teknologi PETRONAS, 31750 Tronoh, Perak, Malaysia

Мерена су физичка својства, као што су густине, вискозности и индекси рефракције, водених раствора калијум-карбоната (PC) помешаног са глицином (Gly), као растварача за уклањање CO_2. Ова својства су мерена на 10 различитих температура, од 298,15 то 343,15 K. Масени удели (w_1+w_2) раствора (PC+Gly) су били 0,05+0,01, 0,10+0,02, 0,15+0,03, 0,20+0,04, 0,25+0,05, 0,30+0,06, 0,35+0,07 и 0,40+0,08 %, редом. Анализа експерименталних резулата показује да густине, вискозности и индекси рефракције водених (PC+Gly) смеша расту са порастом концентрација калијумкарбоната и глицина, и опадају са смањењем температуре. Експериментални подаци за густине, вискозности и индексе рефракције су корелисани као функције температуре, коришћењем методе најмањих квадрата. Предикције података су одређене на основу коефицијената корелација за сва мерена својства, и приказане са стандардном девијацијом. Експериментални подаци су конзистентни са предикцијама.

(Примљено 18. августа, ревидирано 16. октобра, прихваћено 13. новембра 2013)

REFERENCES

1. H. Herzog, B. Eliasson, O. Kaarstad, *Sci. Am*. **182** (2000) 72
2. *Recent Global Monthly Mean CO_2 levels*, National Oceanographic and Atmospheric Administration, Silver Springs, MD, 2012
3. M. Wang, A. Lawal, P. Stephenson, J. Sidders, C. Ramshaw, *Chem. Eng. Res. Des.* **89** (2011) 1609
4. E. S. Rubin, A. B. Rao, *Environ. Sci. Technol*. **36** (2002) 4467
5. *Intergovernmental Panel on Climate Change*, IPCC report, IPCC, Geneva, 2007
6. B. D. Bhide, A. Voskericyan, *Chem. Eng. Trans* .**19** (1998) 37
7. A. Aboudheir, W. El Moudir, *Energy Procedia* **1** (2009) 195

8. B. P. Mandal, M. Guha, A. K. Biswas, S. S. Bandyopadhyay, *Chem. Eng. Sci*. **56** (2001) 6217
9. P. W. Derks, K. J. Hogendoorn, G. F. Versteeg, *J. Chem. Eng. Data* **50** (2005) 1947
10. J.-G. Lu, Y. Ji, H. Zhang, M.-D. Chen, *Sep. Sci. Technol*. **45** (2010) 1240
11. C.-S. Tan, J.-E. Chen, *Sep. Purif. Technol*. **49** (2006) 174
12. A. Jamal, A. Meisen, *Chem. Eng. Sci*. **56** (2001) 6743
13. A. F. Portugal, J. M. Sousa, F. D. Magalhães, A. Mendes, *Chem. Eng. Sci*. **64** (2009) 1993
14. U. E. Aronu, A. Hartono, H. F. Svendsen, *Chem. Eng. Sci*. **66** (2011) 6109
15. T. Kumagai, K. Tanaka, Y. Fujimura, T. Ono, F. Ito, T. Katz, O. Spuhl, A. Tan, P. W. J. Derks, *Energy Procedia* **4** (2011) 125
16. R. K. Bartoo, *Chem. Eng. Prog*. **80** (1984) 35
17. J. T. Cullinane, G. T. Rochelle, *Ind. Eng. Chem. Res*. **45** (2006) 2531
18. H. Y. Jo, M. G. Lee, B. S. Kim, H. J. Song, H. B. Gil, J. W. Park, *J. Chem. Eng. Data* **57** (2012) 3624
19. K. Simons, W. D. W. F. Brilman, H. Mengers, K. Nijmeijer, M. Wessling, *Ind. Eng. Chem. Res*. **49** (2010) 9693
20. R. J. Hook, *Ind. Eng. Chem. Res.* **36** (1997) 1779
21. A. Hartono, U. E. Aronu, H. F. Svendsen, *Energy Procedia* **4** (2011) 209
22. A. Nuchitprasittichai, S. Cremaschi, *Comput. Chem. Eng*. **35** (2011) 1521
23. M. S. Shaikh, A. M Shariff, M. A. Bustam, G. Murshid, *J. Chem. Eng. Data* **58** (2013) 634
24. A. Muhammad, M. I. Mutalib, T. Murugesan, A. Shafeeq, *J. Chem. Eng. Data* **53** (2008) 2226
25. G. Murshid, A. M. Shariff, K. K. Lau, M. A. Bustam, *J. Chem. Eng. Data* **57** (2012) 133
26. M. Roy, R. Sah, P. Pradhan, *Int. J. Thermophys.* **31** (2010) 316
27. Y. M. Tseng, A. R. Thompson, *J. Chem. Eng. Data* **9** (1964) 264
28. S. S. Ubarhande, A. S. Burghate, B. N. Berad, J. D. Turak, *Rasayan J. Chem*. **4** (2011) 585
29. S. Mazinani, A. Samsami, A. Jahanmiri, *J. Chem. Eng. Data* **56** (2011) 3163
30. F. Harris, K. A. Kurnia, M. I. A. Mutalib, T. Murugesan, *J. Chem. Eng. Data* **54** (2009) 144
31. S. Lee, S.-I. Choi, S. Maken, H.-J. Song, H.-C. Shin, J.-W. Park, K.-R. Jang, J.-H. Kim, *J. Chem. Eng. Data* **50** (2005) 1773
32. G. Murshid, A. M. Shariff, K. K. Lau, M. A. Bustam, *J. Chem. Eng. Data* **56** (2011) 2660
33. J. G. Baragi, S. Maganur, V. Malode, S. J. Baragi, *J. Mol. Liq*. **178** (2013) 175
34. M. A. Majid, T. Murugesan, *J. Mol. Liq*. **169** (2012) 95
35. A. B. Knežević-Stevanović, J. D. Smiljanić, S. P. Šerbanović, I. R. Radović, M. Lj. Kijevčanin, *J. Serb. Chem. Soc.* **79** (2014) 77
36. O. Ciocirlan, O. Iulian, *J. Serb. Chem. Soc.* **74** (2009) 317
37. I. R. Radović, M. Lj. Kijevčanin, A. Ž. Tasić, B. D. Djordjević, S. P. Šerbanović, *J. Serb. Chem. Soc.***74** (2009) 1303
38. K. P. Pharm, California State Science Fair, Project No. S1615. (2008) 1.

Journal of the Serbian Chemical Society
JSCS-info@shd.org.rs • www.shd.org.rs/JSCS
J. Serb. Chem. Soc. 79 (6) 729–741 (2014) UDC 556.551+546.3:544.362+579.68(497.11)
JSCS–4622 *Original scientific paper*

Investigation of the microbial diversity of an extremely acidic, metal-rich water body (Lake Robule, Bor, Serbia)

SRĐAN STANKOVIĆ[1]*, IVANA MORIĆ[2], ALEKSANDAR PAVIĆ[2], BRANKA VASILJEVIĆ[2], D. BARRIE JOHNSON[3] and VLADICA CVETKOVIĆ[1]

[1]*University of Belgrade, Faculty of Mining and Geology, Belgrade, Serbia,* [2]*Institute of Molecular Genetics and Genetic Engineering, University of Belgrade, Serbia and* [3]*School of Biological Sciences, Bangor University, Bangor, United Kingdom*

(Received 5 June, revised 24 June, accepted 24 June 2013)

Abstract: An investigation of the microbial diversity in the extremely acidic, metal-rich Lake Robule was performed using culture-dependant and culture-independent (T-RFLP) methods. In addition, the ability of the indigenous bacteria from the lake water to leach copper from a mineral concentrate was tested. T-RFLP analysis revealed that the dominant bacteria in the lake water samples were the obligate heterotroph *Acidiphilium cryptum* (≈50 % of the total bacteria) and the iron-oxidizing autotroph *Leptospirillum ferrooxidans* (≈40 %) The iron/sulfur-oxidizing autotroph *Acidithiobacillus ferrooxidans* was reported to be the most abundant bacteria in the Lake in an earlier study, but it was not detected in the present study using T-RFLP, although it was isolated on solid media and detected in enrichment (bioleaching) cultures. The presence of the two bacterial species detected by T-RFLP (*L. ferrooxidans* and *A. cryptum*) was also confirmed by cultivation on solid media. The presence and relative abundance of the bacteria inhabiting Lake Robule was explained by the physiological characteristics of the bacteria and the physico-chemical characteristics of the lake water.

Keywords: acidophiles; bioleaching; biomining; tailings; T-RFLP.

INTRODUCTION

The Copper Mine Bor has been in operation since 1903, and during that time millions of tons of mine tailings have been deposited in the close proximity of the town of Bor. Exposure of the tailings to air and water initiated the microbially accelerated oxidative dissolution of sulfide minerals, forming an acid mine drainage (AMD) containing elevated concentrations of metal cations and sulfates. It is known that acidophilic bacteria and archaea, some of which are directly involved in the process of sulfide mineral oxidation and thereby accelerate the

* Corresponding author. E-mail: srdjan.stankovic@gmail.com
doi: 10.2298/JSC130605071S

production of AMD by a factor of up to 10^6, rapidly populate acidic environments.[1] This commonly leads to the formation of acidic lakes and ponds under deposits of tailings and in open pits.

Lake Robule is located at the foot of the overburden of the open pit named Visoki planir, which was created during the five-year period from 1975 until 1980. It is the largest overburden of the Copper Mine Bor (100 m in height) and is composed of 150 million tons of waste rocks and off-balanced ore.[2] By preventing water circulation, the Visoki planir overburden created Lake Robule. The lake also collects water draining the overburden after rainfall. The lake is 200 m in length and 150 m in width with a maximum depth of about 10 m. Although water is drained from the lake into the Bor River at a constant rate of about 500 m^3 per day,[3] the lake water level is constant.

Lake Robule has become an extreme environment due to the acidic solutions containing elevated concentrations of metal cations and sulfates continuously flowing into it from the surrounding overburden following rainfall. The input of AMD from the overburden has caused the water of the lake to become highly acidic, and deep red in color due to high concentration of ferric iron. Such an environment is a potential source of acidophilic bacteria that could be used in biohydrometallurgy, specifically for leaching of copper from concentrates, ores and tailings, referred to as bioleaching. Bioleaching technology enables economically feasible exploitation of low-grade ores and tailings, as it is significantly cheaper than the classical pyrometallurgical technology.[4] In addition, the environmental impacts of the bioleaching technology are generally much lower than those associated with the pyrometallurgical processing of copper-containing ores.[5]

It is estimated that tailings of the Copper Mine Bor still contain about one million tons of copper. According to its mineral composition and average contents of copper, the tailing deposits Visoki Planir, Cerovo and the Old Flotation are particularly suitable for microbial leaching. These dumps contain 200 million tons of tailings, with estimated content of 346 000 tons of copper.[6]

It is now accepted that compositions of microbial communities cannot be determined solely using culture-dependant methods[7] and that culture-independent approaches generally yield data that are more comprehensive. In order to better define the bacterial community inhabiting Lake Robule, terminal restriction enzyme fragment length polymorphism (T-RFLP) analysis was used in this study, in parallel with cultivation of acidophilic bacteria on solid media. T-RFLP enables the microbial diversity and relative abundance of microorganisms in samples to be estimated based on the different lengths of polymerase chain reaction (PCR)-amplified DNA (often 16S rRNA genes) that were digested with restriction endonucleases.

The aims of this study were to investigate microbial diversity of the Lake Robule, to isolate and identify indigenous acidophilic bacteria, and to test the bioleaching potential of the microbial community in the lake water.

EXPERIMENTAL

Sampling and measurement of the physicochemical parameters of the lake water

Lake water samples were collected in 50 ml sterile plastic containers on July 26th, 2012. Water temperature, pH and conductivity were measured on site using a Hanna Instruments HI98311 mobile instrument. The redox potential of the water was measured using a combined Pt–Ag/AgCl electrode system.

Copper analysis

The total copper concentrations in the water samples were measured using a modified method described by Anwar *et al*.[8] Cu(II) was reduced to Cu(I) by adding 200 μL of 10 % hydroxylamine solution to 100 μL of water sample. The solution was mixed well and incubated for 5 min at room temperature. First, 1 mL of tartrate buffer (1 mL of 0.5 M HCl added to 100 mL of 0.5 M sodium tartrate and pH adjusted to 5.5) was added and the solution vortexed. Next, 500 μL of phosphate buffer (87.7 mL of 0.2 M NaH_2PO_4 with 13.3 mL of 0.2 M Na_2HPO_4) and 100 μL of 0.1 % bicinchoninic acid (Sigma Chemical, USA) diluted in tartrate buffer was added and the mixture vortexed. Finally, 0.8 mL distilled H_2O was added and the solution was mixed well. After 10 min at room temperature, the absorbance was measured at 562 nm (Cecil CE1011 spectrophotometer).

Iron analysis

The ferrozine assay was used to determine the concentrations of both soluble Fe(III) and Fe(II). The concentrations of Fe(II) were determined using the standard method described by Lovely and Phillips.[9] Then, the total iron concentration was determined by repeating the analysis following addition of hydroxylamine (to reduce the Fe(III) present to Fe(II)). The Fe(III) concentrations were obtained from the difference the obtained values.

Isolation and cultivation of acidophilic bacteria from the Lake Robule on selective solid media

Acidophilic bacteria from Lake Robule were cultivated on overlay solid media[10] that comprised a bottom layer of solid medium inoculated with an acidophilic heterotrophic bacterium *Acidiphilium cryptum* (strain SJH) and a top layer of the same medium inoculated with water from Lake Robule. *A. cryptum* SJH, a heterotrophic acidophilic bacterium, was added to a bottom layer of a plate in order to metabolize products of the hydrolysis of the agarose, which have an inhibitory effect on the growth of most acidophilic chemolithoautotorphs. Bacteria were cultivated on two types of overlay solid media: iFeo, medium, which contained ferrous sulfate as the sole energy source, and is suitable for the cultivation of iron oxidizers such as *Leptospirillum ferrooxidans*, while the FeSo medium that contains ferrous iron, tetrathionate and tryptone soya broth, supports the growth of iron- and sulfur-oxidizers, such as *Acidithiobacillus ferrooxidans*, and also some heterotrophic acidophiles.[11] The iFeo medium contained 1 basal salts of 50×concentrated solution (12.5 g L^{-1} $(NH_4)_2SO_4$, 5 g L^{-1} $MgSO_4 \cdot 7H_2O$), 0.1 % trace elements solution, 25 mM $FeSO_4$, while the composition of the FeSo medium was as follows: 1×basal salts of 50×concentrated solution, 0.1 % trace elements solution, 0.025 % tryptone soya broth, 5 mM $FeSO_4$, and 10 mM $K_2S_4O_6$, in final concen-

trations. All media were gelled using a 0.5 % agarose solution. The inoculated plates were incubated for 30 days at 30 °C.

Extraction and analysis of DNA from the bacterial colonies

A small amount of biomass from several colonies displaying the same morphologies was suspended in 20 μL cell lysis solution (0.05 M NaOH, 0.25 % sodium dodecyl sulfate) and heated at 95 °C for 15 min in a PCR thermocycler. The crude cell lysates were allowed to cool and 180 μL of MilliQ:Tris buffer (0.01 mM Tris, pH 7.5) added. The Fe(III)-encrusted colonies were washed first in 100 mM oxalic acid, and then in sterile ultra-pure water, followed by the addition of the cell lysis solution addition. To identify the isolates, their 16S rRNA genes were amplified using PCR (described below) and the obtained products were digested with the restriction enzyme *Hae*III and the fragment lengths determined using T-RFLP (described below). Bacterial identities were determined by comparing the fragment lengths obtained with those in the databank of acidophilic bacteria maintained at Bangor University, UK.

PCR amplification of 16S rRNA genes

Bacterial 16S rRNA genes were amplified using 27F:
5′-AGAGTTTGATCMTGGCTCAG-3′ and
1387R: 5′-GGGCGGAGTGTACAAGGC-3′
primers. For PCR, a final volume of 25 μL, containing 12.5 μL master mix (Promega, USA), 10 pmol of each primer, 2.5 mM $MgCl_2$. 0.5 μL ultra-pure dimethylsulfoxide and 1 μL DNA template, and ultra-pure water, was used. The PCR reactions were realized in a Techne TC-312 thermocycler. Amplification was performed as follows: initial denaturation 95 °C for 5 min, followed by 30 cycles of denaturation at 95°C for 30 s, annealing 55 °C for 30 s and elongation at 72 °C for 90 s. Final extension was performed at 72 °C for 10 min. The PCR products were analyzed by gel electrophoresis on a 0.7 % agarose gel.

Isolation of DNA from Lake Robule

Approximately 400 mL of lake water was filtered through a 0.2 μm (pore size) sterile membrane filter. The filter was cut into segments and DNA was isolated using a MoBio Ultra Clean Soil DNA isolation kit following manufacturer's instructions. The isolated DNA was used as a template for the amplification of the 16S rRNA genes.

Terminal restriction fragment length polymorphism (T-RFLP) analysis of the amplified 16S rRNA genes

T-RFLP analysis was used to identify the isolated bacteria, and to study the diversity and relative abundance of the microorganisms present in the Lake water samples, as well as in samples following bioleaching of copper concentrate. In this case, PCR amplification was performed as described using a 27F primer labeled with Cy5 dye at the 5′ end (MWG Biotech, Germany) and unlabelled 1387R primer. The PCR products were digested using three different restriction endonucleases, *Hae*III, *Alu*I, and *Cfo*I in three separate reactions. The Reaction mixture consisted of 0.5 μL of enzyme, 1 μL of enzyme specific buffer, 1 μL of PCR product and 7.5 μL of ultra-pure water. The reaction mix was incubated at 37 °C for 1 h. Mixes containing 2 μL of digestion products and 28 μL of sample loading solution were analyzed using a Beckman Coulter CEQ 8000 capillary electrophoresis apparatus. The sample loading solution contained 0.5 μL 600b CEQ DNA size standard dissolved in 27.5 μL of formamide. The T-RFLP analysis for each restriction enzyme was performed in triplicate and the summarized results are presented.

Bioleaching of copper concentrate

To evaluate the bioleaching potential of bacteria inhabiting Lake Robule, a concentrate containing 17 % of copper from the Copper Mine Majdanpek, Serbia, which contained chalcopyrite as the dominant copper sulfide mineral, was used as the test material. The basal salts solution (100 mL, pH 2.0) was transferred into 250 mL conical flasks (in triplicate) and 1 g of concentrate and 1 mL of water from Lake Robule were added. The cultures were incubated at 30 °C and shaken at 150 rpm. The concentrations of soluble iron and copper, pH, redox potentials (using a combined Pt–Ag/AgCl electrode) and the bacteria present in the cultures were determined after three weeks of incubation.

RESULTS

Physical and chemical properties of Lake Robule

The physical and chemical properties of Lake Robule measured on site are given in Table I. The Lake water is highly acidic and characterized by high conductivity due to the presence of elevated concentrations of dissolved ions. The highly positive redox potential of the Lake water is a consequence of the high concentration of Fe(III), which accounts for 99.7 % of the total iron present.

TABLE I. Physical and chemical properties of Lake Robule water

Sampling date	*t* °C	Color	pH	*Eh* mV	Conductivity mS cm^{-1}	$[Fe^{3+}]$ mg L^{-1}	$[Fe^{2+}]$ mg L^{-1}	$[Cu^{2+}]$ mg L^{-1}
26/07/12	26	Deep red	2.55	+850	10	614	1.68	73

T-RFLP analysis of the bacterial community of Lake Robule

Results of T-RFLP analysis of the PCR-amplified 16S rRNA genes sug-

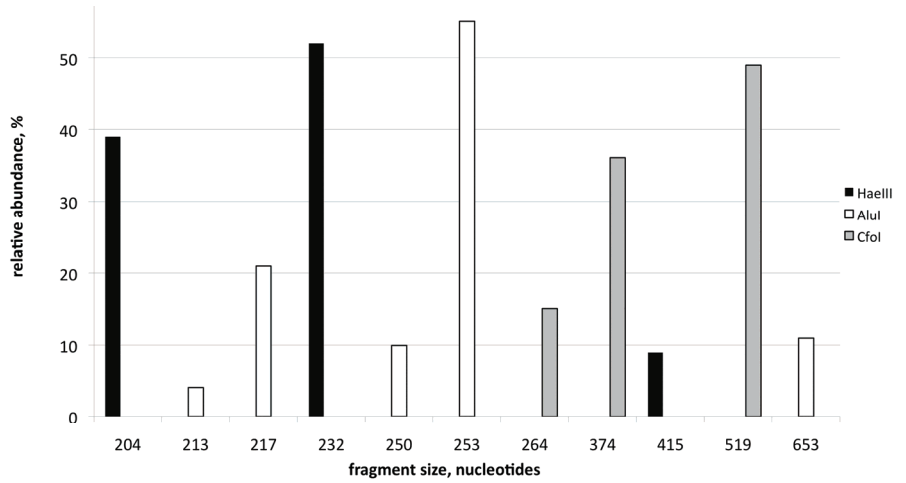

Fig. 1. Analysis of restriction fragments obtained from a sample of Lake Robule water. The length of T-RFs identified after digestion with three endonucleases (*x*-axis) and their relative abundance (*y*-axis).

gested that the bacterial diversity in Lake Robule was very limited, as only three bacterial species were identified (Fig. 1). According to the T-RFLP profiles, the bacteria present in this extreme environment were *L. ferrooxidans*, *A. cryptum* and (more tentatively) *Acidisphaera rubrifaciens*. The presence of *L. ferrooxidans* and *A. cryptum* was confirmed by terminal restriction fragments (T-RFs) produced with all three restriction enzymes, but the presence of *Acd. rubrifaciens* was less certain as only one corresponding T-RF (*Alu*I digests) was detected (Table II). The terminal restriction fragments observed in T-RFLP profiles that could not be related to any fragment in the database are most likely pseudo T-RFs, PCR-related artifacts.[12] The approximate relative abundance of bacteria in the Lake water was calculated from the peak areas of each terminal restriction fragment as a percentage of total peak area. The most abundant bacteria were *A. cryptum* (50 %), followed by *L. ferrooxidans* (40 %), and *Acd. rubrifaciens* (1.3 %). The relative abundance of unidentified T-RFs (pseudo T-RFs) was 8.7 %.

TABLE II. Comparison between the observed T-RFs and those from the database

Enzyme	T-RF from database, nucleotide	Observed T-RF, nucleotide	Identified bacteria
HaeIII	204	204	*L. ferrooxidans*
AluI	217	217	
CfoI	374	374	
HaeIII	232	231	*A. cryptum*
AluI	255	253	
CfoI	519	519	
AluI	213	214	*Acd. rubrifaciens* (?)

Isolation of bacteria from Lake Robule

Three species of acidophilic bacteria were isolated from Lake Robule on overlay plates. Only very small Fe-encrusted colonies (identified as *L. ferrooxi-*

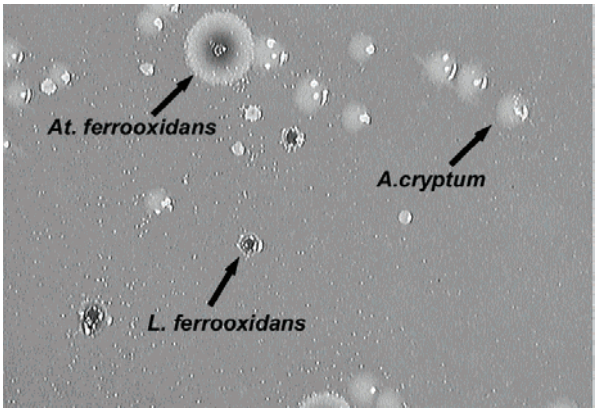

Fig. 2. Colonies of the three species of acidophilic bacteria on a FeSo overlay plate, inoculated with water from Lake Robule.

dans) grew on the iFeo medium. In contrast, three colony variants were identified on the FeSo overlay media: very small Fe-encrusted colonies of *L. ferrooxidans*, larger Fe-encrusted colonies with translucent halos of *At. ferrooxidans* and round, non ferric-iron stained colonies of *A. cryptum*. The colony variants that grew on FeSo overlay plates are shown in Fig. 2. The most abundant colonies were colonies of *A. cryptum*, followed by those of *L. ferrooxidans* and the colonies of *At. ferrooxidans* were the least abundant.

Bioleaching test

After three weeks of the bioleaching experiment, the pH value of the solution was 2.20 and the redox potential was 820 mV. The concentration of the total iron was 815±1.633 mg L^{-1} and the concentration of the total copper was 808.97±5.735 mg L^{-1}. These concentrations of total iron and copper are the mean values of three measurements.

T-RFLP analysis was conducted using only *Hae*III digests, as this restriction endonuclease was able to produce different T-RFs for each of the bacterial species identified in the Lake water. Two bacterial species were identified: *L. ferrooxidans* and *At. ferrooxidans*. However, an additional (and relatively minor) T-RF, not found in the HaeIII digests of the amplified genes from Lake Robule, itself was observed. No acidophilic bacterium corresponding to this T-RF was present in the database. The relative abundances of the microorganisms present in the bioleach liquor are shown in Fig. 3.

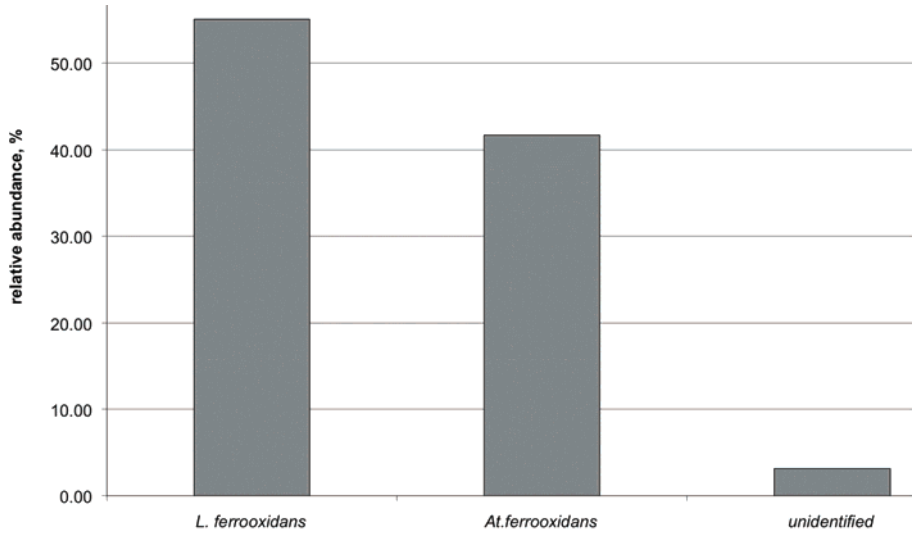

Fig. 3. Relative abundance of bacteria in solution after bioleaching determined by T-RFLP analysis.

DISCUSSION

Lake Robule has been studied for over thirty years. Korać and Kamberović[13] reported that the pH of the lake was 2.97, and that it contained large concentrations of iron, 895 mg L^{-1}, sulfate, 4145 mg L^{-1}, and copper, 55.6 mg L^{-1}. Beškoski *et al.*[3] monitored the physical and chemical properties as well as the microbial diversity of the lake water between 1975 and 2008, and identified *At. ferrooxidans* as the most abundant bacterium in the lake. These authors reported that concentration of copper decreased between 1975, when it was 153 mg L^{-1}, and 2008, when it was 96 mg L^{-1}. The concentration of soluble iron as well as the pH and redox potential fluctuated during this time. The highest and lowest concentrations of iron were detected in 1988, 961 mg L^{-1} and in 1975, 562 mg L^{-1}, respectively. Redox potential of the water was highest in 1988, 527 mV, and lowest in 1975, 297 mV. The redox potential of the lake water was measured by using saturated calomel reference electrode (personal correspondence with the author). The lowest pH of the lake water was detected in 1975, 2.40, and the highest was in 1988, 2.81. Results obtained in the present study were concordant to the results obtained by these authors, with exception of the redox potential of the water (measured with Pt–Ag/AgCl electrode pair), which was higher than any value reported in previous studies. This could be explained by the dominance of Fe(III), which constitutes 99.7 % of total iron in the water.

T-RFLP analysis is a molecular fingerprinting technique that is widely used when studying microbial ecology. It does not require microorganisms to be isolated in order for them to be identified, as it is based on the analysis of genes amplified using environmental DNA as a template.[14] It is a rapid and reliable molecular method for the identification of microorganisms in environmental samples when the microbial diversity of the analyzed sample is low.[15]

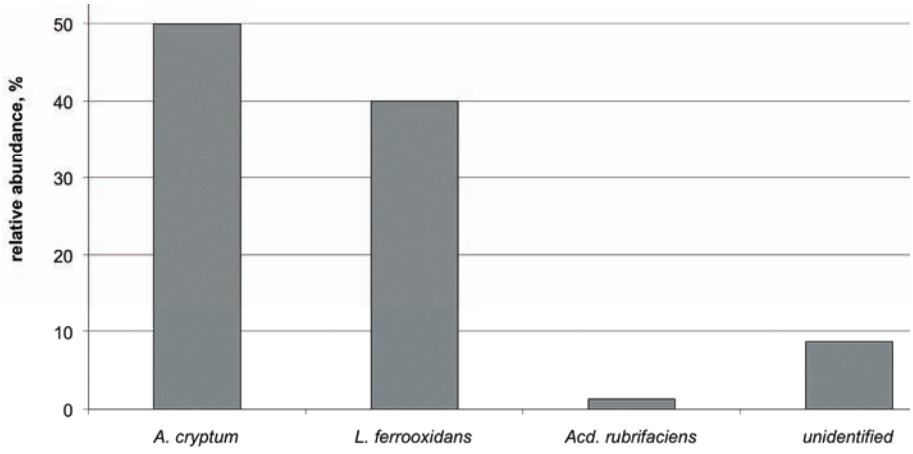

Fig. 4. Relative abundance of bacteria in Lake Robule determined by T-RFLP analysis.

The T-RFLP profiles obtained with three different restriction enzymes confirmed with high confidence that the most abundant bacteria in Lake Robule are *A. cryptum* and *L. ferrooxidans* (Fig. 4). In addition, there is an indication that a bacterium related to *Acd. rubrifaciens* might be present in relatively low numbers, but since only one T-RF characteristic of this bacterium was observed following digestion with AluI, further analysis (*e.g.*, construction and analysis of a clone library) needs to be performed to elucidate this. Interestingly, *At. ferrooxidans*, previously reported as the dominant bacterial species in Lake Robule[3] was not been detected in the Lake water by T-RFLP analysis, although it was isolated on the solid medium (FeSo plates), along with *A. cryptum* and *L. ferrooxidans*. This indicates that while *At. ferrooxidans* is present in the lake, its relative abundance is low compared to those of both *L. ferrooxidans* and *A. cryptum*.

Earlier studies suggested that microbial communities in acidic environments were dominated by *At. ferrooxidans*, but this appears to have been an artifact of the methods, particularly in the enrichment culture and most probably the number counts.[7] Media for cultivation of acidophilic bacteria that have been widely used, and sometimes still are, such as 9K,[16] contain very high concentrations of Fe^{2+} (9 g L^{-1} in 9K) that favor the growth of *At. ferrooxidans*. Even if there is a very small number of *At. ferrooxidans* in a sample, it will be dominant after cultivation in 9K medium. Therefore, the results obtained in such studies are not surprising, as *At. ferrooxidans* thrives in environments with high concentrations of Fe^{2+} and a low redox potential.[17] In contrast, *L. ferroxidans* has a far higher affinity for ferrous ions and greater tolerance to ferric ions, and therefore tends to out-compete *At. ferroxidans* in high redox potential environments.[18]

Both direct plating of mine waters onto overlay media[19] and molecular methods such as T-RFLP and fluorescent *in situ* hybridization (FISH)[7] have revealed that the most abundant bacterium in iron-rich acidic environments is often *L. ferrooxidans*. The concentration of ferric iron in Lake Robule at the time of sampling was 614 mg L^{-1} (11 mM), and the redox potential was 850 mV, which are conditions that are far more conducive for the growth of *L. ferrooxidans* than for *At. ferrooxidans* (Table I). Reports on the composition of microbial community in the Lake published by Beškoski *et al.* (2009) that differ significantly from the results presented in this paper are, probably, the consequence of the methods that were used previously to cultivate bacteria from the Lake water. However, it is also possible that *At. ferrooxidans* was indeed more relatively abundant in the past when redox potentials were generally lower (and more variable) than more recently.

At the end of the bioleaching experiment, only *L. ferrooxidans* and *At. ferrooxidans* were detected in the mineral leachate (Fig. 3). At the start of the experiment, both the ratio of the Fe(III) to Fe(II) concentrations and the redox potential were low, but both increased during culture incubation. Initially, *At. ferrooxi-*

dans would have outgrown *L. ferrooxidans*, since *At. ferrooxidans* has faster growth rate than *L. ferrooxidans* in low redox potential solutions. However, because the leptospirilli have a greater affinity for Fe(II) and are less sensitive to Fe(III), they would become dominant in the later stages of the bioleaching process.[18] These data indicate that *At. ferrooxidans* exist in the lake water, but the numbers of this bacterium in the lake are extremely low, and are undetectable by T-RFLP. The obligatory acidophilic heterotroph *A. cryptum*, the most abundant bacterium in the lake water as determined by T-RFLP analysis and isolation on the solid medium was not detected at the end of the bioleaching period since it is more sensitive to copper than both *At. ferrooxidans* and *L. ferrooxidans*, tolerating up to a maximum of about 10 mM of Cu (635 mg L^{-1}).[20] However, the concentration of copper determined in bioleaching solution was greater than this, *i.e.*, 808.97 mg L^{-1} .

The numbers of heterotrophic acidophiles in acidic, sulfide mineral-rich environments are often much lower than those of chemolithoautotrophic acidophiles, such as *L. ferrooxidans* and *At. ferrooxidans*. Heterotrophic acidophiles in these environments use metabolic products (lysates and exudates) of autotrophic acidophiles as growth substrates, as well as any extraneous organic carbon. In this mutualistic relationship, autotrophs produce growth substrate for heterotrophs, while heterotrophs, utilizing them, eliminate organic compounds (notably small molecular weight aliphatic acids) that are toxic to most acidophiles.[21] Since autotrophic acidophiles produce only small amounts of organic compounds, the numbers of heterotrophic acidophiles are often less than the number autotrophic acidophiles. However, if there is enough organic substrate, acidophilic heterotrophs can grow faster and can outnumber the autotrophs. One potential source of organic matter in the Lake is a municipal waste dump, which is in close proximity to the Lake, while other potential sources could be acidophilic algae. On the bottom of the Lake, green and filamentous biomass exists in the form of a microbial mat, indicating the presence of algae and fungi. Recent reports showed that in acidic environments exposed to sunlight, primary producers of organic matter are algae. Acidophilic algae excrete glycolic acid and sugars and sustain the growth of heterotrophic acidophilic bacteria, including *Acidiphilium* spp.[22] Production of oxygen by algae also helps in the growth of chemolithoautotrophic acidophiles. Since *Leptospirillum* spp. are very sensitive to the presence of organic compounds in the environment (particularly organic acids), it appears that heterotrophic acidophilic bacterium *A. cryptum* efficiently metabolizes organic compounds, facilitating the growth and activity of *L. ferrooxidans* within Lake Robule.

CONCLUSIONS

The bacterial consortium populating Lake Robule is limited in its biodiversity, and is dominated by two bacterial species: *A. cryptum* and *L. ferrooxidans*. The most abundant microorganism in lake is the heterotrophic bacterium *A. cryptum*. This finding suggests that the lake water has a constant supply of organic matter. A possible source of organic matter could be the municipal waste dump that is very close to the lake. Another source of organic matter in the lake is probably acidophilic algae that populate a microbial mat at the bottom of the lake. *L. ferrooxidans* is an autotrophic iron oxidizer. This bacterium thrives in environments, such as that of Lake Robule, that have high concentrations of Fe^{3+} and very positive redox potentials. These conditions are less suitable for the growth of *At. ferrooxidans*, which was not detected by T-RFLP analysis, but was isolated directly from lake water on an overlay solid medium. *At. ferrooxidans* was also detected in the leach liquor from a test performed on the bioleaching of copper from a chalcopyrite concentrate using Lake Robule water as the inoculum. This bacterium prefers low redox potentials and high concentrations of Fe^{2+}, and it grew faster than *L. ferrooxidans* during the initial stages of the bioleaching process. This finding indicates that the lake water contains *At. ferrooxidans*, but in relatively small abundances. Cultivating bacteria from Lake Robule on media with high concentrations of ferrous ions could lead to the wrong conclusions concerning the microbial diversity of the lake. Moreover, this study showed that using only molecular, cultivation independent methods (such as T-RFLP) to evaluate the microbial diversity of environmental samples is not sufficient since *At. ferrooxidans* was not detected by this method. For the most accurate evaluation of microbial diversity under extremely acidic environments, the employment of both molecular- and cultivation-based methods is required.

Physical and chemical properties of the Lake display both seasonal and long-term variations. Consequently, the microbial community of the Lake Robule is also probably subject to variation, and the results presented in this paper are of lake water sampled during the summer months in the recent past. Future research should focus on tracking the changes in physical properties and chemistry of the Lake Robule, followed by an investigation of microbial diversity by combining molecular methods and plating on overlay solid media. This approach would give insight into changes in the microbial communities that populate Lake Robule over time and should explain correlations between changes in physical and chemical properties of the Lake water and the structure of bacterial consortium that inhabits this extreme environment.

Acknowledgements. This study was supported by the Ministry of Education, Science and Technological Development of the Republic of Serbia (Project No. 176016). VC acknowledges the support of the Serbian Academy of Sciences and Arts (Project Geodynamics). IM, AP and BV were supported by the Ministry of Education, Science and Technological Deve-

lopment of the Republic of Serbia (Project No. 173048). SS is grateful to Professor D. Barrie Johnson from Bangor University, UK, for an opportunity to visit his laboratory as a guest research scientist.

ИЗВОД

ИСТРАЖИВАЊЕ МИКРОБИОЛОШКОГ ДИВЕРЗИТЕТА ЕКСТРЕМНО КИСЕЛЕ ВЕШТАЧКЕ АКУМУЛАЦИЈЕ ВОДЕ СА ВИСОКИМ САДРЖАЈЕМ МЕТАЛА (ЈЕЗЕРО РОБУЛЕ, БОР, РЕПУБЛИКА СРБИЈА)

СРЂАН СТАНКОВИЋ[1], ИВАНА МОРИЋ[2], АЛЕКСАНДАР ПАВИЋ[2], БРАНКА ВАСИЉЕВИЋ[2], D. BARRIE JOHNSON[3] и ВЛАДИЦА ЦВЕТКОВИЋ[1]

[1]*Универзитет у Београду, Рударско–геолошки факултет,* [2]*Институт за молекуларну генетику и генетичко инжењерство, Универзитет у Београду и* [3]*School of Biological Sciences, Bangor University, United Kingdom*

Истраживање микробиолошког диверзитета екстремно киселе вештачке акумулације воде, језера Робуле код Бора, спроведено је култивацијом бактерија на селективним чврстим подлогама и применом молекуларне методе која не захтева изолацију и култивацију бактерија из животне средине (T-RFLP). Такође, испитивана је способност нативних бактерија из језера да врше лужење бакра из узорка минералног концентрата. T-RFLP анализом је утврђено да у води језера доминирају облигатно органохетеротрофна бактерија *Acidiphilium cryptum* (≈50 % од укупног броја бактерија) и облигатно аутотрофна бактерија која оксидује гвожђе *Leptospirillum ferrooxidans* (≈40 %). Према резултатима које су пре неколико година објавили други аутори, најзаступљенији микроорганизам у језеру је била аутотрофна бактерија која оксидује гвожђе и сумпор - *Acidithiobacillus ferrooxidans,* међутим присуство ове бактерије у води језера није потврђено T-RFLP анализом. Ова бактерија је изолована на селективној чврстој подлози и детектована T-RFLP методом у раствору након теста биолужења. Присуство две бактеријске врсте које су детектоване T-RFLP методом у води језера (*A. cryptum* и *L. ferrooxidans*) потврђено је култивацијом на селективним чврстим подлогама. Присуство и релативна заступљеност бактерија у језеру Робуле су објашњени у складу са физиолошким карактеристикама ових бактерија и физичко-хемијским особинама језерске воде.

(Примљено 5. јуна, ревидирано 24. јуна, прихваћено 24. јуна 2013)

REFERENCES

1. H. Tributsch, J. Rojas-Chapana, in *Biomining*, D. E. Rawlings, D. B. Johnson, Eds., Springer, Berlin, 2007, p. 263
2. R. Rajković, V. Marinković, R. Lekovski, *Rudarski radovi* **3** (2011) 77 (in Serbian)
3. V. P. Beškoski, P. Papić, V. Dragišić, V. Matić, M. M. Vrvić, *Adv. Mater. Res.* **105** (2009) 71
4. H. R. Watling, *Hydrometallurgy* **84** (2006) 81
5. D. B. Johnson, *Trans. Nonferrous. Met. Soc. China* **18** (2008) 1367
6. G. Bogdanović, M. Trumić, M. Trumić, D. V. Antić, *Reciklaža i održivi razvoj* **4** (2011) 37 (in Serbian)
7. B. J. Baker, J. F. Banfield, *FEMS Microbiol. Ecol.* **44** (2003) 139
8. M. A. Anwar, M. Iqbal, M. A. Qamar, M. Rehman, A. M. Khalid, *World J. Microb. Biot.* **16** (2000) 135
9. D. R. Lovely, E. J. P. Phillips, *Appl. Environ. Microb.* **53** (1987) 1536
10. D. B. Johnson, *J. Microbiol. Meth.* **23** (1995) 205

11. D. B. Johnson, K. B. Hallberg, in *Biomining*, D. E. Rawlings, D. B. Johnson, Eds., Springer, Berlin, 2007, p. 237
12. M. Egert, M. W. Friedrich, *Appl. Environ. Microb.* **69** (2003) 2555
13. M. Korać, Ž. Kamberović, *Metall. Mater. Eng.* **13** (2007) 41
14. W. Liu, T. L. Marsh, H. Cheng, L. J. Forney, *Appl. Environ. Microb.* **63** (1997) 4516
15. J. J. Engbretson, C. L. Moyer, *Appl. Environ. Microb.* **69** (2003) 4823
16. M. P. Silverman, D. C. Lundgren, *J. Bacteriol.* **77** (1959) 642
17. D. B. Johnson, K. B. Hallberg, *Adv. Microb. Physiol.* **54** (2009) 201
18. D. E. Rawlings, H. Tributsch, G. S. Hansford, *Microbiology* **145** (1999) 5
19. K. C. Walton, D. B. Johnson, *Environ. Pollut.* **76** (1992) 169
20. M. F. Said, *Ph.D. Thesis*, University of Wales, Cardiff, 1990
21. D. B. Johnson, *FEMS Microbiol. Ecol.* **27** (1998) 307
22. I. Nancucheo, D. B. Johnson, *Frontiers Microbiol.* **3** (2012) article 325.

Journal of the Serbian Chemical Society
JSCS-info@shd.org.rs • www.shd.org.rs/JSCS
J. Serb. Chem. Soc. 79 (6) 743–757 (2014)
JSCS–4623
UDC 637.4.002.2+661.183.1+
547.459.5+544.4:628.3
Original scientific paper

Treatment of egg processing industry effluent using chitosan as an adsorbent

KARICHAPPAN THIRUGNANASAMBANDHAM, VENKATACHALAM SIVAKUMAR* and JEGANATHAN PRAKASH MARAN

Department of Food Technology, Kongu Engineering College, Perundurai, Erode-638052, TN, India

(Received 1 February, revised 14 May, accepted 15 May 2013)

Abstract: The objective of the present study was to investigate the efficiency of chitosan as an adsorbent for the treatment of wastewater from the egg processing industry. Parameters affecting the effluent treatment process, such as pH, chitosan dosage, settling time and initial chemical oxygen demand (*COD*) on the reduction percentage of turbidity, *COD* and biochemical oxygen demand (*BOD*) were studied. The optimum conditions were found to be pH 4, chitosan dosage of 1.1 g L^{-1} and a settling time of 40 min. The maximum reduction percentage of turbidity, *COD* and *BOD* were found to be 94, 88 and 83 %, respectively. The effective adsorption process was confirmed by FT-IR spectral analysis. The experimental data were analyzed by different isotherm and kinetic models. The Langmuir isotherm type I model satisfactorily described the adsorption mechanism. The rate of *COD* reduction followed a pseudo-first-order kinetic model. A four factor, three levels Box–Behnken response surface design was employed to develop second order polynomial mathematical models from the experimental data.

Keywords: egg wastewater; chitosan; adsorption; isotherms; kinetics; experimental design.

INTRODUCTION

Water is a scarce resource of the world and only 0.03 % is available for human activities.[1] Domestic and industrial sources have made the use of waters unwholesome and have produced great amounts of wastewater. The release of raw wastewater into the environment causes aesthetic problems and has a negative impact on environmental bodies and human living resources. A few decades, there were no stringent laws guiding environmental pollution and hence, many industries discharged untreated or inadequately treated wastewater into the environment.[2] Recently, pollution control boards made stringent regulation to adopt

* Corresponding author. E-mail: drvsivakumar@yahoo.com
doi: 10.2298/JSC130408074T

zero discharge methods in order to protect the ecological system. Therefore, nowadays, effluent treatment is one of the most important targets for various industries.[3] Different type of industries discharge huge amount of wastewaters, of which the egg processing industry generates more than 9.5 billion liters of wastewater annually. The discharge of untreated egg processing industrial wastewater creates many environmental problems due to its high concentrations of organic matter.[4]

Numerous effluent treatment methods, such as anaerobic,[5] aerobic,[6] advanced oxidation processes,[7] ozonation,[8] electro-oxidation,[9] photochemical oxidation using UV/H_2O_2,[10] electrochemical techniques,[11] coagulation–flocculation,[12] ion exchange,[13] membrane processes[14] and biosorption,[15] have been used to treat the various industrial effluents. Among these methods, chemical coagulation is a widely used method for the treatment of industrial effluent, due to its superior removal efficiency of toxic substances.[16] In chemical coagulation processes, aluminum and iron salts are widely used as coagulants that destabilize the colloidal materials and cause the small particles to agglomerate into larger settable flocs; thus, effectively reducing the content of organic matter.[17,18] However, the chemical coagulation method has some disadvantages, such as large chemical addition, sludge generation,[19] economic viability and secondary pollution may arise.[20] Hence, there is critical need to identify a environmental friendly material that has the capability to treat industrial wastewaters efficiently without having any negative impact on the receiving environmental bodies.

Chitosan, which is derived from the de-acetylation of chitin, is one of the most predominantly employed polymeric materials for use as an adsorbent to treat different wastewaters, such as seafood processing wastewater,[21] milk processing wastewater,[22] brewery wastewater,[23] textile wastewater,[24] pulp and paper mill wastewater,[25] olive oil industry wastewater[26] and metal industry wastewater,[27] because of its biodegradability, biocompatibility, adsorption properties and possibilities of regeneration.[28] Moreover, the sludge produced from the chitosan can be efficiently degraded by micro-organisms[29] without causing any harmful effects on ecological systems. An extensive literature survey showed that no research reports are available for the treatment of egg processing industrial wastewater using chitosan as an adsorbent. Hence, the objective of the present study was to investigate and optimize the effects of the operating parameters, such as pH, chitosan dose, settling time and initial concentration on reduction percentage of turbidity, *COD* and *BOD*, on the treatment of wastewater from the egg processing industry. Different isotherms and kinetics models were employed to describe the obtained results. Finally, from the experimental data, second order polynomial models were developed for the responses (turbidity, *COD* and *BOD* reduction) using a four-factor, three-level Box–Behnken response surface design (BBD). BBD is a spherical, revolving response surface methodol-

ogy (RSM) design that consists of a central point and the middle points of the edges of a cube circumscribed on a sphere, which is useful for developing and understanding the performance of complex systems.[30]

EXPERIMENTAL

Wastewater sample

Egg wastewater samples were collected from an egg processing industry located in Erode, Tamilnadu, India. The samples were stored at ≤5 °C in order to avoid changes in the physico-chemical characteristics of the effluent. Chitosan (fine white powder), hydrochloric acid (98.5 % of purity) and sodium hydroxide (98 % of purity) were obtained from Merck Chemicals, Chennai, Tamilnadu, India. The characteristics of effluent used in the present study are given in Table I.

TABLE I. Characteristics of the egg processing industry wastewater

Characteristic	Value
Turbidity, NTU	306–832
COD / mg L^{-1}	1574–4000
BOD / mg L^{-1}	894–2185
pH	6.9–7.5
Conductivity, mS cm^{-1}	0.588–0.724
Total dissolved solids, mg L^{-1}	3120–3876

Experimental procedure

Conventional batch studies were performed with different dosages of chitosan (0.7–1.3 g L^{-1}) in 100 mL of composite wastewater of pH values in the range 2–7. The pH of the effluent was measured and adjusted with 0.1M HCl or NaOH solutions. Then the samples were agitated (1 min at 100 rpm followed by 3 min at 40 rpm) in a combined incubator and shaker (GeNei™ OS-250, India) and then allowed to settled down. The clear supernatant effluent was centrifuged (Remi R-24 Centrifuge, India) and filtered through a 0.45 μm filters. The *COD* and *BOD* content of the filtered effluent were analyzed by the procedures suggested by the American Public Health Association (APHA) standard method of examination of water and wastewater.[31] The turbidity of samples was determined using a turbidity meter (Elico CL52D, India). All the adsorption experiments were performed in triplicate to check the reproducibility of the results. The value of q_e was calculated using the following equation:[32]

$$q_e = \left(\frac{c_0 - c_e}{w} \right) V \quad (1)$$

The value of q_t was calculated using the following equation:[32]

$$q_t = \left(\frac{c_0 - c_t}{w} \right) V \quad (2)$$

where, c_0 is initial *COD* concentration and c_t is concentration of *COD* at time *t*, *V* is the volume of the wastewater sample (L), and *w* is the weight of the chitosan used (g). The reduction efficiency (*RE*) was calculated by the following equation:[33]

$$RE = \left(\frac{c_0 - c_e}{c_0} \right) \times 100 \quad (3)$$

where, c_0 and c_e are the initial and after treatment concentrations, respectively, of *COD* or *BOD*, or the turbidity.

Fourier-transform infrared red (FT-IR) spectroscopic analysis

The FT-IR spectra of chitosan (raw and after adsorption process) were recorded on an FT-IR spectrometer (Instrument model RX_1, India) in the range of 4000–400 cm^{-1} using potassium bromide (KBr) pellets.

Statistical analysis

Different statistical parameters such as standard absolute errors (*SAE*),[34] the Marquardt percent standard deviation (*MPSD*) and average relative error (*ARE*)[35] were used to analyze the various isotherms and kinetic models. The following equations were used to evaluate the different statistical parameters

$$SAE = \sum_{i=1}^{n} \left| q_{e,cal} - q_{e,exp} \right|_i \quad (4)$$

$$MPSD = 100 \sqrt{\frac{\sum_{1-n}^{n} \left(\frac{q_{e,exp} - q_{e,cal}}{q_{e,exp}} \right)}{n - p}} \quad (5)$$

$$ARE = \frac{100}{n} \sum_{i=1}^{n} \left| \frac{q_{e,exp} - q_{e,cal}}{q_{e,exp}} \right|_i \quad (6)$$

where, p is the number of parameters in the isotherm equation and n is the number of data points.

Box–Behnken (BBD) design

Response surface methodology (RSM) is an empirical statistical modeling technique employed for multiple regression analysis using quantitative data obtained from properly designed experiments to solve multivariate equations simultaneously.[36] In the present study, a three-level, four-factor BBD was employed to study the effect of process variables such as the initial *COD* concentration, pH, adsorbent dose and settling time on the reduction efficiency of turbidity, *COD* and *BOD*. The process variables were coded at three levels (low, middle and high, *i.e.*, –1, 0 and +1, respectively) for statistical calculations and the design is given in Table II. The coding of the process variables were realized according to the following equation:[37]

$$x_i = \frac{X_i - X_{cp}}{\nabla X_i} \quad (7)$$

where x_i is a dimensionless value of an independent variable; X_i is the real value of an independent variable; X_{cp}, is the real value of an independent variable at the center point and ∇X_i is the step change of the real value of variable i, corresponding to a variation of a unit for the dimensionless value of the variable *i*.

A total number of 29 experiments were performed in a randomized order. A second order polynomial model was used to fit the experimental data in order to develop mathematical

models to represent the predicted experimental data using a statistical software package (Stat ease design expert 8.0.7.1). The generalized second order polynomial equation is given below:[37]

$$Y = \beta_0 + \sum_{j=1}^{k} \beta_j x_j + \sum_{j=1}^{k} \beta_{jj} x_j^2 + \sum_{i<j=2}^{k} \sum \beta_{ij} x_i x_j + e_i \quad (8)$$

where Y is the response; x_i and x_j are variables (i and j ranged from 1 to k); β_0 is the model intercept coefficient; β_j, β_{jj} and β_{ij} are interaction coefficients of linear, quadratic and the second-order terms, respectively; k is the number of independent parameters (k = 4 in this study); and e_i is the error.

TABLE II. Ranges of the independent variables and their levels

Variable	Factor X	Level		
		–1	0	1
Initial *COD* concentration, mg L^{-1}	X_1	1574	2786	4000
pH	X_2	3	4	5
Chitosan dosage, g L^{-1}	X_3	0.9	1.1	1.3
Settling time, min	X_4	10	30	50

RESULTS AND DISCUSSION

Effects of pH

The effects of different pH values in the range 2–7 on the reductions of turbidity, *COD* and *BOD* were examined. It was observed (Fig. 1) that the reduction percentages of turbidity, *COD* and *BOD* all increased with increasing pH up to 4. In acidic pH, chitosan forms $–NH_3^+$ groups that attract the negatively charged organic matter in the wastewater,[38] which increased the reduction percentage of turbidity, *COD* and *BOD* (88, 80 and 76 %, respectively). Above pH of 4, the positive charge on the chitosan surface decreased[39] and it became insoluble,[40] which negatively affected the treatment process and decreased the reduction percentage of turbidity, *COD* and *BOD*.

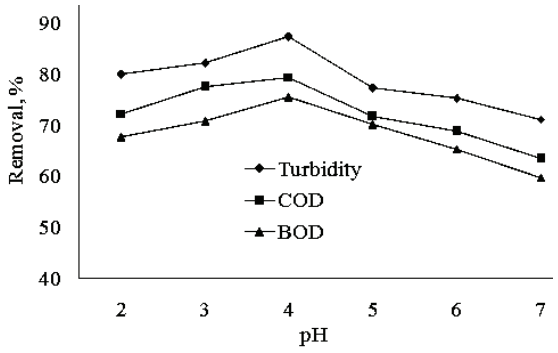

Fig. 1. Effect of pH on the reduction percentage of turbidity, *COD* and *BOD* (chitosan dosage = 0.9 g L^{-1} and settling time = 50 min).

Effects of chitosan dosage

The effects of chitosan dosage on the treatment process were evaluated at different levels (0.7–1.3 g L^{-1}). As shown in Fig. 2, the reduction percentage of turbidity, *COD* and *BOD* increased with increasing chitosan dosage up to 1.1 g L^{-1} and the maximum percentage reductions were found to be: turbidity, 94 %; *COD*, 88 % and *BOD*, 83 %. This is mainly because higher dosages of chitosan increase the number of exchangeable reaction sites[41] available for an effective reduction process of organic matters in the effluent, which could increases the reduction percentage. Beyond a chitosan dosage of 1.1 g L^{-1}, no significant effect on the reduction percentage of turbidity, *COD* and *BOD* were observed.

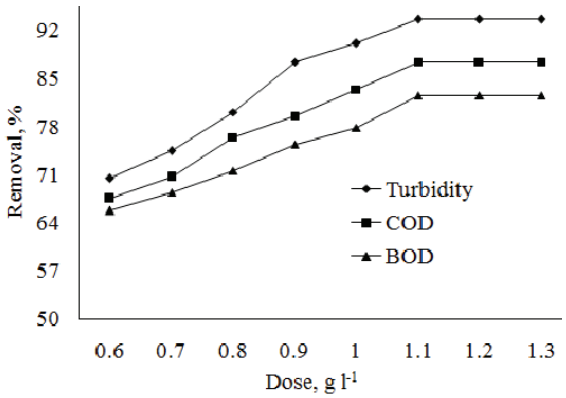

Fig. 2. Effect of the adsorbent dose on the reduction percentage of turbidity, *COD* and *BOD* (pH 4 and settling time = 50 min).

Effect of settling time

To study the effective settling time on the treatment process, studies were performed at different settling times in the range from 10–60 min. The bridging flocculation mechanism of chitosan enhances the compact nature and strength of flocs,[42] which could affect the treatment process significantly. The reduction percentage of turbidity, *COD* and *BOD* increased with settling time up to 40 min resulting in values of 94, 88 and 83 %, respectively (Fig. 3). Thereafter, no significant changes were observed in the reduction percentage of turbidity, *COD* and *BOD*.

Effects of initial concentration

The effects of the initial concentration on the reduction percentage of turbidity, *COD* and *BOD* are shown in Fig. 4, from which it was found that reduction percentages of turbidity were 96, 95 and 94 % for initial values of 306, 416 and 832 NTU, respectively (Fig. 4A). Moreover, the *COD* reduction was found to be 91, 90 and 88 % for initial concentrations of 1574, 2786 and 4000 mg L^{-1},

respectively (Fig. 4B) and *BOD* reduction was found to be 85, 84 and 83 % for initial concentrations of 894, 1324 and 2185 mg L^{-1}, respectively (Fig. 4C) under treatment process conditions of pH 4 and a chitosan dosage of 1.1 g L^{-1}. From the results, it was observed that longer settling times are required to enhance the reduction percentage of turbidity, *COD* and *BOD* when their values are higher.[43]

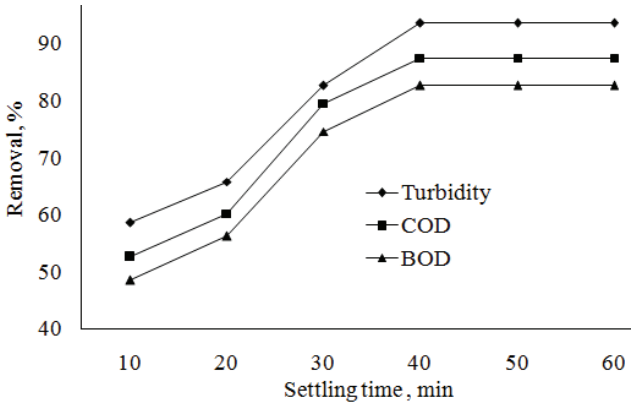

Fig. 3. Effect of settling time on the percentage removal of turbidity, *COD* and *BOD* (pH 4 and chitosan dosage = 1.1 g L^{-1}).

FT-IR analysis

FT-IR spectrophotometric measurements were used to study the mechanism of the treatment process and it is shown in Fig. 5. Curve A shows that, the broad band at 3402 cm^{-1} (N–H stretching) and the peaks at 1604 and 1415 cm^{-1} (N–H bending vibration and N–H deformation) indicating the presence of $–NH_2$ groups on raw chitosan and the band at 1371 cm^{-1} exhibited the presence of O–H group. Both of these functional groups on raw chitosan can serve as reaction sites for the present treatment process.[44] From Fig. 5, it was found that, transmittance shifted from 3402 cm^{-1} (curve A) to lower wave number 3287 cm^{-1} (curve B) shows the interaction between chitosan and organic matters and also disappearance of the peak at 1604 cm^{-1} (curve A) and the formation of a new peak at 1640 cm^{-1} (curve B) was related to consumption of $–NH_2$ groups.[45] It could be concluded that, both $–NH_2$ and –OH groups were involved in this treatment process.

Isotherms

In this study, various isotherm equations, *i.e.*, the Langmuir (type I–IV), Freundlich, Tempkin, and Dubinin–Radushkevich (D–R) models[35] were used to describe the present treatment process. The isotherm parameters and statistical error values for the models are given in Table III. The separation factor (R_L) in Langmuir isotherm models can be used to verify whether the adsorption process is favorable ($0 < R_L < 1$), irreversible ($R_L = 0$), linear ($R_L = 1$) or unfavorable

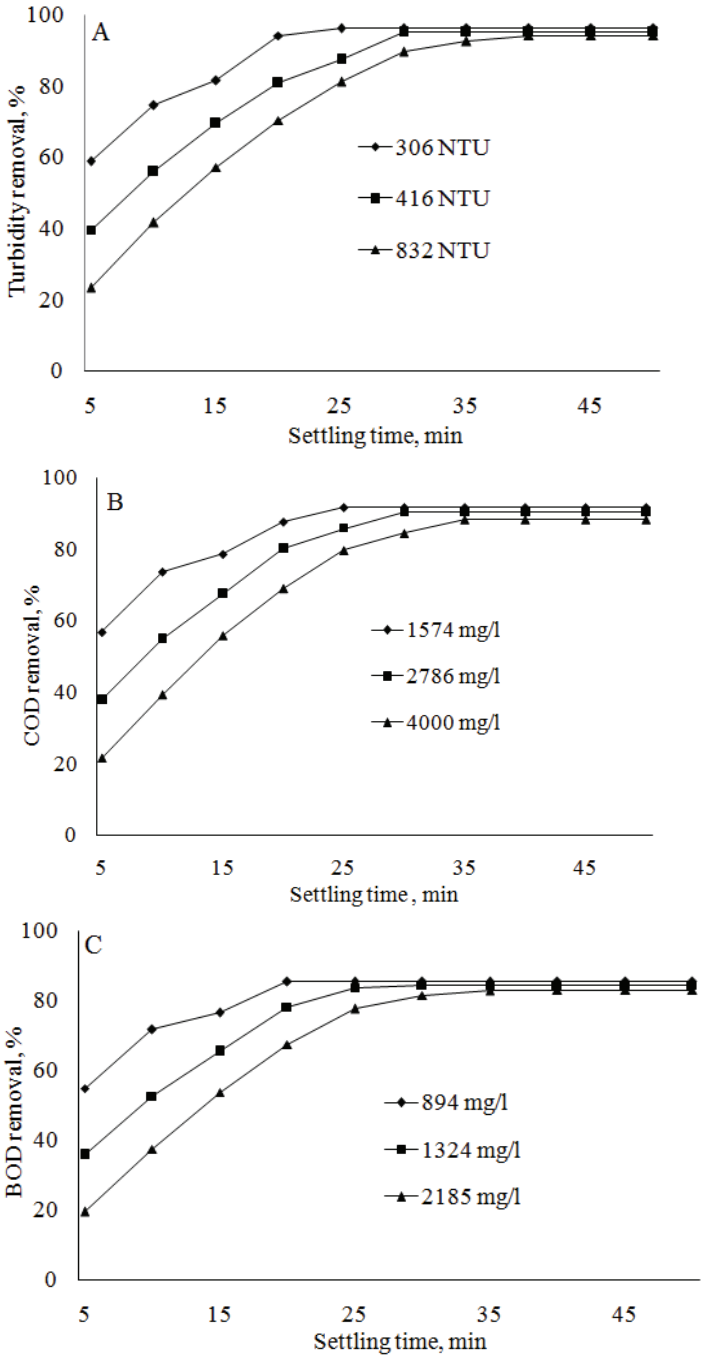

Fig. 4. The effect of initial concentration on reduction percentage of turbidity (A), *COD* (B) and *BOD* (C) (pH 4 and chitosan dosage = 1.1 g L^{-1}).

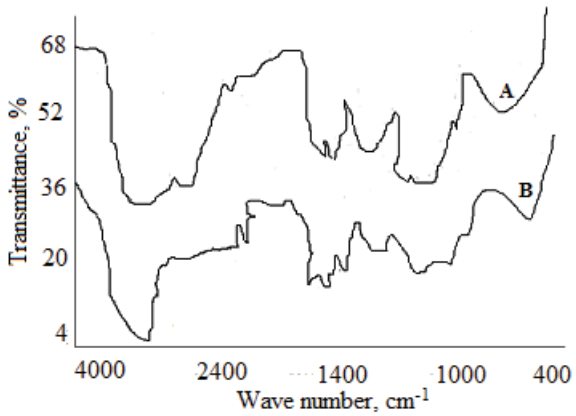

Fig. 5. FT-IR spectra of raw chitosan (A) and after treatment (B).

TABLE III. Isotherm parameters and error analysis values for *COD* reduction; conditions: pH 4; wastewater, 100 mL; adsorbent dose, 1.1 g L^{-1}; *SAE*, sum of absolute errors; *MPSD*, Marquardt percent standard deviation; *ARE*, average relative error

Parameter	Langmuir I	Langmuir II	Langmuir III	Langmuir IV	Freundlich		Tempkin		Dubinin–Radushkevich	
q_m	735.73	781.58	743.04	0.008	K_F	1.85	q_T	149.56	q_{D-R}	785.88
K_L	0.001	655.49	743.04	149.56	n	1.40	K_T	0.01	β	0.0026
R_L	0.27	0.00	0.00	0.00	$1/n$	0.71	B_T	16.84	E	0.11
Statistical error analysis										
Parameter	Langmuir I	Langmuir II	Langmuir III	Langmuir IV	Freundlich		Tempkin		Dubinin–Radushkevich	
SAE	1.70	650.53	612.00	131.03	1673.12		116.56		951.70	
MPSD	1.30	496.44	467.03	99.99	1276.80		88.95		726.27	
ARE	1.28	83.23	82.36	<1000	92.74		804.97		87.89	

($R_L > 1$).[46] In this study, the R_L values ranged from 0 to 0.27, which indicate the Langmuir isotherm model can hardly describe the studied system. In the case of the Freundlich isotherm, the K_F parameter (heterogeneity factor) can be used to indicate whether the process is linear ($K_F = 1$) or whether a chemical process ($K_F < 1$) or physical process ($K_F > 1$) is favorable. The value of K_F obtained in this study was 1.85, which indicates that a physical process was favorable for the studied system. In the Tempkin isotherm model, the positive value of the B_T constant (16.84) showed that the studied system was exothermic in nature. From the Table III, the estimated values of the D–R constants do not represent the experimental data for the reduction of *COD* satisfactorily. The best fitting of the Langmuir (type I–IV), Freundlich, Tempkin, and Dubinin–Radushkevich (D–R) models were analyzed by three different error functions, *i.e.*, *SAE*, *MPSD* and *ARE*, and it was found (Table III) that the Langmuir type I isotherm was the best

model (lowest statistical error value) to describe the present treatment process adequately.

Kinetics

Two kinetic models, *i.e*., pseudo-first-order and pseudo-second-order (type I–IV), were employed to evaluate the present study and the results are given in Table IV. From the Table IV, it could be seen that the q_e values calculated using the pseudo-second-order kinetic models did not fit the experimental q_e values as well as those calculated using the pseudo-first-order kinetic model. The statistical error analysis results also indicated that the pseudo-first-order kinetic model fitted well the obtained experimental data (Table IV). From these results, it was confirmed that the present system followed pseudo-first-order kinetics.

TABLE IV. Kinetic parameters and error analysis values for *COD* reduction; conditions: pH 4; wastewater, 100 mL; adsorbent dose, 1.1 g L^{-1}

Kinetic model	*COD* Concentration mg L^{-1}	$q_{e,exp}$ mg g^{-1}	$q_{e,cal}$ mg g^{-1}	*SAE*	*MPSD*	*ARE*
Pseudo-first-order model						
Lagergren	1574	131.04	120.38	10.66	8.13	8.86
	2786	229.16	221.86	7.30	3.19	3.29
	4000	320.87	386.71	65.84	20.52	17.03
Pseudo-second-order model						
Type I	1574	131.04	155.47	24.43	18.64	15.71
Type II		131.04	0.01	131.03	99.99	< 1500
Type III		131.04	151.52	20.48	15.63	13.52
Type IV		131.04	152.99	21.95	16.75	14.35
Type I	2786	229.16	333.37	104.21	45.47	31.26
Type II		229.16	0.00	229.16	100.00	< 1500
Type III		229.16	308.12	78.96	34.46	25.63
Type IV		229.16	319.23	90.07	39.30	28.21
Type I	4000	320.87	912.53	591.66	184.39	64.84
Type II		320.87	0.00	320.87	100.00	<1500
Type III		320.87	913.09	592.22	184.57	64.86
Type IV		320.87	920.21	599.34	186.79	65.13

BBD analysis

The BBD consisted of 29 experimental runs with 5 center points and the experiments were performed according to the experimental design, and the results are listed in Table V. The statistical analysis was performed using Design Expert Statistical software package 8.0.7.1 (Stat Ease Inc., Minneapolis, USA). The adequacy of the models was justified by Pareto analysis of variance (ANOVA).

TABLE V. Box–Behnken experimental design and the obtained results

Run	*COD* Concentration mg L^{-1}	pH	Chitosan dosage g L^{-1}	Settling time min	Turbidity reduction %	*COD* Reduction %	*BOD* Reduction %
1	2786	3	1.3	30	30.58	28.76	25.67
2	2786	3	1.1	10	9.564	8.46	5.12
3	1574	3	1.1	30	45.85	43.54	40.25
4	1574	5	1.1	30	55.64	53.48	50.84
5	1574	4	1.1	10	65.45	63.47	60.54
6	4000	5	1.1	30	66.34	64.58	61.78
7	2786	5	1.3	30	66.247	64.28	61.72
8	2786	4	0.9	10	45.28	43.58	40.28
9	4000	4	1.3	30	92.54	90.28	87.58
10	2786	4	1.1	30	94.53	90.38	87.54
11	2786	5	0.9	30	64.28	63.54	60.24
12	2786	3	1.1	50	44.78	43.58	40.54
13	2786	4	1.3	10	55.64	54.28	51.42
14	2786	4	1.1	30	94.53	90.38	87.54
15	4000	4	1.1	50	94.28	90.28	87.32
16	2786	4	1.1	30	94.53	90.38	87.54
17	4000	4	0.9	30	85.24	83.56	80.46
18	2786	4	1.3	50	94.28	89.64	86.48
19	2786	4	1.1	30	94.53	90.38	87.54
20	2786	5	1.1	10	30.86	29.34	26.68
21	1574	4	0.9	30	88.64	86.42	83.54
22	4000	3	1.1	30	31.54	30.87	27.84
23	4000	4	1.1	10	34.58	32.84	29.64
24	2786	3	0.9	30	50.84	52.84	49.62
25	2786	5	1.1	50	64.58	63.48	60.48
26	2786	4	0.9	50	84.28	86.94	83.24
27	1574	4	1.1	50	94.25	90.28	87.48
28	2786	4	1.1	30	94.53	90.38	87.54
29	1574	4	1.3	30	94.28	90.78	87.54

Development of mathematical equation and validation

A second order polynomial equation (quadratic) with interaction terms was fitted to the experimental data obtained on the basis of BBD and the final equation obtained in terms of coded factors are given below:

$$Y_1 = 94.53 - 3.30X_1 + 11.24X_2 + 1.25X_3 + 19.59X_4 + 6.25X_1X_2 + \\ + 0.42X_1X_3 + 7.73X_1X_4 + 5.56X_2X_3 - 0.37X_2X_4 - 0.09X_3X_4 - \\ - 3.26X_1^2 - 39.20X_2^2 - 2.83X_3^2 - 19.61X_4^2 \quad (9)$$

$$Y_2 = 90.38 - 2.96X_1 + 10.89X_2 + 0.09X_3 + 19.36X_4 + 5.94X_1X_2 + \\ + 0.59X_1X_3 + 7.66X_1X_4 + 6.21X_2X_3 - 0.25X_2X_4 - 2.00X_3X_4 - \\ - 3.02X_1^2 - 37.23X_2^2 - 1.21X_3^2 - 18.55X_4^2 \quad (10)$$

$$Y_3 = 87.54 - 2.96X_1 + 11.06X_2 + 0.25X_3 + 19.33X_4 + 5.84X_1X_2 + \\ + 0.78X_1X_3 + 7.69X_1X_4 + 6.36X_2X_3 - 0.41X_2X_4 - 1.97X_3X_4 - \\ - 3.01X_1^2 - 37.27X_2^2 - 1.39X_3^2 - 18.71X_4^2 \quad (11)$$

where, Y_1, Y_2 and Y_3 are the predicted reduction percentages of the turbidity, *COD* and *BOD*, respectively, and X_1, X_2, X_3 and X_4 are the initial concentration, pH, adsorbent dose and settling time, respectively. The adequacy and fitness of the models were tested by analysis of the variance (ANOVA) and the results are listed in Table VI. Analysis of the variance followed by the Fisher statistical test (*F*-test) was applied to evaluate the significance of each variable. The high Fisher *F*-values of 89.34, 84.81 and 83.83 for turbidity, and *COD* and *BOD* reduction, respectively, imply that the developed model was statistically significant. The values of R^2 were calculated to be 0.9760, 0.9753 and 0.9750 for turbidity, and *COD* and *BOD* reduction, respectively, which indicated that 97 % of experimental data was compatible. The values of adjusted-R^2 (0.8617 for turbidity, 0.8577 for *COD* and 0.8562 for *BOD*) were also high and showed a high corre-

TABLE VI. ANOVA table of the responses

Source	Turbidity reduction		*COD* Reduction		*BOD* Reduction	
	RC	*P* value	*RC*	*P* value	*RC*	*P* value
Model	94.5273	< 0.0001	90.3776	< 0.0001	17086.7	< 0.0001
X_1	–3.2992	0.0631	–2.9633	0.0856	105.435	0.0876
X_2	11.2362	< 0.0001	10.8908	< 0.0001	1468.29	< 0.0001
X_3	1.25081	0.4568	0.09533	0.9534	0.76768	0.8777
X_4	19.5939	< 0.0001	19.3567	< 0.0001	4481.88	< 0.0001
X_{12}	6.25243	0.0444	5.94252	0.0503	136.308	0.0555
X_{13}	0.4166	0.8851	0.59221	0.8341	2.44662	0.7837
X_{14}	7.72709	0.0163	7.65891	0.0153	236.33	0.0157
X_{23}	5.55675	0.0698	6.205	0.0421	161.671	0.0392
X_{24}	–0.374	0.8968	–0.245	0.9309	0.6561	0.8869
X_{34}	–0.09	0.9751	–2.00	0.4829	15.6025	0.4914
X_1^2	–3.2602	0.1646	–3.0192	0.1875	58.8518	0.1916
X_2^2	–39.204	< 0.0001	–37.225	< 0.0001	9009.27	< 0.0001
X_3^2	–2.8258	0.2244	–1.2067	0.5885	12.5701	0.5362
X_4^2	–19.614	< 0.0001	–18.548	< 0.0001	2271.5	< 0.0001
CV / %	8.37		8.47		8.94	
AP	22.39		22.23		22.16	
R^2	0.976		0.9753		0.975	
Adj-R^2	0.952		0.9506		0.9501	

lation between the observed and the predicted values. The low values of the correlation of variance (8.37, 8.47 and 8.94 for turbidity, *COD* and *BOD* reduction, respectively) clearly represent the high degree of precision and good reliability of the conducted experiments. An adequate precision measures the signal-to-noise ratio and compares the range of the predicted values at the design points to the average prediction error. A value of this ratio greater than 4 is desirable[47] and indicates adequate model discrimination. In the present study, the ratio was found to be >22.15 for all the responses, which indicates an adequate signal. Therefore, the quadratic model was used to navigate the design space. The validation of quadratic model was confirmed by diagnostic plots, such as the predicted *vs*. the experimental values (Fig. 6A, B and C). The data points on this plot lie reasonably close to a straight line and indicate an adequate agreement between the real data and the data obtained from the models.[48]

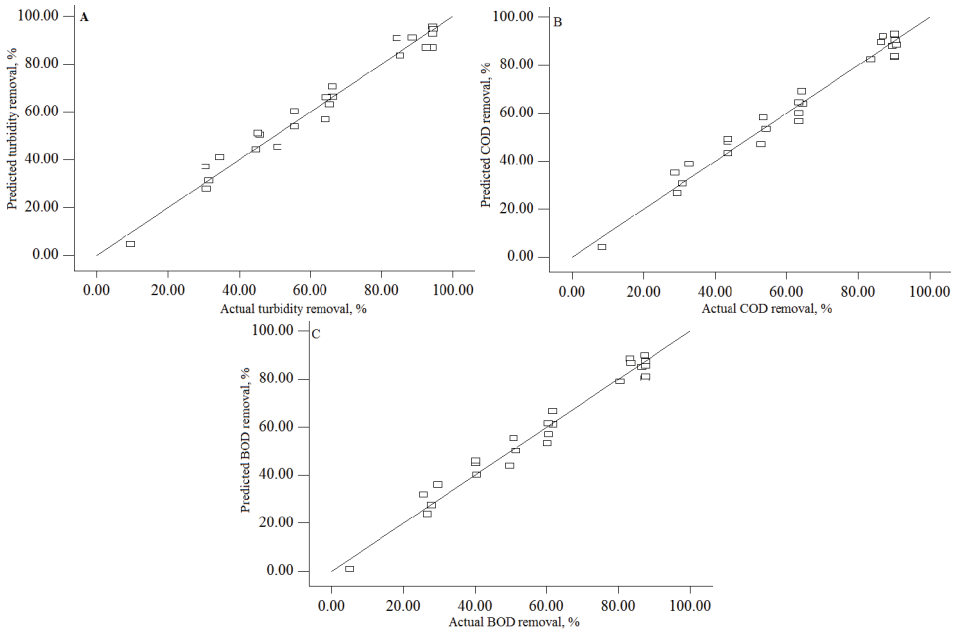

Fig. 6. Experiments *vs*. predicted plot for the reduction of turbidity (A), *COD* (B) and *BOD* (C).

CONCLUSION

The present investigation revealed that chitosan could be used to reduce the turbidity, *COD* and *BOD* from the wastewater from the egg processing industry. Under the optimum conditions of pH 4, a chitosan dosage of 1.1 g L^{-1} and a settling time 40 min, the maximum reductions of turbidity, *COD* and *BOD* of 94, 88 and 83 %, respectively, were attained for initial values of 832 NTU, 4000 and

2185 mg L^{-1}, respectively. The effective adsorption process was confirmed by FT-IR spectroscopy. Various isotherm and kinetic models were fitted to the experimental *COD* reduction data. Among the various isotherm models, the Langmuir isotherm Type I described the process adequately. From the kinetic studies, it was found that, the reduction rate of *COD* followed the pseudo-first-order kinetic model. The developed mathematical models using BBD provided a very high degree of correlation with the experimental data and showed all the independent variables have a significant effect on the responses.

И З В О Д

ТРЕТИРАЊЕ ЕФЛУЕНТА У ИНДУСТИЈИ ПРЕРАДЕ ЈАЈА КОРИШЋЕЊЕМ ХИТОСАНА КАО АДСОРБЕНТА

K. THIRUGNANASAMBANDHAM, V. SIVAKUMAR и J. PRAKASH MARAN

Department of Food Technology, Kongu Engineering College, Perundurai, Erode- 638052, TN, India

Циљ ове студије је био да се испита ефикасност хитосана као адсорбента за третман отпадних вода из индустрије прераде јаја. Одређивани су параметри који утичу на процес адсорпције, као што су pH, доза адсорбента, време деловања и почетна концентрација хемијске потрошње кисеоника (BOD) на проценат умањења замућености, HPK и биохемијске потрошње кисеоника (COD). Нађено је да су оптимални услови pH 4; доза хитосана 1,1 g L^{-1} и време деловања 40 min. Максимално смањење замућености, BOD и COD били су 94, 88 и 83 %. Ефективни процес адсорпције био је потврђен FTIR спектралном анализом. Експериментални резлутати су били анализирани коришћењем различитих изотерми и кинетичких модела. Лангмирова (*Langmuir*) изотерма типа I на задовољавајући начин је описала адсорпциони механизам, а брзина опадања HPK пратила је кинетички модел псеудо-првог реда. На основу експерименталних података развијени су математички модели са полиномима другог реда коришћењем методе Бокс–Бенкенове (*Box–Behnken*) повшине са три нивоа.

(Примљено 1. фебруара, ревидирано 14. маја, прихваћено 15. маја 2013)

REFERENCES

1. C. Allegre, M. Maisseu, F. Charbit, *J. Hazard. Mater.* **116** (2004) 57
2. B. Sarkar, P. P. Chakrabarti, A. Vijaykumar, V. Kale, *Desalination* **195** (2006) 141
3. S. Lacorte, A. Latorre, D. Barceló, A. Rigol, A. Malmqvist, T. Welander, *Trends Anal. Chem*. **725** (2003) 22
4. R. E. Carawan, J. V. Ahambers, R .R. Zall, *The North Carolina Agricultural Extension Service, Raleigh*. **NC. 81** (1979) 785
5. J. P. Guyot, H. Macarie, A. Noyola, *Appl. Biochem. Biotechnol*. **25** (1990) 579
6. G. R. Pophali, R. Khan, R. S. Dhodapkar, T. Nandy, S. Devotta, *J. Environ. Manage.* **85** (2007) 1024
7. E. Neyens, J. Baeyens, *J. Hazard Mater*. **98** (2003) 33
8. V. Fontanier, V. Farines, J. Albet, S. Baig, J. Molinier, *Water Res*. **40** (2006) 303
9. E. Brillas, J. C. Calpe, J. Casado, *Water Res*. **34** (2000) 2253
10. Y. Yang, D. T. Wyatt, M. Bahorsky, *Text. Chem. Color*. **30** (1998) 27
11. G. Chen, *Sep. Purif. Technol*. **38** (2004) 11
12. A. A. Tatsi, A. I. Zouboulis, K. A. Matis, P. Samaras, *Chemosphere* **53** (2003)737

13. A. H. Elshazly, A. H. Konsowa, *Desalination* **158** (2003) 189
14. C. Bhattacharjee, P. K. Bhattacharya, *Sep. Purif. Technol*. **49** (2006) 281
15. P. Lodeiro, R. Herrero, M. E. Sastre de Vicente, *Environ. Chem*. **3** (2006) 400
16. F. M. Menezes, R. Amal, D. Luketina, *Powder Technol*. **88** (1996) 27
17. J. Xu, B. W. Sheldon,, R. E. Carawan, D. K. Larick, A. C. Chao, *Poult. Sci.* **80** (2001) 57
18. R. J. Stephenson, S. J. B. Duff, *Water Res*. **30** (1996) 781
19. A. A. Tatsi, A. I. Zouboulis, K. A. Matis, P. Samaras, *Chemosphere* **53** (2003) 737
20. F. W. Pontius, *J. Am. Waterworks Assoc*. **92** (2000) 18
21. W. A. Bough, *Process Biochem*. **11** (1976) 13
22. F. H. Chi, W. P. Cheng, *J. Polym Environ*. **14** (2006) 411
23. W. P. Cheng, F. H. Chi, R. F. Yu, Y. C. Lee, *J. Polym. Environ*. **13** (2005) 383
24. E. Guibal, J. Roussy, *React. Funct. Polym*. **67** (2007) 33
25. A. C. Rodrigues, M. Boroski, N. S. Shimada, J. C. Garcia, J. Nozaki, N. Hioka, *J. Photochem. Photobiol., A* **194** (2008) 1
26. B. Meyssami, A. B. Kasaeian, *Bioresour Technol*. **96** (2005) 303
27. A. Gamage, F. Shahidi, *Food Chem*. **104** (2007) 989
28. N. V. Ravi Kumar, *React. Funct. Polym*. **46** (2000) 1
29. F. H. Chi, W. P. Cheng, *J. Polym. Environ*. **14** (2006) 411
30. J. Prakash Maran, V. Sivakumar, R. Sridhar, V. Prince Immanuel, *Ind. Crop. Prod*. **42** (2013) 159
31. L. S. Clesceri, A. E. Greenberg, A. D. Eaton, *Standard Methods for Examination of Water & Wastewater*, 21st ed., American Public Health Association (APHA), American Water Works Association (AWWA) & Water Environment Federation (WEF), Washington DC, 2005, pp. 5210–5520B
32. J. Zhu, H. Zhao, J. Ni, *Sep. Purif. Technol.* **56** (2007) 184
33. B. Krajewska, *Sep. Purif. Technol*. **41** (2005) 305
34. I. D. Mall , V. C. Srivastava, N. K. Agarwal, I. M. Mishra, *Colloids Surfaces, A* **264** (2005) 17
35. B. Kayranli, *Chem. Eng. J*. **173** (2011) 782
36. J. P. Maran, V. Sivakumar, R. Sridhar, K. Thirugnanasambandham, *Carbohyd. Polym*. **92** (2013) 1335
37. R. Sridhar, V. Sivakumar, V. Prince Immanuel, J. Prakash Maran, *Environ. Prog. Sustain. Energy* **31** (2012) 558
38. R. P. Jill, H. S C. Chihpin, C. C. Ying, *Colloids Surfaces, A* **147** (1999) 359
39. A. L. Ahmad, S. Sumathi, B. H. Hameed, *Water Res*. **39** (2005) 2483
40. M. A. A. Hassan, T. P. Li and Z. Z. Noor, *J. Chem. Nat. Res. Eng*. **4** (2009) 43.
41. K. Thirugnanasambandham, V. Sivakumar, J. Prakash Maran, *Carbohyd. Polym*. **97** (2014) 451
42. A. L. Ahmad, S. Sumathi, B. H. Hameed, *Chem. Eng. J*. **118** (2006) 99
43. D. Asandei, L. Bulgariu, E. Bobu, *Cell. Chem. Technol*. **43** (2009) 211
44. T. S. Anirudhan, S. Rijith, *Colloids Surfaces, A* **351** (2009) 52
45. A. Pawlak, M. Mucha, *Thermochim. Acta* **396** (2003) 153
46. V. Vimonses, L. Shaomin, J. Bo, C. W. K. Chow, S. Chris, *Chem. Eng. J*. **148** (2009) 354
47. J. Prakash Maran, S. Manikandan, K. Thirugnanasambandham, C. V. Nivetha, R. Dinesh, *Carbohyd. Polym*. **92** (2013) 604
48. P. M. Jeganathan, S. Venkatachalam, T. Karichappan, S. Ramasamy, *Prep. Biochem. Biotech*. **44** (2014) 56.